MICROCYCLE SPECTRAL ESTIMATION

Thesis by

David J. Blakemore

In Partial Fulfillment of the Requirements

For the Degree of

Doctor of Philosophy

California Institute of Technology

Pasadena, California

1966

(Submitted May 26, 1966)

ACKNOWLEDGEMENTS

The author would like to acknowledge the financial support of the Radio Corporation of America, via an RCA fellowship and the Naval Ordnance Test Station, via a research contract (N123 (60530) 54717A) with the California Institute of Technology.

The research reported on in this thesis is entirely the work of the author, except for contributions by

H. C. Martel
Glenna
J. A. Bard
D. J. Anton
T. H. Davey
D. J. Griep
U. Hartman
H. C. Martel
W. H. Corcoran
J. H. Osugi
A. R. Jones
J. N. Franklin
T. L. Grettenberg
K. Matsumoto
H. C. Martel
J. Miyamoto
J. K. Lo
J. S. Hughes
J. Conforti, Jr.
S. Farber
T. Kruger
H. C. Martel
J. P. Stenbit
D. Laird
C. B. Ray
J. Elliot

1. ABSTRACT

This thesis attempts to estimate the power spectral density of low frequency semiconductor noise over a range of 10 decades, from a microcycle (10^{-6} cps) to 10 kilocycles (10^{+4} cps). It is concluded that the behavior is more complex than a simple inverse proportionality to frequency. The spectrum is approximately 1/f in the region around 100 cps and changes gradually to $1/f^2$ as the frequency decreases to the microcycle region. These spectra represent the noise properties of the first stage transistors of a grounded input dc differential amplifier. The estimated spectra at very low frequencies still reflect strong temperature influences.

In order to obtain these measurements it was necessary to control the temperature environment of the noise source. This was accomplished first by passive attenuation and later by active control. The noise source was placed in a circulating oil bath whose temperature was sensed electrically and controlled to a .001°C range. In conjunction with the temperature control activity the power spectral density of room temperature variations was estimated in the frequency range from .1 cps down to 5×10^{-8} cps. Other spectra of interest estimated over the low frequency range were for line voltage amplitude fluctuations and operational amplifier drift. A brief description of the equipment constructed to obtain sample functions of the noise processes is included.

The analytical portion of this work is concerned with the mathematical techniques employed in obtaining power spectral density estimates. The basic scheme employed is that of Blackman and Tukey which consists of estimating the auto-correlation function and Fourier transforming the result. A formula is developed for calculating the variance of the spectral estimator actually employed in the computations. The bias and variability are presented for the estimator when estimating a spectra containing a spectral line. A confidence interval approach to the variability of the spectral estimator is examined. A confidence interval which depends only on the data is constructed around the spectral density estimate. A technique for utilizing the available knowledge concerning the expected variability of the spectral estimate is developed. The result is formulated in terms of a maximum liklihood estimator for the average spectral density when several independent estimates are available. Some possible sources of low frequency bias in the spectral estimate are considered in detail. Among these are the effect of mean removal and certain deterministic disturbances such as steps. Prewhitening for $1/f$ and $1/f^2$ spectra is examined and shown to lead to very great improvement in the spectral estimate. Some suggestions as to more efficient methods of spectral estimation data collection and processing are offered.

TABLE OF CONTENTS

TABLE OF CONTENTS (CONTINUED)

LIST OF FIGURES

2. INTRODUCTION

Does 1/f Noise Really Exist?

The internal noise generated by solid state devices has long been known to have an "excess" component - that is, a component in addition to the thermal or Johnson Noise Model. This noise is usually designated as "excess" because of the distribution of the extra energy with frequency; not because of a large deviation from the anticipated total rms value. The power spectral density of this excess noise increases with decreasing frequency in contrast with the thermal noise spectrum which is constant, or "white." This "1/f Noise," as it has come to be called, is usually modeled as $1/f^a$ where $a > 0$. Is this really a valid characterization? How far down in frequency does this 1/f behavior continue?

Much effort has been expended toward determining the "cause" of 1/f Noise. More precisely, the research has been directed toward a further understanding of the physics of the processes which generate the semiconductor noise. It is generally accepted that 1/f Noise is a collector junction phenomenon. However, there seem to be a large number of competing theories purporting to explain the 1/f behavior. For instance, Bell in Reference [1] presents a model claimed to lead to a 1/f type spectra. A great deal of the confusion which surrounds the subject stems from the great variety of experimental results available. It would appear to be useful for the solid state theoreticians to have a more definite idea of exactly what the "facts" are which require explanation.

Rollin and Templeton [2], [3] seem to have made one of the earliest concentrated attacks on the low frequency noise behavior problem in 1953. They used what may be called the "tape recorder speed-up" technique. This consists of recording the raw data on magnetic tape, playing the tape back repeatedly at greatly increased speeds, and utilizing a wave analyzer to determine the frequency distribution of the energy. This scheme permits use of commercially available instrumentation (wave analyzer or equivalent) which operates in the audio frequency (20 cps - 20,000 cps). Rollin and Templeton had to compensate for the frequency response of their tape recorder system. Because of the large dynamic range involved coupled with the inability to measure the frequency response to a sufficiently high accuracy, their results may have contained a considerable amount of bias. They presented results for carbon resistors, wire-wound resistors, and germanium filaments.

Subsequently, several other researchers investigated a variety of random processes using this technique. The last work on low frequency semiconductor noise seems to have been that of Winston and Firle in 1955 [4]. They investigated fluctuations in voltage across reversed biased germanium and silicon diodes. They obtained spectral estimates by two essentially equivalent schemes. One was a photographic playback version of the "tape recorder speed-up" scheme and the other was an equivalent numerical analysis on a digital computer.

The modern technique of power spectral density estimation achieved wide acceptance primarily due to the work of Blackman and Tukey in 1958 [5]. Parzen has attacked the problem of obtaining consistent estimates of the spectra [6]. He has also found for a specific class of windows (a shaping function applied to the correlation function estimate as discussed in Section 3.1.1) and spectra the "optimum" windows in terms of variability of the estimator [7]. A number of new wrinkles have been added but the basic scheme of estimating the auto-correlation function and Fourier transforming remains unchanged. Parzen and a number of others who have done similar work have exposed the fact that for most spectra of practical interest the variability of the estimates is not a strong function of the particular window. Until recently [8, 9] almost no attention has been given to the bias properties of various spectral estimators. It is an extremely difficult subject to handle with any degree of generality since bias errors depend intimately on the "right answer." Most of the discussion of the low frequency bias problem in Section 3.3 is concerned with spectra of the 1/f type since it was of most interest for this work.

Both of the spectral estimation schemes used by Winston and Firle lead to a poor spectral estimator in the statistical sense. Appendix A shows that their spectral estimate has a variance which is a large fraction of its mean <u>at all frequencies</u>. The bias properties are also calculated but appear not to be very serious for the specific case of 1/f Noise. Winston and Firle's data appears to have a scatter

which agrees with such a formulation. They fit a least squares straight line to the data on a log-log scale leading to a value for a in $1/f^a$ which is "greater than unity." This calculation could be very unreliable with their estimator. Because of the advances made in the art of spectral estimation during the intervening years, it was hoped that another look at the problem might add something.

How do you do the job better? Winston and Firle investigated the noise voltage properties of a back biased p-n junction. For greater applicability to practical engineering situations it would be prefer able to measure the noise properties of transistors in operating circuits. The approach chosen for this work was to attempt to measure the noise properties of transistors in an amplification mode via a differential amplifier noise source. Section 4.1 discusses the design of the noise source. An attempt was made to establish what can be inferred about the properties of a single transistor from the measured properties of the noise generator.

Winston and Firle found it necessary to construct an elaborate temperature control system. Are there perhaps other environmental factors which should be controlled? Was this control really required? Could it have been avoided by more clever data processing? Is it possible, as in many engineering measurement applications, to utilize more sophisticated mathematical analysis and numerical computation techniques and a less sophisticated physical experiment while still obtaining at least comparably accurate results? The easy availability

and low cost of large digital computation facilities lead one to hope this might be the case. Of course, as a practical matter what one actually does is to build the best physical apparatus one can afford and then apply the best computation techniques available.

However, in one sense this is not what you would really like to do. You would like to build apparatus and use data processing just sophisticated enough to answer the desired question, thereby saving time and money for use in answering the next question. For instance, consider the 1/f Noise case. It would be nice to control the environment and process the data just cleverly enough to be able to determine at what frequency the spectra no longer increases with decreasing frequency (if such a break frequency exists). The difficulty of course is that it is not at all obvious beforehand how much control would be "enough." Would temperature control to .1^{o}C be sufficient if good spectral estimators were employed? This would depend on what the 1/f break frequency turned out to be. But this situation is, in fact, very general. In many experiments one never really knows how good to make an experiment until one knows the results of the experiment. To avoid having to do the experiment several times successively more accurate, one usually adopts the approach of doing it as well as possible subject to economic type constraints. It never seems to be obvious that one "over designed" the experiment because the questions change as the answers begin to arrive.

This discussion is particularly relevant to the temperature control problem for a 1/f Noise source. Section 4.2 presents a complete discussion of the temperature dependence problem and the solutions adopted. When the research reported in this thesis was begun, results roughly comparable (except more accurate) to those of Winston and Firle were obtained with no active temperature control. Temperature control was then resorted to and lower frequency, more accurate results were sought. Eventually, a point was reached such that the temperature control was not sufficient to avoid distorting the results. As a natural consequence of such a situation a number of doubts were created.

Do a great many "noises" have a 1/f type spectra? If so, doesn't this throw a lot of suspicion on the measurement technique? Are the estimates being biased by some as yet unknown phenomenon? Motivated by just such considerations, spectra of some other noise processes of interest were also estimated at low frequencies. Among these were the variations in room temperature, the amplitude of the 60-cycle line, and operational amplifier noise. Section 5. discusses these results in detail.

Can we really estimate power spectral densities at microcycle type frequencies? Sections 3.2 and 3.3 can be regarded as sort of an error analysis of the numerical computation procedure used to obtain power spectral density estimates from raw data. Aside from the standard results concerning amplitude and time sampling some

other errors are considered. Suppose the data contains a bad point or an extraneous step function, "What is the effect on the spectral estimate?" What is the effect of removing the sample mean? Can the spectral estimate be improved by our a priori knowledge that we expect to obtain 1/f type results? What equipment is required to obtain data from which spectral estimates at very low frequencies can be formed? Since we are planning to use the digital computer to obtain the spectral estimates from the raw data this question reduces to consideration of what raw data it is relevant to collect and in what form. Section 4.3 discusses the equipment mechanized to collect the raw data for the various experiments while Section 3.2.3 deals with the specific computational tools utilized.

As a final note before launching into the gory details of this research it seems appropriate to deal for a moment with the question of, "Why do we care about 1/f Noise, anyway?" There are several reasons not the least of which is that insatiable curiosity the author shares with the elephant's child. The aim of providing better information to aid in understanding the 1/f Noise generation phenomenon was mentioned above. On a more practical level knowledge of low frequency noise behavior is required to make a sensible long-term design of an electronic instrument. Suppose one intends to put a piece of equipment, say an amplifier, in a spacecraft (or anywhere else) unattended for some long period of time. Need provision be made for resetting its zero?; If so, how often? Will it be necessary to control various parts of the environment to guarantee meeting the

long-term stability requirements?

It seems to be an unfortunate fact that the "drift" properties of electronic devices are very poorly understood especially by many of the people who are in the business of manufacturing and selling the devices. A great deal of effort goes into formulating and designing instruments to meet other types of specifications. However, very few manufacturers even formulate a "drift" specification in a rational manner, let alone meet it. In fact, "drift" ought to be considered as a random process, i.e., "noise," which has most of its energy at very low frequencies. This of course implies that measuring the "peak drift" over a given time span is not a very relevant way of specifying it. Low frequency spectral estimation techniques offer one rational way of describing "drift." If one has an accurate characterization of the random process one can then make meaningful statistical statements as to what may be expected in the time domain. For instance, one might say of a given instrument, "If the instrument is operated in a typical air conditioned laboratory its "drift" referred to the input will be less than 7μ-volts 95% of the time."

3. SPECTRAL ESTIMATION

3.1 General

3.1.1 Spectral Estimation Formulae

All of the spectral estimates of this thesis were obtained by utilizing Blackman and Tukey [5] type spectral estimators. Basically, this technique consists of estimating the correlation function and Fourier transforming the result to form a spectral estimate. The power spectral density is an ensemble property of the random process. But, in general one has available only one sample function from the process. Therefore, the assumption that the process is ergodic is indispensible and all attempts at forming averages must be along time rather than across an ensemble. The auto-correlation function of the process is estimated by sliding the data past itself, multiplying, and summing. (In the discrete case these estimates are called "mean lagged products" for obvious reasons). Specifically, we have as our estimated correlation function

$$\hat{R}_o(\tau) = \begin{cases} \dfrac{1}{T_N - |\tau|} \displaystyle\int_{-\left(\frac{T_N - |\tau|}{2}\right)}^{\left(\frac{T_N - |\tau|}{2}\right)} x(t + \tfrac{\tau}{2})\, x\, (t - \tfrac{\tau}{2})dt & |\tau| < T_M \\ 0 & \text{otherwise} \end{cases} \quad (1)$$

where $x(t)$ is the data and T_N is the total data record length, and this formula is applied only for lags (τ's) less than some maximum value T_M, $T_M < T_N$. This truncation

can be written explicitly as

$$\hat{R}(\tau) = D(\tau)\,\hat{R}_o(\tau) \tag{2}$$

where $D(\tau)$ is called the "lag window" and is identically zero for $|\tau| > T_M$. The shape of this window for $|\tau| < T_M$ affects the properties of the spectral estimate as will be discussed below, but it is important to note that the truncation can never be eliminated entirely because the finite data record length precludes estimating the correlation function over an infinite range. This "windowed" correlation function is then Fourier transformed to yield an estimated spectrum as follows:

$$\hat{S}(f) = \int_{-\infty}^{\infty} \hat{R}(\tau)\, e^{-j2\pi f\tau}\, d\tau \tag{3}$$

Notice that this scheme does not directly estimate the desired quantity, the power spectrum. An intermediate quantity, the correlation function, is estimated and this result is shaped and transformed to obtain the final estimate. While the properties of this estimator can be calculated (see below) it has never been shown that this procedure is in any way "optimum" or most efficient. On the other hand, no one has proposed any very acceptable, practical alternative approaches.*

* Parzen's "Reproducing Kernel Hilbert Space" approach is apparently an attempt to do this, but has not received very wide acceptance.

3.1.2 Properties of the Estimate

The estimated power spectral density at any given frequency is a random variable and a property of particular interest is its average value. One wants to know specifically how the average value of the estimate is related to the correct answer. Taking the ensemble average of Equation (3) above and inserting Equation (2) we have

$$E[\hat{S}(f)] = \int_{-\infty}^{\infty} e^{-j2\pi f\tau} D(\tau)\, E\left[\hat{R}_o(\tau)\right] d\tau \tag{4}$$

where E refers to the expected value, and the order of integration has been interchanged. To find the expected value of the correlation function estimate, we rewrite Equation (1) as

$$\hat{R}_o(\tau) = \frac{1}{T_N} \int_{-\frac{T_N}{2}}^{\frac{T_N}{2}} f(t,\tau)\, x\left(t + \frac{\tau}{2}\right) x\left(t - \frac{\tau}{2}\right) d\tau \tag{5}$$

where

$$f(t,\tau) \triangleq \begin{cases} \dfrac{T_N}{T_N - |\tau|} & -\left(\dfrac{T_N - |\tau|}{2}\right) < t < \dfrac{T_N - |\tau|}{2} \\ 0 & \text{otherwise} \end{cases} \tag{6}$$

Since the data is bounded in amplitude and the limits are finite, we can calculate the expected value

as

$$E\left[\hat{R}_o(\tau)\right] = \frac{1}{T_N}\int_{-\frac{T_N}{2}}^{\frac{T_N}{2}} f(t,\tau)\, R_x(\tau)dt \qquad (7)$$

where we have used the stationarity assumption implied by the ergodicity of $x(t)$ to write τ as the argument of the correlation function. Direct calculation via Equation (6) now yields

$$E\left\{\hat{R}_o(\tau)\right\} = R_x(\tau) \quad \text{for} \quad |\tau| < T_M \qquad (8)$$

which inserted in Equation (4) gives

$$E[\hat{S}(f)] = Q(f) \circledast S_x(f) = \int_{-\infty}^{\infty} Q(f-f')\, S_x(f')df' \qquad (9)$$

where $\circledast$ denotes the operation of convolution and $Q(f)$ is the fourier transform of the "window" $D(\tau)$.

$$Q(f) \triangleq \int_{-\infty}^{\infty} e^{-j2\pi f\tau} D(\tau)d\tau \qquad (10)$$

The significance of the "window" can now be seen directly from Equation (9). Recalling that $D(\tau)$ is identically zero for $\tau > T_M$ we see that $Q(f)$ will be basically $\frac{\sin x}{X}$ like in character with a width of at least $\frac{1}{2T_M}$. Therefore, the "window" is analagous to the narrow band filter in the wave analyzer. It is the width in frequency over which the average value of the

estimate samples the real spectrum. The specific window most used in this work was the "hanning" window given by

$$D(\tau) = \begin{cases} \frac{1}{2}\left(1 + \cos\frac{\pi\tau}{T_M}\right) & |\tau| \geq T_M \\ 0 & \text{otherwise} \end{cases} \qquad (11)$$

for which $Q(f)$ is shown in Figure (1). Reference [5] contains definitions and normalized plots of several other window functions.

Equation (9) indicates one of the central difficulties of power spectral density estimation. Namely, that properties of the estimator are expressible (to date, at least) only as integrals involving the actual spectrum, which at that point is presumably unknown. Therefore, all that is possible is a kind of hypothesis testing operation. One postulates a correct result, and then notes that the estimated spectrum is, or is not, consistent with the postulated result. One way to circumvent this difficulty through confidence interval statements is discussed in Section 3.1.4.

Another very general result for this type of spectral estimator is also obvious. Most estimates of the spectrum will be biased, since Equation (9) indicates that the average value of the estimate will be exactly equal to the actual value of the spectrum at a given frequency only through a numerical coincidence for

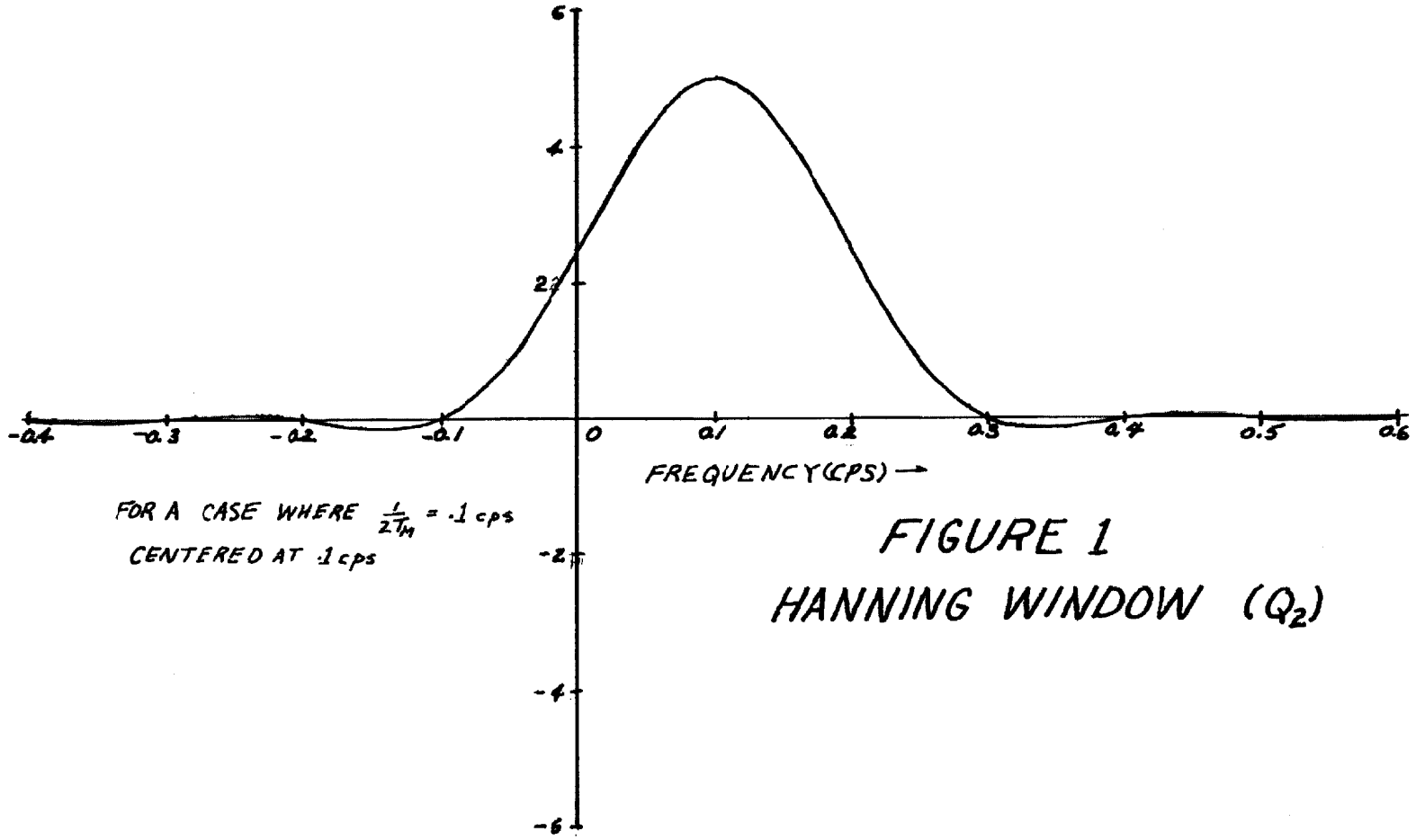

FOR A CASE WHERE $\frac{1}{2T_M} = .1$ cps
CENTERED AT .1 cps

FIGURE 1
HANNING WINDOW (Q_2)

everything except a white (constant) spectrum.* It has been shown by Parzen and others that these types of estimators are asymptotically unbiased in the limit as T_N goes to infinity. This is a consequence of the fact that $Q(f)$ becomes a delta function as T_M grows without limit. As a practical matter it is neither very interesting, nor surprising that an unbiased estimator can be obtained with a record of infinite length. However, it is important to notice that with a fixed finite record of length T_N, the best results are obtained from a bias standpoint when the real spectrum is "smooth" over distances of a few times $1/2T_M$ in frequency.

The other statistical property of the spectral estimate, which is of primary interest, is its variance. Following the example of Blackman and Tukey the covariance between the spectral estimate at two different frequencies will be calculated. This procedure has the advantage of yielding considerably more information with only a slight increase in computational complexity. It makes the correlation between adjacent estimates readily available as well as the variance at a given frequency. Thus, we

---

* See Section 6. below, which discusses this facet more fully.

wish to calculate

$$\mathrm{Cov}\left[\hat{S}(f_1)\ ,\ \hat{S}(f_2)\right] = E\left\{\left[\hat{S}(f_1)-E\left[\hat{S}(f_1)\right]\right]\left[\hat{S}(f_2)-E\left[\hat{S}(f_2)\right]\right]\right\} \quad (12)$$

From Equations (2) and (3) it is obvious that we must calculate

$$\mathrm{Cov}\left[\hat{R}_o(\tau_1)\ ,\ \hat{R}_o(\tau_2)\right]$$

which in turn requires a formula for

$$\mathrm{Cov}\left[x\left(t_1 - \frac{\tau_1}{2}\right)x\left(t_1 + \frac{\tau_1}{2}\right)\ ,\ x\left(t_2 - \frac{\tau_2}{2}\right)x\left(t_2 + \frac{\tau_2}{2}\right)\right]$$

$$= E\left\{x\left(t_1 - \frac{\tau_1}{2}\right)x\left(t_1 + \frac{\tau_1}{2}\right)\ x\left(t_2 + \frac{\tau_2}{2}\right)x\left(t_2 - \frac{\tau_2}{2}\right)\right\} \quad (13)$$

$$- E\left\{x\left(t_1 - \frac{\tau_1}{2}\right)x\left(t_1 + \frac{\tau_1}{2}\right)\right\}\ E\left\{x\left(t_2 - \frac{\tau_2}{2}\right)x\left(t_2 + \frac{\tau_2}{2}\right)\right\}$$

At this point it is necessary to make the assumption that the data, x(t), is a sample function from a zero mean, gaussian random process, in order to evaluate the expected value of the four-fold product.* This is not to imply that the spectral estimation technique will not work in non-zero mean or non-gaussian cases, only that the properties of the estimator are then more difficult to calculate. Our data will, in general, have a mean, and the effect of its removal is discussed below in Section 3.3.1.

* Stationarity has been assumed previously.

Proceeding then, under the assumption that $x(t)$ is gaussian and zero mean, we write the expected value of the fourfold product as *

$$E\left[x\left(t_1 - \frac{\tau_1}{2}\right) x\left(t_1 + \frac{\tau_1}{2}\right) x\left(t_2 - \frac{\tau_2}{2}\right) x\left(t_2 + \frac{\tau_2}{2}\right)\right]$$

$$= R_x(\tau_1)\, R_x(\tau_2) - R_x\left[t_1 - t_2 + \frac{\tau_1 - \tau_2}{2}\right] R_x\left[t_1 - t_2 - \frac{\tau_1 - \tau_2}{2}\right]$$

$$+ R_x\left[t_1 - t_2 + \frac{\tau_1 + \tau_2}{2}\right] R_x\left[t_1 - t_2 - \frac{\tau_1 + \tau_2}{2}\right] \qquad (14)$$

which yields

$$\mathrm{Cov}\left[\left(t_1 - \frac{\tau_1}{2}\right)\left(t_1 + \frac{\tau_1}{2}\right), x\left(t_2 - \frac{\tau_2}{2}\right)\left(t_2 + \frac{\tau_2}{2}\right)\right]$$

$$= \iint_{-\infty}^{\infty} e^{j(\omega_1+\omega_2)(t_1-t_2)} S(f_1) S(f_2) \left[e^{j(\omega_1-\omega_2)\left(\frac{\tau_1+\tau_2}{2}\right)} + e^{j(\omega_1-\omega_2)\left(\frac{\tau_1-\tau_2}{2}\right)} \right] df_1\, df_2$$

where $\omega_1 = 2\pi f_1$, $\omega_2 = 2\pi f_2$, and the correlation functions have been written as the inverse transform of the corresponding spectral densities.**

Now changing variables to

$$f' = f_1 + f_2$$

$$f = f_1 - f_2$$

and recognizing that the spectral density is an even

---

* See for instance, Davenport and Root, [10] Problem # 2, page 168.

** The notation $\omega = 2\pi f$ will be used for all ω's and f's regardless of subscripts or superscripts throughout this Thesis.

function we obtain

$$\mathrm{Cov}\left[x\left(t_1 - \frac{\tau_1}{2}\right) x \left(t_1 + \frac{\tau_1}{2}\right), x\left(t_2 - \frac{\tau_2}{2}\right) x \left(t_2 + \frac{\tau_2}{2}\right)\right]$$

$$= 4 \iint_{-\infty}^{\infty} \cos 2\omega'(t_1-t_2) \cos \omega\tau_1 \cos \omega\tau_2 \, S(f'+f)S(f-f')\,df\,df' \tag{15}$$

Utilizing this result we return to calculate the desired covariance of Equation (12) through the use of Equations (1), (2), and (3). We have

$$\mathrm{Cov}\left(\hat{S}(f_1), \hat{S}(f_2)\right) = \iint_{-\infty}^{\infty} e^{-j(\omega_1\tau_1+\omega_2\tau_2)} D(\tau_1)\, D(\tau_2) \left(\frac{1}{T_N-|\tau_1|}\right)\left(\frac{1}{T_N-|\tau_2|}\right) \cdot$$

$$\int_{-\frac{T_N-|\tau_1|}{2}}^{\frac{T_N-|\tau_1|}{2}} \int_{-\frac{T_N-|\tau_2|}{2}}^{\frac{T_N-|\tau_2|}{2}} \tag{16}$$

$$\mathrm{Cov}\left[x\left(t_1 - \frac{\tau_1}{2}\right) x \left(t_1 + \frac{\tau_1}{2}\right), x\left(t_2 - \frac{\tau_2}{2}\right) x \left(t_2 + \frac{\tau_2}{2}\right)\right] dt_1\, dt_2\, d\tau_1\, d\tau_2$$

The variance calculation to this point has exactly parallel that of Blackman and Tukey. At this point they choose, for calculational convenience, to approximate $\hat{R}_o(t)$ by an estimator where the integration limits do not depend on t; namely by

$$\hat{R}_o'(\tau) \triangleq \begin{cases} \dfrac{1}{T_N'} \displaystyle\int_{-\frac{T_N'}{2}}^{\frac{T_N'}{2}} x(t + \tfrac{\tau}{2})\, x(t - \tfrac{\tau}{2})dt & |\tau| < T_M \\ 0 & \text{otherwise} \end{cases} \qquad (17)$$

where $T_N' = T_N - \alpha T_M$ and α is on the order of $\frac{1}{3}$ but depends on the window used.* This particular approximation seems to have nothing to especially recommend it for the work in this thesis. It does, however, have a serious disadvantage in that the variance calculated is for an estimator that is not, in fact, used. It is preferable to calculate the second order properties of the estimator actually used.

Since in most cases the approximation above concerning α is a good one, the two different schemes yield results which differ only slightly. But this fact in itself, is a comforting one to have available. We shall therefore proceed using the correct correlation function estimator of Equation (1). Utilizing once more, the formulation of Equations (5) and (6) and inserting the result of Equations (15) into (16) we obtain:

*

$$\alpha \triangleq \frac{1}{T_M} \frac{\displaystyle\int_0^{T_M} \tau\, D(\tau)d\tau}{\displaystyle\int_0^{T_M} D(\tau)d\tau}$$

$$\mathrm{Cov}\left[\hat{S}(f_1),\hat{S}(f_2)\right] = 4\int_{-\infty}^{\infty}\cos\omega_1\tau_1\cos\omega_2\tau_2\cos\omega\tau_1\cos\omega\tau_2\,D(\tau_1)D(\tau_2)$$

$$S(f+f')S(f-f')\,\frac{1}{T_N^2}\int_{-\frac{T_N}{2}}^{\frac{T_N}{2}} f(t_1,\tau_1)f(t_2,\tau_2)\cos 2\omega'(t_1-t_2)\,dt_1dt_2\,df\,df'\,d\tau_1\,d\tau_2 \qquad (18)$$

Where use has been made of the "evenness" of the windows and spectra and the order of integration has been interchanged. The t_1 and t_2 integrations can be carried out directly by expanding the cosine term and utilizing the fact that $f(t,\tau)$ is even in t. Thus,

$$\frac{1}{T_N^2}\int_{-\frac{T_N}{2}}^{\frac{T_N}{2}} f(t_1,\tau_1)\,f(t_2,\tau_2)\cos 2\omega'(t_1-t_2)\,dt_1dt_2 \qquad (19)$$

$$= \frac{\sin\omega'(T_N-|\tau_1|)}{\omega'(T_N-|\tau_1|)}\;\frac{\sin\omega'(T_N-|\tau_2|)}{\omega'(T_N-|\tau_2|)}$$

which in turn gives for the covariance

$$\mathrm{Cov}\left[\hat{S}(f_1),\hat{S}(f_2)\right] = 4\int_{-\infty}^{\infty}\cos\omega_1\tau_1\cos\omega_2\tau_2\cos\omega\tau_1\cos\omega\tau_2\,D(\tau_1)D(\tau_2)$$

$$S(f+f')S(f-f')\;\frac{\sin\omega'(T_N-|\tau_1|)}{\omega'(T_N-|\tau_1|)}\;\frac{\sin\omega'(T_N-|\tau_2|)}{\omega'(T_N-|\tau_2|)}\;d\tau_1d\tau_2df'df \qquad (20)$$

While this formula is not simple, it is apparently the best that can be obtained without approximations of some kind. As will become apparent shortly, it is really no more complicated to apply in a practical calculation than the simpler appearing versions because both reduce to the same approximate formula.

For comparison, if we had utilized the approximation of Blackman and Tukey, we would have arrived at

$$\mathrm{Cov}\left\{\hat{S}(f_1),\hat{S}(f_2)\right\} = 4\iiint_{-\infty}^{\infty} \cos\omega_1\tau_1 \cos\omega_2\tau_2 \cos\omega\tau_1 \cos\omega\tau_2 \, D(\tau_1)D(\tau_2) \, S(f+f')S(f-f') \left(\frac{\sin\omega' T_N'}{\omega' T_N'}\right)^2 d\tau_1 d\tau_2 df' df \tag{21}$$

which is their result. The f' integration decouples in this approximation. Recognizing the τ integrals as windows evaluated at specific frequencies the result can then be rewritten as in Reference [5] .

$$\mathrm{Cov}\left\{\hat{S}(f_1),\hat{S}(f_2)\right\} = \int_{-\infty}^{\infty} \left[Q(f+f_1) + Q(f-f_1)\right]\left[Q(f+f_2) + Q(f-f_2)\right] \Gamma(f)df \tag{22}$$

where

$$\Gamma(f) \triangleq 4\int_{-\infty}^{\infty} S(f+f')\, S(f-f') \left(\frac{\sin\omega' T_N'}{\omega' T_N'}\right)^2 df'$$

The approximate result, Equation (22), is much easier to interpret than Equation (20). However, with the aid of "hindsight" most of the intuitive arguments can be applied to either form. The more accurate result then shows that

as expected, the classical formulation is a good approximation. We shall illustrate this point with typical numerical values in the next section. But, first however, it is useful to see what form the first order correction terms take analytically.

Returning to Equation (20) we see that the f' integration does not separate out neatly as in the approximate case, because of the τ_1, τ_2 dependence of the f' integrand. One approach is to expand this integrand in a two-dimensional Taylor series in $\left|\frac{\tau_1}{T_N}\right|$ and $\left|\frac{\tau_2}{T_N}\right|$ about the point $\tau_1 = 0$, $\tau_2 = 0$. The zeroth order term is then identical with Equation (22), the approximate answer, except that T_N replaces T_N'. Thus, we define

$$\Gamma(f,\tau_1\tau_2) \triangleq 4\int_{-\infty}^{\infty} S(f+f')S(f-f') \frac{\sin \omega' T_N\left(1 - \frac{|\tau_1|}{T_N}\right)}{\omega' T_N\left(1 - \frac{|\tau_1|}{T_N}\right)} \frac{\sin \omega' T_N\left(1 - \frac{|\tau_2|}{T_N}\right)}{\omega' T_N\left(1 - \frac{|\tau_2|}{T_N}\right)} df' \tag{23}$$

and wish to expand $\Gamma(f,\tau_1,\tau_2)$ as follows

$$\Gamma(f,\tau_1,\tau_2) = \Gamma(f,o,o) + \left(\frac{|\tau_1|}{T_N}\right) \frac{\partial \Gamma(f,\tau_1,\tau_2)}{\partial\left(\frac{|\tau_1|}{T_N}\right)}\Bigg|_{\tau_1=\tau_2=0} + \left(\frac{|\tau_2|}{T_N}\right) \frac{\partial \Gamma(f,\tau_1,\tau_2)}{\partial\left(\frac{|\tau_2|}{T_N}\right)}\Bigg|_{\tau_1=\tau_2=0} + \cdots \tag{24}$$

We will depend on the fact that the windows $D(\tau_1)$ and $D(\tau_2)$ are zero for τ's greater than T_M which is much less than T_N to make second order terms in $\frac{|\tau|}{T_N}$ negligible.

It is now obvious, as alluded to above, that

$$\Gamma(f,o,o) = 4 \int_{-\infty}^{\infty} \left(\frac{\sin \omega' T_N}{\omega' T_N}\right) S(f+f')\, S(f-f')\, df' \qquad (25)$$

and that this term in the covariance is just Equation (22) with T_N instead of T_N'. Calculating the partial derivatives of $\Gamma(f,\tau_1,\tau_2)$ and evaluating at $T_1 = T_2 = 0$ yields

$$\left.\frac{\partial\Gamma(f,\tau_1,\tau_2)}{\partial\left(\frac{|\tau_1|}{T_N}\right)}\right|_{\tau_1=\tau_2=0} = \left.\frac{\partial\Gamma(f,\tau_1\tau_2)}{\partial\left(\frac{|\tau_2|}{T_N}\right)}\right|_{\tau_1-\tau_2-0} = \Gamma(f,o,o) - \Gamma'(f,o,o) \qquad (26)$$

$$\Gamma'(f,o,o) \triangleq 4 \int_{-\infty}^{\infty} S(f+f')\, S(f-f')\, \frac{\sin 2\omega' T_N}{2\omega' T_N}\, df' \qquad (27)$$

Returning to Equation (24) we obtain

$$\Gamma(f,\tau_1,\tau_2) = \Gamma(f,o,o) \left\{1 + \frac{|\tau_1|}{T_N}\left[1 + \frac{\Gamma'(f,o,o)}{\Gamma(f,o,o)}\right] + \frac{|\tau_2|}{T_N}\left[1 + \frac{\Gamma'(f,o,o)}{\Gamma(f,o,o)}\right] + \cdots\right\}$$

In order to facilitate interpretation of the τ_1 and τ_2 integrations we will factor the first order terms into product form as follows:

$$\Gamma(f,\tau_1,\tau_2) \approx \Gamma(f,o,o) \left\{1 + \frac{|\tau_1|}{T_N}\left[1 + \frac{\Gamma'(f,o,o)}{\Gamma(f,o,o)}\right]\right\} \left\{1 + \frac{|\tau_2|}{T_N}\left[1 + \frac{\Gamma'(f,o,o)}{\Gamma(f,o,o)}\right]\right\} \qquad (28)$$

We can write Equation (28) as*

$$\Gamma(f,\tau_1,\tau_2) \approx \Gamma(f,o,o)\ D'(\tau_1)\ D'(\tau_2) \tag{29}$$

where

$$D'(\tau) \triangleq \begin{cases} 1 + \dfrac{|\tau|}{T_{NR}} & |\tau| < T_{NR} \\ 0 & \text{otherwise} \end{cases} \tag{30}$$

and

$$T_{NR} = T_N \Big/ \left(1 + \frac{\Gamma'(f,o,o)}{\Gamma(f,o,o)}\right)$$

When inserted into Equation (20) this result yields a formula comparable to Equation (22), namely

$$\mathrm{Cov}\left\{\hat{S}(f_1),\hat{S}(f_2)\right\} \approx \int_{-\infty}^{\infty} \left[Q''(f-f_1) + Q''(f-f_1)\right]\left[Q''(f+f_2) + A''(f-f_2)\right] \Gamma(f)df \tag{31}$$

where

$$\Gamma(f) = 4 \int_{-\infty}^{\infty} S(f+f')\ S(f-f') \left(\frac{\sin \omega' T_N}{\omega' T_N}\right)^2 df'$$

and Q" is the Fourier transform of the product of the old "window" D(t) and the new "window" D'(t) i.e.,

$$Q''(f) \triangleq \int_{-\infty}^{\infty} D(\tau)\ D'(\tau)\ e^{-j\omega\tau}\, d\tau = Q(f) \circledast Q'(f) \tag{32}$$

where Q'(f) is, of course, the Fourier transform of D'(t)

$$Q'(f) = \int_{-\infty}^{\infty} D'(\tau)\ e^{-j\omega\tau}\, d\tau = T_{NR} \left(\frac{\sin \pi f\ T_{NR}}{\pi f\ T_{NR}}\right)^2$$

---

* We will show in Sections 3.1.3. that Γ' is closely related to Γ in the usual case so that $T_{NR} = \frac{2}{3} T_N$.

It is now apparent that to first order the effect of the approximation in Equation (17) which leads to Equation (22) is represented by the change in the window from $Q(f)$ to $Q(f) \circledast Q'(f)$. Normally $T_N \gg T_M$ and $T_{NR} \gg T_M$ which implies that $Q'(f)$ is much "narrower" than $Q(f)$. Therefore, $Q''(f)$ is very nearly equal to $Q(f)$. Thus, the approximation is very good. The first order error can be evaluated numerically in any given case. The variance of $S(f)$ is, of course, obtained by setting $f_1 = f_2$ yielding

$$\mathrm{var}\left[\hat{S}(f_1)\right] \approx \int_{-\infty}^{\infty} \left[Q''(f+f_1) + Q''(f-f_1)\right]^2 \Gamma(f)\,df \qquad (33)$$

It is perhaps pertinent to mention that the form of the modified window $Q''(f)$ can be calculated exactly. We merely perform the convolution indicated in Equation (32). For illustrative purposes we shall consider the case of the Q_o window. Because the operations involved in obtaining Q'' from Q are linear, the modified window for Q_2 etc., can then be obtained by simple algebra in the frequency domain. (See Equation (67)). Thus, we have

$$Q''(f) = \int_{-\infty}^{\infty} T_{NR}\left(\frac{\sin \pi T_{NR}}{\pi T_{NR}}\right)^2 2T_M \left(\frac{\sin 2\pi T_M(x-f)}{2\pi T_M(x-f)}\right) dx$$

This integral is evaluated by expanding the denominator via a partial fraction expansion to yield

$$\frac{1}{x^2(x-f)} = -\frac{1}{fx^2} - \frac{1}{f^2x} + \frac{1}{f^2(x-f)}$$

and then utilizing DW 858.704 and DW 858.713 [12]* for these integrations which are not identically zero. After simplification the result is

$$Q''(f) = \left(1 - \frac{T_M}{T_{NR}}\right)\frac{\sin 2\pi fT_M}{\pi f} + \left(\frac{1}{\pi^2 T_{NR}}\right)\frac{\sin^2 \pi fT_M}{f^2}$$

which can be rewritten as

$$Q''(f) = \left(1 - \frac{T_M}{T_{NR}}\right)Q_o(f) + \frac{T_M}{T_{NR}}\,Q_1(f) \qquad (34)$$

where Q_o is the rectangular window and Q_1 is the triangular window. i.e.,

$$D_o(\tau) = \begin{cases} 1 & |\tau| \le T_M \\ 0 & |\tau| > T_M \end{cases} \qquad D_1(\tau) = \begin{cases} 1 - \frac{|\tau|}{T_M} & |\tau| \le T_M \\ 0 & |\tau| > T_M \end{cases}$$

$$Q_o(f) = 2T_M\,\frac{\sin 2\pi fT_M}{2\pi fT_M} \qquad Q_1(f) = T_M\left(\frac{\sin \pi fT_M}{\pi fT_M}\right)^2 \qquad (35)$$

Thus, the modified window is a slightly reduced copy of the original window plus a small copy of the next higher order window. As advertised, if $T_M \ll T_N$ and the spectral density is "smooth," (see next section) then the modified

*This notation refers to the integral # in Dwight's Table of Integrals.

window will be very nearly the original window. A case when this would not be true would be if the real spectral density something like $1/f$ or $1/f^2$ noise with a lower break frequency much smaller than $\frac{1}{2T_M}$, the minimum resolution point. Then for calculating the variance at the point $f_1 = \frac{1}{2T_M}$ we would have

$$\left[Q''(f+f_1) + Q''(f-f_1)\right]^2 = \left\{\left[Q_o(f+f_1) + Q_o(f-f_1)\right]\left(1 - \frac{T_M}{T_{NR}}\right)\right.$$

$$\left. + \frac{T_M}{T_{NR}}\left[Q_1(f+f_1) + Q_1(f-f_1)\right]\right\}^2$$

to be integrated in Equation (33) to yield the variance. The first term is just the ordinary result. Its contribution to the variance will be small even though $S(f)$, and hence $\Gamma(f)$, is very large near the origin (relative to its size at f_1). This is because $Q_o(f)$ has its first zero at the origin when located at $f_1 = \frac{1}{2T_M}$. This same behavior is not true of $Q_1(f)$ when located at $f_1 = \frac{1}{2T_M}$ since its first zero is at $\frac{1}{T_M}$. Therefore, the Q_1 terms might make a significant contribution to the $\text{var}\{\hat{S}(f_1)\}$ regardless of the $\frac{T_M}{T_N}$ multiplier. Perhaps a less confusing way to view this same phenomenon is to return to Equation (34) for $Q''(f)$. From this equation we see that the odd zeros of $Q''(f)$ counting from the

center are those of $Q_o(f)$ shifted outward slightly because the $Q_1(f)$ term is always positive. The even zeros do not change because $Q_1(f)$ also has zeros at these points. Thus, when the variance at the odd points (R = 1, .3, ...) is evaluated, we expect to obtain slightly larger results than at the even points, particularly for spectra which have something like a "pole" at the origin. Also, it is obvious that this extra variability at both the odd and the even points grows smaller as the point in question, f_1, proceeds from the minimum resolution point $\frac{1}{2T_M}$ to the maximum point $\frac{1}{2\Delta t}$.

3.1.3 Approximate Variance Formula

From the results of the last section it is obvious that calculation of the variance of the spectral estimator is complex. In order to plan experiments and obtain rough estimates of the accuracy of a given measurement, it is desirable to have available some sort of approximate formulation. To this end, let us consider the case where the true power spectrum is "smooth." By this we mean that S(f) does not change rapidly in value on the frequency scale of a few times $1/T_M$. With this assumption we formulate some useful approximations.

Part of the motivation for the choice of this particular assumption is evident from Equation (31). We wish to evaluate $\Gamma(f)$ in a simple manner. The $\left(\frac{\sin \omega' T_N}{\omega' T_N}\right)^2$ term behaves essentially like a delta function, provided $S(f')$ does not change rapidly in f'; hence, the choice of "smooth" over at least a few $\frac{1}{T_N}$'s. An alternative approach is to assume S(f) is white noise. The same results would be obtained. It would become obvious that a constant spectrum was a more severe restriction than necessary, and that "smoothness" would be sufficient.

In any case, with the smoothness assumption we now have

$$\Gamma(f) \approx \frac{2}{T_N} \left[S(f)\right]^2 \qquad (36)$$

so that in Equation (31) or (33) we are integrating the modified windows against approximately $\left[S(f)\right]^2$. All of the usual windows employed are basically of width $\frac{1}{T_M}$ or greater in frequency. For instance, the hanning window employed most frequently in this thesis has a central blob of width $\frac{2}{T_M}$ and side lobes of width $\frac{1}{2T_M}$.* Thus, since $Q'(f)$ is of "width" $\frac{1}{T_N}$ we can say that

$$Q''(f) \approx Q(f) \quad \text{provided } T_N \gg T_M \tag{37}$$

Thus we have

$$\text{var}\left[\hat{S}(f)\right] \approx \frac{2}{T_N} \int_{-\infty}^{\infty} \left[Q(f+f_1) + Q(f-f_1)\right]^2 \left[S(f)\right]^2 df \tag{38}$$

It is now clear why $S(f)$ must be "smooth" over distances of order $1/T_M$ for the approximation to be useful. This is, of course, a more stringent restriction on the spectrum than the $\frac{1}{T_N}$ smoothness requirement. If both these conditions do hold the windows squared are approximately δ functions of strength T_M centered at $\pm f_1$ with negligible overlap at the origin. (This can be verified by inserting any of the explicit formulae for $Q(f)$ and integrating). Consequently we have

$$\text{var}\left[\hat{S}(f_1)\right] \approx \frac{T_M}{T_N} \left[S(f_1)\right]^2 \tag{39}$$

---

* For reduced confusion the notation will be chosen consistent with Reference [5] and the hanning window will be referred to as Q_2.

It is important to note where the approximations occurred and what types were involved at each point. The approximation leading to $\Gamma(f)$ in Equation (36) is only one of smoothness of $S(f)$ on a $\frac{1}{T_N}$ scale. This result would be exact if $S(f)$ were really a constant (white noise). The approximation leading to Equation (37) which says that the modified window is approximately equal to the original window, is dependent only on T_M, T_N, and the particular window used. It is independent of the spectra being estimated and in this way is analagous to Blackman and Tukey's α calculation mentioned above (see footnote to Equation (16)). The advantage here is that without a great deal of difficulty $Q''(f)$ can be calculated exactly. The approximation of Equation (37) can be eliminated and the variance calculated for the estimator actually used. These two approximations are combined to yield Equation (38). Thus, for a white noise and accurately calculated $Q''(f)$, Equation (38) can be made exact. This is still true when we proceed to the final result, Equation (39). The T_M/T_N result presented there depends on ignoring the overlap of the two window functions. Again, if the spectrum is white, then this approximation is only a function of the windows and Equation (39) could be made exact with more detailed calculation. As it stands it is approximate, and for any non-white noise it is more approximate.

Some words on the significance of Equation (39) are in order. First of all the presence of the T_M/T_N shows immediately why, as mentioned several times already, the usual case is $T_N \gg T_M$. This case leads to a smaller variance for the estimator. A criterion often chosen for the estimator is the ratio of its standard deviation to its mean. Applying the same $1/T_M$ smoothness approximation to Equation (9), we see that the estimate is approximately unbiased, and we have

$$E\left[\hat{S}(f)\right] \approx S(f) \tag{40}$$

so that

$$\frac{\sqrt{\text{var}\left[\hat{S}(f)\right]}}{\text{mean}\left[\hat{S}(f)\right]} \approx \sqrt{\frac{T_M}{T_N}} \tag{41}$$

This is a rough measure of the percentage accuracy of the estimator. It says, for instance, that if $S(f)$ were gaussian (patently false, but perhaps not a bad approximation), then 68% of the time the estimate would be within $100\sqrt{\frac{T_M}{T_N}}$ percent of its average value (approximately the correct result).

The major trade-off involved in power spectral density estimation is now apparent. The resolution of the estimate is about $1/T_M$, because of the window. Thus, to increase resolution we must increase T_M. If we desire to keep the variance constant at this increased

resolution, we must increase T_N proportionately. But this requires more data! Therefore, if we have a fixed record length, the variance of the estimated spectra must be traded off against resolution in the estimated spectra. As T_M is decreased to decrease the variance, the window gets broader and one gets a lower variance estimate of the spectrum averaged over a broader range in frequency. Thus, it is really a variance-uncertainty trade-off. We are trading one kind of uncertainty in the result for another. Phrased still another way, this can be called a variance-confidence trade-off, or indeed a variance-variance trade-off.

It is, of course, important to note that one type of variability might be much more acceptable than the other in a given problem. For instance, if one knows the noise is white and desires only to estimate accurately how much of it is present (i.e., $|S(f)|$), the resolution is clearly not very important, while the variance of the estimate at a given frequency is paramount. On the other hand, the opposite case could occur. Suppose that we know that a line is present in the spectrum and its magnitude is known but not its location. Obviously, we desire all possible resolution at the expense of variability.

It is also of interest to examine briefly the covariance between adjacent estimates in an approximate form. Following the above "smoothness" approximation, we can see Equation (36) and (37) remain unchanged while the approximate form of Equation (31) becomes

$$\mathrm{Cov}\left[\hat{S}(f_1), \hat{S}(f_2)\right] \approx \frac{2}{T_N} \int_{-\infty}^{\infty} \left[Q(f+f_1) + Q(f-f_1)\right] \left[Q(f+f_2) + Q(f-f_2)\right]\left[S(f)\right]^2 df \tag{42}$$

From this result it is apparent that if f_1 and f_2 are close together on a $\frac{1}{T_M}$ scale, then the two windows overlap considerably and the spectral estimates at the two points are highly correlated. If f_1 and f_2 are separated by many $\frac{1}{T_M}$'s then the product of the windows is small and the covariance is small. When $(f_1 - f_2)$ is small multiple of $\frac{1}{2T_M}$ the covariance is dependent upon the particular window used. For instance, with the hanning window the covariance is approximately $\frac{1}{2}$ at adjacent points in a discrete estimation i.e., $f_1 - f_2 = \frac{1}{2T_M}$. But for the rectangular window (i.e., no shaping of correlation estimate, only truncation) the covariance, at this separation, is nearly zero. Thus, for most windows little independent information is obtained from estimates closer together in frequency than $\frac{1}{2T_M}$. Note, that by using the hanning window to decrease the variance of the estimate, the correlation between adjacent

estimates separated by $\frac{1}{2T_M}$ has risen, so that in a way no "new" information is obtained until the separation becomes $\frac{1}{T_M}$ or so.

It was claimed above that $\Gamma'(f,o,o)$ is simply related to $\Gamma(f,o,o)$. We will now demonstrate this for the case under discussion where $S(f)$ is "smooth" over many $\frac{1}{T_M}$'s. Returning to the definition of Γ' in Equation (27) we see that proceeding just as above, we obtain

$$\Gamma'(f,o,o) \approx \frac{\left[S(f)\right]^2}{T_N}$$

and that $S(f)$ need only be "smooth" on a scale of a few $\frac{1}{T_N}$'s. Since in this approximation $\Gamma(f,o,o)$ was given by Equation (36) to be $\frac{2[S(f)]^2}{T_N}$ we see, in fact, that

$$\frac{\Gamma'(f,o,o)}{\Gamma(f,o,o)} = \frac{1}{2} .$$

With all this discussion of the "smooth" spectra case it might seem that it is the only one of interest. Unfortunately, nature is not so benevolent. Distressingly often the situation arises where the spectrum we're trying to estimate has discontinuities of one kind or another. By "discontinuities" we refer to large changes in the magnitude of the spectra on a frequency scale small compared to $\frac{1}{T_M}$ or $\frac{1}{T_N}$. This phenomenon can come about in many different ways, some of which will be

demonstrated below; but the general problem is that of a line in the spectral density.

In this case none of the "smoothness" approximations made above hold and we must return to Equation (33) and the definition of $\Gamma(f)$. For this purpose let us suppose that the real spectrum $S(f)$ consists of white noise plus a δ function.

$$S(f) = N_o + \frac{A^2}{2}\left[\delta(f+f_o) + \delta(f-f_o)\right] \tag{43}$$

Assuming the noise to be white and the line to be a δ function are not necessary, only convenient. It will be clear that any smooth component and any shape spike would do. Now we insert this spectrum into the definition of $\Gamma(f)$ and obtain

$$\begin{aligned}\Gamma(f) = 4 \int_{-\infty}^{\infty} \Big\{ & N_o^2 + \frac{A^2}{2} N_o \Big[\delta(f+f'+f_o) + \delta(f+f'-f_o) + \delta(f-f'+f_o) \\ & + \delta(f-f'-f_o)\Big] \\ & + \frac{A^4}{4}\Big[\delta(f+f'+f_o)\,\delta(f-f'+f_o) + \delta(f+f'+f_o)\,\delta(f-f'-f_o) \\ & + \delta(f+f'-f_o)\,\delta(f-f'+f_o) \\ & + \delta(f+f'-f_o)\,\delta(f-f'-f_o)\Big]\Big\} \left(\frac{\sin \omega' T_N}{\omega' T_N}\right)^2 df'\end{aligned} \tag{44}$$

The three terms in the brackets shows the respective contributions of the white noise itself, the interaction between the white noise and the line, and the line itself. If we call the integral on the first of these $\Gamma_N(f)$, we have already seen in Equation (36) that for the "smoothness" approximation it is given by

$$\Gamma_N(f) \approx \frac{2}{T_N}\left[S(f)\right]^2 = \frac{2\,N_o^2}{T_N}$$

Calling the term representing the interaction between the smooth spectrum and the spectral line, $\Gamma_i(f)$ we have

$$\Gamma_i(f) = 2A^2 N_o \int_{-\infty}^{\infty} \left[\delta(f+f'+f_o) + \delta(f+f'-f_o) + \delta(f-f'+f_o) + \delta(f-f'-f_o)\right] \left(\frac{\sin \omega' T_N}{\omega' T_N}\right)^2 df'$$

which yields

$$\Gamma_i(f) = 4A^2 N_o \left[\left(\frac{\sin(\omega+\omega_o)T_N}{(\omega+\omega_o)T_N}\right)^2 + \left(\frac{\sin(\omega-\omega_o)T_N}{(\omega-\omega_o)T_N}\right)^2\right] \quad (45)$$

Finally the term contributed by the δ function alone $\Gamma_\delta(f)$, is

$$\Gamma_\delta(f) = A^4 \int_{-\infty}^{\infty} \left[\delta(f+f'+f_o)\,\delta(f-f'+f_o) + \delta(f+f'+f_o)\,\delta(f-f'-f_o) + \delta(f+f'-f_o)\,\delta(f-f'+f_o) + \delta(f-f'-f_o)\,\delta(f-f'-f_o)\right] \left(\frac{\sin \omega' T_N}{\omega' T_N}\right)^2 df'$$

A convenient way to put this into tractable form is to insert it in Equation (33) and carry out the f and f′ integrations together. The component in the variance due to the spectral line, $\mathrm{var}\left[\hat{S}(f)\right]$, then becomes

$$\mathrm{var}_{\delta}\left[\hat{S}(f_1)\right] = \frac{A^4}{2} \int_{-\infty}^{\infty} \left[2\,\delta(f)\left(\frac{\sin \omega T_N}{\omega T_N}\right)^2 + \delta(f+f_o)\left(\frac{\sin(\omega+\omega_o)T_N}{(\omega+\omega_o)T_N}\right)^2 + \delta(f-f_o)\left(\frac{\sin(\omega-\omega_o)T_N}{(\omega-\omega_o)T_N}\right)^2 \right] \left[Q''(f-f_1) + Q''(f-f_1)\right]^{-2} df$$

which, since Q" is an even function, is just

$$\mathrm{var}_{\delta}\left[\hat{S}(f_1)\right] = A^4\left\{4\left[Q''(f_1)\right]^2 + \left[Q''(f_o+f_1) + Q''(f_o-f_1)\right]^2\right\} \quad (46)$$

Note that up to this point no approximations have been made on this component of the variance (other than representing the "line" as a δ-function). If the real spectrum had been only the line, the average value of the estimates obtained via Equation (9) would be

$$\begin{aligned} \mathrm{mean}\left\{\hat{S}(f_1)\right\} &= Q(f) \circledast \frac{A^2}{2}\left[\delta(f+f_o) + \delta(f-f_o)\right] \\ &= \frac{A^2}{2} \int_{-\infty}^{\infty} \left[\delta(f'+f_o) + \delta(f'-f_o)\right] Q(f_1-f')df' \quad (47) \\ &= \frac{A^2}{2}\left[Q(f_1+f_o) + Q(f_o-f_1)\right] \end{aligned}$$

It is immediately apparent that S is a very bad estimator for a line spectrum. The modified window is approximately equal to the actual window as shown above and for f_1 larger than a few $\frac{1}{T_M}$, Q(f) is very small so

that we have

$$\mathrm{var}_{\delta}\left[\hat{S}(f_1)\right] \approx A^4 \left[Q(f_c+f_1) + Q(f_o-f_1)\right]^2 \qquad (48)$$

and hence

$$\frac{\sqrt{\mathrm{var}_{\delta}\left[\hat{S}(f_1)\right]}}{\mathrm{mean}_{\delta}\left[\hat{S}(f_1)\right]} \approx 2$$

This is a very discouraging, although not surprising, conclusion. It tells you not to bother to try to estimate something which is too narrow for you to see! Your estimate will only be within 200% of its average value, 68% of the time or so; and that average value itself will be of minimum width $\frac{1}{T_M}$ and hence biased. A sketch of Equations (46) and (47) is perhaps in order. We are assuming the real spectrum is two lines at $\pm f_o$ with total power A^2

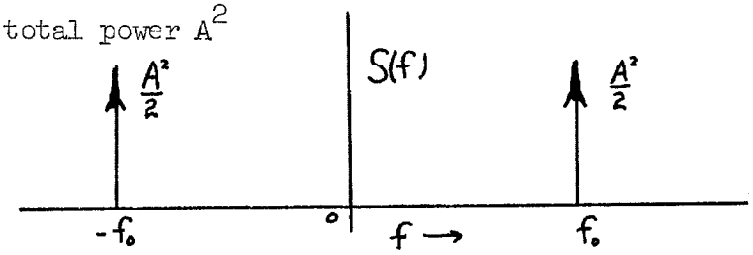

Equation (47) says that the average value of the estimated spectrum is two windows centered at $\pm f_c$.

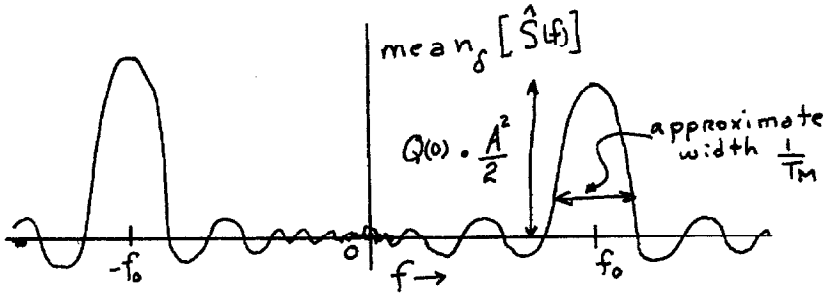

Equation (46) indicates that the variance is the square of the modified windows located at $\pm f_o$ plus four times the square of a modified window located at the origin.

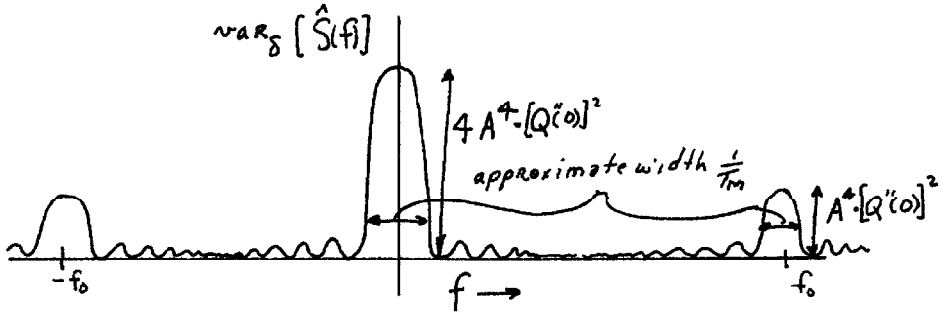

Notice that there is a large variance around the origin even though the average value is small.

Now returning from the digression concerning a line spectrum alone, to complete the variance calculation we insert the other two contributions to $\Gamma(f)$ into Equation (33) and perform the f integration. The white noise contribution from $\Gamma_w(f)$ is

$$\mathrm{var}_w\left[\hat{S}(f_1)\right] = \frac{2N_o^2}{T_N}\int_{-\infty}^{\infty}\left[Q''(f+f_1) + Q''(f-f_1)\right]^2 df$$

which, as before, in the smoothness approximation yields

$$\mathrm{var}_w\left[\hat{S}(f_1)\right] \approx N_o^2 \frac{T_M}{T_N} \tag{49}$$

The contribution resulting from interaction of the spectral line and the white noise is

$$\mathrm{var}_i\left[\hat{S}(f_1)\right] = \int_{-\infty}^{\infty} \left[Q''(f+f_1) + Q''(f-f_1)\right]^2 \Gamma_i(f)\,df$$

$$= 4A^2 N_o \int_{-\infty}^{\infty} \left[Q''(f+f_1) + Q''(f-f_1)\right]^2 \left[\left(\frac{\sin(\omega+\omega_o)T_N}{(\omega+\omega_o)T_N}\right)^2 + \left(\frac{\sin(\omega-\omega_o)T_N}{(\omega-\omega_o)T_N}\right)^2\right] df$$

Now if we take the normal case where $T_N \gg T_M$ then the $\left(\frac{\sin x}{x}\right)^2$ terms are much narrower than the windows and we have approximately

$$\mathrm{var}_i\left[\hat{S}(f_1)\right] \approx \frac{A^2 N_o}{T_N}\left[Q''(f_o+f_1) + Q''(f_o-f_1)\right]^2 \tag{50}$$

which again is the square of the sum of two modified windows located at $\pm f_o$ but whose amplitude now depends on T_N. A sketch of this result follows:

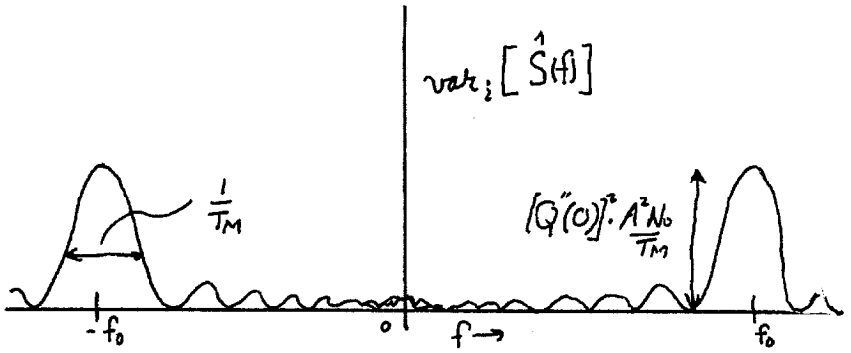

If we combine these results for the normal case we now have for the variance of the spectral estimate when the real spectrum is given by Equation (43) the formula

$$\text{var}\left[\hat{S}(f)\right] \approx A^4 \left\{4\left[Q''(f)\right]^2 + \left[Q''(f_o+f) + Q''(f_o-f)\right]^2\right\} + \frac{N_o A^2}{T_N}\left[Q''(f_o+f) + Q''(f_o-f)\right]^2 + N_o^2 \frac{T_M}{T_N} \tag{51}$$

The average value of the spectral estimate is, of course, given by

$$\text{mean}\left[\hat{S}(f)\right] = \frac{A^2}{2}\left[Q(f+f_o) + Q(f-f_o)\right] + N_o \tag{52}$$

where the equality should be approximately for a "smooth" but not "white" spectrum. The two important features of having a line present in a spectrum to be estimated are now evident. First the estimate of the original spectrum is ruined in the variance sense within a few $\frac{1}{T_M}$'s of the origin and for a few $\frac{1}{T_M}$'s around the spectral line. In addition, the estimate is biased in that it measures the line itself spread out to a few $\frac{1}{T_M}$'s

around its actual location. The extent to which both of these detrimental effects occur at a given frequency depends not only on the relative size of the line but also on the particular window.

3.1.4 Confidence Interval for Spectral Estimate

The difficulty referred to above of having the answer to the question, "How good is the estimator?", depend on the correct result can be partially removed through use of confidence intervals. The key is to ask the right question. Suppose we ask how large an interval in spectral density around the estimated spectrum is required to guarantee a given probability of including the correct result. This question can be answered in a form which does not involve knowledge of the correct result. We will apply the general procedure for finding confidence intervals outlined by Mood.*

Suppose that we consider our spectral estimate at a given frequency, $\hat{S}(f)$, to be a normally distributed random variable. Since we have only one sample, we clearly need to have some sort of constraint between the mean and variance in order to make it a one parameter distribution. Motivated by the $\frac{T_M}{T_N}$ percentage estimator

* Reference [11], pgs. 256ff.

result of Equation (41) let us suppose that, in fact, the standard deviation is known to be a given fraction of the mean i.e., let us assume

$$\sqrt{\text{var}\left[\hat{S}(f)\right]} = g \text{ mean}\left[\hat{S}(f)\right] \tag{53}$$

where $g < 1$ and corresponds to $\frac{T_M}{T_N}$. It should be noted that we are making the assumption that $\hat{S}(f)$ is gaussian which is in itself an approximation. In order to simplify the notation for this section let us redefine

$$\hat{S}(f) \triangleq S$$

$$\text{mean}\left[\hat{S}(f)\right] = \bar{S} \triangleq \mu$$

$$\sqrt{\text{var}\left[\hat{S}(f)\right]} = \sqrt{\text{var } S} \triangleq \sigma$$

The mean to variance constraint assumption becomes

$$\sigma = g\mu \tag{54}$$

and we are now asking the following question, "What size interval should we construct around our sample mean (maybe one sample) to guarantee a given probability of covering the population mean?" We call our one sample mean, S, an estimate of the mean

$$S = \hat{\mu} .$$

Then we know by assumption that the density of $\hat{\mu}$ with μ as parameter is

$$p(\hat{\mu};\mu) = p(S;\mu) = \frac{1}{\sqrt{2\pi}\, g\mu} e^{-\frac{(\hat{\mu}-\mu)^2}{2g^2\mu^2}} \tag{55}$$

We desire to find two values of S, S_1 and S_2, such that the random interval (S_1, S_2) contains the true mean μ with a given probability, say $1-R_1-R_2$. These values will, of course, depend on what our particular data point is, so we want $S_1(\hat{\mu})$, $S_2(\hat{\mu})$ such that

$$P(S_1(\hat{\mu}) < \mu < S_2(\hat{\mu}) = 1-R_1-R_2 \tag{56}$$

We expect R_1 and R_2 to be small (i.e. a high "confidence" in the interval) and the reason for separating them will become obvious shortly. $S_1(\hat{\mu})$ and $S_2(\hat{\mu})$ must satisfy*

$$R_2 = P\left\{\hat{\mu} < S_2(\hat{\mu})\right\} = \int_{-\infty}^{S_2(\hat{\mu})} p(\hat{\mu} \; ; \; \mu)d\hat{\mu}$$

$$R_1 = P\left\{\hat{\mu} > S_1(\hat{\mu})\right\} = \int_{S_1(\hat{\mu})}^{\infty} p(\hat{\mu} \; ; \; \mu)d\hat{\mu} \tag{57}$$

Now using Equation (55) we can obtain

$$R_1 = \tfrac{1}{2} - \tfrac{1}{2} N\left(\frac{1}{g}\left[\frac{\hat{\mu}}{S_1(\hat{\mu})} - 1\right]\right)$$

$$R_2 = \tfrac{1}{2} - \tfrac{1}{2} N\left(\frac{1}{g}\left[1 - \frac{\hat{\mu}}{S_2(\hat{\mu})}\right]\right) \tag{58}$$

where N(x) is the normal integral tabulated by Dwight 1045, [12] namely

$$N(x) = \frac{1}{\sqrt{2\pi}} \int_{-x}^{x} e^{-\frac{z^2}{2}} dz$$

* The logic involved here is adequately detailed in Mood.

And if we denote by $N^{-1}(x)$ the inversion of this operation (which can only be done numerically, but is extensively tabulated) the equations can be inverted to yield

$$S_1(\hat{\mu}) = \frac{\hat{\mu}}{1 + g\, N^{-1}(1-2R_1)}$$
$$S_2(\hat{\mu}) = \frac{\hat{\mu}}{1 - g\, N^{-1}(1-2R_2)} \qquad (59)$$

Which is the result desired for Equation (56) above and yields

$$P\left\{\frac{\hat{S}(f)}{1 + g\, N^{-1}(1-2R_1)} < \text{mean}\left\{\hat{S}(f)\right\} < \frac{\hat{S}(f)}{1 - g\, N^{-1}(1-2R_2)}\right\} = 1-R_1-R_2 \qquad (60)$$

We could now (in theory at least) choose R_1 and R_2 to minimize the length of the interval. Notice that Equation (60) tells us what size interval to construct around the data point as a function only of that data point in order to guarantee a given probability of covering the average answer. This appears to be in a sense more useful than the earlier $\sqrt{T_M/T_N}$ variance result. However, the appearance is mostly illusion since roughly the same approximations are involved in saying that the standard deviation is a fixed fraction of the mean as those which lead to the earlier approximate variance result. In practice, either method seems to yield very similar results as the following example indicates.

Suppose we have, as is typical of many of the experimental results in this thesis, 10000 equi-spaced data points and we estimate the spectra at 100 points. Then this corresponds to a $\sqrt{T_M/T_N}$ ration of .1 which yields approximately a 10% estimator. The 2σ variance band (95%) would be + .82 db and - .92 db. Therefore we can expect the estimated spectrum to lie within this range around any postulated correct result about 95% of the time. On the other hand, if we take $g = .1$ and ask for a corresponding confidence of 95%, we obtain a + .78 and - .95 db band around the data point. Therefore, we can expect the postulated result to lie within this range around our estimated spectrum about 95% of the time. These are very similar results.

Along the same lines of what we can say, given a batch of spectral estimation data, it is interesting to ask the following question. Suppose we have estimated the spectrum of a given process several times. Can we use the information we have about the variance of these different results to improve our estimate of the spectrum? Maintaining the notation from above, this is saying, "If we have samples $S_1, \ldots, S_n$ and we know a mean to variance constraint exists, $\sigma = g\mu$, then how should we estimate $\mu = \bar{S}$?" Without the constraint, the minimum variance unbiased estimate is the sample mean

$$\hat{\mu} = \frac{1}{N} \sum_{i=1}^{N} S_i = \bar{S}_i$$

With the constraint and the assumption that the various experiments are independent we have that the S_1 are jointly gaussian so that

$$p(S_1, S_2, \ldots S_N|\mu) = \frac{1}{(2\pi)^{N/2} (g\mu)^N} e^{-\sum_{i=1}^{N} \frac{(S_i-\mu)^2}{2g^2\mu^2}}$$

Taking the derivative of the logarithm and setting it equal to zero we find the maximum likelihood estimator for the mean to be

$$\hat{\mu} = \frac{\bar{x}}{2g^2} \left\{ -1 + \sqrt{1 + 4g^2 \frac{r}{\bar{x}^2}} \right\} \tag{61}$$

where $\bar{x}$ is the sample mean, $\frac{1}{N} \sum_{i=1}^{N} S_i$, and $r = \frac{1}{N} \sum_{i=1}^{N} S_i^2$. Recalling that g represents a sort of fractional accuracy of our spectral estimate, it is clear that for our applications we will have $g \ll 1$. Using this assumption, we can form an expansion for $\hat{\mu}$ as follows:

$$\hat{\mu} \approx \bar{x} \left[\frac{r}{\bar{x}^2} - g^2 \left(\frac{r}{\bar{x}^2} \right)^2 + 2g^2 \left(\frac{r}{\bar{x}^2} \right)^3 + 5g^6 \left(\frac{r}{\bar{x}^2} \right)^4 + \ldots \right] \tag{62}$$

Since $\frac{r}{\bar{x}^2}$ is on the order of unity this tells us how to modify the sample mean in order to make use of our knowledge about the one parameter nature of the distribution. As a practical matter the correction will be insignificant in most cases as illustrated by the following numerical example.

Suppose we have 5 samples with values 95, 104, 97, 108, 80 and that the true distribution has $\mu = 100$, $\sigma = 10$ (i.e., $g = .1$). Then the sample mean would be

$$\bar{x} = 96.8$$

and Equation (62) above tells us to use

$$\hat{\mu} = 97.7$$

On the other hand, suppose the 80 were a 120 so the samples were

95, 104, 97, 108, 120

then $\bar{x}$ would be

$$\bar{x} = 104.8$$

and our estimate would be

$$\hat{\mu} = 104.4$$

In each case our knowledge that the standard deviation was one tenth the mean allowed us to adjust the estimate toward the correct result. But not by much!

3.2 Practical Computational Considerations

When it comes to the real job of actually estimating a power spectral density from data, there are a number of relevant details which do not appear in the above discussion. This section will attempt to discuss these in some detail. The first has to do with the sampled nature of the data.

3.2.1 Aliasing (Frequency Folding)

The numerical calculations leading to a power spectral density estimate are performed on a large digital machine. It is, in fact, the very speed of the machine which makes power spectral density estimation a feasible endeavor. Therefore, the data must be in sampled form. That is, the sample function from the continuous random process must be sampled in time to form a discrete set of numbers which can form the starting point for the machine computations. For convenience, samples equi-spaced in time are chosen for this analysis. Section 6. below suggests some alternate schemes which might prove more efficient and/or be easier to implement. But for the data analyzed in this thesis we have available only equi-spaced samples of the noise processes whose spectra it is desired to estimate.

The spectrum of a sample function obtained in this way from a continuous process (equi-spaced samples) is just the original spectrum repeatedly folded back on itself at all multiples of the Nyquist folding frequency and summed. Physically, this merely says we cannot tell how many wiggles the signal has between our time samples unless we have some prior knowledge about its spectrum. More precisely, if our noise process is $n(t)$ and we sample every Δt seconds then we have available the function $x(t)$ given by

$$x(t) = \sum_{n=-\infty}^{\infty} n(t)\, \delta(t-n\Delta t)$$

for which it is well known that the spectrum is*

$$S_x(f) = \sum_{q=-\infty}^{\infty} S_n\left(f - \frac{q}{\Delta t}\right) \qquad |f| < \frac{1}{2\Delta t} \qquad (63)$$

and where $S_x(f)$ is periodic in frequency with period $\frac{1}{\Delta t}$. This frequency folding is commonly referred to by Tukey's coined term of "aliasing" because energy at some frequencies masquerades as energy at others.

It is now apparent that for any digital power spectral density estimation scheme, this feature is present and must be dealt with in a satisfactory way. First,

---

* See Blackman and Tukey or almost any sample data control systems text for a derivation.

it is significant to note that if the original spectrum is "white" (constant) over a frequency band appreciably larger than $\frac{1}{2\Delta t}$, there will be trouble. The estimated spectrum is limited to $|f| < \frac{1}{2\Delta t}$. In this case the estimate would bear very little resemblance to the real spectrum even if the estimation were perfect. Thus, in order to do a sensible job of estimating a nearly white spectrum it must be low pass filtered at a frequency somewhere near (preferably less than) $\frac{1}{2\Delta t}$. It is also important to realize that this filtering must be done in analog form before the sampling is done. The aliasing occurs with the sampling and cannot subsequently be undone by further digital processing. The computer does not know how to tell which energy at a given frequency belongs there.

However, the situation changes slightly for many of the spectra dealt with in this thesis. Many of them fall off with frequency like $\frac{1}{f}$ or even as fast as $\frac{1}{f^2}$. From even a cursory inspection of the numbers, it is clear that aliasing is insignificant in this case for all but a few frequencies very near $\frac{1}{2\Delta t}$. Therefore, for many of the data runs of this thesis anti-aliasing filters were unnecessary.

3.2.2 Discrete Estimation Formulae

As discussed in the previous section, we must work with discrete samples from the random processes. Thus, it is obvious that the correlation function can be estimated only at discrete points rather than on a continuous basis. Therefore, we modify Equation (1) of Section 3.1.1 to calculate "mean lagged products" as**

$$\hat{R}(R\Delta t) = C_R = \frac{1}{N-R} \sum_{q=0}^{N-R} x(q\Delta t)\, x((q+R)\Delta t) \quad R = 0, \ldots, M \tag{64}$$

which yields an estimate of the correlation function at points Δt apart from zero to $M\Delta t$. In the discrete case a convolution interval becomes a sum so that it is easier to "window" the estimate in the frequency domain after it has been Fourier transformed. Accordingly, a "raw spectral estimate", V_R is formed by taking a finite Fourier cosine transform*

$$V_R = \Delta t \left[C(o) + 2 \sum_{q-1}^{M-1} C(q\Delta t) \cos\left(\frac{qR\pi}{M}\right) + C(M\Delta t) \cos R\pi \right] \quad R = 0, 1, \ldots, M \tag{65}$$

The final spectral estimate U is then obtained by

---

* The correlation function and spectrum are even because of stationarity.

** The notation is changed to C's for the discrete case rather than R's to reduce confusion by conforming to Blackman and Tukey's notation.

convolution with the "window" as

$$\hat{S}\left(\frac{R}{2M\Delta t}\right) = U_R = a_o V_R + \sum_{j=1}^{\infty} \left[V_{R+j} + V_{R-j}\right] a_j \qquad (66)$$

where the "a_j" represents the Fourier transform of the lag window. For the "hanning" window (Q_2) used most extensively in this thesis they are

$$a_j = \begin{cases} \frac{1}{2} & i = 0 \\ \frac{1}{4} & i = 1 \\ 0 & \text{otherwise} \end{cases} \qquad (67)$$

3.2.3 Program Description

To carry out the computations leading to a spectral estimate a FORTRAN program was written for the 7094 digital computer. It would have been possible to obtain an existing program which performed many of the calculations. The major motivation for creating another was convenience. It was considered important from the viewpoint of input data processing and output data presentation to have a format that was very convenient, since it was to be used extensively. For instance, it was found to be imperative in many cases to "prewhiten" the data; (digitally filter to obtain favorable spectra, as discussed below and in Section 3.3.2), a feature which is not generally directly available in spectral estimation programs. Our program is included in Appendix [B] and

a detailed listing will not be presented here although a general description is perhaps in order.

The program mechanization selected first computes the finite cosine table to be used later in the calculations for Fourier transformation. This step may be omitted if the current run is a repeat of an immediately prior estimation for which the cosine table is still available in memory.

The program then digitally filters the input data to form a new random process whose spectrum is related to the original spectrum by the magnitude squared of the filter transfer function (known). With some a priori knowledge of the input spectrum,this technique allows improvement of the spectral estimate's properties. This improvement is obtained by shaping the spectrum to be estimated to be more nearly constant. As indicated in Section 3.1.2 above, this helps lower the variance of the estimate as well as reduce its bias. A much more detailed discussion of the bias problem will be presented below for some specific cases.

The sample mean is computed next. This computation is done by data thirds in order to maintain the option of removal of a linear trend from the data. The mean lagged products are then formed. Appropriate constants are subtracted from each to remove either a constant or a linear trend from the data. The mean removal, at least, was

always employed and is discussed in detail below in Section 3.3.1.

The raw spectral estimates are now formed by finite Fourier transformation by the cosine table generated earlier. Application of the "window" then yields the spectral estimate. The effect of any digital filter used to prewhiten the data is then removed yielding a final spectral estimate for the actual input data.

Our program is written as a subroutine so that it may be called by a main program which can further process any of the desired results. We used this technique to do various data plotting jobs while avoiding the recompiling of the basic spectral estimation formulae.

3.2.4 Quantization

Because all of the data processing is done digitally, the original continuous data must, of course, be quantized. While the exact spectral effect of time sampling can be calculated as indicated above in Section 3.2.1 the exact effect of amplitude sampling can not. The difficulty lies in a practical calculation of the second order statistics of the quantized signal. Various approximate formulations are available. The one presented here is original although not unique. We have chosen to separate the analysis of time sampling and amplitude quantization effects. Both,

in fact, occur together and it is possible that the way to an exact description of their effects is to solve the problem all at once.* We desire a description of the spectrum of the quantized output in terms of the spectrum of the input. We shall proceed by characterizing the output as the input plus an error term, utilizing the approximation that the error and the input are independent, assuming the error is white, obtaining a formula for the spectrum of the error and thereby for the quantized signal.

We consider a quantizer, E, whose input is a random process n(t) and whose output is another random process n′(t). There are many specific ways to mechanize a quantizer. We consider only one although it will be obvious that in our approximation most others would yield the same results. Suppose E is defined by

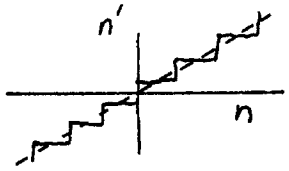

$$n' = \begin{cases} (2N+1)\,\frac{\epsilon}{2} & o < N\epsilon < n < (N+1)\epsilon \\ -(2N+1)\,\frac{\epsilon}{2} & o > -N\epsilon > n > -(N+1)\epsilon \end{cases} \qquad (68)$$

* Reference [13] is Widrow's version of such an attempt. For a certain class of signals he shows that the error has approximately a white spectrum.

Then if we write the output in terms of the input as

$$n' = n + e$$

we can specify the error, e, in terms of n as follows:

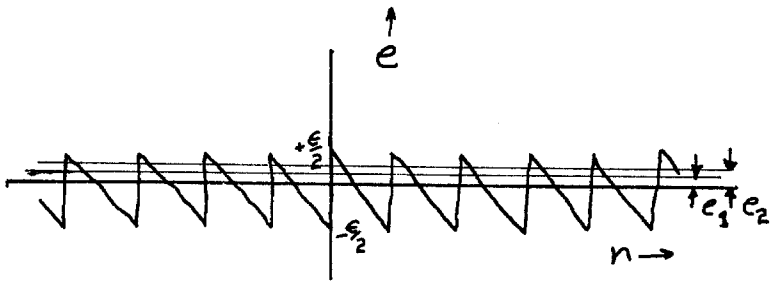

$$e = \left\{ \begin{array}{ll} \frac{\epsilon}{2} - (n - N\epsilon) & N\epsilon < n < (N+1)\epsilon \\ & N = 0, \pm 1, \pm 2, \pm 3, \ldots \end{array} \right\} \qquad (69)$$

Now let us calculate p(e) from the gaussian distribution as *

$$p(e) = \lim_{\Delta e \to 0} \frac{1}{\Delta e} \frac{1}{\sqrt{2\pi}\,\sigma} \sum_{N=-\infty}^{\infty} \int_{N\epsilon + \epsilon/2 - e - \Delta e}^{N\epsilon + \epsilon/2 - e} e^{-n^2/2\sigma^2} dn \qquad \epsilon/2 \geq e \geq 0$$

Approximating the integrand of each term by its first order Taylor series and noting that the approximation becomes exact in the limit we obtain

$$p(e) = \frac{1}{\sqrt{2\pi}\,\sigma} \sum_{N=-\infty}^{\infty} e^{-\frac{1}{2\sigma^2}\left[(N+\frac{1}{2})\,\epsilon - e\right]^2} \qquad (70)$$

---

* We calculate p(e) only for $e \geq 0$ since it is an even function by symmetry.

$p(e)$ is approximately constant and equal to $\frac{1}{\epsilon}$ since its integral must be unity. A bound on the first order correction term can be obtained as follows. Suppose we expand $p(e)$ in a Taylor series about the origin.

$$p(e) \approx p(o) + p'(o)e + p''(o)\frac{e^2}{2} + \cdots\cdots$$

The linear term is zero because $p(e)$ is even but this fact can also be shown immediately from Equation (70) above by differentiation because the sum obtained for $p'(e)$ is identically zero at $e = o$. The first correction term is then quadratic.

Let us evaluate $p(\epsilon/2)$. From Equation (70) we have

$$p\left(\frac{\epsilon}{2}\right) = \frac{1}{\sqrt{2\pi}\,\sigma} \sum_{N=-\infty}^{\infty} \exp\left(-\tfrac{1}{2}\left(\frac{N\epsilon}{\sigma}\right)^2\right) \tag{71}$$

which becomes on utilizing DW 552.6 [12],

$$p\left(\frac{\epsilon}{2}\right) = \frac{1}{\epsilon}\left[1 + 2\sum_{N=1}^{\infty} e^{-2\left(\frac{N\pi\sigma}{\epsilon}\right)^2}\right] \tag{72}$$

a series which converges a great deal faster in the cases of interest where $\left(\frac{\sigma}{\epsilon}\right)$ is large. Thus $p\left(\frac{\epsilon}{2}\right)$ is slightly larger than $\frac{1}{\epsilon}$. The deviation of $p(o)$ from $\frac{1}{\epsilon}$ can be bounded as follows. From Equation (70) by differentiation we

obtain

$$p'(e) = \frac{-1}{\sqrt{2\pi}\,\sigma^3} \sum_{N=-\infty}^{\infty} [(N+\tfrac{1}{2})\epsilon - e]\, e^{-\frac{[(N+\frac{1}{2})\epsilon - e]^2}{2\sigma^2}}$$

$$p''(e) = \frac{1}{\sqrt{2\pi}\,\sigma^3} \sum_{N=-\infty}^{\infty} e^{-\frac{[(N+\frac{1}{2})\epsilon - e]^2}{2\sigma^2}} + \frac{1}{\sqrt{2\pi}\,\sigma^5} \sum_{N=-\infty}^{\infty} [(N+\tfrac{1}{2})\epsilon - e]^2\, e^{-\frac{[(N+\frac{1}{2})\epsilon - e]^2}{2\sigma^2}}$$

which indicates that the function $p(e)$ is concave upward and increases monatonically from the origin in both directions in the region $-\frac{\epsilon}{2} < e < \frac{\epsilon}{2}$. Therefore, the behavior is as shown in exaggerated form in the sketch below. Since we know that $\int_{-\epsilon/2}^{\epsilon/2} p(e) = 1$, we know that the area above

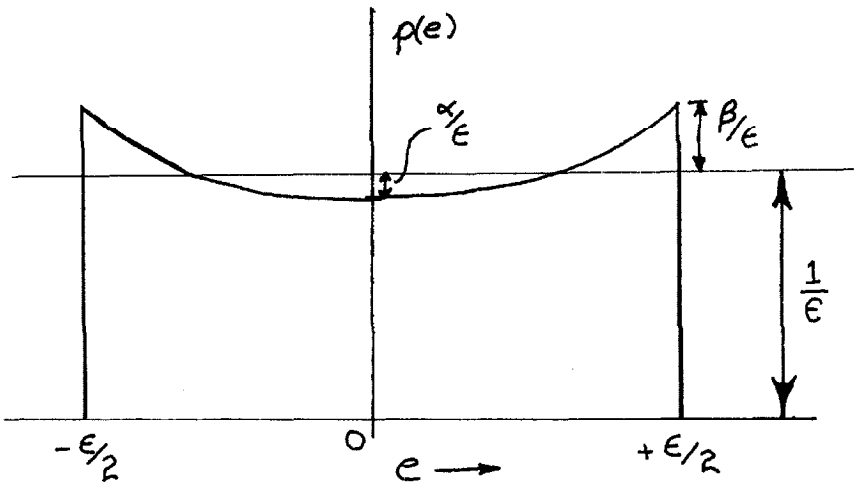

the $\frac{1}{\epsilon}$ line must equal that below it which combined with the concavity implies that $\beta > \alpha$. Since β is given by Equation (22) we have

$$\alpha < \beta = 2 \sum_{N=1}^{\infty} e^{-2\left(\frac{N\pi\sigma}{\epsilon}\right)^2} \tag{73}$$

as bounds for the error in calling the quantization error uniformly distributed. It is interesting to note that the probability density of the error is very uniform. Even when ϵ is equal to σ the maximum percentage error β is on the order of 10^{-7}. Therefore it is an excellent approximation to take

$$p(e) \approx \left\{ \begin{array}{ll} \frac{1}{\epsilon} & |e| < \frac{\epsilon}{2} \\ 0 & \text{otherwise} \end{array} \right\} \tag{74}$$

which of course implies

$$E(e) = 0$$

$$E(e^2) = \frac{\epsilon^2}{12}$$

Consider the error e(t) to be a stationary random process. If we assume its spectrum is white over the estimation bandwidth for any given run, $\frac{1}{\Delta t}$, we arrive at a level for this spectrum, N_o, of*

$$N_o = \epsilon^2 \frac{\Delta t}{12} \tag{75}$$

* Note this puts the quantization noise over the same band as the spectral estimates, $-\frac{1}{2\Delta t} < f < +\frac{1}{2}\Delta t$, which includes negative frequencies.

The validity of this assumption is very difficult to evaluate because it involves the second order statistics of the output of the quantizer.

3.3 Low Frequency Bias

The particular interest of this thesis is in the behavior of several random processes at very low frequencies. Therefore, the various phenomena which lead to inaccuracies in the spectral estimates at low frequencies will be examined in detail. There are two reasons for concentrating on the bias of the estimate. First, it is the area which has typically been ignored in previous studies. In addition, an estimator's bias is the most annoying property empirically because it is so slippery. One can repeat the experiment a large number of times and obtain results whose spread agrees very well with the estimator's expected variance. And yet the results can all be in error by a considerable amount and lead to erroneous conclusions. Finally, the exasperating feature is that after the source of the bias has been found and eliminated, the results again appear consistent to the same extent as previously. Thus, one is always left with some lingering doubt about whether there is still some undiscovered bias lurking in the estimate. We shall now consider specifically some of the prominent sources of low frequency biases in spectral estimates.

3.3.1 Mean Removal

Recalling the analysis of the previous sections it will be noted that all discussion was for a zero mean random process. Since this will almost never be the case, the mean is removed during the spectral estimation process. Were this not done the spectrum being estimated would have a spectral line at the origin. The estimate would then be ruined in a bias and a variance sense in the vicinity of the origin as discussed above. The method of mean removal used in our computations was to employ the sample mean as an estimate of the mean and subtract its square from the mean lagged products at each point to obtain auto-correlation function estimates.* This choice is motivated by the following case. Suppose our data $x(t)$ was actually from a stationary zero mean noise process $n(t)$ plus an additive constant m;

$$x(t) = n(t) + m$$

Then the correlation functions are

$$R_x(\tau) = R_n(\tau) + m^2$$

and m^2 is just the right thing to remove from our estimated correlation function to obtain the correct result. Moreover if $n(t)$ were white the sample mean would be a minimum variance, unbiased estimator for m.

* We will also consider in this section mean removal by subtraction of the sample mean from each data point.

However, in real cases several questions arise. What is the effect of such a calculation for real data? In particular, how can this effect be expressed in terms of spectral densities? How serious is the fact that the noise is not white? Is the use of the sample mean adequate?

We shall answer these questions in a very straight forward manner by calculating the average value of the spectral density estimated by the actual computational formula employed. The estimate of the spectrum at frequency $R/2\ M\Delta t$ is V_R given by *

$$V_R = \Delta t \sum_{q=-M+1}^{M} C_q \cos \frac{Rq\pi}{M} \qquad R = 0,1, \ldots\ldots, M \tag{76}$$

and

$$C_R = \frac{1}{N-R} \sum_{q=1}^{N-R} Z_q Z_{q+R} - (\bar{Z})^2 \qquad R = 0,1, \ldots\ldots, M \tag{77}$$

where the Z_i are the data points and $\bar{Z}$ is the sample mean. We shall calculate the properties for this Q_o window estimate first, then extend to those for the more complex windows (i.e. U_R). To investigate the bias properties we take the ensemble average and maneuver it algebraically until we obtain an expression containing

* This differs from Equation (64) above only in that the mean removal is included.

terms for which we have a ready explanation.

Inserting Equation (77) into Equation (76) yields

$$E\left\{V_R\right\} = E\left[\hat{S}\left(\frac{R}{2M\Delta t}\right)\right] = \Delta t \sum_{q=-M+1}^{M}\left[R_z(q\Delta t) - E\{\bar{Z}^2\}\right]\cos\frac{Rq\pi}{M}$$

which can be written as

$$E\left[V_R\right] = \Delta t \int_{-\infty}^{\infty} R_z(\tau)\cos\left[2\pi\left(\frac{R}{2M\Delta t}\right)\tau\right]\sum_{q=-M+1}^{M}\delta(\tau - q\Delta t)d\tau$$

$$- 2M\Delta t\ \delta_{R,o}\ E[(\bar{Z})^2]$$

where $\delta_{i,j}$ is the Kronecker delta given by $\delta_{i,j} = \begin{Bmatrix} 0 & i\neq j \\ 1 & i=j \end{Bmatrix}$

This can be further juggled by including a window to obtain

$$E\left[V_R\right] = \Delta t \int_{-\infty}^{\infty} R_z(\tau)\, D(\tau)\cos\omega_r\tau \sum_{q=-\infty}^{\infty}\delta(\tau - q\Delta t)d\tau - 2M\Delta t\ \delta_{R,o}\ E[(\bar{Z})^2]$$

where $\omega_r = 2\pi\left(\frac{R}{2M\Delta t}\right)$ and $D_o(\tau) = \begin{Bmatrix} 1 & |\tau| < M\Delta t \\ \frac{1}{2} & |\tau| = M\Delta t \\ 0 & \text{otherwise} \end{Bmatrix}$

It is now evident that the τ integration can be considered as a convolution evaluated at the specific frequency $R/_{2M\Delta t}$ while the train of δ functions performs, the expected aliasing in the frequency domain. Thus

$$E\left[V_R\right] = \Big[\underbrace{S_z(f)}_{\text{spectral density}} \circledast \underbrace{Q_o(f)}_{\text{windowed with } Q_o \text{ window}} \circledast \underbrace{\sum_{q=-\infty}^{\infty} \delta(f - {}^{q}/_{\Delta t})}_{\text{aliased}} \Big]_{\substack{f = {}^{R}/_{2M\Delta t} \\ \text{evaluated at appropriate discrete frequency}}} \qquad (78)$$

$$2M\Delta t\ \delta_{o,R}\ \ E[(\bar{Z})^2]$$

where Q_o is, of course, the Fourier transform of $D_o(\tau)$ given by

$$Q_o(f) = 2M\Delta t \left(\frac{\sin 2M\Delta t \pi f}{2M\Delta t \pi f} \right)$$

and the triple convolution is evaluated at frequency $\frac{R}{2M\Delta t}$ as indicated.

This formula is exactly as expected in that it contains: the effects of the aliasing due to discrete sampling; the effects of the window (simple Q_o in this case); and has a term removed from the dc estimate (R=0) which would be m^2 if the $\bar{Z}$ were a perfect estimate of the mean. It is the verification that the discussions of Section 3.1 do in fact hold for the discrete version. In order to formulate the effect of the actual mean subtraction term in a more amenable manner, we proceed as above to eventually obtain an integral on the spectral density.

The sample mean squared is given by

$$\bar{Z}^2 = \frac{1}{N^2} \sum_{q=1}^{N} \sum_{\ell=1}^{N} Z_q Z_\ell$$

Its expected value is a sum of correlation functions times coefficients which can be written as an integral against a train of δ functions.

as

$$E[\bar{Z}^2] = \frac{1}{N^2} \int_{-\infty}^{\infty} \sum_{q=-N+1}^{N-1} (N - |q|) R_Z(\tau) \delta(\tau - q\Delta t) d\tau$$

which upon further manipulation becomes

$$E[\bar{Z}^2] = \frac{1}{N} \int_{-\infty}^{\infty} \sum_{q=-\infty}^{\infty} \delta(\tau - q\Delta t) R_Z(\tau) D_t(\tau) d\tau$$

where

$$D_t(\tau) = \begin{cases} 1 - \dfrac{|\tau|}{N\Delta t} & -N\Delta t \le \tau \le N\Delta t \\ 0 & \text{otherwise} \end{cases}$$

whose Fourier transform is

$$Q_t(f) = N\Delta t \left(\frac{\sin \pi f N \Delta t}{\pi f N \Delta t} \right)^2$$

Again it is clear that in the frequency domain this is just an aliased convolution evaluated at the origin so

that

$$E[\bar{Z}^2] = \Big[\underbrace{S_z(f)}_{\text{spectral density}} \circledast \underbrace{\left(\frac{\sin \pi f N \Delta t}{\pi f N \Delta t} \right)^2}_{\text{windowed}} \circledast \underbrace{\sum_{q=-\infty}^{\infty} \delta\left(f - \frac{q}{\Delta t}\right)}_{\text{aliased}} \Big]_{\substack{f=0 \\ \text{evaluated at frequency origin}}} \quad (79)$$

Now returning to the previous equation for $E(V_R)$ we can examine the estimate at the origin for the Q_o window as*

$$E\{V_o\} = \left[S_z(f) \circledast \sum_{q=-\infty}^{\infty} \delta\left(f - \frac{q}{\Delta t}\right) * 2M\Delta t \left\{ \left(\frac{\sin 2\pi f M \Delta t}{2\pi f M \Delta t} \right) - \left(\frac{\sin \pi f N \Delta t}{\pi f N \Delta t} \right)^2 \right\} \right]_{f=0} \quad (80)$$

But a convolution evaluated at the origin is just the integral of the product of the two quantities. Thus, the average value of the estimate at dc is an integral. The integrand is the aliased (real) spectrum multiplied by a $\frac{1}{2}$ $M\Delta t$ width "window" with a $\frac{1}{N\,\Delta t}$ size "hole" in it. The equivalent window for V_o looks like the following sketch.

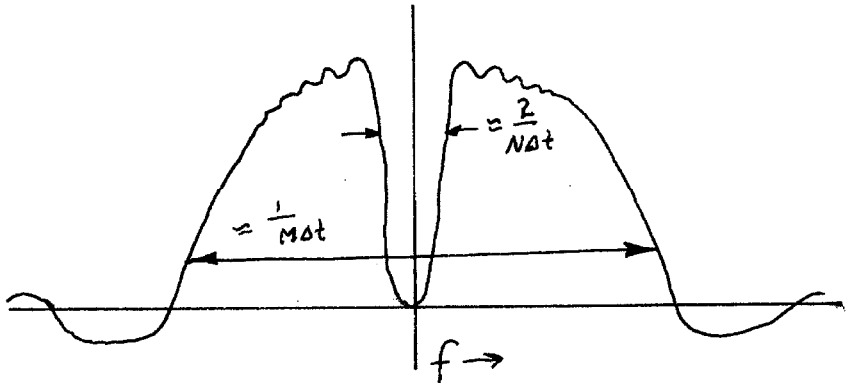

* For other windows one must use their explicit formulae instead of the simple $\frac{\sin x}{x}$ but the result is the same in principle.

Therefore, in the usual case the scheme removes the mean as advertised. But it should be pointed out that V_o is really not an estimate of the power spectral density at the origin. Figure (2) is a plot of the "equivalent window" for V_o of Equation (80) on a log-log scale. It is clear that V_o is really an estimate at some frequency less than $\frac{1}{2}$ MΔt but considerably greater than zero. Blackman and Tukey apparently recognize this and consequently recommend considering the V_o point as an estimate at $\frac{1}{3}$ of the lowest point, $\frac{1}{2}$ MΔt x $\frac{1}{3}$. However, if one postulates a true spectrum and can carry out the necessary integrations, then V_o can be plotted at exactly the appropriate point for that particular spectrum.

There is one additional consideration associated with the mean removal situation which warrants a moment's discussion. This concerns the specific method of mean removal. The above discussion considered removal of the square of the sample mean from each "lagged product." An alternate scheme is to remove the sample mean from each raw data point before calculating the mean lagged products. Suppose that in place of Equation (77) above we were to employ

$$C'(R) = \frac{1}{N-R} \sum_{q=0}^{N-R} (x_q - \bar{x})(x_{q+r} - \bar{x}) \qquad (81)$$

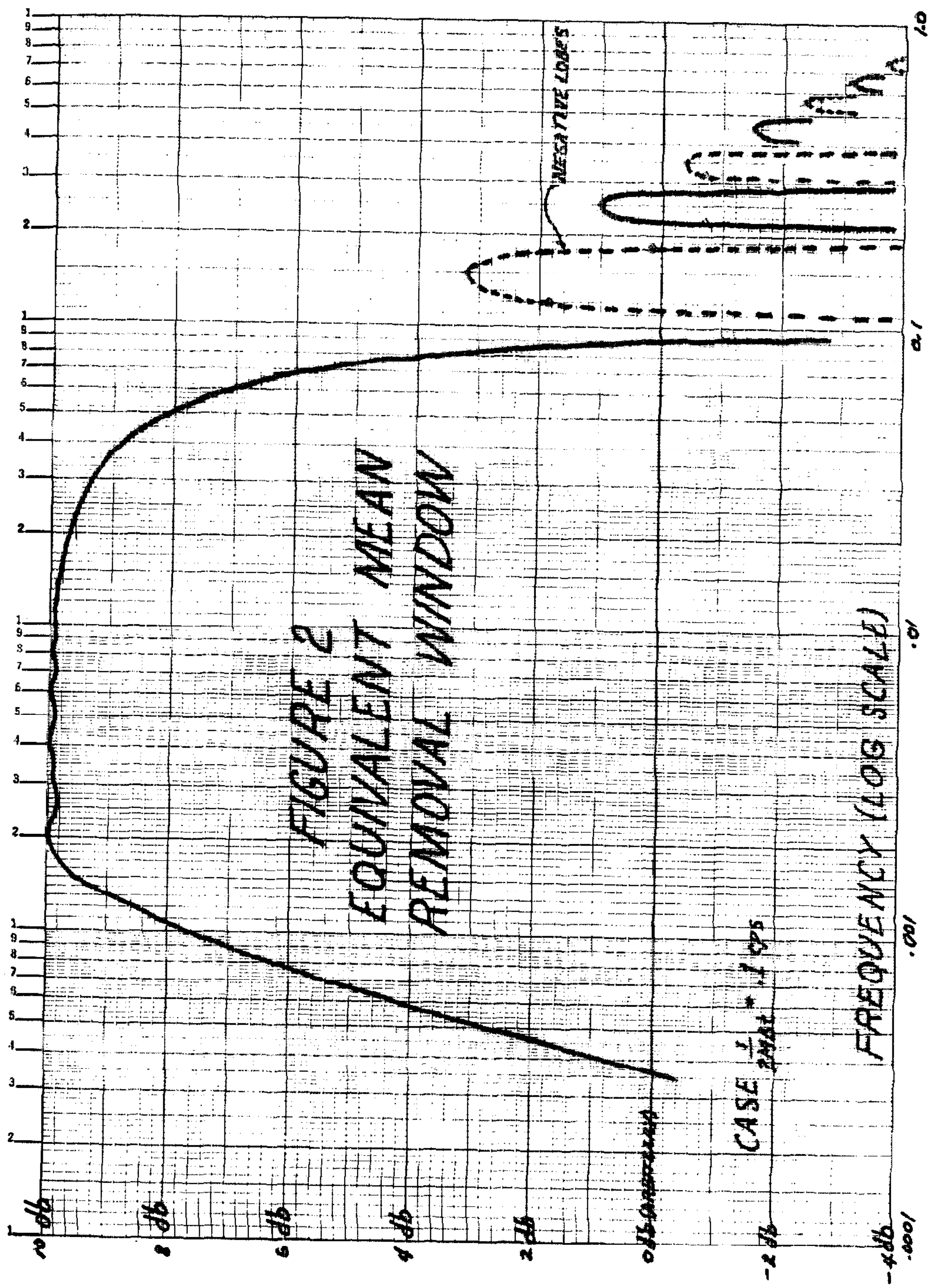
FIGURE 2
EQUIVALENT MEAN
REMOVAL WINDOW
NEGATIVE LOBES
CASE 1/2MΔt = .1 cps
FREQUENCY (LOG SCALE)
.001
.01
0.1
1.0
10 db
8 db
6 db
4 db
2 db
0 db
-2 db
-4 db

Rewriting this and adding and subtracting terms from the sums yields

$$C'(R) = \frac{1}{N-R} \sum_{q=0}^{N-R} x_q x_{q+r} - \bar{x}^2 + \frac{\bar{x}}{N-R} \left\{ \sum_{N-R+1}^{N} (x_q - \bar{x}) + \sum_{0}^{R} (x_q - \bar{x}) \right\}$$

But the first two terms are just the previously discussed method of mean removal so that this result can be written

$$C'(R) = C(R) + D(R)$$

where

$$D(R) \triangleq \frac{\bar{x}}{N-R} \left\{ \sum_{N-R+1}^{N} (x_q - \bar{x}) + \sum_{0}^{R} (x_q - \bar{x}) \right\}$$

represents the difference between the two methods of mean removal. It is clear that the ensemble average of D(R) is identically zero. Thus, "on the average" the methods are identical and hence the above discussion concerning $E(V_r)$ holds equally well for either scheme. For a given specific set of data D(R) will have some value and hence there will be some finite difference in the power spectral density estimated from any particular sample function.

Consider the case of $1/f^2$ noise where the process contains a great deal of energy at frequencies below the minimum resolution, $\frac{1}{2M\Delta t}$. Then the time data will (may) have slow, large amplitude fluctuations. Thus, for short hunks of data at the ends the samples are quite likely to all be on the same side of the mean. In D(R) this will make all of the terms in either or both of the summations possess the same sign. Thus, as R increases

the sums will grow in magnitude so that D(R) will be increasing in R. This in turn implies that $C'(R)$ contains a term increasing approximately linearly in R which is not contained in C(R). For 1/f type spectra the correlation function decreases monotonically with τ i.e., as $\ln \tau$ for 1/f noise, $e^{-\tau}$ for $1/f^2$ noise. Because $C'(R)$ decays more slowly in the τ domain its Fourier transform will decay more rapidly in the frequency domain. Hence, the bias created will tend to make the estimated spectral density steeper. In this respect the effects of this error source are very similar to those of long step function type disturbances (see Section 3.3.3).

A numerical illustration is provided by the following case. Figure (3) shows a spectrum estimated from 10000 raw data points with $\Delta t = 5$ sec and $\bar{x} = .5986399$. It is a Q_2 estimate with M = 100, and the mean was removed according to Equation (77) by subtracting the square of the sample mean from all the mean lagged products. The circles represent the result of an estimation with the same parameters from the same data but with the sample mean subtracted from each data point. The differences appear to be significant only for small R. For this particular case the sample mean is some 778 times the standard deviation of the noise. Thus, effects such as D(R) which depend on this ratio become more important.

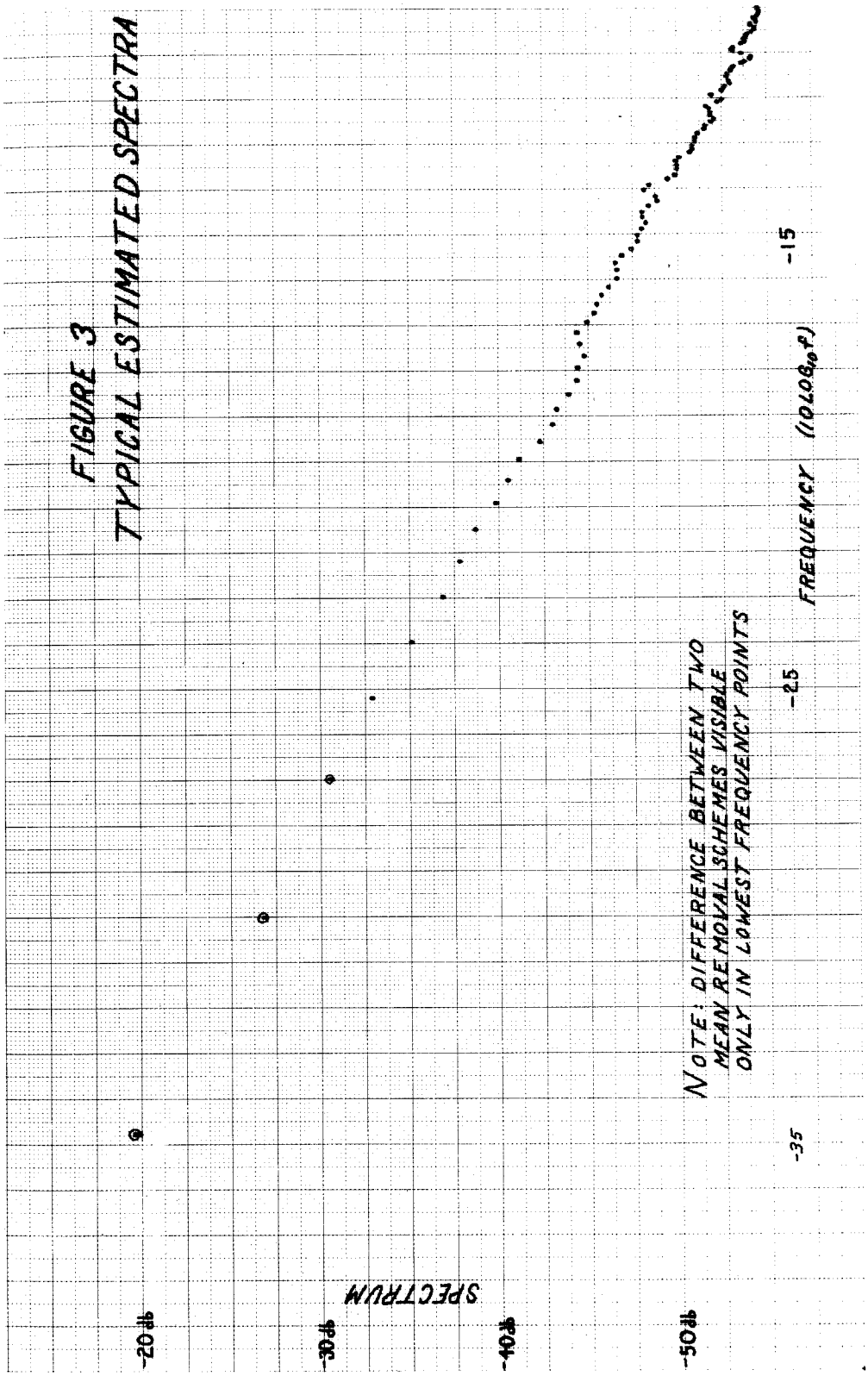
FIGURE 3
TYPICAL ESTIMATED SPECTRA
SPECTRUM
-20 db
-30 db
-40 db
-50 db
-15
-25
-35
FREQUENCY (10LOG10 f)
NOTE: DIFFERENCE BETWEEN TWO
MEAN REMOVAL SCHEMES VISIBLE
ONLY IN LOWEST FREQUENCY POINTS

This error source (which mean removal scheme is chosen) is not properly characterized as a bias since on the average there is no contribution. The question one is concerned about it, "What happens for a particular sample function?" But this is really a question of variability in the usual sense. How much is the result likely to vary from one sample function to another?

What we should really do is calculate the variance of our power spectral density estimates for the computation scheme we actually use. We should not assume, as was done by Blackman and Tukey and in Section 3.1.2 above, that we are working with a zero mean random process. We should take account of the fact that we are removing the mean.

Returning to the discussion of Section 3.3.1 we will now wish to replace $x(t)$ by $x(t) + m - \bar{x}$ to explicitly exhibit its mean and the sample mean removed. Let us ignore the fact that $\bar{x}$ is slightly correlated to each of the x's and write

$$m - x \triangleq \delta$$

and assume that δ is a zero mean random variable which is statistically independent of $x(t)$. This process will calculate the effect on the covariance of the spectral estimator introduced by removal of the sample mean

directly from the data. We will have added onto the right hand side of Equation (13) the terms

$$2[\text{var}(\delta)]^2 + \text{var}\,\delta\left[R(t_2-t_1+\frac{\tau_1}{2}-\frac{\tau_2}{2}) + R(t_2-t_1-\frac{\tau_1}{2}-\frac{\tau_2}{2}) + R(t_2-t_1+\frac{\tau_1}{2}+\frac{\tau_2}{2}) + R(t_2-t_1+\frac{\tau_2}{2}-\frac{\tau_1}{2})\right]$$

where $\text{var}(\delta)$ is the variance of the sample mean as an estimate of the true mean. Again proceeding to write the correlation functions as inverse transforms of the corresponding spectral densities yields the two terms

$$2(\text{var}\,\delta)^2 + 4(\text{var}\,\delta)\int_{-\infty}^{\infty} S(f)\cos\omega\,(t_2-t_1)\cos\tfrac{\omega}{4}\tau_2\cos\tfrac{\omega}{4}\tau_1\,df$$

added to the right hand side of Equation (15). Now insertion back into Equation (16) as was done in Equation (17) before yields Equation (20) with the two additional terms appearing on the right hand side as

$$\frac{2(\text{var}\,\delta)^2}{T_N^2}\,Q(f_1)\,Q(f_2)$$

$$+ 4\,\text{var}\,\delta\iiint_{-\infty}^{\infty}\left[\cos\omega_1\tau_1\cos\omega_2\tau_2\cos\tfrac{\omega}{4}\tau_1\cos\tfrac{\omega}{4}\tau_2\right.$$

$$\left.D(\tau_1)\,D(\tau_2)\,S(f)\,\frac{\sin\frac{\omega}{2}(T_N-|\tau_1|)}{\frac{\omega}{2}(T_N-|\tau_1|)}\,\frac{\sin\frac{\omega}{2}(T_N-|\tau_2|)}{\frac{\omega}{2}(T_N-|\tau_2|)}\right]d\tau_1 d\tau_2 df$$

This can be written approximately in terms of the modified windows by the same technique used before as

$$\frac{2[\text{var } \delta]^2}{T_N^2} Q(f_1)\, Q(f_2) + \frac{(\text{var } \delta)}{T_N} \int_{-\infty}^{\infty} \left[Q''(f_1 + \frac{f}{4}) + Q''(f_1 - \frac{f}{4})\right] \left[Q''(f_2 + \frac{f}{4}) + Q''(f_2 - \frac{f}{4})\right] S(f)\, df \tag{82}$$

where $Q''(f)$ is as defined in Equation (32). The degree of approximation here is the same as that utilized in deriving Equation (31) in that we have ignored terms in $(\frac{\tau}{T_N})^2$ in the τ_1, τ_2 integrations. We expect $\bar{x}$ to be a good estimate of the mean so that the first term should usually be negligible.

In the case of a "smooth" spectrum this additional term in the variance ($f_1 = f_2$) simplifies to

$$2(\text{var } \delta)^2 \left(\frac{T_M}{T_N}\right)^2 + \frac{(\text{var } \delta)}{2} \frac{T_M}{T_N} [S(f)]$$

This is in addition to the previously calculated $\frac{T_M}{T_N}$ term so that if we write the total variance for the smooth spectra case we have

$$\text{var } \hat{S}(f) \approx \frac{T_M}{T_N} \hat{S}(f) \left[1 + \frac{1}{2} \left(\frac{\text{var } \delta}{S(f)}\right) + 2 \frac{T_M}{T_N} \left(\frac{\text{var } \delta}{S(f)}\right)^2\right] \tag{83}$$

This result indicates that the deviation from the expected variance increases as $S(f)$ decreases. For $1/f$ or $1/f^2$ type spectra which decay with increasing frequency this additional variability is largest at the highest frequencies. Thus, it seems not to help explain any unexpected low frequency behavior.

3.3.2 Prewhitening

As Sections 3.1.2 and 3.1.3 above have shown the statistical properties of the spectral estimate are much more desirable if the spectrum to be estimated is white or at least "smooth." That this is particularly true of the spectral estimate's bias will be further illustrated here. The situation is not unlike that in most estimation problems. We can almost always do a better job of estimating something if we know the answer or some approximation to it beforehand. In this case the general technique is to force the data to be white by putting it through a filter whose transfer function is the inverse of the presumed final result. The spectral estimation is done on this result which is presumably white or nearly so. Thus, all the advantages of the "smooth" estimation case can be obtained. The final spectral estimate is then obtained by undoing the filter which can be done exactly since the filter was known. While this procedure may seem rather trivial and of little consequence, as a practical matter it is extremely important. Blackman and Tukey stress the need for prewhitening repeatedly. They're warnings should not go unheeded. For instance, in the 1/f noise case proper prewhitening has probably been the single

most important factor in obtaining useful results. Since the low frequency semiconductor noise case is the one of particular interest for this thesis let us move on to an examination of the prewhitening problem in detail for this case.

Let us consider a power spectral density which goes as 1/f for decreasing frequencies. It might appear smooth on a log-log plot but this is a deception. It has a logarithmic singularity at the origin and is definitely not "smooth" over linear frequency spacings on the order of $\frac{1}{2T_M}$'s.

A spectrum which actually behaves as 1/f all the way to the origin is disturbing for several reasons. First, it would not be integrable and hence imply infinite total power in the random process.* In addition, some of the integrals which appear in the calculations for the mean and the variance of the spectral estimate at low frequencies would not converge because their integrands are windows multiplied by 1/f type kernels. A 1/f spectrum will also have divergent total power because of its behavior at high frequencies. However, because of aliasing difficulties in a practical estimation problem we will arrange to be dealing with a basically low pass spectrum.

* It is not, however, clear that we could ever expect to measure a significant amount of this infinite power. We may not live long enough!

Let us consider then a 1/f spectrum which is white below some lower "break" frequency, f_o, and zero above some upper "cutoff" frequency, f_c, as shown in Figure (4) and given by

$$S(f) = \begin{cases} \frac{K}{f_o} & |f| < f_o \\ \frac{K}{|f|} & f_o < |f| < f_c \\ 0 & |f| > f_c \end{cases} \qquad (84)$$

where K sets the absolute level of the spectrum. For any given spectral estimation run f_c will be something on the order of $\frac{1}{2\Delta t}$ whereas f_o might be something like a micro cycle (10^{-6} cps). It is interesting to note that having idealized the situation to this extent we can at least calculate a correlation function, a feat which could not be managed when the spectrum diverged like 1/f at the origin and decayed only like 1/f at infinity. The inverse Fourier transform of Equation (84) yields the correlation function as

$$R(\tau) = 2k \left\{ \frac{\sin 2\pi f_o \tau}{2\pi f_o \tau} + C_i (2\pi f_o \tau) - C_i (2\pi f_c \tau) \right\} \qquad (85)$$

where $C_i(x)$ is the cosine integral $\int_x^\infty \frac{\cos \alpha}{\alpha} d\alpha$. It seems clear that cutting off the 1/f behavior at low frequencies

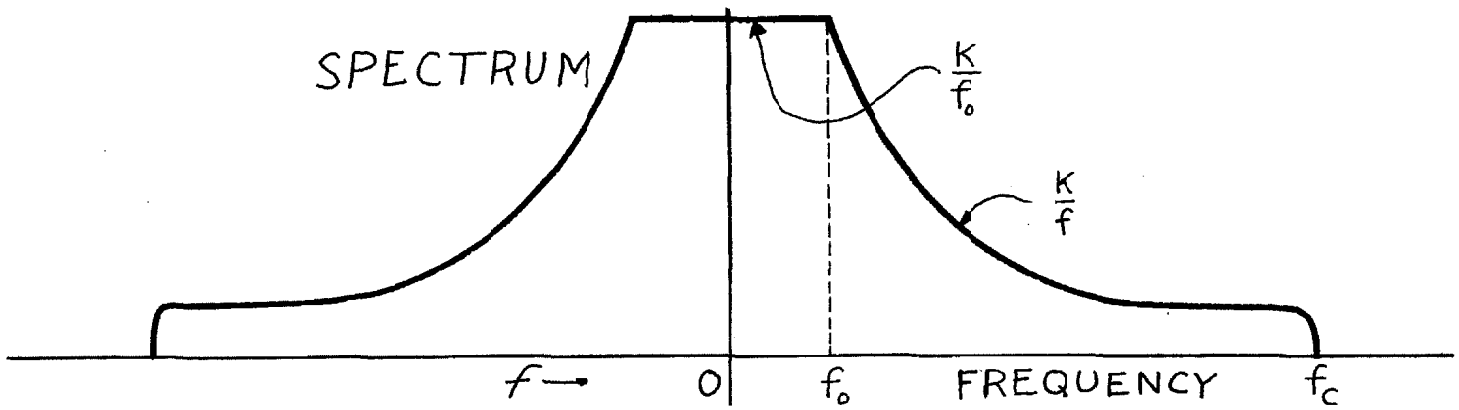

CORRELATION FUNCTION

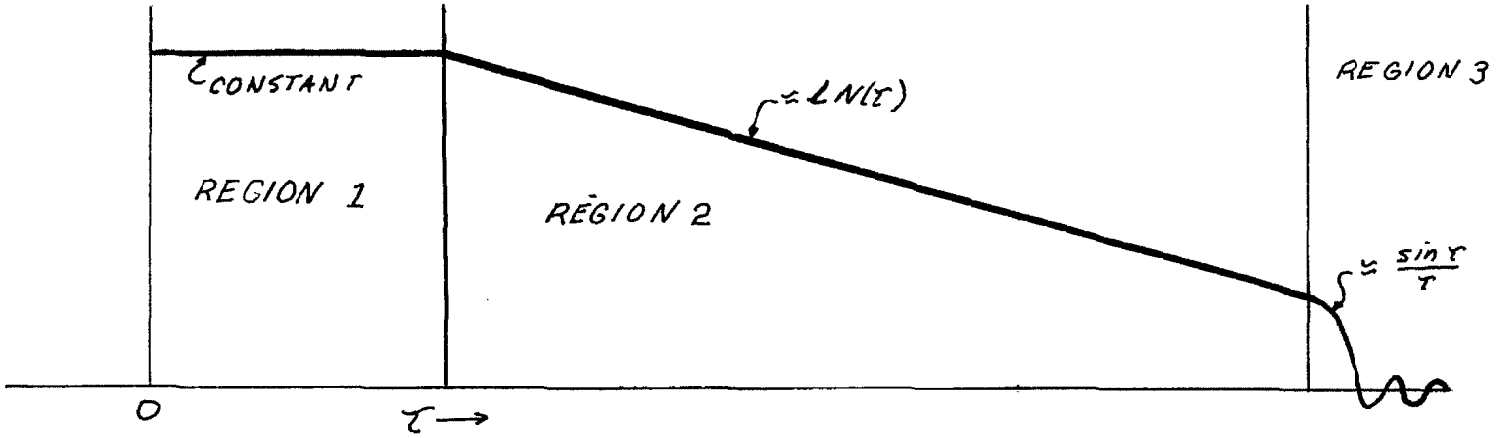

FIGURE 4
HYPOTHETICAL 1/f SPECTRUM

in a different manner would merely change the "shape" of the $\frac{\sin x}{x}$ term to the Fourier transform (i.e. "window") for whatever shape is chosen as the truncation in the frequency domain. Using asymptotic expansions for the cosine integral

$$C_i(x) \approx \left\{ \begin{array}{ll} \frac{\sin x}{x} & x \gg 1 \\ -\ln \frac{1}{\gamma x} & x \ll 1 \end{array} \right\}_{\gamma = 1.781072} \tag{86}$$

we obtain approximate expressions for the correlation function in the three regions of interest.

$$R(\tau) \approx \left\{ \begin{array}{ll} 2k \left[1 + \ln \left(\frac{f_c}{f_o} \right) \right] & \tau \ll \frac{1}{2\pi f_c} \quad \text{region 1} \\ 2k \left[\ln(2\pi\gamma f_c \tau) \right] & \frac{1}{2\pi f_c} \ll \tau \ll \frac{1}{2\pi f_o} \quad \text{region 2} \\ 2k \left[\frac{\sin 2\pi f_c \tau}{2\pi f_c \tau} \right] & \tau \gg \frac{1}{2\pi f_o} \quad \text{region 3} \end{array} \right\} \tag{87}$$

where we have used the assumption mentioned earlier that $f_c \gg f_o$.

In the first region the correlation function is a large positive constant which grows logarithmically as we let the 1/f behavior extend to the origin. Note that with our discrete estimation scheme we will never be able to measure this region's behavior. Our minimum

resolution in the correlation function estimates is $\tau = \Delta t$ but region 1 occurs for $\tau \ll \frac{1}{2\pi f_c} = \frac{\Delta t}{\pi}$.

. Therefore, almost all of this $R(\tau)$ contribution would appear in the $\tau = 0$ point for our scheme. This is one way of viewing the origin of the bias in the spectral estimator.

In the second region $R(\tau)$ has a lograthmic behavior with τ. We are interested in considering the case where our minimum resolution in frequency, $\frac{1}{2M\Delta t}$, is much larger than f_o, the 1/f break frequency. Thus, region 2 is all we will ever be able to see as τ increases since it extends in τ to something like $\frac{1}{2\pi f_o}$ which is larger than the maximum τ point $2M\Delta t$. The $\frac{\sin x}{x}$ behavior of the correlation function in region 3 won't be seen until we get down in frequency to where we can resolve the f_o break point. This means essentially record lengths long compared to $\frac{1}{f_o}$.

But let us return to the question of bias. We wish to calculate the average value for our spectral estimator for the particular case of 1/f noise of the assumed shape. From the preceeding section we have that the average value of the estimate at frequency $R/2M\Delta t$

for the "Q_o" window is given by

$$E(V_o) = \left[S(f) \circledast \sum_{q=-\infty}^{\infty} \delta\, f - \frac{q}{\Delta t} \circledast 2M\Delta t \left\{ \frac{\sin 2\pi f M\Delta t}{2\pi f M\Delta t} - \left(\frac{\sin \pi f N\Delta t}{\pi f N\Delta t} \right)^2 \right\} \right]_{f=0}$$

$$E(V_R) = \left[S(f) \circledast \sum_{q=-\infty}^{\infty} \delta\, f - \frac{q}{\Delta t} \circledast Q_o(f) \right]_{f = \frac{1}{2M\Delta t}} \qquad (88)$$

We will calculate the bias for the Q_o estimate and recombine these results according to Equation 67 to obtain the bias results for the Q_2 window. Because we are considering the aliased power spectrum of the noise to be given by Equation (84) we see that the bias calculations will involve integrals of the truncated 1/f function against $\frac{\sin x}{x}$ and $\left(\frac{\sin x}{x}\right)^2$ type kernels. Although these integrals converge they are not readily obtainable via any of the standard reference tables. The easiest method of evaluating them is to return to the τ domain where the windows take simple forms. In particular, the Q_o window is, of course, just unity over a fixed τ length and the $\left(\frac{\sin x}{x}\right)^2$ is a triangle in the τ domain. For $R > 0$, and a Q_o window,

$$E\left(V_R\right) = \int_{-\infty}^{\infty} S_a(f')\, Q_o\left(f' - \frac{R}{2M\Delta t} \right) df'$$

$$= 2\int_{o}^{M\Delta t} R_a(\tau) \cos\left(2\pi \frac{R}{2M\Delta t}\, \tau \right) d\tau \qquad (89)$$

where $R_a(\tau)$ is the correlation function corresponding to the aliased spectrum $S_a(f)$. If we use Equation (85)

for this correlation function we have

$$E\left\{V_R\right\} = 2\int_0^{M\Delta t} 2k\left[\frac{\sin 2\pi f_o \tau}{2\pi f_o \tau} + \int_{2\pi f_o \tau}^{2\pi f_c \tau} \frac{\cos x}{x}\, dx\right] \cos\frac{R\pi}{M\Delta t}\, d\tau$$

With the use of integration by parts and trigonometric identities we obtain

$$E\left\{V_R\right\} = \frac{k}{\pi f_o}\left[Si\left(R\pi + 2\pi f_o M\Delta t\right) - Si\left(R\pi - 2\pi f_o M\Delta t\right)\right]$$

$$- 2k\frac{M\Delta t}{R\pi}\left[Si\left(R\pi + 2\pi f_c M\Delta t\right) - Si\left(2\pi f_c M\Delta t - R\pi\right)\right. \quad (90)$$

$$\left. -Si\left(R\pi + 2\pi f_o M\Delta t\right) - Si\left(R\pi - 2\pi f_o M\Delta t\right)\right]$$

where $Si(x)$ is the sine integral, $\int_0^x \frac{\sin x}{x}\, dx$. This expression is exact in that the only assumption involved is that the aliased power spectral density is the truncated 1/f spectrum of Equation (84). Since V_R is the estimate of the spectrum of $f = \frac{R}{2M\Delta t}$, we see that to calculate the bias Equation (90) should be compared with

$$S\left(\frac{R}{2M\Delta t}\right) = \frac{k\, 2M\Delta t}{R} \quad (91)$$

which is the correct result at this frequency. In developing approximate formulae from Equation (90) we note that we have already assumed that

$$f_o \ll \frac{R}{2M\Delta t} \leq f_c \quad (92)$$

which imples that

$$2\pi f_o M\Delta t \ll R\pi \leq 2\pi f_c M\Delta t$$

where the equality sign holds only for M = 100.

The differences between Si functions then become integrals of the $\frac{\sin x}{x}$ kernel over very small regions around the points $R\pi$. Using a first order Taylor series approximation to the $\frac{\sin x}{x}$ in this region we have

$$E\left\{V_R\right\} \approx \frac{k}{R/_{2M\Delta t}} \left[\frac{2}{\pi} Si(R\pi) + \frac{(-1)}{3R} \left(\frac{f_o}{1/_{2M\Delta t}}\right)\left(1 + \frac{2f_o}{1/_{2M\Delta t}}\right) - \frac{\left(Si\left(2\pi f_c M\Delta t + R\pi\right) - Si\left(2\pi f_c M\Delta t - R\pi\right)\right)}{\pi}\right] \qquad (93)$$

The last term will be exactly zero to the extent that the cutoff frequency, f_c, is really the aliasing frequency, $\frac{1}{2\Delta t}$, and will be negligibly small in any case. Equation (93) is written with the correct result at the frequency $R/_{2M\Delta t}$ factored out. Therefore, the extent to which the expression in square brackets is not equal to unity will be the fractional bias. For this case of the Q_o window, Table (1) shows this bias vs R for the first few terms under the assumption (92).

R	% Bias of Q_o Spectral Estimate at $R/_{2M\Delta t}$ for Truncated 1/f Spectrum	
1	+ 17%	+ .68 db
2	- 9%	- .41 db
3	+ 6.7%	+ .28 db
4	- 4.5%	- .2 db
.	.	.
.	.	.
.	.	.

TABLE (1)

We must now calculate the bias of our estimate V_o considered as an estimate at the origin. This result will be important for computing the bias of the Q_2 estimate. However, as pointed out in Section 3.3.1 this point is actually an estimate at some point other than the origin due to the mean removal scheme. Thus, we can also ask what frequency this point should be plotted at such that it will be an unbiased estimate of the spectrum at that frequency. To calculate $E(V_o)$ we return to Equation (88), insert the truncated 1/f noise of Equation (84) as the aliased spectrum, and integrate all the

integrals only over the positive frequency domain since the functions are even in f. This procedure leads to

$$E(V_o) = \frac{4KM\Delta t}{f_o}\int_o^{f_o}\frac{\sin 2\pi fM\Delta t}{2\Delta fM\pi t}\,d \;-\; \frac{4KM\Delta t}{f_o}\int_o^{f_o}\left(\frac{\sin \pi fN\Delta t}{\pi fN\Delta t}\right)^2 df$$

$$+\frac{2K}{\pi}\int_{f_o}^{f_c}\frac{\sin 2\pi fM\Delta t}{f^2}\,df \;-\; \frac{4KM}{\pi^2N^2\Delta t}\int_{f_o}^{f_c}\frac{\sin^2 \pi fN\Delta t}{f^3}\,df$$

The first integral is just a Si function and the other three can be expressed in terms of sine and cosine integrals. The following formulae obtained by repeated integration by parts will be useful.

$$\int_o^A \frac{\sin^2 x}{x^2}\,dx = Si(2A) - \frac{\sin^2 A}{A}$$

$$\int_A^B \frac{\sin rx}{x^2}\,dx = r\left[\frac{\sin rA}{rA} - \frac{\sin rB}{rB} + Ci(rB) - Ci(rA)\right]$$

$$\int_A^B \frac{\sin^2 rx}{x^3}dx = r^2\left[\tfrac{1}{2}\left(\frac{\sin rA}{rA}\right)^2 - \tfrac{1}{2}\left(\frac{\sin rB}{rB}\right)^2 + \frac{\sin 2rA}{2rA} - \frac{\sin 2rB}{2rB} + Ci(2rB) - Ci(2rA)\right]$$

Utilization of these results in conjunction with the expression for $E(V_o)$ above yields

$$E(V_o) = 4KM\Delta t \left[\frac{Si(2\pi f_o M\Delta t)}{2\pi f_o M\Delta t} + \frac{\sin(2\pi M\Delta t f_o)}{2\pi f_o M\Delta t} - 2\,\frac{Si(2\pi f_o N\Delta t)}{2\pi f_o N\Delta t} - \frac{\sin(2\pi f_c M\Delta t)}{2\pi f_c M\Delta t} \right.$$

$$+ \tfrac{1}{2}\left(\frac{\sin \pi f_o N\Delta t}{\pi f_o N\Delta t}\right)^2 + \tfrac{1}{2}\left(\frac{\sin \pi f_c N\Delta t}{\pi f_c N\Delta t}\right)^2 - \frac{\sin(2\pi f_o N\Delta t)}{2\pi f_o N\Delta t} + \frac{\sin(2\pi f_c N\Delta t)}{2\pi f_c N\Delta t}$$

$$\left. + Ci(2\pi M\Delta t f_c) - Ci(2\pi f_o M\Delta t) - Ci(2\pi f_c N\Delta t) + Ci(2\pi f_o N\Delta t) \right] \quad (94)$$

This expression is exact but not very useful. To form more tractable approximations we need to say something about the size of $2\pi f_o N\Delta t$. This is equivalent to asking if even our total record length, $(N\Delta t)$, is long enough to be near resolving f_o. A typical set of parameters might be $M = 100$ and $N = 10^4$. If we take f_o on the order of 10^{-5} and let Δt range from 10^{-4} to 10^3 then there are clearly two different ranges of approximations of interest. At the high frequency end where we cannot resolve f_o at all Equation (94) becomes

$$E(V_o) \approx \frac{K}{1/2M\Delta t} \left[-1 + 2 \ln \frac{N}{M} \right] \qquad \Delta t \ll \frac{1}{2\pi f_o N} \quad (95)$$

This result is in the form one would expect. It does not depend on f_o explicitly since we have assumed we cannot "see" f_o but it depends on its presence through the ratio of our total record length to the maximum lag at

which the correlation function is estimated. Another way of interpreting this effect is as the ratio between the minimum frequency resolution point and the size of the "hole" in the window due to the removal of the sample mean. At the low frequency end, where $1/2N\Delta t$ resolves f_o but $1/2M\Delta t$ does not, we have

$$E[V_o] \approx \frac{K}{1/2M\Delta t}\left[4 + 2\ln\left(\frac{1}{\gamma\, 2\pi f_o M\Delta t}\right)\right] \qquad \Delta t \gg \frac{1}{2\pi f_o N} \tag{96}$$

which again shows the expected dependence; that is, it now depends on how far the minimum frequency resolution point is above the 1/f break frequency.

One expects the bias during the transition region, where neither of these two approximations is strictly valid, to vary smoothly between them. This could be verified for any particular case by inserting numerical values into the exact formula, Equation (94). However, a good indication that this is in fact the case is given by the following typical calculation. Taking a case which is just at the upper borderline of the low frequency case, $M = 100$, $N = 10^4$, $\Delta t = 5$, $f_o = 10^{-5}$ and evaluating the result utilizing both approximate formulae we obtain

high frequency case $\quad E(V_o) \approx (K/1/2M\Delta t)$ (8.2)

low frequency case $\quad E(V_o) \approx (K/1/2M\Delta t)$ (9.76)

which are not very different.

The bias of these results when considered as estimates of S(o) is large since the correct result there is K/f_o. But we are now in a position to calculate that point, f', for which they are in fact unbiased estimates of S(f). The most convenient form for this result is as a fraction of the lowest frequency point R = 1 where $f = 1/2M\Delta t$. Thus we calculate $(f'/1/2M\Delta t)$ as

$$\left(\frac{f'}{1/2M\Delta t}\right) = \frac{K/2M\Delta t}{E(V_o)} = \begin{cases} -1 + 2 \ln \frac{N}{M} & 2\pi f_o N\Delta t \ll 1 \\ 4 + 2 \ln \frac{1}{\gamma\, 2\pi f_o M\Delta t} & 2\pi f_o N\Delta t \gg 1 \end{cases} \tag{97}$$

For a typical low frequency case of M = 100, $N = 10^4$, $f_o = 10^{-5}$, Δt = 5 sec this says the zero point estimate should be plotted 1/(10)th of the way between the origin and the R = 1 point. This is about 1 decade on a log f scale.

We are also now in a position to complete a table of percentage biases for the Q_2 estimate by using the $\frac{1}{4}$, $\frac{1}{2}$, $\frac{1}{4}$ coefficients of Equation (67) applied to the Q_o results. This yields biases as indicated in Table (2).

R	% Bias of Q_2 Estimates for Q_o Estimates of a Truncated 1/f Spectrum		% Bias of Q_2 Estimates for Perfect Q_o Estimates of a Truncated 1/f Spectrum	
0	0	0	-	-
1	+ 313%	+ 4.94 db	+ 315%	+ 4.98 db
2	+ 21.5%	+ .85 db	+ 16.5%	+ .66 db
3	-< 1%	- .01 db	+ 6.5%	+ .27 db
4	.	.	+ 3.3%	+ .14 db
.	.	.	.	.
.	.	.	.	.
.	.	.	.	.

TABLE (2)

The R = 0 point is considered as an estimate at the point f′ just calculated and hence is unbiased by definition. The other biases involving the V_o point assume the high frequency case is involved but as the calculation above indicates it makes little difference most of the time.

The bias of the spectral estimator becomes even more pronounced for the case of $1/f^2$ spectra. This is to be expected since one is now estimating on the slope of a much steeper function. Let us take as the correct result an RC noise spectrum with a very low break frequency,

f_t. i.e.,

$$S(f) = \frac{K_t}{f^2 + f_t^2} \tag{98}$$

where K_t sets the absolute level. We will be particularly interested in the case where $f >> f_t$ and the spectrum is decaying as the square of the frequency. Let us proceed to calculate the expected value of the Q_o spectral estimate at $f = R/2M\Delta t$

$$E(V_R) = \int_{-\infty}^{\infty} \frac{K_t}{f_2 + f_t^2} \, Q_o\left(f - \frac{R}{2M\Delta t}\right) df \tag{99}$$

where we have made the approximation of ignoring the aliasing since the spectral density is decaying as $1/f^2$. Making use of the formula for the Q_o window given earlier in Equation (35) and the fact that*

$$\int \left[\frac{\sin(x-R\pi)}{(x-R\pi)}\right] \frac{dx}{(x^2 + a^2)} = \frac{\pi}{a^2 + (R\pi)^2} \left[1-(-1)^{R_e}-a\right] \tag{100}$$

we have

$$E(V_R) = \frac{K_t}{\left(\left(\frac{R}{2M\Delta t}\right)^2 + f_t^2\right)} \left[1-(-1)^{R_e}-2\pi f_t M\Delta t\right] \tag{101}$$

---

* This integral is obtained by integrating the product of the Fourier transforms of the factors in the integrand in the Fourier transformed domain.

For the case where our frequency resolution is much too large to "see" f_t then

$$f_t \ll \frac{1}{2M\Delta t} \Longrightarrow 2\pi f M\Delta t \ll 1$$

and we have approximately

$$E(V_R) \approx \frac{K_t}{\left(R/_{2M\Delta t}\right)^2} \begin{cases} 2 & R \text{ odd} \\ 2\pi f_t M\Delta t & R \text{ even} \end{cases} \qquad (102)$$

This is a very interesting and rather unusual result. It says that since $K\left(R/_{2M\Delta t}\right)^2$ is the correct result you will be biased upward by a factor of 2 at every other point and downward by a large factor at the points in between. This behavior correlates very well with typical experimental data as Figure (5) illustrates. The dashed line shows what is believed to be the correct result for this data which goes as $1/f^2$ in this range. The points are the Q_o estimates directly from the data with the lables indicating the values of R for the first few points. For this particular run Δt = 5 sec, M = 100 and if one postulates $f_t = 10^{-5}$ cps then Equation (102) predicts + 3 db for the odd points and - 15 db for the even points which agrees with the data within the expected variability of these points.

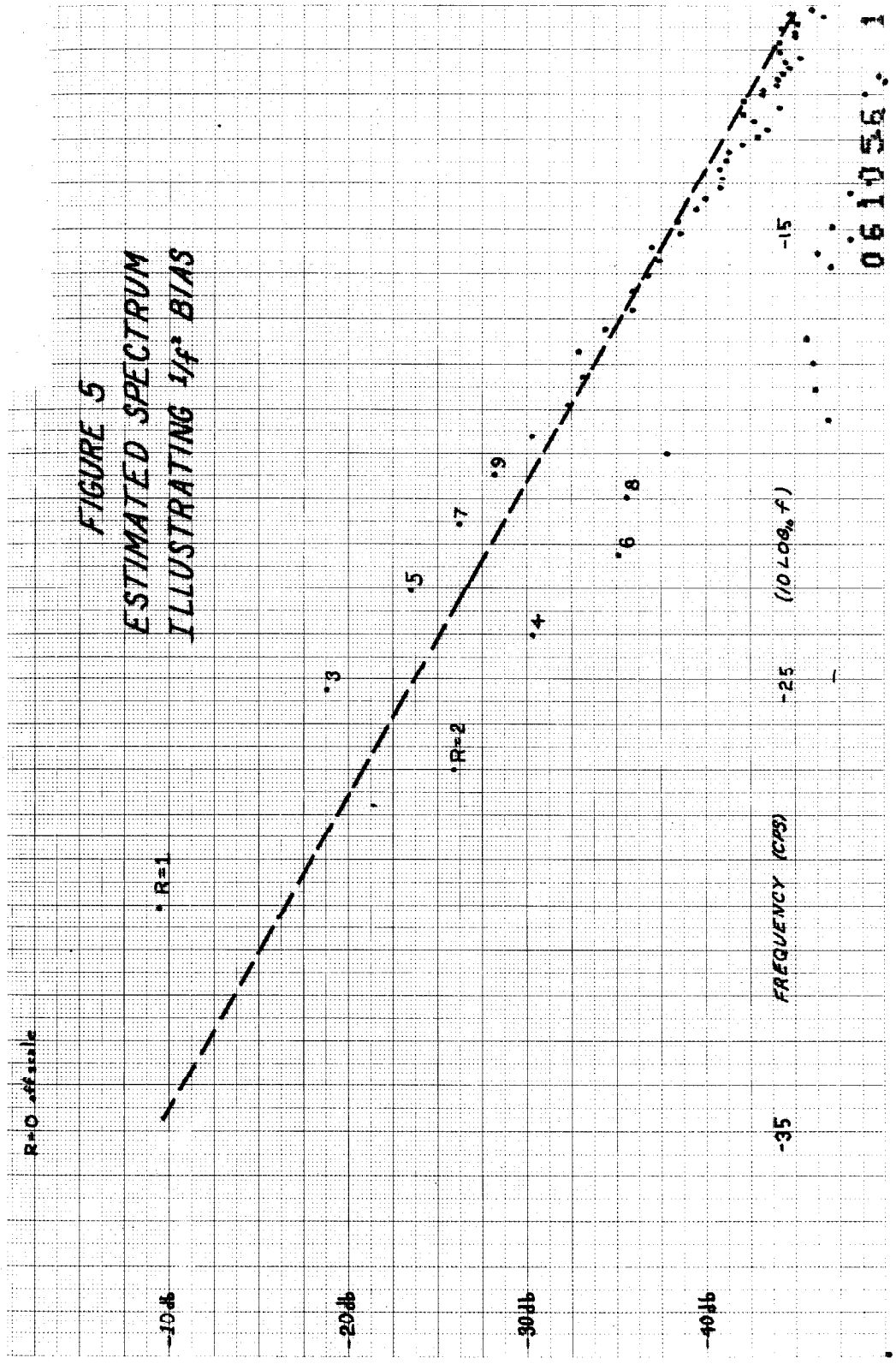
FIGURE 5
ESTIMATED SPECTRUM
ILLUSTRATING 1/f² BIAS
R=0 offscale
-10db
-20db
-30db
-40db
R=1
R=2
.3
.4
.5
.6
.7
.8
.9
-35
-25
-15
FREQUENCY (CPS)
(10 LOG10 f)
0 6 1 0 5 5 . 1

As a preliminary to calculating the bias for the Q_o estimate it is necessary to find $E(V_o)$. We start with the assumed spectrumof Equation (84) and again ignoring aliasing obtain from Equation (80) that

$$E\{V_o\} = \int_{-\infty}^{\infty} \left[\frac{K_t}{f^2 + f_t^2}\right] 2M\Delta t \left[\frac{\sin 2\pi fN\Delta t}{2\pi fM\Delta t} - \left(\frac{\sin 2\pi fN\Delta t}{2\pi fN\Delta t}\right)^2\right] df$$

Making use of Dwight 859.005 [12] and*

$$\int_{-\infty}^{\infty} \left(\frac{\sin x}{x}\right)^2 \frac{dx}{(x^2 + a^2)} = \frac{\pi}{a^2} + \frac{\pi}{2a^3}\left(e^{-2a} - 1\right) \qquad (103)$$

we obtain

$$E\{V_o\} = \frac{K_t}{f_t^2}\left[\pi\left(1 - e^{-2\pi f_t M\Delta t}\right) - \frac{2M}{N} + \frac{M\left(1 - e^{-2\pi N\Delta t f_t}\right)}{N^2\pi\Delta t f_t}\right]$$

Again making the assumption that $\pi f_t \ll \frac{1}{2M\Delta t}$ we have

$$E\{V_o\} = \begin{cases} \frac{K_t}{f_t^2}\left\{\pi^2 \frac{f_t}{1/2M\Delta t}\right\} & 2\pi f_t N\Delta t \ll 1 \\ K/f_t^2\left\{\pi^2 \frac{f_t}{1/2M\Delta t} - \frac{2M}{N}\right\} & 2\pi f_t N\Delta t \gg 1 \end{cases} \qquad (104)$$

where in the first case even the total record length $N\Delta t$ is insufficient to resolve f_t. These results are written in a form which exhibits thedeviation of the estimate, V_o, from the actual behavior of the origin, K/f_t^2. They show

* Franklin [14] pg. 225.

that V_o underestimates the true spectrum at the origin by about 1/10th of the ratio between the break frequency of the noise, f_t, and the estimation resolution $1/2M\Delta t$. A more informative way to write this result is as

$$E\{V_o\} = \frac{K_t}{\left(1/2M\Delta t\right)^2} \left\{\pi^2 \frac{\left(1/2M\Delta t\right)}{f_t}\right\} \qquad (105)$$

which shows how much bigger V_o estimates the noise to be than the correct answer at the R = 1 point. Since the noise is increasing like $1/f^2$ in this region Equation (105) can be used to determine at what frequency f' the V_o estimate is an unbiased estimate. This calculation yields

$$\left(\frac{f'}{1/2M\Delta t}\right) = \frac{1}{\pi}\sqrt{\frac{f_t}{1/2M\Delta t}} \qquad (106)$$

which tells at what fraction of $1/2M\Delta t$ the V_o point should be plotted. For the typical run referred to above and shown in Figure (5) this fraction is about 1/10π. The point labled R = 0 in this figure when plotted at this point (logarithmically a decade and a half away in frequency from the R = 1 point) π³ appears quite reasonable, again within the variability expected.

We are now in a position to evaluate the bias of the Q_2 (hanning window) estimate using the $\frac{1}{4}$, $\frac{1}{2}$, $\frac{1}{4}$ coefficients as given by Equation (67). The biases for R even with the Q_o window and R = 0 and 1 with the Q_o window will depend on an assumption about f_t but the others can be evaluated in percentage terms without this assumption because the odd R terms dominate. As a typical case let us again use the data of Figure (5) emplcyed above for which $2M\Delta t = 10^3$ and f_t is assumed to be 10^{-5} cps. Then the data of Table (3) results where the last column

R	% Bias of V_R					
	Q_o		Q_2		(perfect Q_o)	
0	0%*	0 db	-50%*	- 3 db*	+ 500%*	+ 6.99 db
1	100%	+ 3 db	+ 12500%	20.97 db*	+ 25000%*	34 db*
2	-97%*	-15 db*	+ 125%	+ 3.52 db	+ 100%	3.03 db
3	100%	+ 3 db	+ 3.8%	+ .16 db	+ 20%	.8 db
4	-97%*	-15 db*	.	.	.	.
.	.		.	.	.	.
.	.		.	.	.	.
.	.		.	.	.	.

TABLE (3)

* These points depend on assumption about f_t.

presents the fractional bias of the Q_2 estimate for perfect Q_o points including R = 0. The R = 0 point is considered an estimate at the f′ given by Equation (106) for this table and so is unbiased for Q_o by definition. The data of Table (3) indicates why prewhitening is so important when dealing with $1/f^2$ spectra. The biases are very pronounced at the few lowest points. But these are just the points of most interest for this type of spectra since they "cover more ground" on the logarithmic frequency scale. Hence, it is important to recapture them via prewhitening.

The above discussions have adequately demonstrated that attempting to form spectral density estimates on a $1/f$ or $1/f^2$ sloping spectrum leads to very bad estimates. The major remedial action taken during this research was to prewhiten the data. The scheme utilized was basically that recommended by Blackman and Tukey. In the discrete case the prewhitened data, z_j's, are formed from the raw data x_i's by

$$z_j = \sum_{i=o}^{K} A_i \, x_{i+j} \qquad j = 1, 2, \ldots, N - K \qquad (107)$$

Where the A_i's can be viewed as the sampled data version of the impulse response of a linear filter. The magnitude

squared of this filter will then be given by

$$|Y(f)|^2 = B_0 + 2B_1 \cos 2\pi f + 2B_2 \cos 2(2\pi f) + \cdots\cdots$$
$$= \sum_{n=-K}^{K} B_1 \cos 2\pi f n \qquad (108)$$

And the B's will therefore relate $S_z(f)$ to $S_x(f)$ as

$$S_z(f) = |Y(f)|^2 S_x(f)$$

We will be most interested in two kinds of filters

$$|Y(f)|^2 = \begin{cases} |f| & |f| \le \frac{1}{2\Delta t} \quad \text{1/f prewhitening} \\ f^2 & |f| \le \frac{1}{2\Delta t} \quad \text{1/f}^2 \text{ prewhitening} \end{cases} \qquad (109)$$

where each will be periodic in frequency with period $1/\Delta t$ just as the aliased spectral density. Looking back at Equation (108) we see that a simple method of realizing B's is to expand Equation (109) in a finite cosine series. This procedure yields

$$|Y(f)|^2 = \begin{cases} \frac{1}{2} - \frac{4}{\pi^2} \sum_{n=1,\ \text{odd}}^{\infty} \frac{1}{n^2} \cos 2n\pi f\Delta t & \text{1/f prewhitening} \\ \frac{\pi^2}{3} + 4 \sum_{n=1}^{\infty} \frac{(-1)^n}{n^2} \cos 2n\pi f\Delta t & \text{1/f}^2 \text{ prewhitening} \end{cases} \qquad (110)$$

But neither of these expansions is really zero at the origin for any finite number of terms. This feature is

very important when we are dealing with cases where the $1/f$ or $1/f^2$ behavior continues for several decades below the minimum frequency resolution point, $\frac{1}{2M\Delta t}$. In order to force the prewhitening filter to be identically zero at $f = 0$ we subtract the partial sum from $|Y(f)|^2$ for any given number of terms. Then we have

$$|Y(f)|^2 = \begin{cases} \frac{4}{\pi^2} \sum_{n=1}^{k+1} \frac{1}{n^2} - \frac{4}{\pi^2} \sum_{n=1,\ \text{odd}}^{k+1} \frac{1}{n^2} \cos 2n\pi f\Delta t & 1/f \text{ prewhitening} \\ 4 \sum_{n=1}^{K+1} \frac{(-1)^{n+1}}{n^2} + 4 \sum_{n=1}^{K+1} \frac{(-1)^n}{n^2} \cos 2n\pi f\Delta t & 1/f^2 \text{ prewhitening} \end{cases} \tag{111}$$

which yields

$$B_k = \begin{cases} \frac{4}{\pi^2} \sum_{n=1}^{K+1} \frac{1}{n^2} & k = 0 \\ -\frac{4}{\pi^2} \frac{1}{k^2} & k = \text{odd} \\ 0 & k = \text{even} \end{cases} \quad 1/f \text{ prewhitening} \tag{112}$$

$$B_k = \begin{cases} 4 \sum_{n=1}^{K+1} \frac{(-1)^{n+1}}{n^2} & k = 0 \\ \frac{(-1)^k}{k^2} & k \geq 1 \end{cases} \quad 1/f^2 \text{ prewhitening}$$

The coefficients which must be applied to the raw data in the time domain, the A's, are obtained from the filter characteristic, the B's, by a self convolution. Writing out these formulae in detail yields

$$
\begin{aligned}
B_o &= A_o^2 + A_1^2 \ldots\ldots\ldots\ldots + A_K^2 \\
B_1 &= A_oA_1 + \ldots\ldots\ldots + A_{K-1}A_K \\
B_2 &= A_oA_2 + \ldots\ldots\ldots + A_{K-2}A_K \\
B_3 &= A_oA_3 + \ldots\ldots + A_{K-3}A_K \\
&\vdots \qquad\qquad \vdots \qquad\qquad \vdots \\
B_K &= A_oA_K
\end{aligned}
\tag{113}
$$

These nonlinear algebraic equations must be inverted to find the proper A's for the set of B's of Equation (112). By inserting the numerical values for the first few cases, i.e., K small, a form for rough approximations to the A's for all K can be obtained. A short computer program was written by K. Matsumoto to solve the equations iteratively starting from the approximate results for any given K.

Since the partial sum is removed the values for all of the A's change, depending on how many A's are computed. It was found, for this work, that very adequate results were obtained utilizing K = 9 (or 10 A's) for 1/f prewhitening and K = 8 (or 9 A's) for $1/f^2$ prewhitening. Table (4) lists these prewhitening coefficients. In addition, Table (5) lists the A's for K = 49 (or 50 A's). They would presumably only be used in a case where it was very important to maintain a 1/f behavior very accurately and to very low frequencies.

1/f Prewhitening		$1/f^2$ Prewhitening	
A_0 =	+ 1.2460762	A_0 =	+ .85900591
A_1 =	- .88669391	A_1 =	- .9380654
A_2 =	- .096221262	A_2 =	+ .18554991
A_3 =	- .12234353	A_3 =	- .086138683
A_4 =	- .037616304	A_4 =	+ .031371809
A_5 =	- .047103651	A_5 =	- .03445261
A_6 =	- .017285854	A_6 =	+ .0063926557
A_7 =	- .022159825	A_7 =	- .023757884
A_8 =	- .0070501685		
A_9 =	- .0099076437		

TABLE (4)

PREWHITENING COEFFICIENTS

TABLE (5)

PREWHITENING COEFFICIENTS FOR 1/f SPECTRA

A_0	=	+ 1.3221297	A_{26}	=	- .0024582738
A_1	=	- .82051718	A_{27}	=	- .0029221055
A_2	=	- .080650110	A_{28}	=	- .0021067328
A_3	=	- .11433732	A_{29}	=	- .0025097537
A_4	=	- .036575483	A_{30}	=	- .0018054929
A_5	=	- .049030906	A_{31}	=	- .0021588768
A_6	=	- .022105715	A_{32}	=	- .0015443690
A_7	=	- .028579432	A_{33}	=	- .0018566522
A_8	=	- .015215286	A_{34}	=	- .0013155949
A_9	=	- .019185228	A_{35}	=	- .0015933982
A_{10}	=	- .011264811	A_{36}	=	- .0011130872
A_{11}	=	- .013950386	A_{37}	=	- .0013615906
A_{12}	=	- .0087319731	A_{38}	=	- .00093192328
A_{13}	=	- .010670907	A_{39}	=	- .0011551859
A_{14}	=	- .0069819628	A_{40}	=	- .00076793013
A_{15}	=	- .0084483139	A_{41}	=	- .00096909006
A_{16}	=	- .0057063556	A_{42}	=	- .00061729365
A_{17}	=	- .0068545374	A_{43}	=	- .00079864464
A_{18}	=	- .0047384243	A_{44}	=	- .00047603093
A_{19}	=	- .0056621074	A_{45}	=	- .00063890126
A_{20}	=	- .0039806248	A_{46}	=	- .00033888270
A_{21}	=	- .0047399473	A_{47}	=	- .00048294127
A_{22}	=	- .0033722939	A_{48}	=	- .00019550028
A_{23}	=	- .0040076400	A_{49}	=	- .00031501684
A_{24}	=	- .0028738183			
A_{25}	=	- .0034133139			

The accuracy with which the A's of Table 4 represent the respective functions can be illustrated by calculating the filter characteristic (magnitude squared)

at equi-spaced points in frequency. Figure (6) is such a graph for the 1/f prewhitening filter. Both scales are logarithmic so that a straight line would represent exactly an f characteristic. The deviation at very low frequencies results from the fact that the filter characteristic is zero at the origin. (Within round off error). The filter has been evaluated at 100 points because M = 100 is the case most frequently utilized in the experimental work below. Figure (7) is a similar plot of the $1/f^2$ prewhitening filter and exhibits similar behavior relative to a square law.

An interesting intuitive understanding of these prewhitening filters is obtained by examining the effects in the time domain for typical data. If we are estimating on the slope of 1/f or $1/f^2$ type spectral densities the sample function in the time domain will appear very smooth or slowly varying. Because most of the energy in the process is contained at frequencies well below $\frac{1}{2M\Delta t}$ the numerical values obtained by sampling the process every Δt seconds will not change rapidly. Consider construction of a given z_i from x_i and the 9 adjacent x's by the A's listed in Table (4). The 10 A's sum to

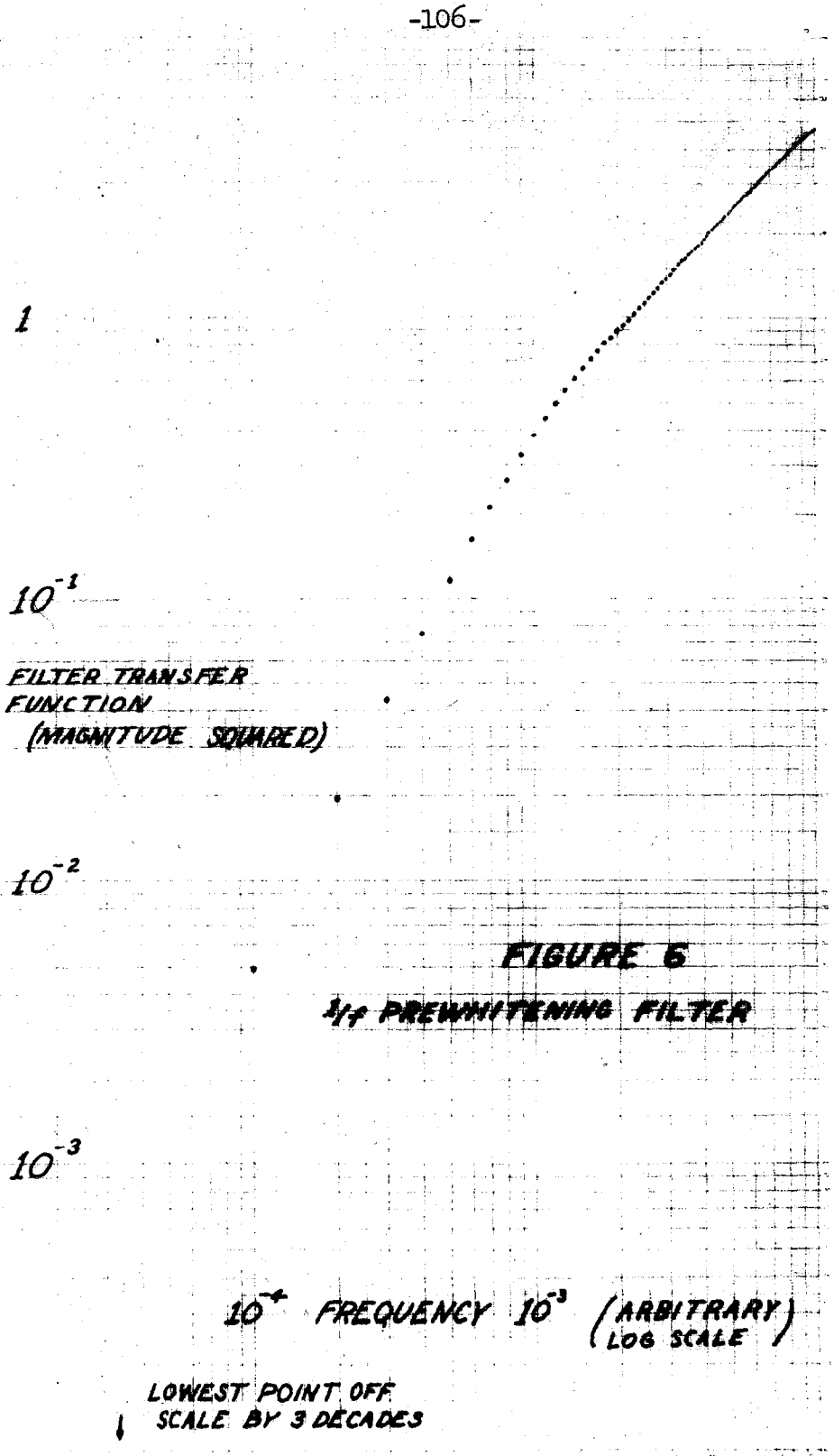

FIGURE 6

1/f PREWHITENING FILTER

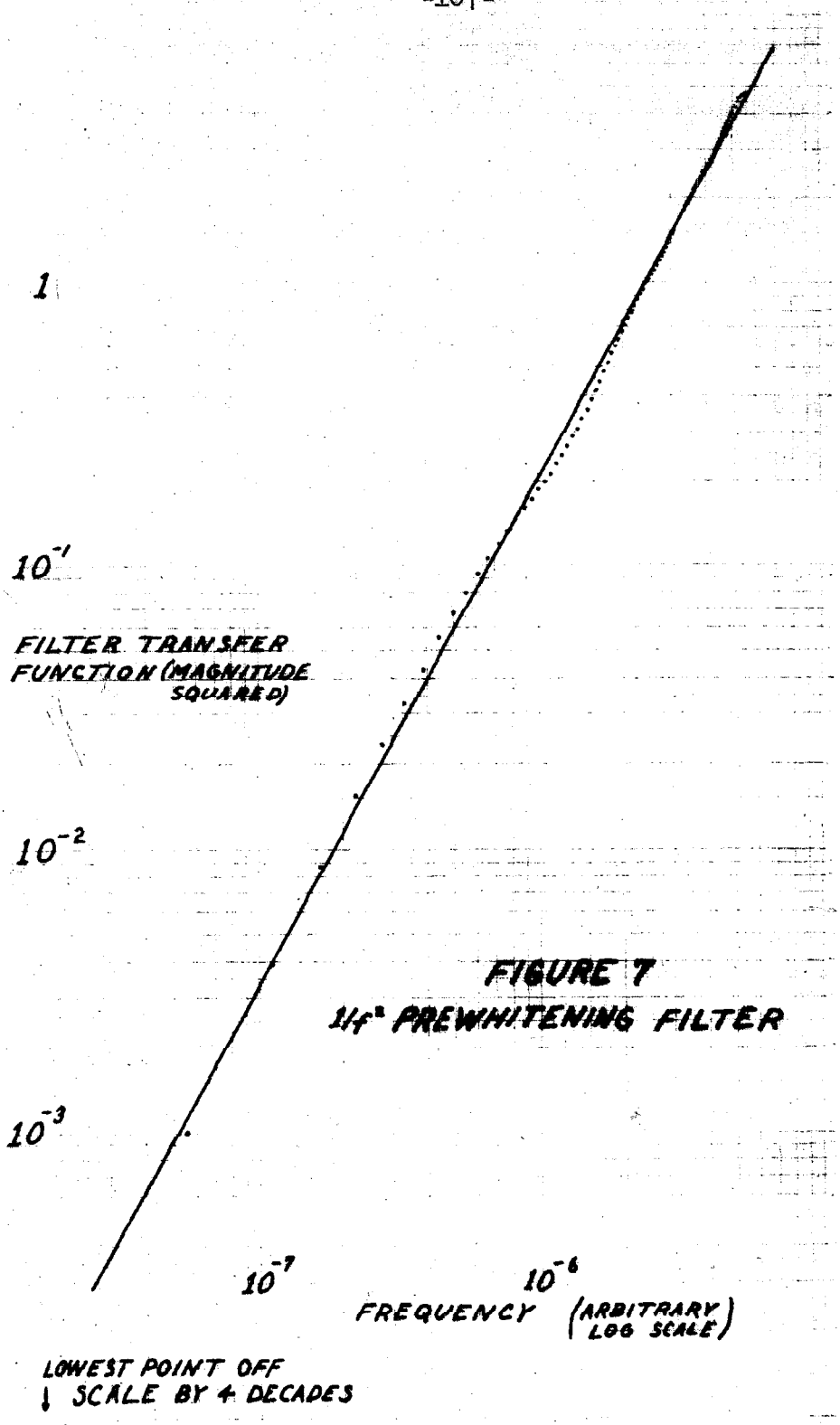

FIGURE 7

$1/f^2$ PREWHITENING FILTER

approximately zero so that, because the data is very smooth, the resulting z_i's will be small and oscillate about zero. But this is just one description of a process which is more "white" than the original spectrum. Table (7) illustrates this behavior by listing a typical sequence of raw data points and the corresponding prewhitened data points. These are from a process whose spectrum is approximately 1/f in the region of interest.

Raw Data	Prewhitened Data
.6648	
.6375	
.6473	
.6512	
.6395	
.6505	
.6458	
.6442	
.6454	
.6491	+ .005132
.6548	- .011872
.6575	- .003256
.6580	+ .011284
.6518	- .012720
.6529	+ .004729
.6479	- .000448
.6497	- .004585
.6522	- .006874
.6519	- .007442
.6428	- .001840
.6428	- .001672
.6441	+ .008327

TABLE (7)

PREWHITENED DATA

An illustration of the effectiveness of such prewhitening is given by Figure (8) . This is a spectrum estimated from prewhitened data. The corresponding spectrum from the raw data, Figure (5) , was shown earlier to illustrate the bias which enters when estimating on the slope of a $1/f^2$ spectrum. The gain achieved by prewhitening is quite striking. The tremendous biases in the unprewhitened estimated spectrum are not longer present. The variability on this run appears to now be consistent with the $\frac{M}{N}$ approximation. That the spectrum estimated upon is now approximately white is best illustrated by the estimated spectrum before the effect of the prewhitening filter has been removed. Figure (9) shows the spectrum estimated from the prewhitened data corresponding to the spectra of Figures (5) and (8) . When $|Y(f)|^2$ is removed the spectrum of Figure (9) becomes that of Figure (8) . By forcing $|Y(f)|^2$ to zero at the origin we have overpowered the problem so that the spectrum being estimated upon goes to zero at the origin. This seems to be necessary because the bias contributions from a non-smoothness in which the spectrum goes to zero are not nearly as serious as those where the spectrum increases appreciably.

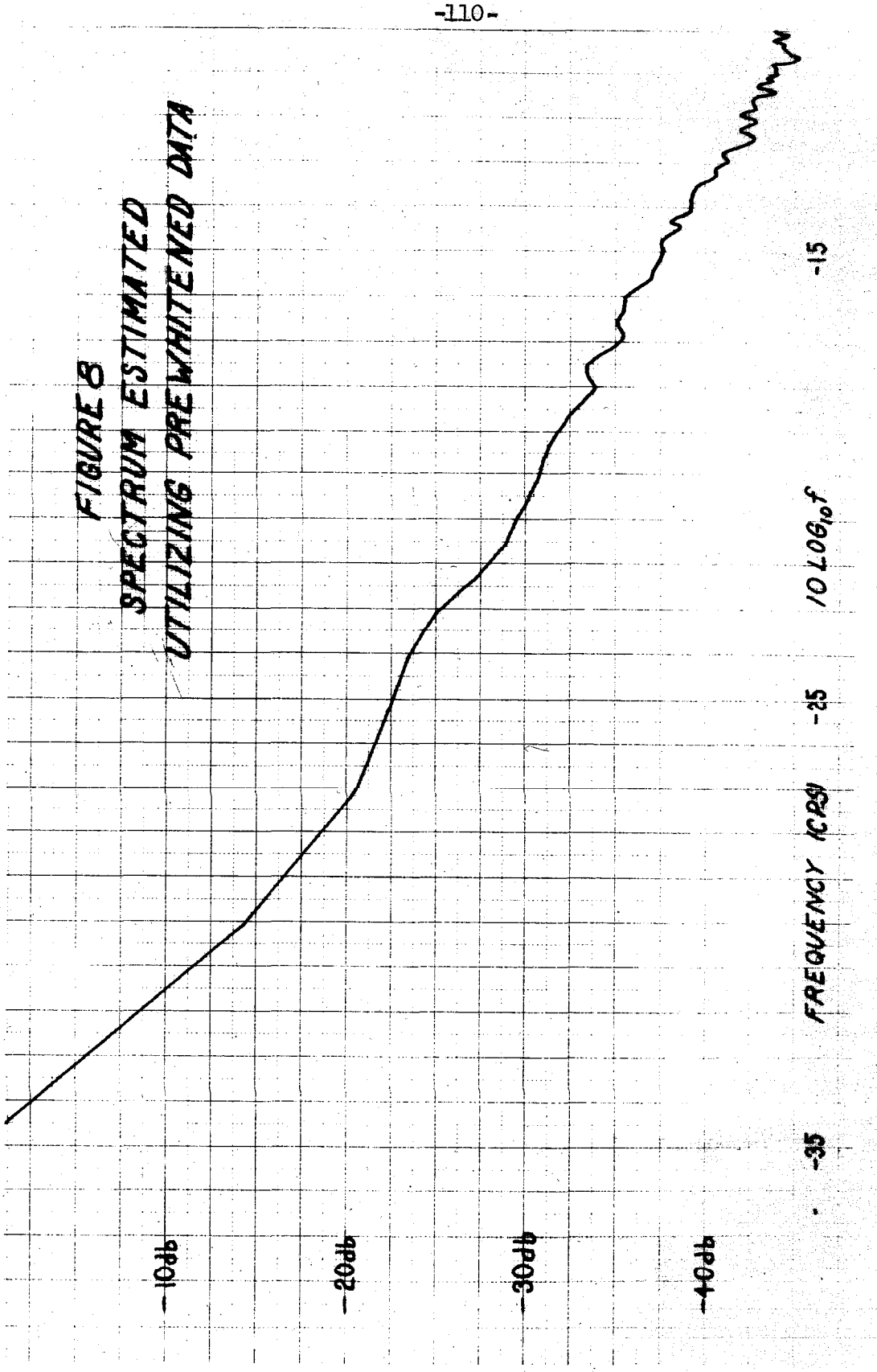
FIGURE 8
SPECTRUM ESTIMATED
UTILIZING PREWHITENED DATA
-10db
-20db
-30db
-40db
-35
-25
-15
FREQUENCY (CPS)
10 LOG10 f

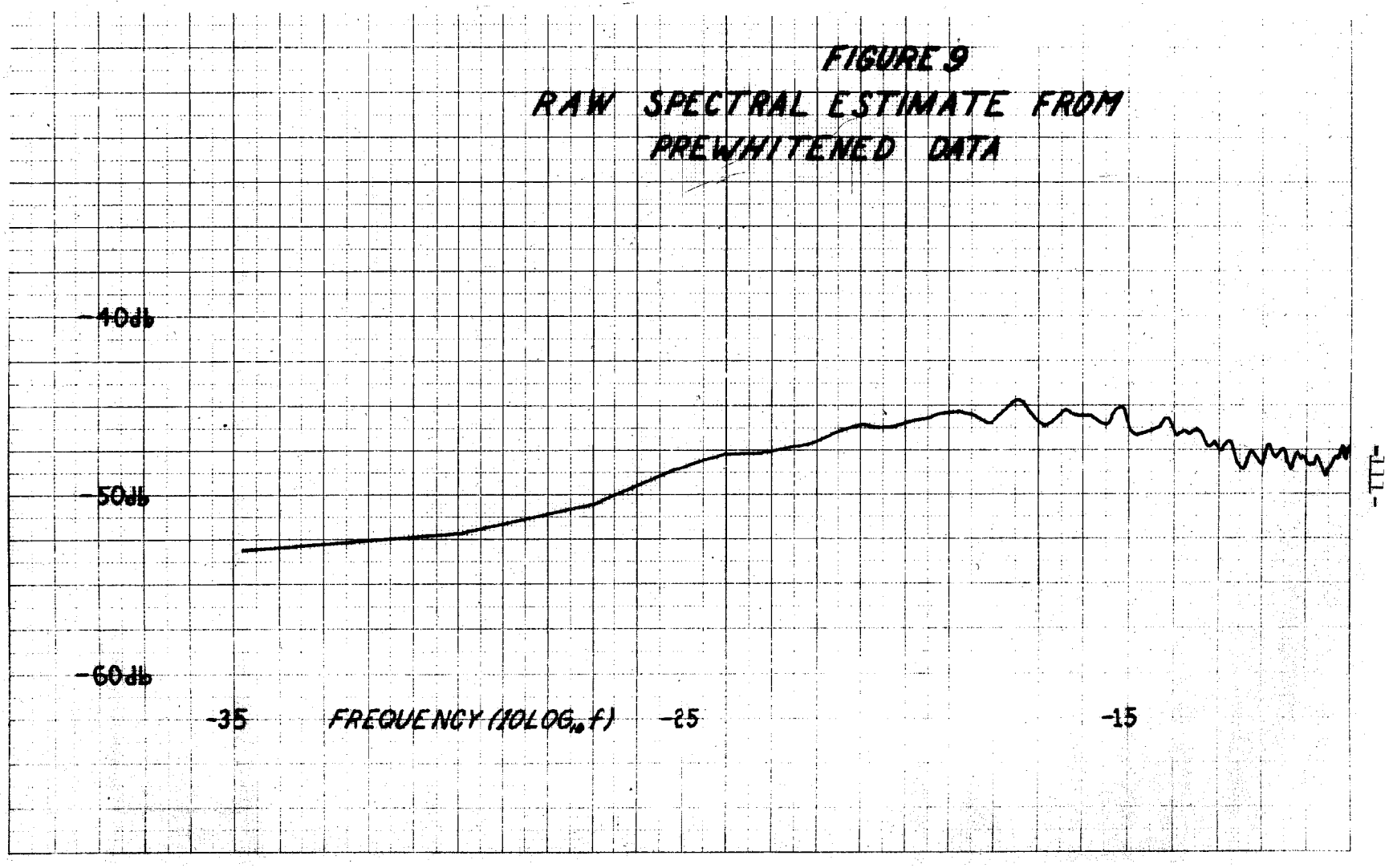
FIGURE 9
RAW SPECTRAL ESTIMATE FROM
PREWHITENED DATA
-40db
-50db
-60db
-35
FREQUENCY (10LOG10 f)
-25
-15

3.3.3 Impulsive or Step Type Disturbances

At the very practical level a severe bias is often introduced by impulsive or step type disturbances in the data. The question is, "What is the effect on the power spectral density estimate of a big glitch in the raw data?"

First consider the simple case of one isolated "bad point." Suppose out of our N discrete samples x_i one is equal to a large constant A, say

$$x_i' = \begin{cases} x(t = i\Delta t) = x_i & i = 1, N \quad i \neq K \\ A & i = K \end{cases} \Bigg\} \; A \gg \sigma \qquad (114)$$

where we shall assume that A is much larger than the RMS value of the noise because this is the case of interest. If A is the same order as σ, not only would the effects be greatly reduced, but it would presumably be difficult to decide that the point was "bad." The sketch below illustrates the situation under consideration.

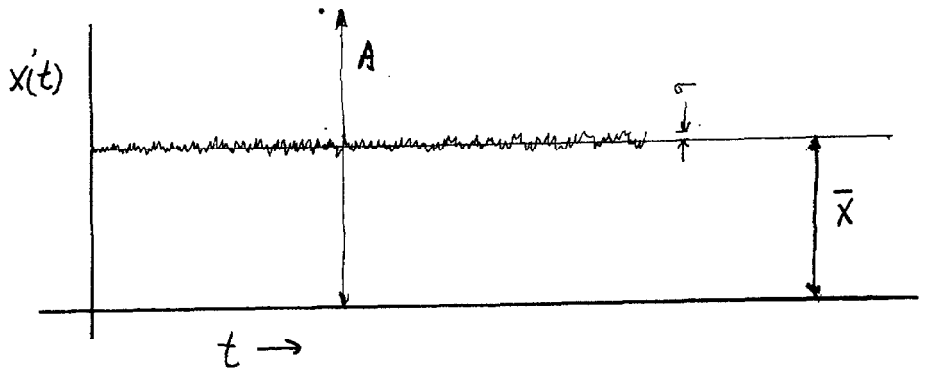

This new random process is, of course, non-stationary and a spectral density for it is nonsense.* However, as a practical matter it is important to know the properties of such data since this situation occurs fairly often. In particular, it is pertinent to ask how a power spectral density estimated from this data by the usual techniques compares with the "real" spectrum of $x(t)$. On an intuitive basis it seems clear what the answer should be. The spectral estimator assumes that the waveform with which it is presented is a sample function from an ergodic random process. Thus, the real process must contain a "lot", in some sense, of "spikes" in the time domain. Therefore, it has a great deal of energy at even very high frequencies. Thus, the original spectrum of $x(t)$ must have been "whitened" in some way.

Computationally, the situation is even more clear. The record is shifted by itself and multiplied to form mean lagged products. Since A is much larger than σ the value for $C(o)$, i.e., the square of all the x_i's, will be essentially

$$C'(o) \approx C(o) + \frac{A^2}{N} - \frac{2\bar{x}A}{N} - \frac{A^2}{N^2} \approx C(o) + \frac{A^2}{N} \qquad (115)$$

where the first term is the "ordinary" result, the

* The non-stationarity is not, in fact, implied rigorously. It is possible to think of stationary ensembles from which this would be a typical sample. However, in most cases such processes are not very realistic physically.

last two terms arise because of the mean removal (see Equation (77)), and $\bar{x}$ is the sample mean excluding A. The other mean lagged products are changed only by terms on the order of $\approx A/N$ which are much smaller. It is now clear that, since C(o) is an estimate of σ_x^2, if

$$A >> \sqrt{N}\,\sigma$$

there will be trouble. In this case

$$C'(o) >> C(o)$$

$$C'(R) \approx C(R) < C(o) \quad R > 0$$

which is the estimator's best approximation to "white" noise, i.e., a δ function in τ. Another way of viewing this is that when the finite cosine transform is computed via Equation (65) the C(o) term will dominate. The raw spectral estimates, V_R's, as well as the windowed spectral estimates, U_R's will be approximately constant

$$\hat{S}\left(\frac{R}{2M\Delta t}\right) = V_R \approx U_R \approx \Delta t\, C'(o) \approx \frac{\Delta t A^2}{N} \qquad (116)$$

Thus the estimated spectrum will, in fact, be "white." A significant point which should not be overlooked is that the disturbance in the frequency domain goes as the square of the amplitude in the time domain.

An excellent illustration of this behavior in action is given by Figure (10). This is a plot of an estimated spectrum from N = 6230 points of which one is in error and equal to A = 3.04 . The "real spectrum" is plotted below for comparison and from it we determine that $\sigma = .0136$ and $\bar{x} = .664$ and for this run $\Delta t = 5$ sec so that the level of the incorrect "white" spectrum agrees well with the approximate prediction of Equation (75) (ie. -21db).

The case of a number of isolated "bad" points possibly of different heights A_i becomes slightly more complex. It seems clear that the basic "whitening" will still take place and that we will have something like $V(R) \approx \frac{\Delta t}{N} \Sigma A_i^2$. But if any of the disturbances are within $M\Delta t$ (the largest lag estimated) of each other there will be, in addition, another large term in the correlation function estimate. This will in turn lead to a spike in the spectral density at the corresponding frequency. Note that this implies the A_i involved occur within the same M/N th fraction (something like 1/100th for our data) of the data.

Next, consider the case of series of adjacent "bad points." Suppose the available signal is just the

FIGURE 10
ESTIMATED SPECTRUM
ILLUSTRATING IMPULSIVE TYPE BIAS

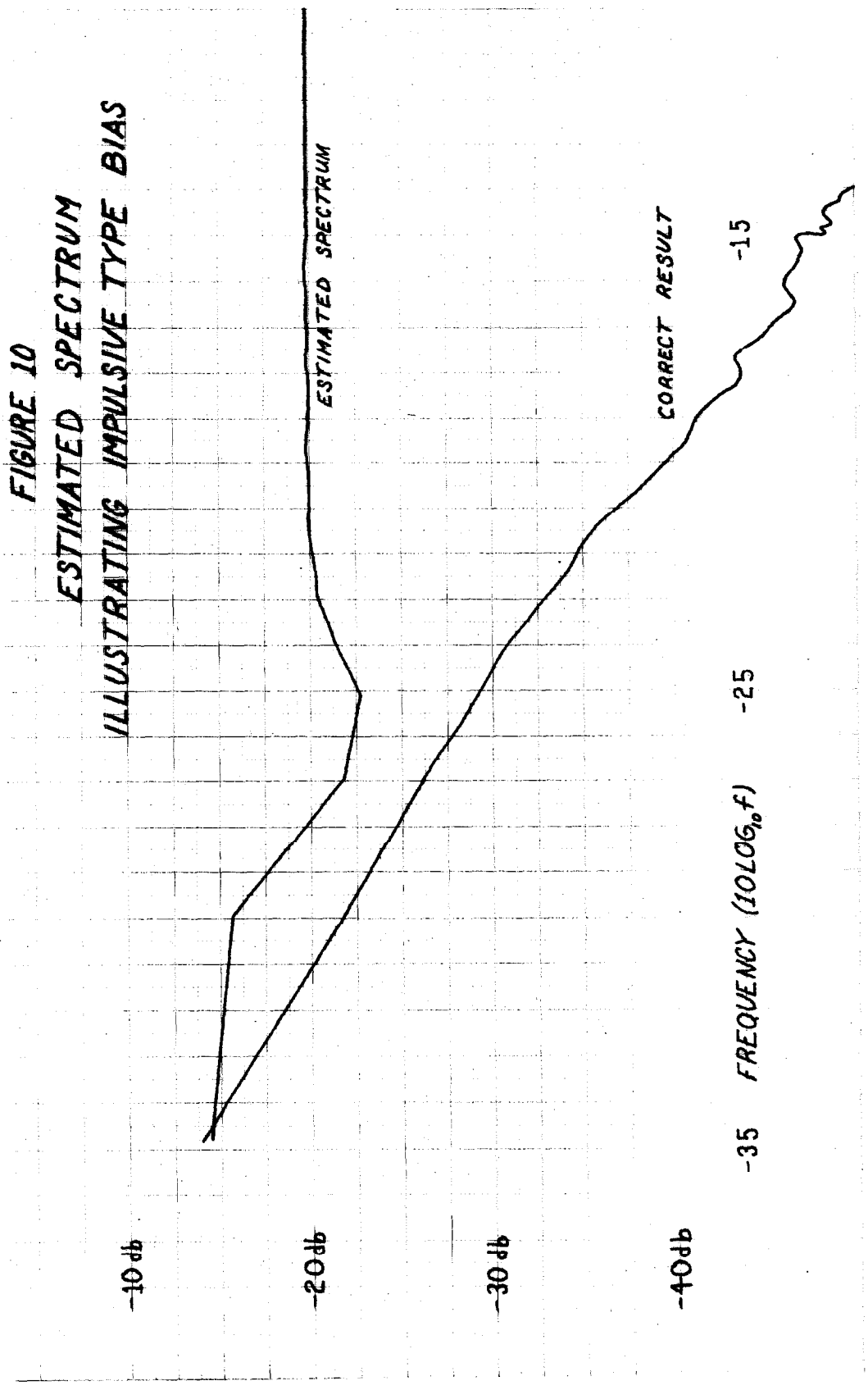

sampled noise everywhere except at K consecutive points where it is larger by A;

$$x_i' = \begin{cases} x_i & o \le i \le k \ , \ K + k \le i \le N \\ A + x_i & k \le i \le k + K \end{cases} \qquad (117)$$

so that the situation is as sketched below where again we have assumed $A \gg \sigma$ (but not necessarily $A \gg \bar{x}$).

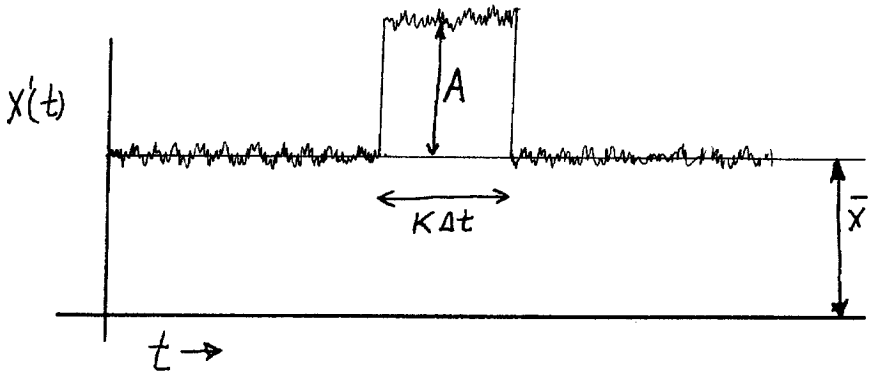

As before $x'(t)$ is decidedly non-stationary, barring an inventive job of ensemble creation, and we shall only ask what the effect is on the estimated spectrum. There seems to be two distinct cases of interest depending on length of the disturbance.

First, suppose that $K \ll M$ and the disturbance is still short relative to the maximum correlation function lag estimated. Then the correlation function at zero

will be given by

$$C'(o) = \frac{1}{N} \sum_{i=o}^{N} x_i^2 + \frac{KA^2}{N} + \frac{2A}{N} \sum_{i=k}^{k+K} x_k^2 - \frac{\bar{x}^2}{N} - \frac{2K\bar{x}}{N} A - \left(\frac{K}{N} A\right)^2 \quad (118)$$

which since $K \ll M \ll N$ becomes approximately

$$C'(o) \approx C(o) + \frac{KA^2}{N} \quad (119)$$

and similarly

$$\begin{aligned}
C'(1) &\approx C(1) + \left(\frac{K-1}{N}\right) A^2 \\
C'(2) &\approx C(2) + \left(\frac{K-2}{N}\right) A^2 \\
&\cdot \quad \cdot \quad \cdot \\
&\cdot \quad \cdot \quad \cdot \\
&\cdot \quad \cdot \quad \cdot \\
C'(K-1) &\approx C(K-1) + \frac{1}{N} A^2 \\
C'(K) &\approx C(K) \\
&\cdot \quad \cdot \\
&\cdot \quad \cdot \\
&\cdot \quad \cdot \\
C'(M) &\approx C(M)
\end{aligned} \quad (120)$$

Thus, the estimated correlation function will be approximately the ordinary estimate plus a triangle of height A^2/N and

width $K\Delta t$ as illustrated schematically in the sketch. This implies

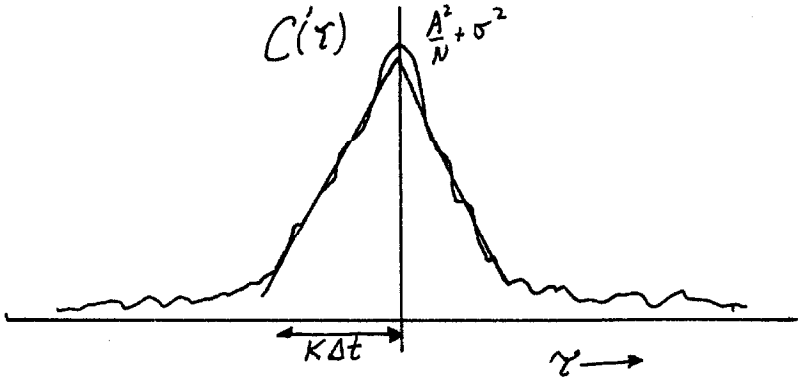

that the spectral estimate $\hat{S}'(f)$ will be approximately the ordinary estimate plus the Fourier transform of the triangle which is a $\left(\frac{\sin x}{x}\right)^2$ of height $\frac{A^2 K\Delta t}{N}$ and width $\frac{1}{K\Delta t}$ centered at the origin. As $K \to 1$ this $\left(\frac{\sin x}{x}\right)^2$ extends over the whole estimation bandwidth and whitens the data in agreement with the discussion above. But as K increases the effective area of the disturbance in the frequency domain shrinks back toward the origin.

Figure (11) illustrates this type of bias in action. The "real" spectrum is also shown and from its calculation we learn that $\bar{x} = -.078$, $\sigma = .36$, while for this run Δt was 5 minutes and N was 10000. The data leading to the biased curve had 10 points 10 times too large i.e., $A \approx 3.0$. Here we have that

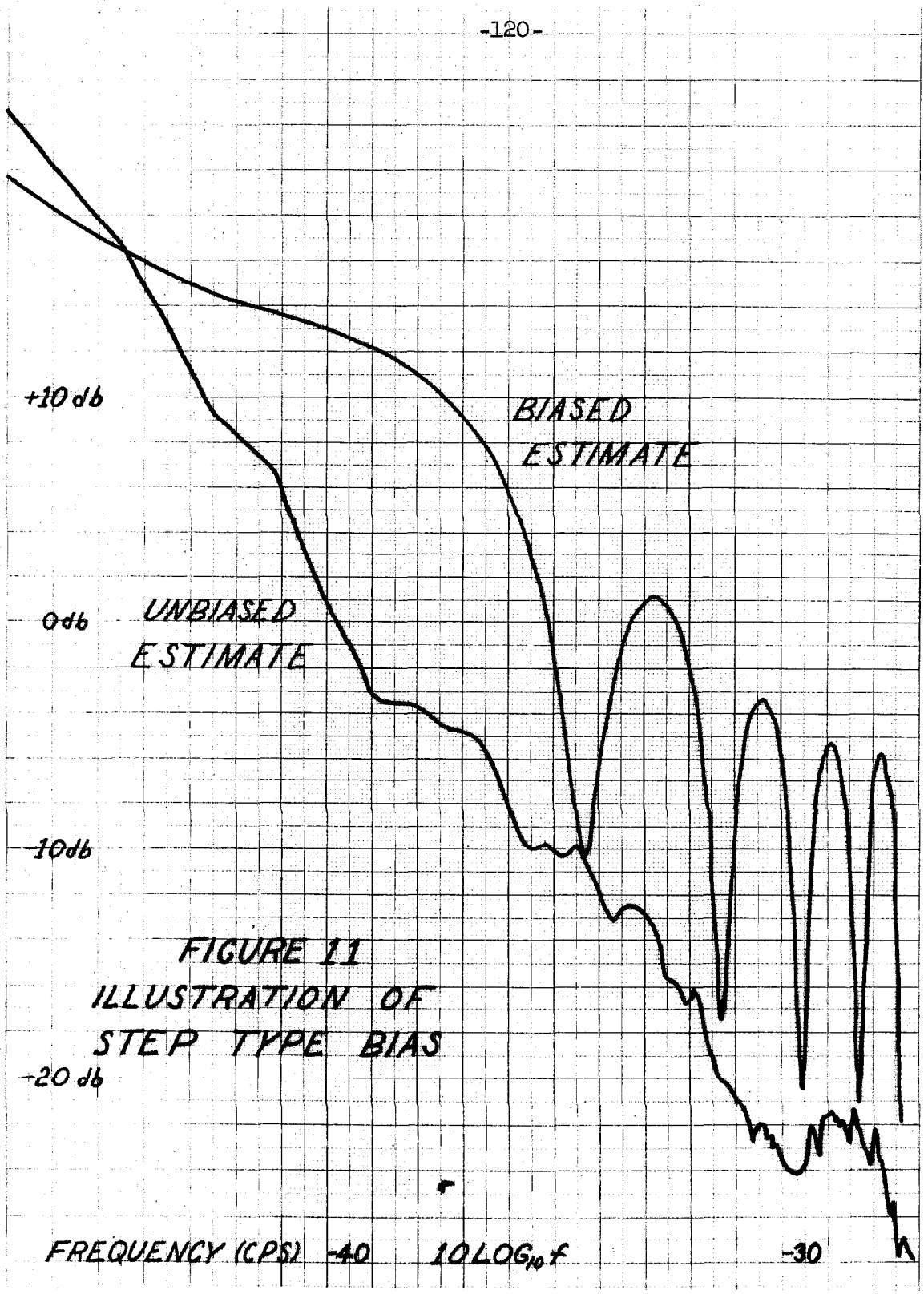

FIGURE 11
ILLUSTRATION OF
STEP TYPE BIAS

$\frac{K}{M} = 1/10$ and this corresponds to the point at which the first large dip in the biased spectrum occurs. The other zeros of the $\left(\frac{\sin x}{x}\right)^2$ curve also show up as large dips since the correct result is "down" a large distance even on a logarithmic scale. For anyone unfamilar with the distortions introduced by a log-log scale a glance at Figure (12) will be helpful in the sense of "calibration." It shows another function, the hanning window (see Section (3.1.2)) which is not a $\left(\frac{\sin x}{x}\right)^2$ but of similar shape, plotted on a log-log scale.

As the second case suppose K >> M and the disturbance takes up a large fraction of the record. Now, of course, it is perhaps presumptuous to specify either case as the "disturbance" but this can be accounted for by the sign of A and the analysis is unaffected. Returning to the formula for the calculation of the mean lagged products including the mean removal, Equation (77), and utilizing our definition of x_i, Equation (114), we see that the new correlation function is expressible in terms of the old as

$$C_R' = C_R + \frac{1}{N-R}\left\{A\sum_{i=k=R+1}^{k} x_i + A\sum_{i-k+1}^{k+K-R} x_{i+R} + A\sum_{i=k+1}^{k+K-R} x_{i+R} + A\sum_{i=k+K-R+1}^{k+K} x_{i+R}\right\} - \frac{2\bar{x}KA}{N} - \left(\frac{AK}{N}\right)^2 + \frac{A^2(K-R)}{N-R}$$

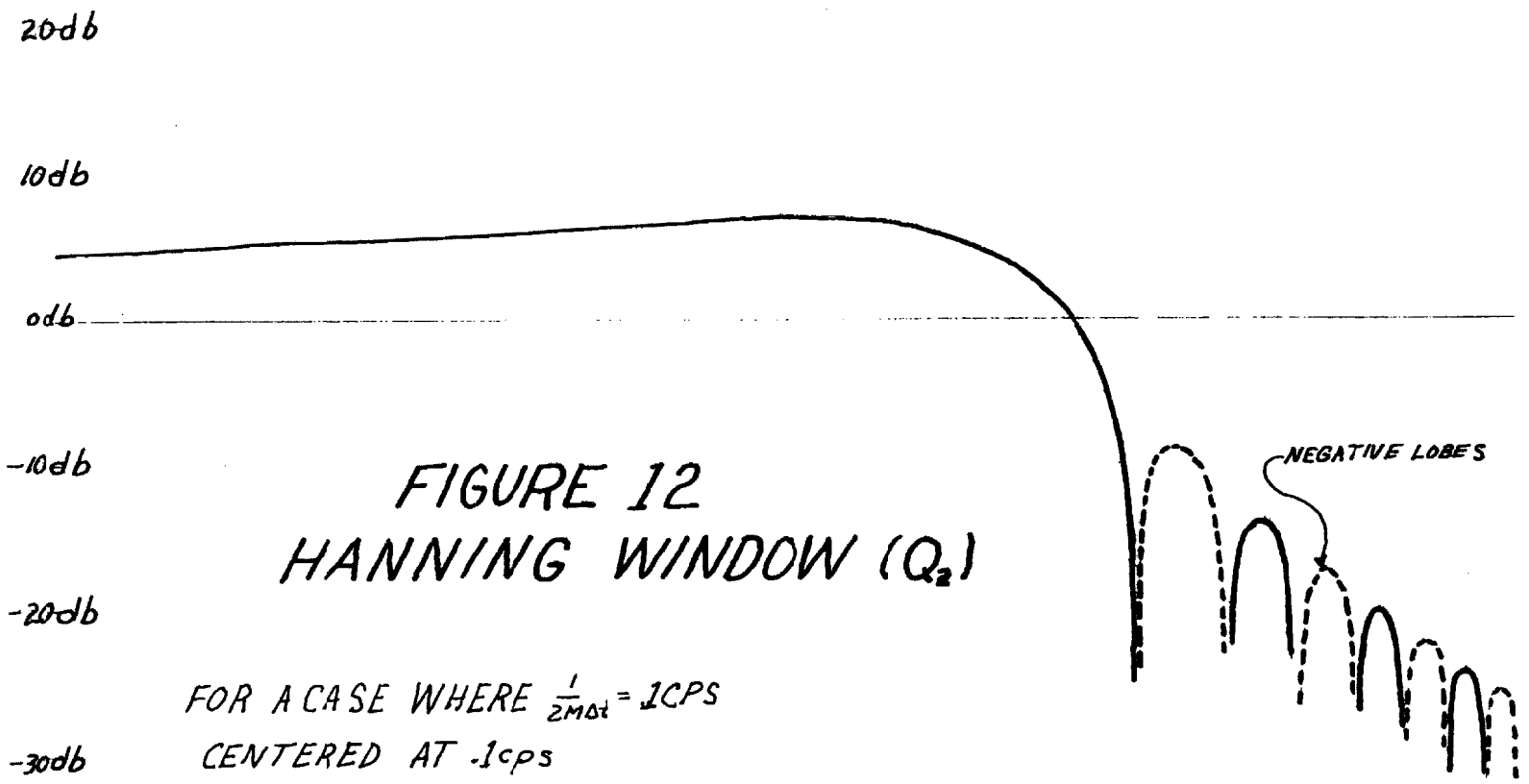

FIGURE 12
HANNING WINDOW (Q_2)

FOR A CASE WHERE $\frac{1}{2M\Delta t} = .1CPS$
CENTERED AT .1cps

which simplifies to $C'(R) = C(R) + f(R)$ where

$$f(R) = \frac{A}{N-R}\left\{\sum_{i=k-R+1}^{k+K+R} x_i + \sum_{i=k+R+1}^{k+K-R} x_i - 2\bar{x}K\left(1 - \frac{R}{N}\right)\right. \qquad (121)$$

$$\left. + A\left[K\left(1 - \frac{K}{N}\right) - R\left(1 - \frac{K^2}{N^2}\right)\right]\right\} \qquad (\bar{x} > 0)$$

If x_i is written as a fluctuation about its mean, $\bar{x}$, the small correction term on the $\bar{x}$ coefficient will be the only $\bar{x}$ contribution remaining i.e., for $x_i \triangleq \bar{x} + \delta_1$

$$f(R) = \frac{A}{N-R}\left\{\sum_{i=k-R+1}^{k+K+R} \delta_i + \sum_{i=k+R+1}^{k+K-R} \delta_i + 2\bar{x}\,\frac{KR}{N}\right. \qquad (122)$$

$$\left. + A\left[K\left(1 - \frac{K}{N}\right) - R\left(1 - \frac{K}{N}\right)^2\right]\right\}$$

where the δ_i summations will vanish if the expected value is taken since they are zero mean. It is now clear that because $N \geq K >> M \geq R$, $f(R)$ is always positive. Rewriting Equation (121) and taking the expected value we see that

$$E\left[f(R)\right] = \frac{A}{N-R}\left\{AK\left(1 - \frac{K}{N}\right) + R\left(\frac{2\bar{x}K}{N} - A\left(1 - \left(\frac{K}{N}\right)^2\right)\right)\right\} \qquad (123)$$

By expanding the denominator and combining terms this can be put in the form

$$E\left[f(R)\right] = a + bR + cR^2 + \ldots\ldots \qquad 0 \le R \le M$$

where

$$\begin{aligned} a &= A^2 \frac{K}{N}\left(1 - \frac{K}{N}\right) \\ b &= \frac{A}{N}\left[2\bar{x}\frac{K}{N} - A\left[1 - \left(\frac{K}{N}\right)\right]\right] \\ c &= \frac{A}{N^2}\left[2\bar{x}\frac{K}{N} - A\left(1 - \frac{K}{N}\right)\right] \\ &\cdot \quad \cdot \quad \cdot \\ &\cdot \quad \cdot \quad \cdot \\ &\cdot \quad \cdot \quad \cdot \end{aligned} \tag{124}$$

Thus f(R) is, on the average, a linear increasing term added to the correlation function ($R > 0$).

For 1/f type spectra the correlation functions decay in the τ domain rather smoothly. For instance, as $\ln \tau$ for 1/f noise and $e^{-\tau}$ for $1/f^2$ noise. Thus, the addition of the step to the data will cause the correlation function decay in τ to be more gradual. This implies a faster decay, i.e. steeper slope, in the frequency domain because of the Fourier transform relationship. Hence, the effect of the step is to bias the spectral density "upward" at the low frequency end. This would imply estimating an a in $1/f^a$ which was too large.

To obtain a quantitative measure for the size of this effect we shall calculate the spectral estimate that would arise from f(R) alone via Equation (76) for the V's. Thus,

$$E\left[V_R\right] = \Delta t \left[a + 2\sum_{q=1}^{M-1} (a + bq) \cos q \frac{R\pi}{M} + (a + bM) \cos R\pi\right]$$

The effect of the constant "a" in the C's is to add $2Ma\Delta t$ to V_o while leaving the other V's unaffected. Therefore, the only terms which will contribute to the V_r for $R > 0$ are the b terms. Thus,

$$E\left[V_R\right] = b\Delta t \left[M(-1)^R + 2\sum_{q=1}^{M-1} q \cos q \frac{R\pi}{M}\right]$$

which by utilizing Jolley 428 [15] becomes

$$E\left[V_R\right] = b\Delta t \begin{cases} M^2 & R = 0 \\ -\dfrac{1}{\sin^2 \frac{R\pi}{M}} & R \text{ odd} \\ 0 & R \text{ even} \end{cases} \qquad (125)$$

Now including the V_o contributions from the a term we have for the bias in a Q_o estimate from this "long step"

effect

$$E\left[V_R\right] = \Delta t \begin{cases} bM^2 + 2aM & R = 0 \\ \dfrac{-b}{\sin^2 \frac{R\pi}{2M}} & R \text{ odd} \\ 0 & R \text{ even} \end{cases} \tag{126}$$

Therefore, the Q_2 biases would be given by

$$E\left[U_R\right] \approx M\Delta t \begin{cases} a + \dfrac{Mb}{2}\left[1 - \left(\dfrac{2}{\pi}\right)^2\right] & R = 0 \\ \dfrac{a}{2} + \dfrac{Mb}{4}\left[1 - 2\left(\dfrac{2}{\pi}\right)^2\right] & R = 1 \\ \dfrac{-b}{2M \sin^2 \frac{R\pi}{2M}} & R \geq 2 \end{cases} \tag{127}$$

An illustration that this analysis is reasonably correct is given by the following set of data. Figure (3) shows a spectrum from the Mark I noise source derived from 10000 raw data points taken at 5 second intervals. Because a number of independent measurements were made this estimate is believed to approximate the actual spectral density well over this region (see Section 5.2 below). This spectrum is a Q_2 estimate from data pre-whitened for 1/f and is plotted from -60 db to -10 db vertically with the frequency scale running (logarithmically) from 10^{-4} cps to 10^{-1} cps. The raw data for this run is very "smooth" in the sense of lacking step or impulsive type disturbances. Figure (13)

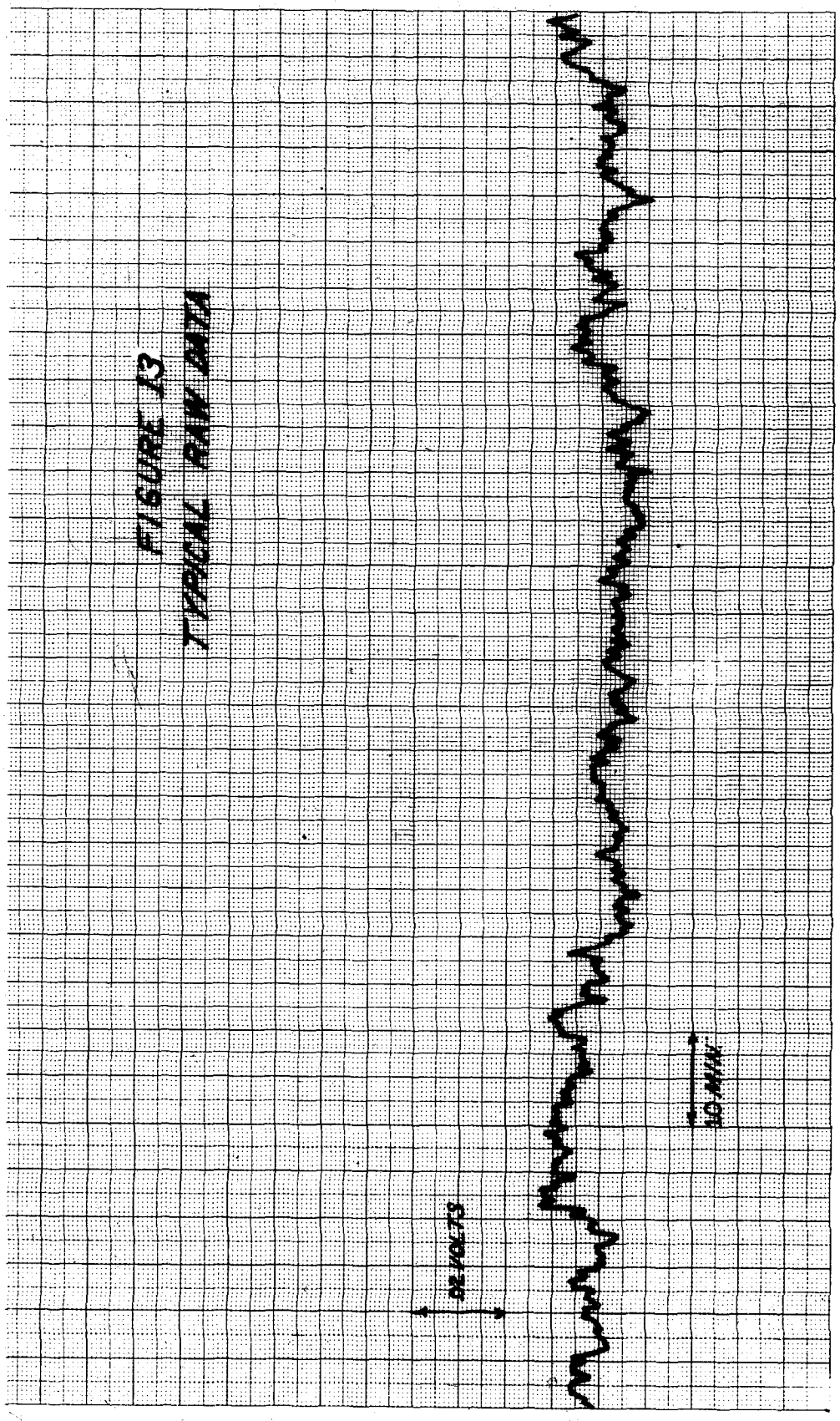

FIGURE 13
TYPICAL PAM DATA

shows a section of 1/ 11th of the raw data. The vertical scale is + .55 to + .75 volts and the horizontal scale is such that the data shown covers 150 minutes of time (900 points). The sample mean for this data (all 10000 points) is a .5986399. Assuming the noise to be gaussian the square root of the correlation function estimate at the origin is an estimator for σ, the rms value. In this case we find $\sigma \approx .00770$. A step was intentionally inserted in the "middle half" of the data. In the notation used above this is

$K = N/_2 = 5000$, $k = 2500$

The size of the step, A, was varied through the values .01, .05, .1, .2. Since for this data M = 100, $\Delta t = 5$ this yields for a and b the values shown in Table (8)

A	a	b	a(empirical)	b(empirical)
.01	2.5×10^{-5}	5.94×10^{-7}	4.06×10^{-5}	5.96×10^{-7}
.05	62.5×10^{-5}	28.7×10^{-7}	70.3×10^{-5}	28.9×10^{-7}
.1	250×10^{-5}	54.9×10^{-7}	266×10^{-5}	55.3×10^{-7}
.2	1000×10^{-5}	99.7×10^{-7}	1031×10^{-5}	100.6×10^{-7}

TABLE (8)

If a and b are formed exmpirically from the data via

$$a(\text{empirical}) \triangleq C'(o) - C(o)$$

$$b(\text{empirical}) \triangleq \frac{[C'(M) - C(M)] - [C'(o) - C(o)]}{M}$$

the last two columns in this table result. These results are seen to agree with the analytical predictions quite well. Perhaps a more impressive illustration is given by Figure (14), which shows the correlation function estimated from the data with no step, C(R), and the correlation function estimated from the data with a step of .01, C'(R). The other line on the graph is their difference which exhibits a surprising linearty. In fact, the deviation at the uppermost end is adequately explained via the cR^2 terms of Equation (124).

The results in spectral density are not as easily displayed. Table (9) presents the calculated Q_2 bias for R = 0, 1, and 6, from Equation (127) using the calculated values for a and b along with the empirical biases obtained by substracting the known correct result from the estimated value. Again the calculated results would only be expected to equal an ensemble average of the empirical results so the agreement is quite good. Figure (15)

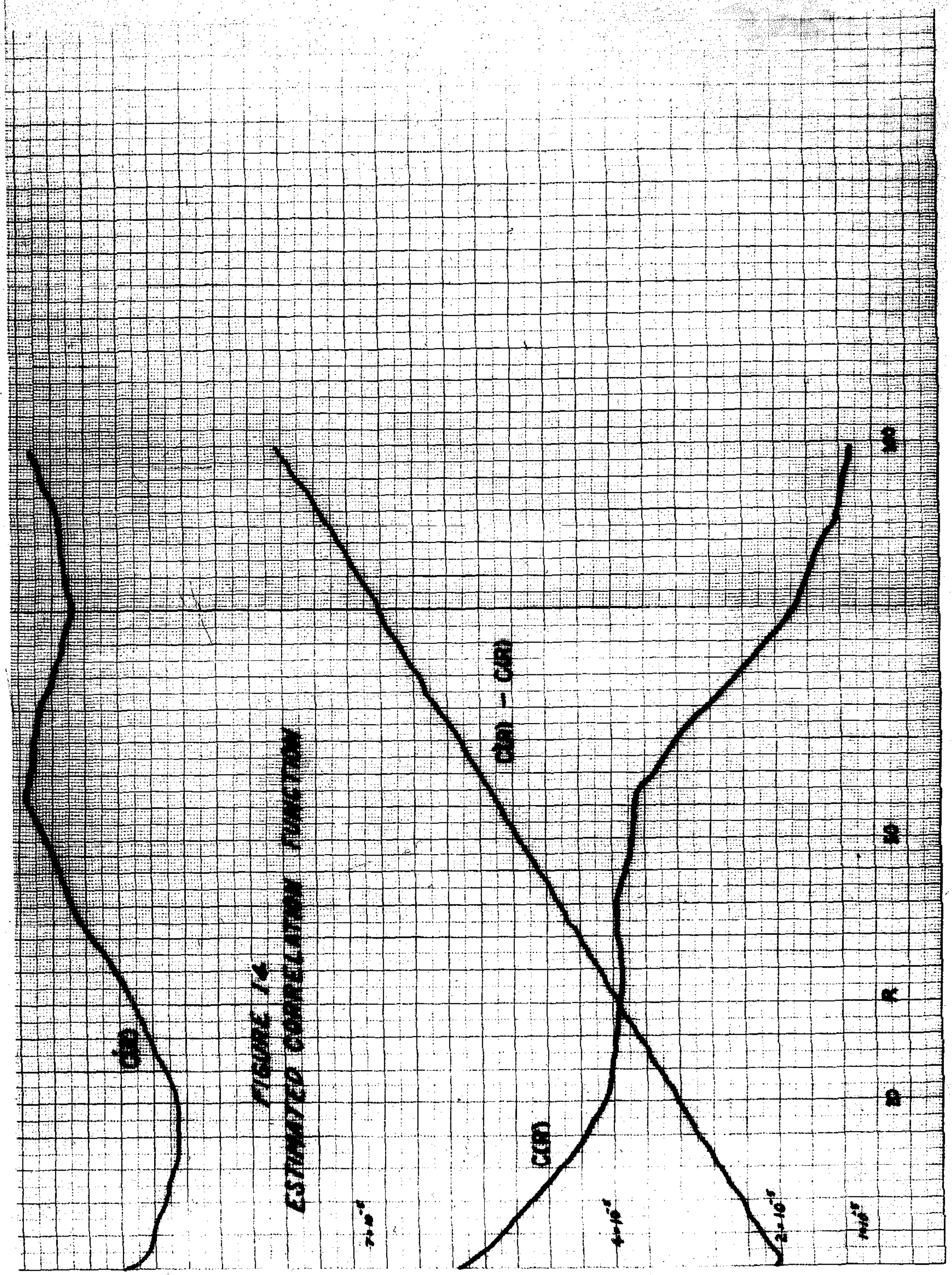

FIGURE 14
ESTIMATED CORRELATION FUNCTION

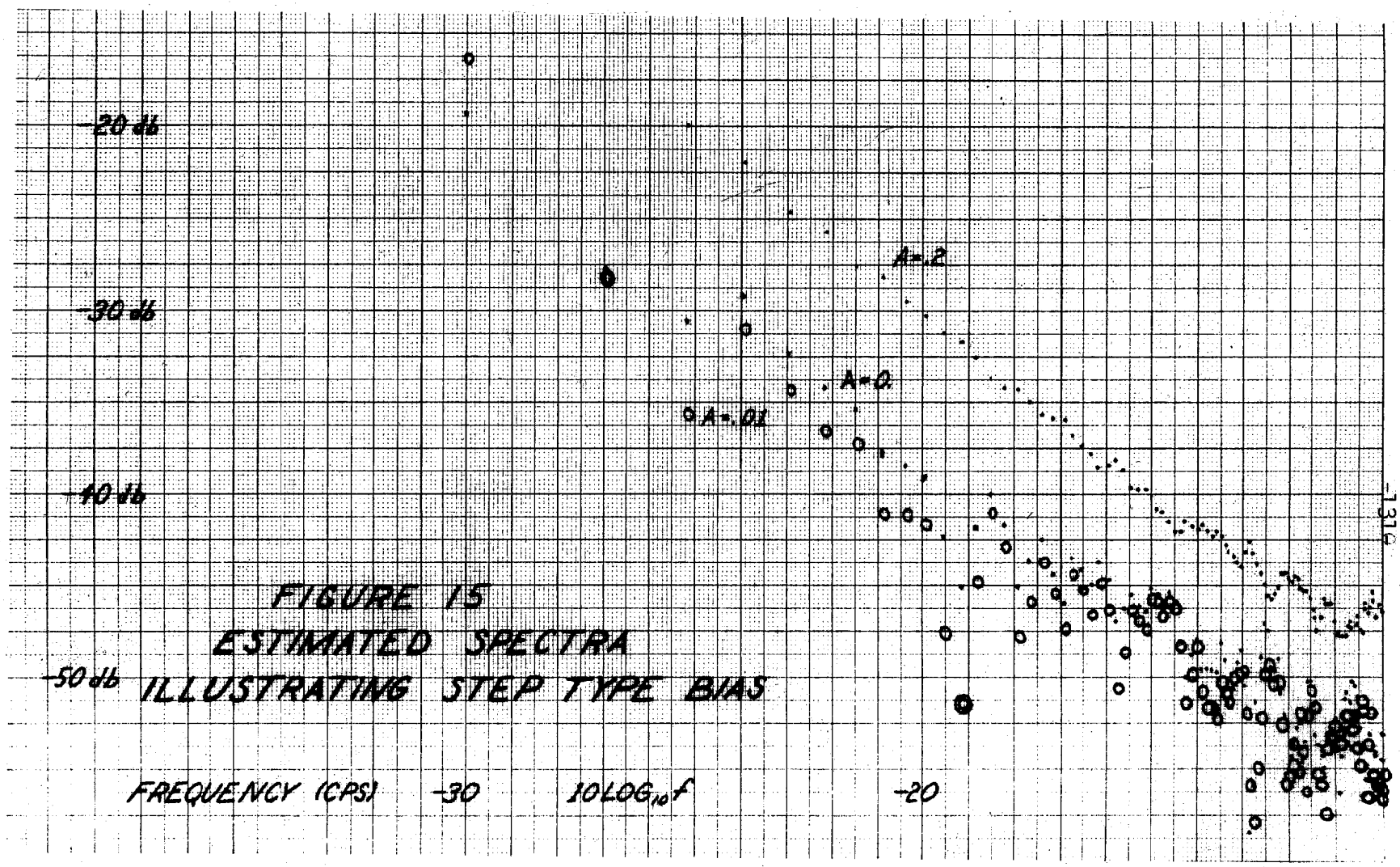

FIGURE 15
ESTIMATED SPECTRA
ILLUSTRATING STEP TYPE BIAS

Q_2 Spectral Estimate

Calculated

A	R = 0	R = 1	R = 6
.01	+ 2.139×10^{-2}	+ $.77 \times 10^{-1}$	- 1.65×10^{-4}
.05	+ 3.56×10^{-1}	+ 1.634×10^{-1}	- 8.02×10^{-4}
.1	+ 1.332	+ 6.39×10^{-1}	- 15.35×10^{-4}
.2	+ 5.15	+ 2.52	- 27.9×10^{-4}

Empirical

A	R = 0	R = 1	R = 6
.01	+ 1.929×10^{-2}	+ 1.148×10^{-2}	- 1.74×10^{-4}
.05	+ 3.98×10^{-1}	+ 1.824×10^{-1}	- 8.85×10^{-4}
.1	+ 1.423	+ 6.767×10^{-1}	- 16.90×10^{-4}
.2	+ 5.36	+ 2.601	- 30.77×10^{-4}

TABLE (9)

shows three spectral densities. These are Q_2 estimates where no prewhitening was applied and are thus poor estimates of the real spectrum (i.e., see bias discussion for $1/f^2$ noise in Section 3.3.2). However, the difference between the curves indicates the effect of the "long step" type bias. One is the estimated spectrum for no step (points). The second is for a step of .01 (circles). The third is for a step of .2 (points). This is a log-log scale. As the step bias begins to dominate all of the

estimated points become negative. The logarithm of their magnitude is plotted. The curve for A = .2 is all negative. There are no negative points on the spectrum for A = 0 and only the two points doublecircled (R = 2 and R = 12) are negative for the A = .01 case. The bias is as advertised in Equation (127), negative, increasing with A, and decreasing with R. But since the correct spectrum is decaying as $1/f^2$ and the bias also decays as $1/f^2$ it appears to remain a constant percentage which is a fixed displacement on a logarithmic scale. The R = 0 point is not plotted on these curves. The intermediate spectra for A = .05, .1 are not plotted to reduce the confusion somewhat. By the time the step is as large as .2 the spectrum is always negative and very smooth because all of the variability contributed by the original random process has disappeared. It is interesting to note the amount of success that prewhitening achieves in reducing the effects of this bias. Figure (16) shows the Q_2 prewhitened 1/f estimates for A = .01, .05, .1, .2. The curve for the smallest step .01 coincides nearly exactly with the undisturbed case. The bias does increase with step size although not as severely in the unprewhitened case. Also, no points are negative in

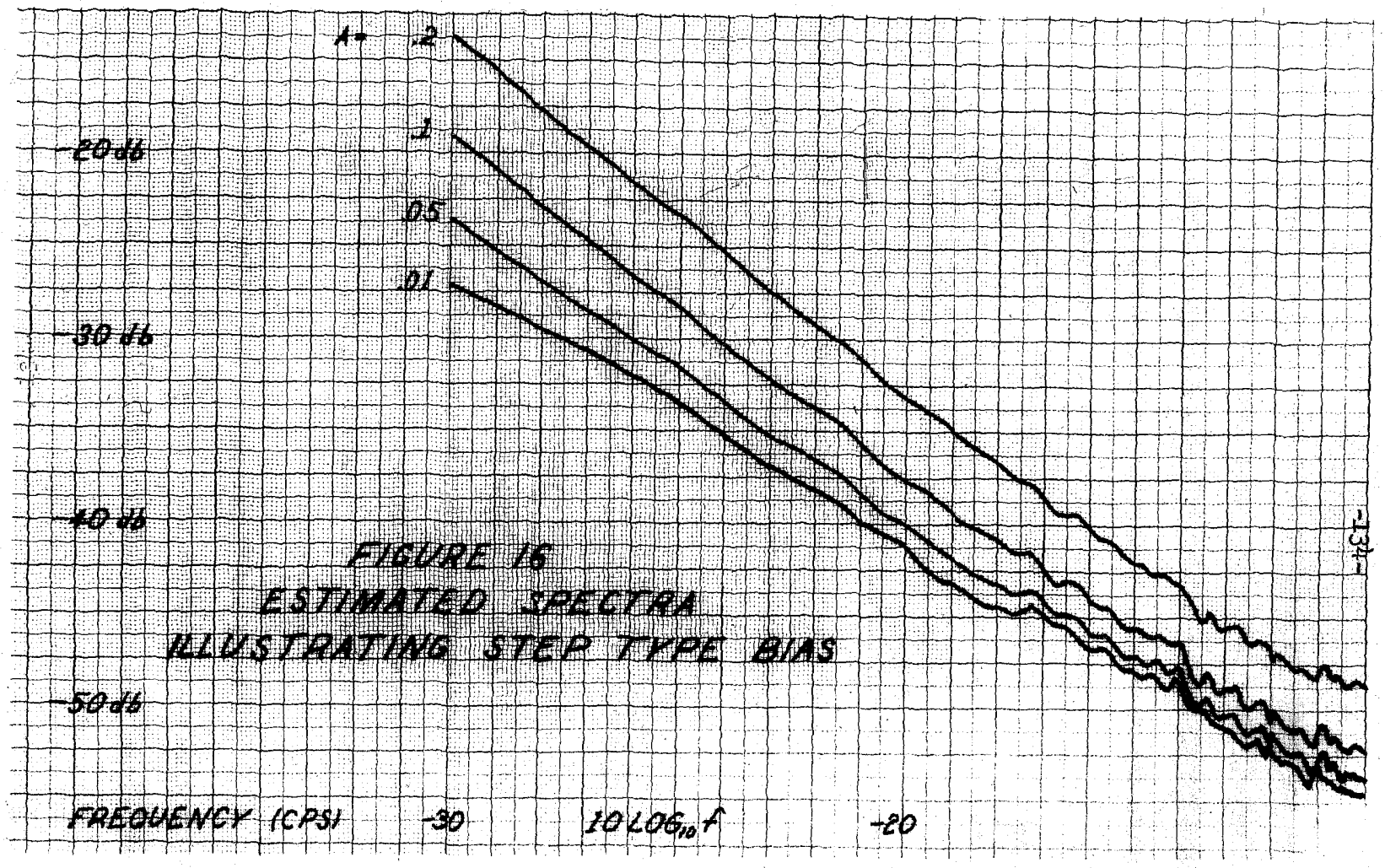

FIGURE 16
ESTIMATED SPECTRA
ILLUSTRATING STEP TYPE BIAS

the prewhitened case so that the bias effect has in fact been reduced a great deal. When you consider that a step of .2, in a piece of data for which $\sigma \approx .0077$, is a 26σ disturbance these results are quite remarkable.

4. LOW FREQUENCY SPECTRAL ESTIMATION EXPERIMENTS

The major portion of the experimental work of this thesis is concerned with obtaining estimates of the power spectral density of 1/f noise or excess noise in semiconductors. This section discusses the planning and motivation of the experiments. Also covered is the design of the noise generator and the measurement of some of its basic circuit properties. The experimental results themselves are presented below in Section 5.

4.1 1/f Noise

The basic motivation for investigating 1/f noise is that the questions are interesting. The answers may, in fact, turn out to be very dull, but the questions are intriguing.

Is the phenomenon really 1/f? Winston and Firle, for instance, fitted a least squares line (on a logarithmic scale) through their data and claimed that the spectrum went as $1/f^a$ with $a > 1$. As Appendix A indicates, their conclusion is open to considerable question because of the grossness of their spectral estimator. The question of whether a simple exponential model is adequate to explain the data remains. But if the

behavior really is 1/f, how does one deal with the infinite power implied for the random process? Or does it stop being 1/f at some very low frequency? And if so, at what frequency?

As mentioned in Section 2. a knowledge of the real spectrum of low frequency semiconductor noise is required in order to design any piece of dc equipment which must operate for a long period of time. How long can it be left alone before the zero must be reset? If the time between calibrations is a design parameter, how should it be set to guarantee a given probability of not having the "drift" exceed a given value? How important is it in terms of drift to control the temperature variations is the immediate environment?

The experimental program undertaken in this thesis is not intended to investigate the solid-state physics of the generation of semiconductor noise. The objective is to measure the noise properties of the whole device, a transistor, in an operating circuit. From the experimental viewpoint the proper approach is to control everything (i.e., all relevant parameters of the circuit and its environment). Then by relaxing control on one item at a time the effect of each on the end result can be ascertained irrevocably The properties of ordinary transistors in ordinary circuits could then be calculated by noting what lack of control of the environment was implied in each case. Unfortunately, no one has yet been able to decide

exactly what environmental conditions require control and to what extent, let alone actually control them.

The basic difficulty is of a very practical mundane nature. The rms value of the noise generated by a transistor in normal operating circumstances is on the order of fractions of microvolts. Transistor operating voltages are at least fractions of volts. Therefore, a dynamic range of 10^6 is involved. In order to measure the noise one must be able to measure, record, and process variations which are seven or eight decades smaller than the mean operating voltages. This requirement can, of course, be eliminated step wise by successive amplification and subtraction of constants. Two major difficulties arise. First, one must either know in advance the constant or dc value which is present so that it may be taken out to an extremely high accuracy, or one must be very clever about taking it out "adaptively" in order not to distort the subsequent spectral estimation results. Secondly, one must always face the unpleasant reality that amplifiers have internally generated noise as well as limited dynamic range.

Considerations such as these led us to utilization of the concept of differential amplification. It was found that by surrendering on the goal of measuring the properties of one transistor directly and utilizing a grounded input differential

amplifier as our noise source we could obtain reasonable measurements in the laboratory. This implies in our case that we are actually measuring the difference properties of two transistors. This proves to be useful not only for eliminating the operating point effects, which can be adjusted to be the same for both transistors, but for eliminating the effects of external conditions such as temperature to which the two transistors react similarly. And, if one considers the two transistors to be statistically independent samples from the same ensemble, the spectrum measured is a constant times that for one transistor. Even if the net results were only the noise properties of a group of components in a particular configuration (which it will be argued is not the case) these results would still be useful because this specific combination, the dc differential amplifier, is very commonly employed.

The schematic for the particular noise generator used for most of the measurements of this thesis is shown in Figure (17) This device was constructed by H. C. Martel and will be referred to henceforth as the "Mark I." The first stage is the noise generator. The second two stages are only for amplification near the source in an attempt to minimize the introduction of external noise. The emmitter follower final stage, is mainly for impedance matching. It is desirable to

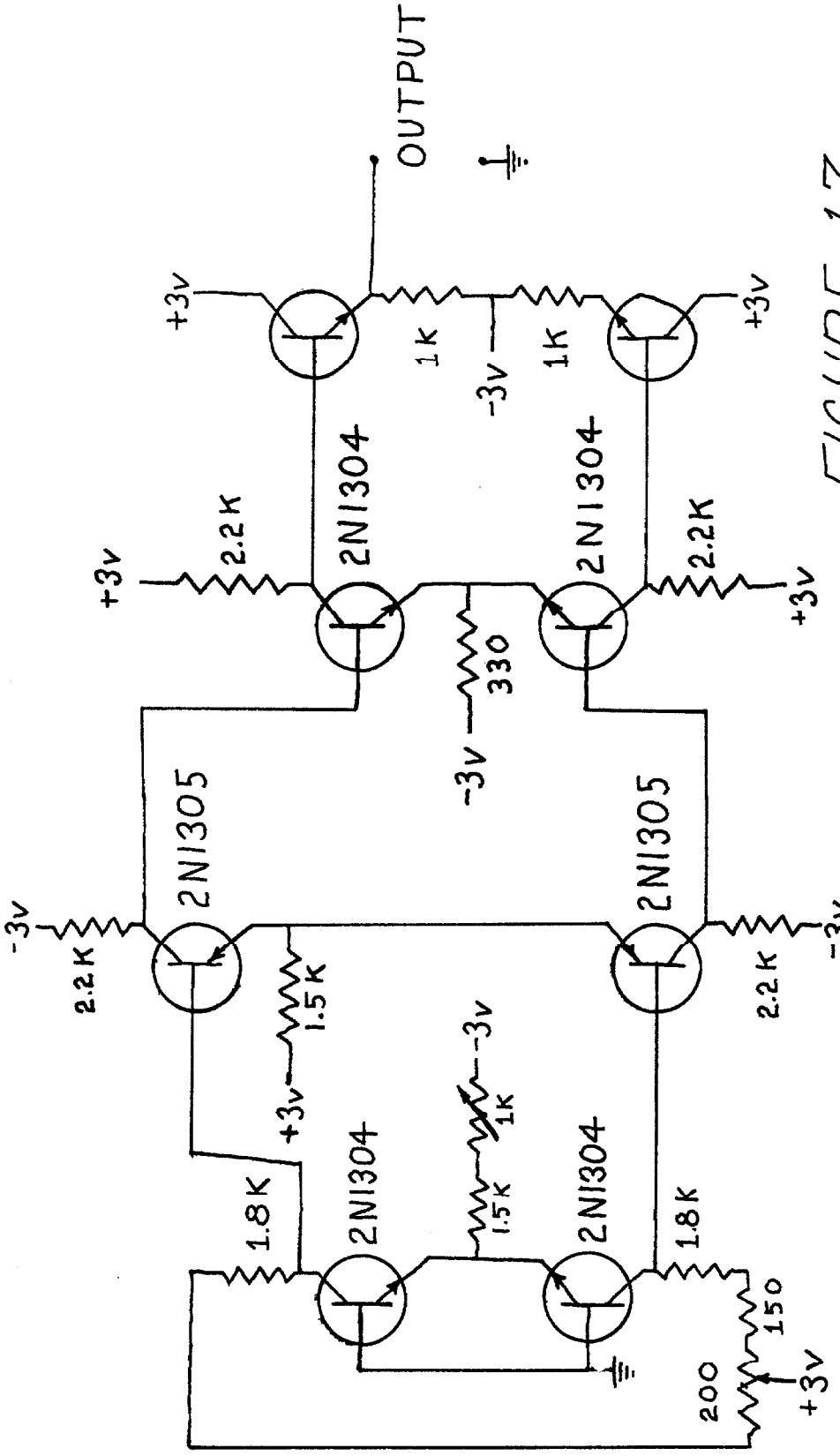

FIGURE 17

MARK I NOISE GENERATOR

have essentially a voltage source. The claim that the noise is contributed mainly by the first stage is substantiated by noting that the noise of the second stage would have to be larger than that of the first by a factor equal to the current gain of the first stage in order to make a significant contribution to the output. This argument extends, of course, to the next stage. First stage V_{be} variations appear in the output. This circuit is one often used in practice and it is the simplest version of the V_{be} variation cancelling configuration recommended by Hoffait and Thorton in Reference [16]. As mentioned above, amplification was provided internal to the noise generator because of the size of the semiconductor noise relative to the input drift/noise of readily available amplifiers, i.e., a typical operational amplifier has a few microvolts of drift/noise referred to its input. Really, this is begging the question because the stages of gain internal to Mark I have an equivalent drift referred to their input, which may or may not be as large as μ-volts. We actually measure the combined noise properties of the whole differential amplifier.

In any attempt to refer the measured spectral densities and rms values back to the input of the noise generator, the gain must be known. The measurement which was made was a transfer gain between voltage at the output and current of the

collector of the noise generating transistor (upper first stage in Figure (17)). This measurement was made with the circuit under operating conditions by injecting .374 μa in addition to the bias current point via a current source. In order to obtain a current source with a high enough impedance to guarantee no loading of the circuit, a 500 v power supply and a very large resistance was employed. The resistance was then varied and a differential transfer gain of about 1.07 volts output per micro-amp of current at this collector was measured. This is probably no better than a 5% measurement but it should be accurate enough for the desired applications.

In addition, to refer the assumed output properties back to the input, a differential mode gain for Mark I must be known. One form of approximate result can be obtained via the formualation of Reference [17]. Assume that the interstage loading can be ignored and that the equivalent internal emmitter resistance is on the order of 100 Ω. Then the differential mode gain, exclusive of the emmitter follower output stages, is about 8700. Another method of obtaining the differential mode gain is to refer the measured transfer gain of 1 volt/μa back from the collector of the first stage to its base via the short circuit current gain, β. Then calculating the voltage drop implied when this current flows in the equivalent input impedance

of the transistor yields a value for differential mode voltage gain. Specifically, if β is 30 and the equivalent input impedance is 3 kΩ, then the differential mode gain would be 10000. This is about 1.2 times the previous result, so for this crude calculation they are not inconsistent.

For the first sets of experimental data taken with the Mark I noise source, the power supply was batteries. Initially, four 1.5 volt "D" cells (normal flashlight size) were used. It was observed that long scale (a few weeks) linear trends in the data appeared to correlate with the battery voltage decay. Then a power supply consisting of several rechargeable nickle-cadmium cell batteries and a 20 volt regulated dc supply operating from the 60~ line was employed. This too eventually proved unsatisfactory, and a special regulated supply was constructed. In order to decide what degree of control was actually required, rough measurements were made of the extent to which power supply voltage variations appear in the output. Let the positive and negative power supply voltages be E_1 and E_2, respectively, and define $\bar{E}$ and ΔE by

$$\bar{E} \triangleq \frac{E_1 + |E_2|}{2}, \Delta E \triangleq E_1 + E_2, N \triangleq \text{Mark I Noise Generator Output}$$

Then by varying the two power supplies independently, one can obtain a common mode gain, $\Delta N/(\bar{E})$, and a differential mode gain, $\Delta N/\Delta(\Delta E)$. Figures (18) and (19) show

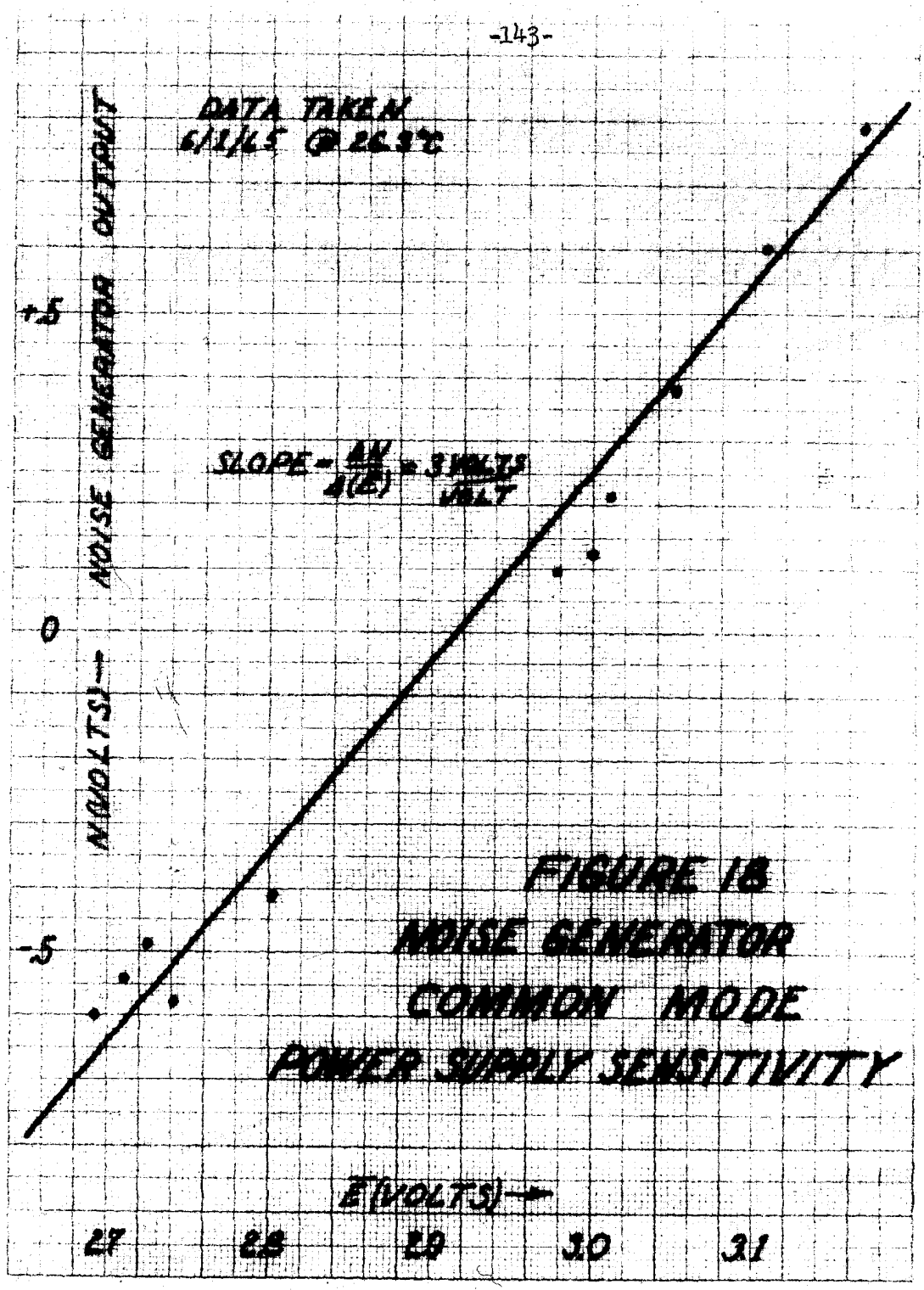

FIGURE 18
NOISE GENERATOR
COMMON MODE
POWER SUPPLY SENSITIVITY

FIGURE 19
NOISE GENERATOR DIFFERENTIAL MODE POWER SUPPLY SENSITIVITY

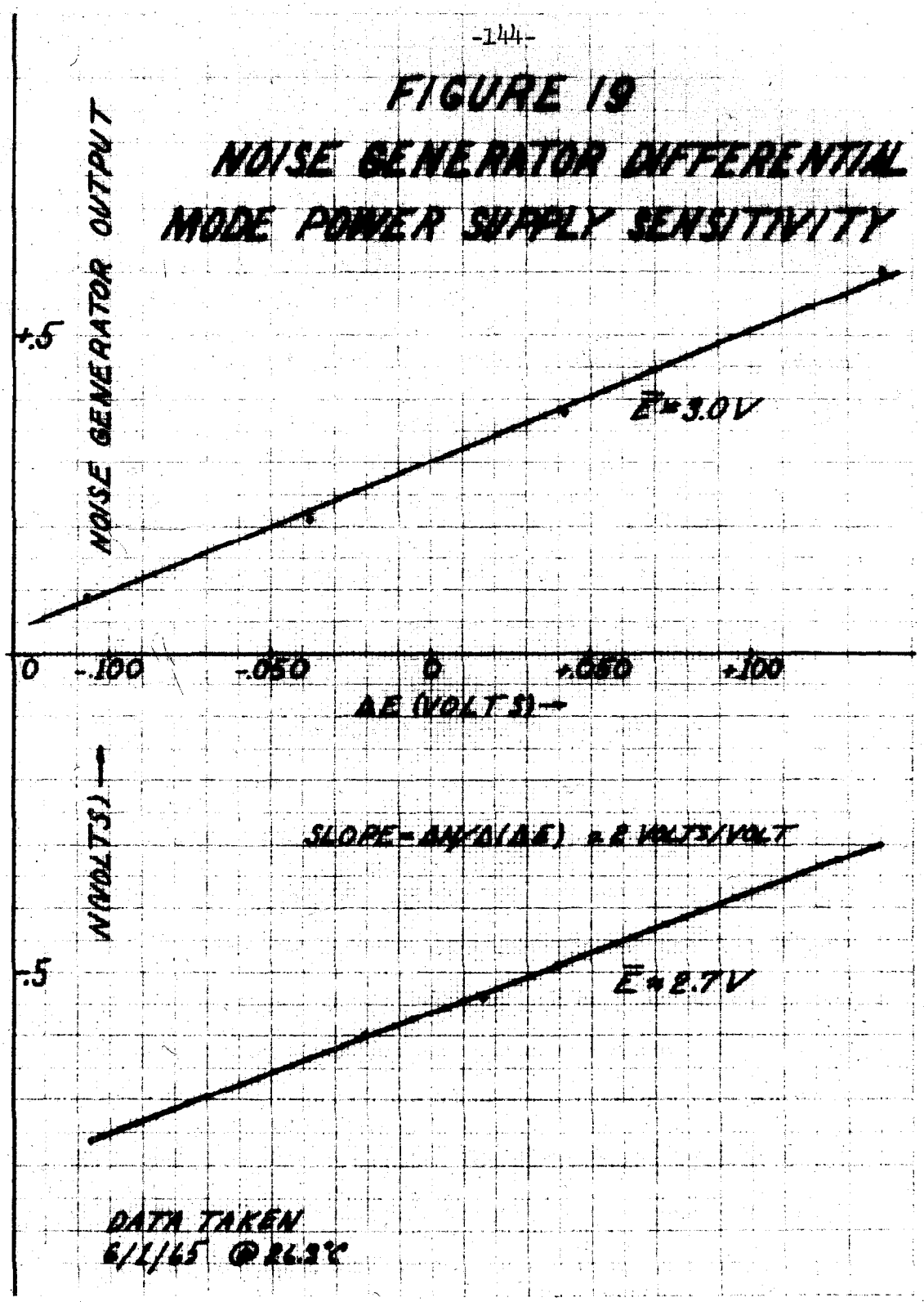

the data leading to values for these two gains of

$$\frac{\Delta N}{\Delta(\bar{E})} \approx 3 \text{ volts/volt}$$

$$\frac{\Delta N}{\Delta(\Delta E)} \approx 2 \text{ volts/volt}$$

This data was taken with the noise generator in temperature controlled oil bath at 26.3°C on June 1, 1965. It was also taken at a particular (arbitrary) setting of the noise generator zero adjust balance pot (see Figure (17)). These latter two facts are not now thought to be relevant, but that is no guarantee that they will not be desired at some future date. The data from which the spectral densities for Mark I are estimated was taken later at 45.9°C at a different setting of the balance pot.

After this investigation, it appeared from past Mark I noise measurements that power supplies with stability on the order of a millivolt would be required. At the 3-volt level this is something on the order of .033%. The device conveniently available as a starting point was a commercial two-unit solid-state 20-volt regulated supply made by Avtel Corporation, which operated from the 60~ line. The first unit supplies a 27.5 volt dc signal. The reference is a 3N39 Zener-transistor package which has an advertised temperature coefficient of .005%/°C over

the range - 20 to + 71°C and operates at 9 volts. For room temperature variations of ± 5°C, this implies something on the order of ± 69 mv on the 27.5 volt output assuming temperature variations are the major contributor to the drift. The second unit follows with a solid-state dc regulator which further attenuates this temperature drift, via feedback and a more stable Zener. The observed long-term variation in the 20-volt output is on the order of ± 10 mv. Better regulation of the high frequency ripple is presumably the primary purpose of the second unit.

A simple series regulator was designed to provide a stable 3-volt output from this 20-volt input. The schematic is shown in Figure (20). Two units were constructed and the outputs adjusted to the desired values. The expected output variation has 4 major components. First, the amount of the input voltage variations which feed through the 36K resistor and appear across the output will be small since this is a negative feedback circuit with a reasonably high loop gain. For this particular case numerically, it can be shown that the ± 10 mv input variations are reduced to less than ± 100 μ volts at the output. Secondly, the input voltage variations will cause a change in the Zener current and hence its voltage which (through the voltage divider) is the reference for the

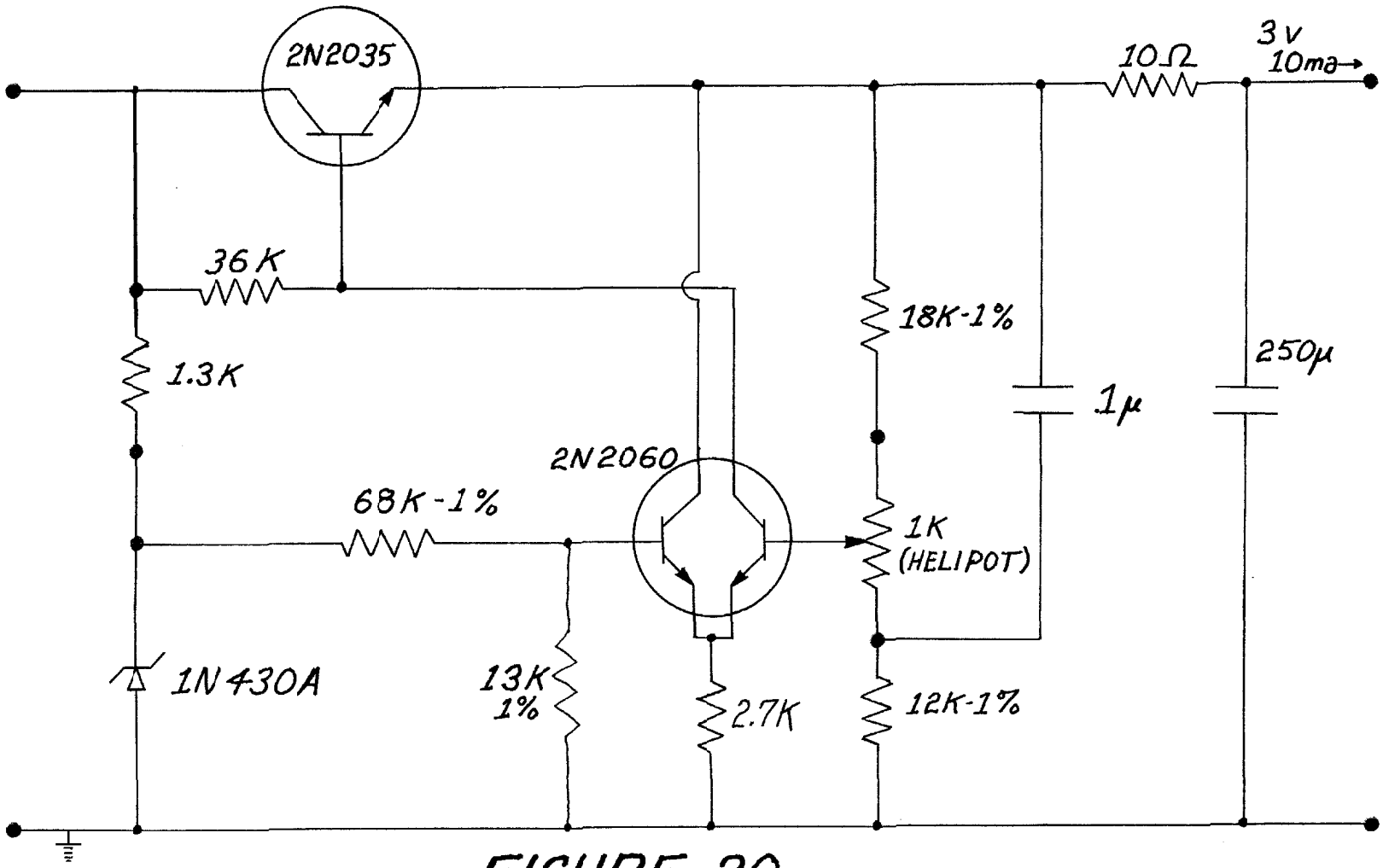

FIGURE 20

SERIES REGULATOR FOR MARK I POWER SUPPLY

differential amplifier comparator against the output. Using the 15 Ω dynamic impedance as per specifications for the Zener, this source yields output variation of ± 40 μv for input changes of ± 10 mv. Third, there will be an output component due to the mismatch of the temperature coefficients of the base emmitter junctions in the two 2060 transistors. These units are nominally temperature matched and packaged in a single case and have a specification on their ΔV_{be} mismatch of 10 μv/°C. A room temperature variation of ± 5°C will then case a variation projected to the output of about ± 120 μv. Finally, there will be a change in output voltage due to the variation in Zener voltage with temperature. The specifications on this particular diode (Hoffman 1N430A) indicate a maximum change with temperature of ± 7 mv out of the 8.5 volt operating range which would cause a ± 2.5 mv change in the output. This is obviously the determining factor. However, the ± 7 mv specification is for a much wider temperature range (-55 → + 100°C) and was felt to be pessimistic. Therefore, the temperature coefficient of the Zener voltage was measured for the unit actually used. The maximum voltage variation observed as measured by a 5 digit, digital voltmeter over the temperature range 15 - 35°C was ± .5 mv. This value yields a somewhat more realistic value of less than ± 200 μv of output variation.

The measurements on the Zener's temperature coefficient were all made in a short time, less than 1 hour. Some pains were taken to insure that the case was actually at the measured temperature. It is possible, however, that a longer-term effect was overlooked. For instance, it could be that the junction material itself, which is at least somewhat thermally insulated from the case, must be at a given temperature for some long period of time to reach "equilibrium" in some sense before its temperature effects are seen in full force. It was assumed that this was not the case and an approximate error budjet for the power supply was constructed as shown in Table (10). Both the sum and the RSS of these values are shown.

Source	Approximate Magnitude
Input variations direct	$< \pm$ 100 μv
Input variations through Zener	$\pm$ 40 μv
ΔV_{be} of 2N2060	$\pm$ 120 μv
Temperature coefficient of Zener	$\pm$ 200 μv
(RSS)	+ 257 μv
(SUM)	$\pm$ 460 μv

TABLE (10)

ERROR BUDJET FOR MARK I POWER SUPPLY

The sum is a reasonable measure if one claims the errors are all dominantly the result of solid-state temperature effects which would be expected to proceed together. The RSS is a reasonable measure if one claims the errors are statistically independent random variables. A realistic estimate is undoubtedly somewhere between the two but even the more pessimistic is less than 1 millivolt.

4.2 Temperature Dependence

As is well known, the voltage across a back-biased p-n junction varies with temperature. For germanium at room temperature, this variation is of the order of 2 millivolts per degree centigrade. The Mark I noise generator will have a differential mode output due to the difference between the temperature coefficients of the base-emmitter junctions of the first stage transistors.

If the temperature coefficients of the two initial transistors are matched to something on the order of 10%, this will represent a differntial mode temperature signal of 200 μ volts/^{o}C. Operated on by the differential mode gain of Mark I, this would be expected to yield an output on the order

of 1.7o volts/^{o}C. This parameter was actually measured to be 4.4 volts/^{o}C.* The measurement was made by observing the rate of decline from a specific voltage in the presence of a known rate of temperature decline. Since no attempt was made to match the first stage transistors with respect to temperature coefficients, the implied discrepancy is not surprising. Further demonstration that Mark I measures temperature is given by Figure (21). The upper curve is the room temperature as a function of time over a 5-day period. The lower is a record of the output of Mark I operated in the room over the same time period.** The two curves are plotted on the same time scale and when compared show clearly that Mark I is an excellent differential temperature sensor. The differential temperature "gain" implied by this data is 5 - 10 volts/^{o}C. Unfortunately, temperature changes are not the effect it is desired to measure.

---

* This gain measurement was made with the large aluminum block shown in Figure (22) immersed in oil.

** Again, the large aluminum block was used and the whole system was allowed to reach thermal equilibrium before data was taken.

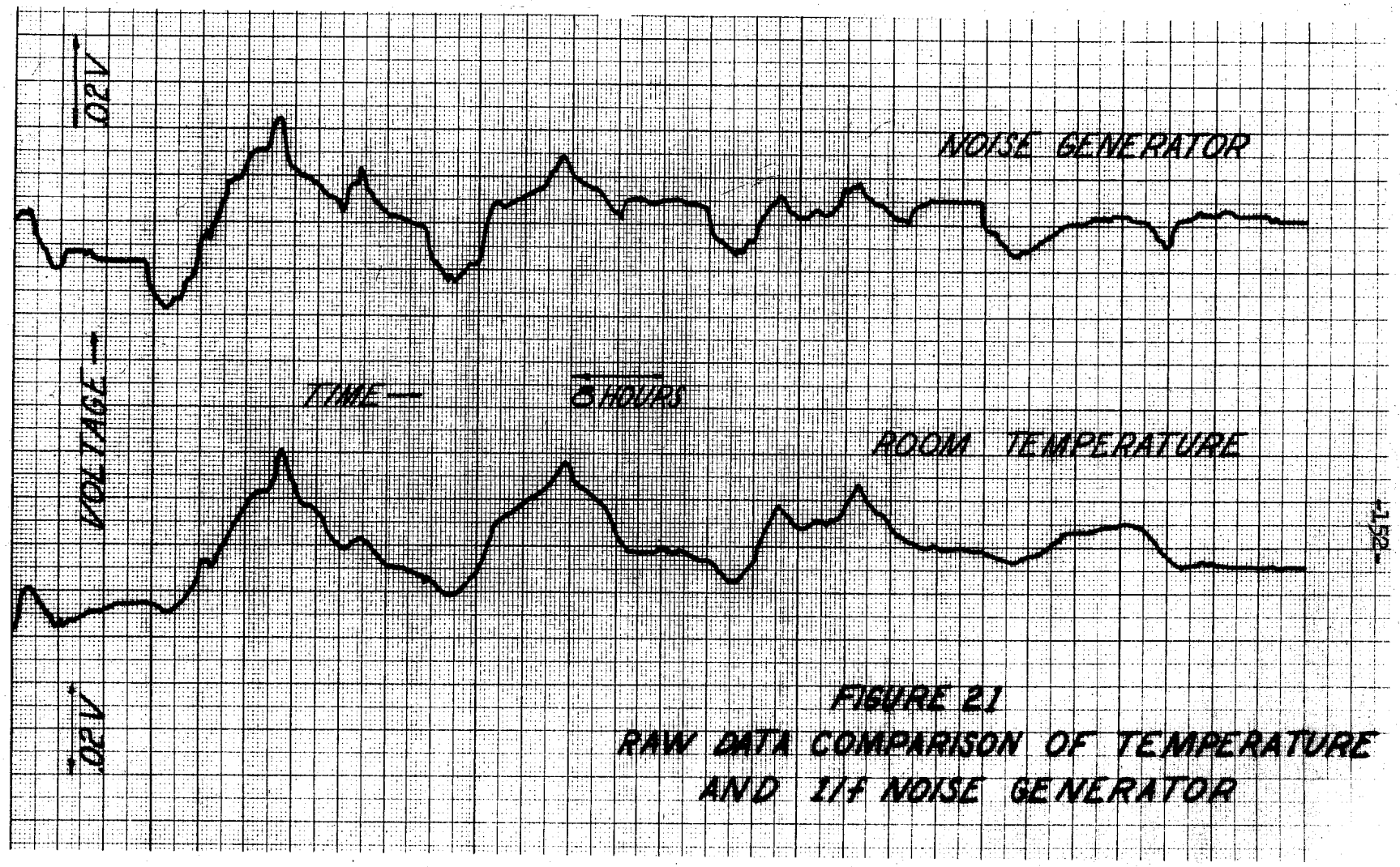

FIGURE 21
RAW DATA COMPARISON OF TEMPERATURE
AND 1/f NOISE GENERATOR

Two distinct approaches were considered for eliminating the effects of temperature. One was to simply place the offending equipment in a temperature controlled environment. This was the approach taken by Winston and Firle [4] and ultimately resorted to in this research. The scheme used will be described in detail in Section (4.2.2), but there are a few general comments which are of interest here. First of all, to be effective in this case, the temperature control must be extremely accurate. This is difficult to accomplish and maintain, especially over long periods of time. Secondly, one encounters the normal difficulties of deciding how much control is required and what amount of the experimental apparatus should be temperature controlled. The method has the advantage, however, of being direct and straightforward. Control is exerted directly on the variable which is producing undesirable consequences.

An alternate approach is to eliminate the effects of temperature through attenuation. That is one can attempt to isolate the noise generator from the environment in such a way that any changes in the temperature (of the room say), are not felt at the noise generating junctions to any significant extent. This method has the advantage of being a great deal more simple to accomplish for all but the lowest frequencies.

It has two major disadvantages. It does not appear to be feasible at very low frequencies (i.e., for very long times) and it affects only the temperature changes impinging from the external environment. Temperature vairations due to variations in internal power dissipated will be unaffected.

4.2.1 Thermal Isolation

The method of thermal isolation was utilized for a series of experiments with the Mark I noise source and was accomplished as follows. The cases of the two first stage transistors, (which generate the noise) were connected by an approximation to a thermal short circuit. This was mechanized by fitting the two transistors snuggly into holes drilled into a small block of aluminum. Electrical insulation was not maintained since the base is connected to the case for this transistor and the two bases are connected in the noise generator circuit . (see figure 17)

The block of aluminum and all other circuit components (see Figure (17) of Section (4.1)) except the batteries, balance pot and on-off switch were mounted on a small circuit board (1x2 inches) which in turn was tightly encased in a larger aluminum block (1x2x3inches) made in halves with the leads extending through small

drilled holes. This whole assembly was mounted together with the batteries, on-off switch, and balance potentiometer in an aluminum box with the output appearing on a BNC connector mounted through the box. Thus, except for leakage, no room air circulated inside the box and none of the box air circulated inside the aluminum block housing the circuit components. In addition, the only thermal gradients that could exist between the two input transistor cases were those which could not be eliminated by the thermal conductivity of their connecting aluminum block. Each stage of thermal isolation is essentially a low pass filter between room temperature variations and the temperature at the transistors.

If the geometry, shown schematically in Figure (22), is modeled for approximate purposes as plane parallel as shown in Figure (23), we can calculate an approximate transfer function between temperature changes in the room environment, ΔT_e, and temperature changes at the device, ΔT_d. We will ignore all corner effects for this approximate discussion. Let the equivalent air gaps d_1 and d_2, areas S_1 and S_2, and temperature difference of the aluminum block ΔT_1, be as shown in the figure. We will also assume that the thermal

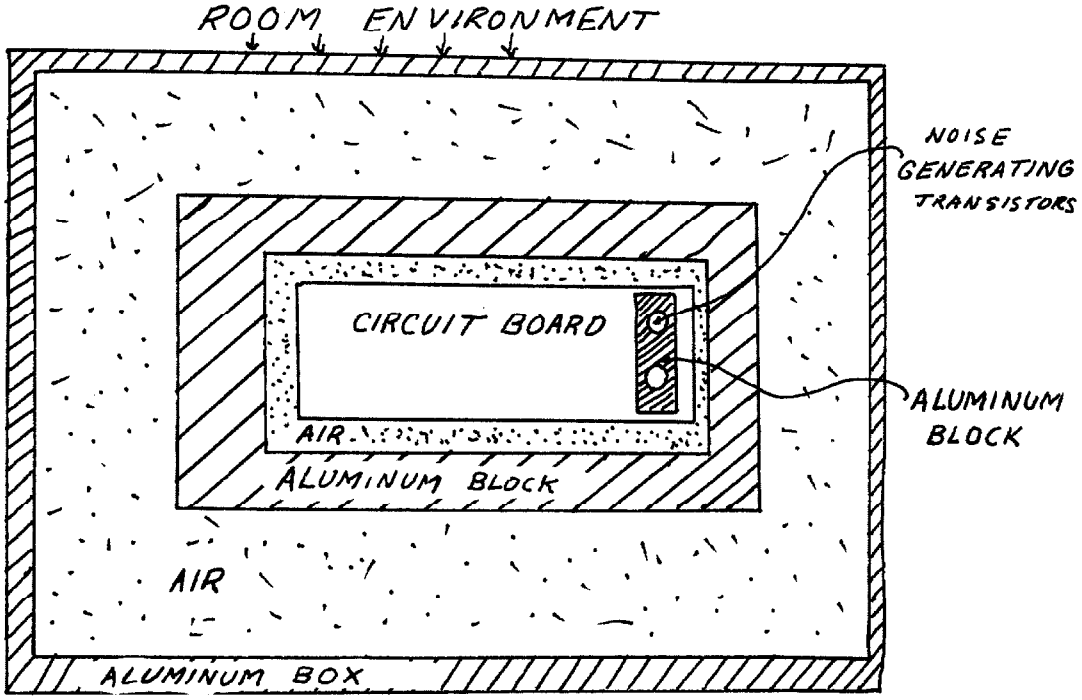

FIGURE 22
ACTUAL GEOMETRY

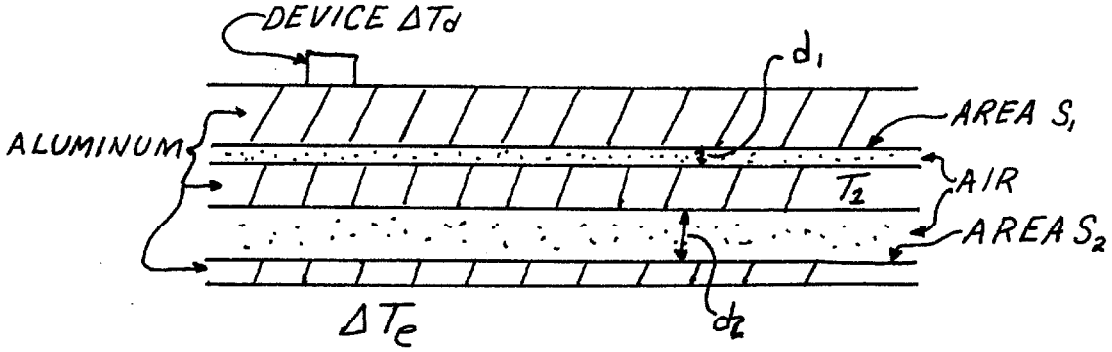

FIGURE 23
APPROXIMATE GEOMETRY

conductivity of the aluminum is high enough so that all of the aluminum reaches the same temperature instantaneously. Then on setting the rate of heating of the device equal to the heat conducted across the air gap we will have for the first stage

$$K_1 \frac{d\,\Delta T_d}{dt} = k \frac{S_1 \Delta T_1}{d_1}$$

where K_1 is the thermal capacity of the small aluminum block (and contents) and k is the thermal conductivity of the air. For the second stage we have similarly

$$K_2 \frac{d\,\Delta T_1}{dt} = k \frac{S_2}{d_2} \Delta T_e$$

where K_2 is the thermal capacity of the large aluminum block. Ignoring initial conditions and combining the Laplace transforms of these two equations yields

$$\frac{\Delta T_d}{\Delta T_\ell} = \frac{1}{\left[1 + \left(\frac{K_1 d_1}{k S_1} s\right)\right]\left[1 + \left(\frac{K_2 d_2}{k S_2} s\right)\right]}$$

for the desired approximate transfer function where s represents the Laplace variable. Thus, we have that the device is linked to the room thermally through two time constants which depend on the geometry and the materials.

We are now able to ascertain to what extent this thermal isolation scheme will be useful. Let us suppose that the room temperature is a disturbance and we desire as little as possible of it to appear in our estimated spectral density for the device. In order to achieve this one must have the "break frequency," $\frac{ks}{2\pi Kd}$ of one of the two temperature "filters" considerably lower than the lowest frequency at which we wish to obtain estimates f_ℓ. (How much lower depends on the particular spectrum of the disturbance). Thus we must have

$$\frac{ks}{2\pi Kd} \ll f_\ell$$

Using .221 cal/g$^\circ$C as the thermal capacity of aluminum and .616 cal/sec-cm$^\circ$C as the thermal conductivity of air this reduces to

$$.443\ \frac{S}{Md} \ll f_\ell$$

Where M is the mass of aluminum in grams. M will most likely not be much over 100 and $\frac{S}{d}$ will certainly be at least 10. Thus, it is rather unlikely that f_ℓ can be taken much below 10^{-2} or 10^{-3} cps. One expects, then, that if this scheme is used, any estimates below a millicycle or so will consist largely of temperature spectral density. This was in fact exactly what occurred

for Mark I as illustrated and discussed in Section 5.2.* (see figure 51)

4.2.2 Thermal Control

Because of the inability to isolate the noise generator from room temperature variations at frequencies below a millicycle by the technique just described the more straight forward approach of thermal control was eventually employed. The following is a description of the scheme used to accomplish the thermal control.

To get an idea of the magnitude of the problem let us examine how well the temperature must be controlled. Let's suppose that we will be using as our random noise process the output of Mark I on a ± 1 volt scale at its output. The temperature coefficient of Mark I referred to its output is on the order of 4.4 volts/^{o}C of temperature change to the large block of aluminum. We will wish to quantize the output, say visually which is the most crude, at least at the ± .01 level. Thus to make the temperature "noise" at least as small as the largest quantization noise we expect we must control the temperature to about four times better than ± .01^{o}C. Such control is not achieved easily.

---

*One can make a similar calculation for an evacuated cavity containing the noise generator. For the parameters under consideration such a grey body calculation yields a limit of 10^{-4} or 10^{-5} cps as the break frequency.

As mentioned earlier when one adopts the approach of controlling the temperature, the ideal situation would be to control the temperature of the noise generating junction itself. To avoid becoming completely enmeshed in solid-state physical difficulties it was decided for this research to settle for the case (can) of the transistor. Thus, a large thermal capacity, constant temperature, heat sink in good thermal contact with the first stage transistor cases is desired. Because of its non-inflammability, high thermal capacity, and electrical insulation properties silicon oil was chosen.*

4.2.2.1 Temperature Sensing

The next obvious obstacle to construction of the temperature controlled bath was a sensor with which to sense temperature variations of less than $\pm .01^{\circ}C$. As a general rule of thumb one expects to need a sensor that is somewhat better in terms of resolution than the eventual control desired. However, by far the most severe constraint was the length of time over which the sensor must be accurate on an absolute scale. Since it was hoped to obtain spectral density estimates to a microcycle (10^{-6} cps) the data record lengths would have to be on the order of a

* Specifically GE SF-81(50).

few months to secure reasonable variance estimates. Because of the continuing extreme sensitivity of the noise source to temperature changes any "drift" in the calibration of the temperature sensor would show up directly in the noise output voltage. In order to operate a control system of this kind in a continuous manner, a continuous electrical output from the temperature sensor was desired. To accomplish these objectives at modest cost, some amount of ingenuity was required.

Resistence bridges were rejected for several reasons. First, none was found commercially available at the time which would sense temperature to .001^{o}C. Secondly, those available at the .01^{o}C level were found to be quite expensive and in general provided only a manual readout of the temperature. Design and construction of a sensitive temperature bridge was considered. As in the commerical cases the resolution was limited and the cost was high due to the extreme stability required of the non-sensing members of the bridge. The temperature sensing resistor in such arrangements is usually platinum (or an alloy) which has a temperature resistence coefficient of

about 4% per degree centigrade. Thus, to sense .001°C requires detection of a change in the resistance of 4 parts in 10^5. This requires at least one of the other legs of the bridge to be 10 times better or 4 parts in 10^6 over a period of several months. Even when they can be purchased, such resistors are quite expensive. The maximum amount of power which may be dissipated into resistors of this degree of stability is usually quite small. Thus, when a bridge circuit is used one finds that at the maximum resolution the available signals are of the order of microvolts (10^{-6}). It is difficult as well as expensive to obtain an amplifier which will amplify μ volts stably over a period of several months. For instance, most standard analog computer type dc amplifiers have an equivalent noise referred to the input on the order of several μ volts.

This same difficulty of stable automatic measurement of μ volts over long periods also precluded the use of thermo couples where the voltages generated are on the order of hundredths of millivolts per degree centigrade.

The solution finally adopted was to measure the temperature stably over long periods with a mercury differential thermometer. The constancy of the thermal coefficient of expansion of the mercury in the double glass envelope is thus presumed to yield the required absolute repeatability of the temperature measurements over long periods of time. The conversion to an electrical output is obtained via a capacitive measurement of the height of the mercury.* Figure (24) illustrates this process schematically. The variable capacitance, C_T,

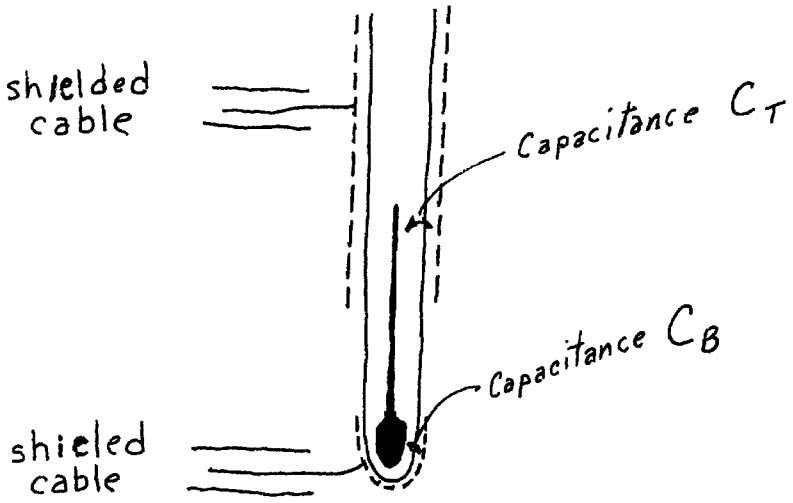

Figure 24
Thermometer Geometry

* The original idea for this scheme was generated in a discussion of the problem between the author and A. R. Jones in the fall of 1964 at which time it was thought to be impractical.

is between the mercury column in the capillary tube and a strip of conducting paint on the calibrated section of the outside of the glass envelope. Except for end effects and leakage fields this capacitance is exactly proportional to the temperature (i.e., to the h eight of the mercury assuming the capillary tube is of constant diameter). This capacitance C_T is much smaller than C_B, the capacitance between the bottom mercury bulb and the conducting paint covering the bottom of the outside of the glass. Hence, when these two capacitors are put in a circuit in series the effective value of the capacitance is essentially C_T. C_B is of course constant, since the bottom bulb is always full. The basic circuit chosen to measure this capacitance (shown in the Sketch below) was extremely simple and used available components.

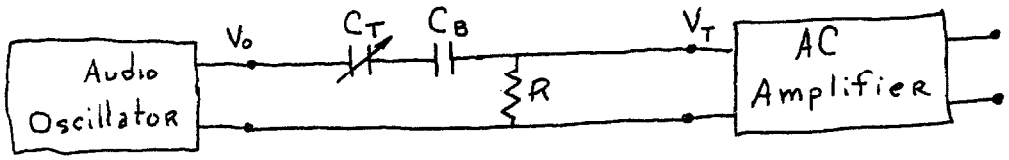

Ignoring the output impedance of the oscillator and the input impedance to the amplifier we have*

$$\frac{V_T}{V_o}(s) = \frac{RC_T s}{1+RC_T s}$$

It is clear that provided $|RC_T s| \ll 1$ the magnitude of the ac voltage appearing across the resistor will be directly proportional to C_T and hence to the temperature. However, note that the size of the voltage available to amplify is also proporitonal to $RC_T s$. This voltage must be kept large compared with the noise of the amplifier referred to its input. Since this is typically a few microvolts, the magnitude of V_T must be kept at least as large as a 100 microvolts or so and preferably a millivolt. This yields a lower bound for $RC_T 2\pi f$ of 10^{-3} or so.** But C_T is fixed at about $0 \rightarrow .4\mu\mu f$ by the size of the capillary tube, the dielectric constant of the glass, and the geometry; none of which are really in our control. Also an upper bound of something

---

* Appendix C contains an error analysis of this scheme.

** V_T was not increased simply by increasing V_o because it was felt undesirable to have large ac voltages and fields in the vicinity of the noise source in the oil bath.

on the order of a few megaohms for R is given by the AC amplifiers available which have input impedances of a few hundreds of megaohms. Practical considerations regarding sensitivity to 60~ noise pickup indicate a choice of the operating frequency at least in the high audio frequency range. The actual values chosen were 1 megaohm and 10 kilocycle. The thermometer used for the thermal control systems sensor was a Beckman differential thermometer with a linear range of 5°C and a calibrated resolution of .001°C over this range.† It can be set to have its zero point be anywhere between 0°C and + 100°C by extruding mercury to a special storage container at the top of the instrument. This temperature sensing scheme has the advantage of requiring only one $50 thermomenter plus readily available laboratory equipment and semi-infinite graduate student labor. The amplifier and oscillator stability need only be as good as the desired temperature sensing.

---

† Catalog #61055 in C. F. Braun 1964 catalog.

In practice the actual circuit used was as shown in Figure (25) with the addition of: a blocking capacitor at the output of the ac amplifier to remove any dc bias in its output, a 10 Kc band pass filter to eliminate to 60μ hum pickup*, a diode and capacitor acting as a peak rectifier to produce a dc voltage proportional to temperature, and dc amplifier to drive a recorder and the heater coil circuitry.

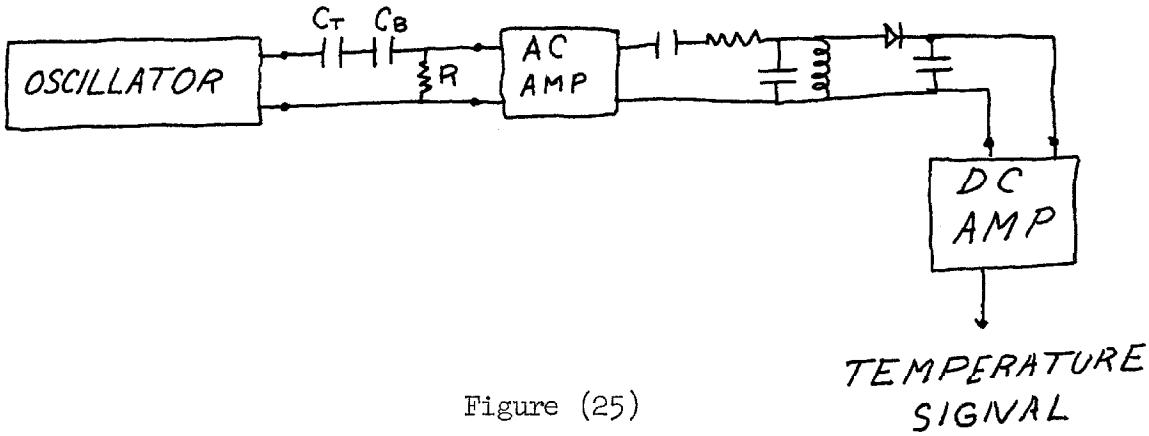

Figure (25)

Actual Temperature Measuring Circuit

Figure (26) is a calibration curve for the temperature curve for the temperature sensor obtained by using the visual calibration on the glass as the standard. It can be read with a lens to .001°C. The data appears to be consistent with a sensor which is accurate to at least ± .01°C.

* This filter provides an attenuation of 250 in the time domain to 60 ~ signals relative to the 10Kc component. The oscillator was tuned to the center frequency of this filter.

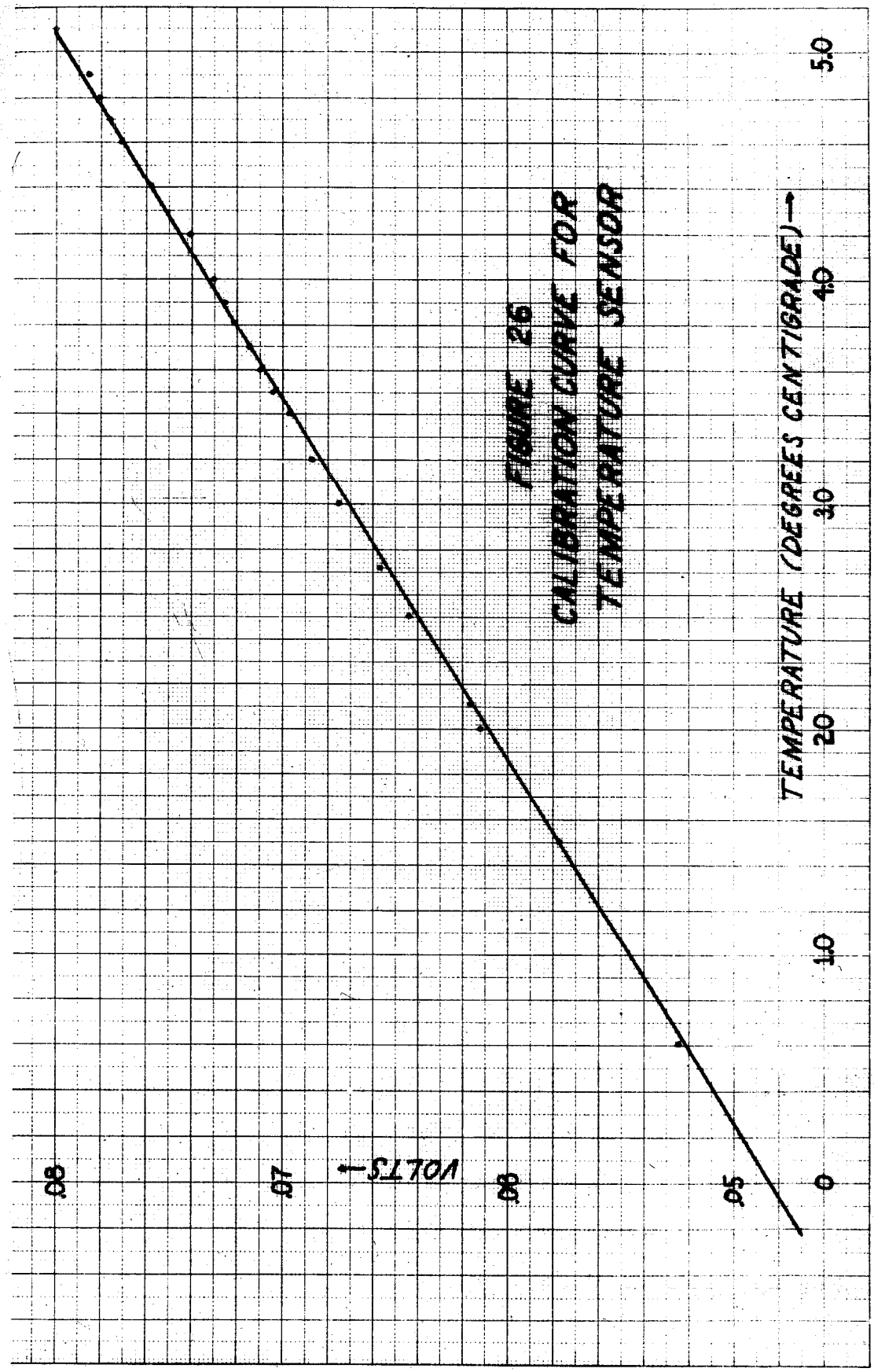

FIGURE 26
CALIBRATION CURVE FOR
TEMPERATURE SENSOR

A similar setup using a .1°C resolution thermometer with a range + 15° to + 35°C was used to measure and record the room temperature beginning March 26, 1965. This is the record that was used to obtain the spectral densities of room temperature discussed in Section 5.1.

4.2.2.2 Thermal Control System

A very simple system was used to control the temperature of the oil bath. A constant current was run through a nichrome wire resistance heater coil to maintain the steady-state temperature of the oil at about 45°C. A one-sided control system was then utilized to hold the temperature to this value by changing the heating through variation of the current in the heater coil. This steady temperature was chosen to provide ample distance for decay to room temperature as the cooling agent.

In order to avoid temperature gradients in the oil it was stirred violently by a 6" diameter propeller located at the bottom of the dewar containing the oil and turned at about 175 rpm by a motor and pulley through an O-Ring Drive. A baffle was inserted in the dewar to avoid vortexing, increase turbulance, and guarantee good mixing of the fluid.

DC current and proportional control was chosen for the heaters rather than a bang-bang or 60 ∿system in order to avoid limit cycles and large 60∿fields in the dewar which might contribute to the measured power spectral density of the noise source.*

The temperature control situation is thus as illustrated in Figure(27) with the heater coils acting on the oil and the electrical thermometer described above sensing the resultant oil temperature and driving the heater coils through the amplifier. The steady-state temperature is obtained through a constant current in the heater

---

* Recall that a sharp line in the spectrum "ruins" the estimator over a considerable range of frequency in both directions depending on the magnitude of the line.

coils and the room temperature disturbance acts on the oil.

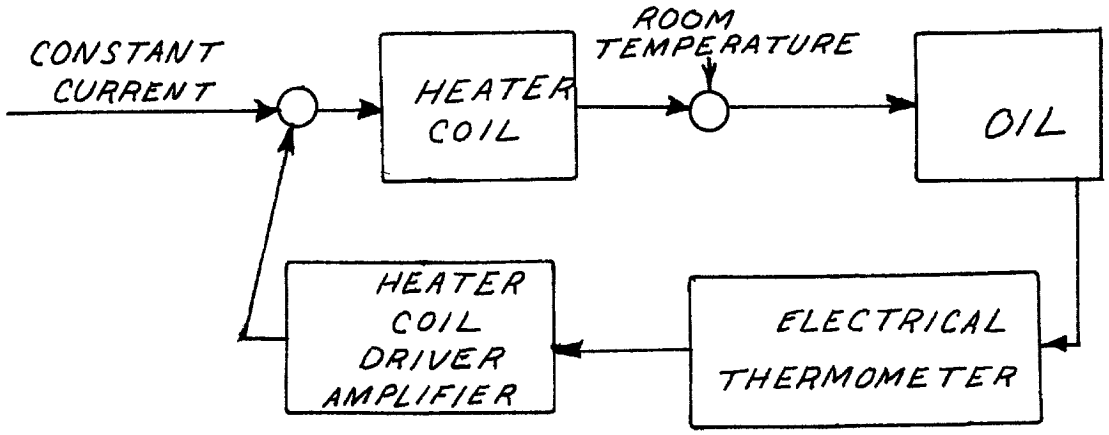

FIGURE 27

As a model for the temperature sensor we shall take

$$\frac{K_2}{\tau_t s+1}$$

This is the transfer functions between the temperature of the oil in ^{o}C and the sensor output in volts. K_2 is the dc gain in volts/^{o}C and τ_1 represents the thermal time constant between the oil temperature and the mercury temperature due to the glass around the bulb of the thermometer. Otherwise, the electronic system is assumed to be

instantaneous which seems an adequate approximation for this analysis. Since the amplifier in the sensor is variable gain and the oscillator voltage can be adjusted somewhat, the numerical value of K_2 is not entirely fixed. However, it is nominally a few tenths of a volt per degree centigrade. The time constant τ_t was included because this is probably an adequate model of the most significant non-ideality present in the sensor. It is difficult to measure due to the limited linear range of the sensor and it was hoped that a design largely independent of τ_t could be obtained. Note that all poles in the ac amplifier and the dc amplifier of the temperature sensing circuit are ignored.

To this same degree of approximation, then the poles of the heater coil driver amplifier will also be ignored. All of these will be at least as high as 10Kc and so should in fact be unimportant in such a "slow" system. The model for the dc amplifier will thus be just a transfer gain K_3 in amps/volt. This gain is available as a design parameter and its variability was accomplished as follows. A circuit normally

employed as a regulated power supply was utilized to achieve the large steady current in the heater coil as shown in Figure (28). This circuit was

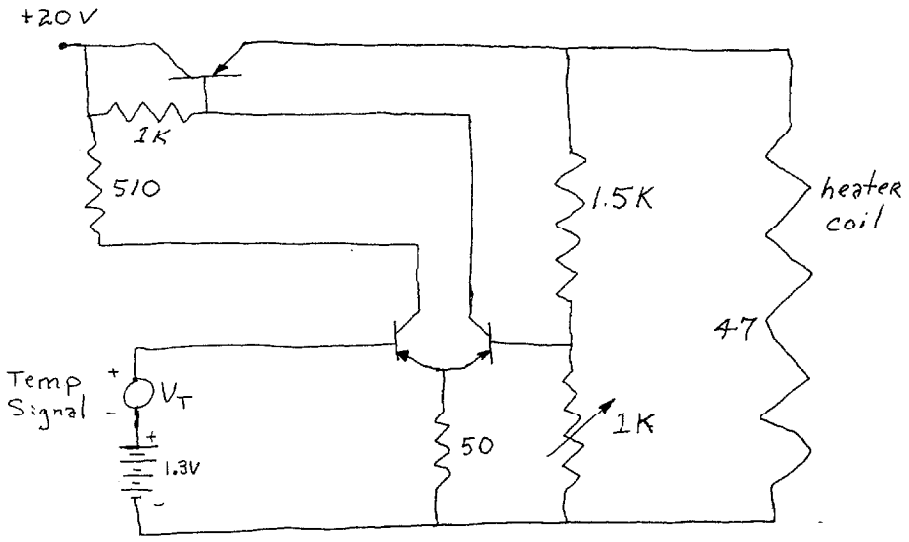

FIGURE 28
HEATER COIL DRIVER CIRCUIT

chosen to allow a large steady current at the null of the temperature sensor ($\approx 45^{\circ}C$) as well as a high gain from variations in the temperature voltage signal to the heater coil current.

To derive a model for the oil and heater let us begin with the differential equation describing the temperature of the oil. This is

$$C_o \frac{dT}{dt} = -K_o(T - T_r) + i^2R + H_o - L_o - R_o \quad (128)$$

where: C_o is the thermal capacity (specific heat) of the oil in $\frac{\text{watt-sec}}{^oC}$

K_o is the thermal conductivity of the oil in watts/^oC

T is the oil temperature in ^oC

T_r is the room temperature in ^oC

i is the heater current in amps

R is the heater coil resistance in ohms

H_o is the heat in watts due to the stirring

L_o is the conductive heat loss through all parts immersed in the oil in watts

R_o is the heat loss through radiative transfer to the surroundings in watts

t is time in seconds.

There are several simplifying assumptions made here. All of the oil is assumed to be at a constant temperature, T. The extensive stirring and baffle included to increase turbulence are intended to justify the neglecting of temperature gradients in the fluid, but this is probably the most severe approximation involved in the above equation. The amount of the mechanical energy input of the stirring blade which is converted to

heat in the oil H_o is assumed to be constant. Since the stirring speed will be kept constant this is not an unreasonable approximation. The amount of heat lost by conduction through parts immersed in the oil, L_o, is assumed to be constant. This will not, in fact, actually be the case since each part will conduct an amount of heat depending on its thermal conductivity and the temperature gradient across it. These parts consist of a lucite baffle, a lucite heater coil support, a metal stirring shaft, a wide range glass thermometer, the ground shield around the fine thermometer and the thermometer itself, and the cables and leads for whatever experiment packages are in the oil. It was expected that to achieve actual closed-loop control to a .001°C these conduction effects would have to be compensated for, but as a first approximation we shall ignore them. The loss through radiative transfer, R_o, is assumed to be constant but should be negligible in any case so that this is not a severe approximation. In addition, the thermal time constant required for the heater wire to change its temperature is assumed to be negligible.

The control variable is i, the disturbance is T_r, and it is desired to control T. As mentioned above in order to operate a "one-sided" control by heating only (or the lack of it) we must "bias" T above room temperature. This will be accomplished by a constant current i_o and lead to a constant oil temperature T_o (in the absence of disturbances). If we also separate the room temperature into its steady state and variable component we have the following set of linearization assumptions:

$$T = T_o + \Delta T \qquad \Delta T \ll T_o$$

$$T_r = \bar{T}_r + \Delta T_r \qquad \Delta T_r \ll \bar{T}_r$$

$$i = i_o + \Delta i \qquad \Delta i \ll i_o$$

Inserting these definitions into the differential equation describing the oil we see that i_o must be chosen so that

$$i_o = \sqrt{\frac{K_o(T_o - \bar{T}_r) - H_o + L_o + R_o}{R}}$$

Where we have ignored the $(\Delta i)^2$ term compared to $2i_o\Delta i$. Ignoring initial conditions, the remaining linearized incremental differential equation in

the Laplace domain is

$$C_o \Delta T = - K_o(\Delta T - \Delta T_r) + 2i_o \Delta i R$$

which simplifies to

$$\Delta T = \left(\frac{2i_o R}{C_o s + K_o}\right) \Delta i + \left(\frac{K_o}{C_o s + K_o}\right) \Delta T_r$$

A complete block diagram for the incremental system is now given in Figure (29).

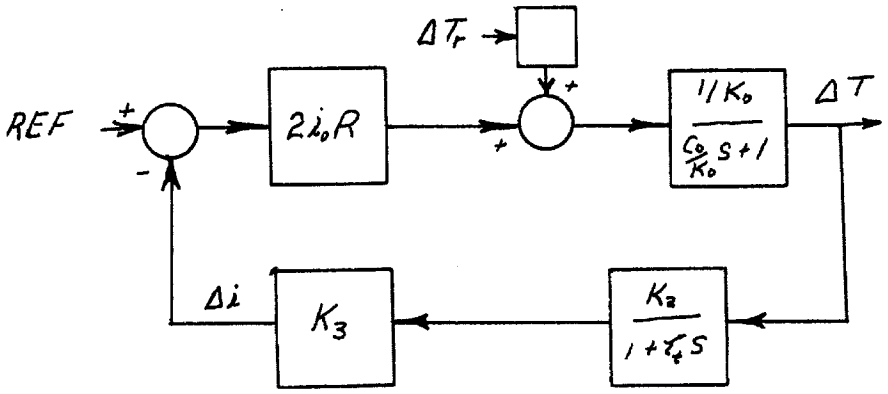

Figure (29)

Linearized Incremental Block Diagram
of Thermal Control System

In order to ascertain the largest admissible value of K_3, a root locus can be constructed for the expression

$$\frac{2i_o R K_3 K_2}{C_o \tau_t \left(S + \frac{K_o}{C_o}\right)\left(S + \frac{1}{\tau_t}\right)}$$

which is the complete open-loop transfer function in the absence of noise. It will look approximately as shown below since $\frac{1}{\tau_t} \gg \frac{K_o}{C_o}$

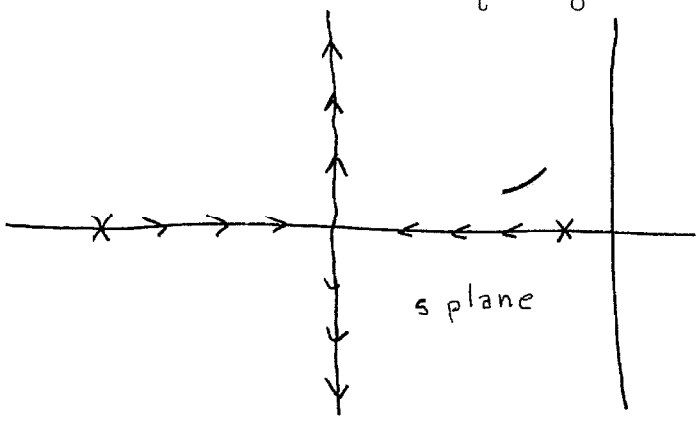

This would lead us to believe that the system is always stable, which is of course, false. The locus will actually turn into the right half plane at large values of gain due to the presence of the amplifier poles. If these had, in fact, been included, the locus would look more like the following sketch (note the scale is now expanded).

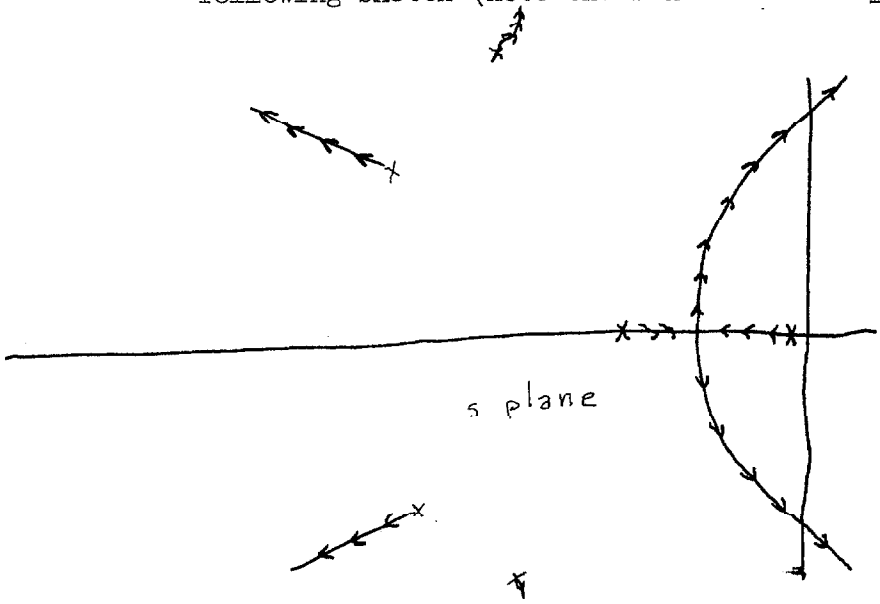

But notice that long before such an instability is reached, the system is highly underdamped and will have very undesirable behavior in the presence of the noise, ΔT_R. An alternate approach is to construct a Bode plot of the closed-loop transfer function and choose K_3 to yield a specific gain or phase margin. Numerically, this is the technique which was utilized as will be related shortly. First, however, let us examine the problem from the viewpoint of disturbance attenuation.

The closed-loop transfer function between ΔT_R and ΔT is after simplification

$$\frac{\Delta T}{\Delta T_R} = \frac{K_o(\tau_t s+1)}{2i_o R K_3 K_2 + K_o(\tau_t s+1)\left(C_o/K_o s+1\right)} = \frac{K_o(\tau_t s+1)}{(s+s_1)(s+s_1^*)} \tag{129}$$

where s_1 and its complex conjugate s_1^* are the poles located on the root locus pictured above for a particular value of K_3. For large values of K_3, $I_m\{s_1\} \gg R_e\{s_1\}$ and we have approximately

$$|s_1| \approx \sqrt{\frac{2i_o R K_3 K_2}{C_o \tau_t}}$$

$$R_e\{s_1\} = -\frac{1}{2\tau_t}$$

Since $|s_1| \gg \frac{1}{\tau_t}$ the two poles of the disturbance attenuation transfer function dominate the behavior and a Bode plot of it would appear as shown in Figure (30). For comparison, the open-loop disturbance attenuation, $\frac{1}{C_o/K_o s+1}$,

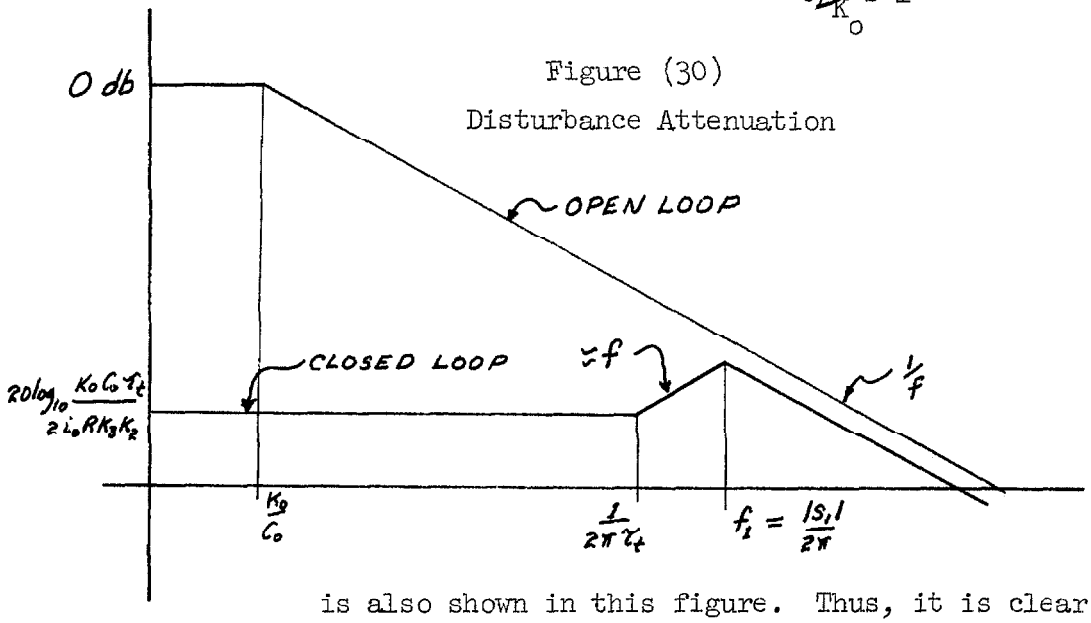

Figure (30)
Disturbance Attenuation

is also shown in this figure. Thus, it is clear that a great deal of noise attenuation is gained by employing closed-loop control. This is especially true for this particular case where the disturbance is room temperature variations. The results of Section 5.1 below indicate this spectrum varies roughly as $1/f^2$ over a very wide frequency range and so the total disturbance power remaining in ΔT varies as the cube of the lower $1/f^2$ band edge in the open loop case but only as the first power of this value in the closed-loop case. To be specific, suppose we model

the power spectral density of the disturbance ΔT_R as

$$S_{\Delta T_R}(f) = \frac{N_o}{1 + \left(f/f_T\right)^2}$$

where N_o is the low frequency ("white") value of the spectrum and f_T is the "break frequency." Then we have in the open loop case

$$S_{\Delta T}(f) = \left(\frac{N_o}{1 + \left(f/f_T\right)^2}\right)\left(\frac{1}{1 + \left(\frac{C_o}{K_o}2\pi\right)^2 f^2}\right)$$

and in the closed-loop case

$$S_{\Delta T}(f) = \frac{N_o}{\left[1 + \left(f/f_T\right)^2\right]}\left(\frac{K_o C_o \tau_t}{2i_o R K_3 K_2}\right)^2 \left[\frac{(2\pi f \tau_t)^2 + 1}{\left(f/f_T\right)^2 + 1}\right]$$

Now if we calculate the total power in the remaining noises utilizing the approximations that $\frac{K_o}{2\pi f_o} \approx f_T \ll \frac{1}{2\pi\tau_t} \ll f_1$ and approximating the functions by their straight line approximate bode plots we have

$$\overline{\Delta T^2}_{\text{open loop}} \approx N_o f_T$$

$$\overline{\Delta T^2}_{\text{closed loop}} \approx N_o f_T \left(\frac{K_o C_o \tau_t}{2i_o R K_3 K_2}\right)^2$$

which is deceptively simple looking only because both the transfer functions and the noise fall off rapidly with f and hence only low frequency behavior is important. Numerically, we have:

$K_o = 1.28$

$\tau_t = 1$

$C_o = 6.65 \times 10^4$

$i_o = .250$

$R = 45$

$K_2 = 10$

$K_3 = .3$

So that the attenuations factor is

$$\frac{K_o C_o \tau_t}{2 i_o R K_3 K_2} = 126$$

These numerical values are the system parameters actually used for the experiments reported on below. The quantities i_c, K_2, K_3, and R are directly measurable. The value for τ_t was estimated approximately from an experiment where the differential thermometer's response to a large known step of temperature was measured. This was a rather crude measurement and the 95% confidence limits on the value for τ_t are probably

about - 20% + 200%. Such an underestimate of τ_t would lead to a consequent understating of the attenuation. A larger value seems more nearly in accordance with the observed behavior of the oil. Over the 7 month period from September '65 to April '66 the oil temperature was recorded some several dozen times at random occasions (including early morning hours). The maximum temperature excursion observed* was $\pm .3^{\circ}C$ while the maximum room temperature excursions over this period were on the order of $\pm 5^{\circ}C$. This indicates an empirical attenuation figure of about 160.

The values for K_o and C_o were obtained from transient and steady state measurements on the oil. From the basic differential equations describing the oil temperature equations (4.2.2.1) with no heating we have

$$K_o(T-T_R) = H_o - L_o - R_o$$

in the "steady state" (with no disturbances). The steady state heat input due to the stirring (175 rpm) less the radiative and conduction losses

* This excludes changes in system operation such as stirring failure, battery changing, etc.

was found in terms of K_o by this method. A period of time many days in length was employed and "average" behavior was utilized since a completely disturbance free environment was not available. The result was that about a $4.5^{\circ}C$ temperature differential was maintained between the room and the oil by the stirring minus the losses. From measurements of the decay from steady state with heating current back to $4.5^{\circ}C$ above the room without heating current via

$$C_o \left.\frac{dT}{dt}\right|_{t=o} = - K_o(T-T_R) + H_o - L_o - R_o$$

we obtain a value for $\frac{K_o}{C_o}$ of

$$K_o/C_o = 1.93 \times 10^{-5} \text{ sec}^{-1}$$

From measurements of the heating up of the oil from $4.5^{\circ}C$ above the room to steady state at $45.9^{\circ}C$ via

$$C_o \left.\frac{dT}{dt}\right|_{t=o} = i_o^2 R$$

we obtain

$$C_o = 6.65 \times 10^4 \text{ watt/sec}^{\circ}C$$

which then yields

K_o = 1.28 watts/^oC and $H_o - L_o - R_o$ = 5.76 watts

While none of these measurements are terribly accurate, they are precise enough for use in indicating that the system's performance is essentially as expected according to the design analysis.

4.3 Experimental Equipment Description

As described above, the method used to estimate power spectral densities in this thesis was to obtain a sample function from the noise process and utilize the Blackman and Tukey technique. Because the estimation was done on a digital machine discrete samples were required. The samples were obtained in three different ways for various parts of this work.

First for high frequencies (i.e., rapid sampling rates) the analog-to-digital conversion equipment of the CIT computing center was utilized. The Packard Bell Multiverter operated directly on an amplified version of the noise process. The sampled, quantized result was fed to the 7040-7094 where it was recorded on magnetic tape. This was an entirely on-line operation performed completely in real time. The magnetic tape data could then be used at any future time as an input to the spectral estimation program for the 7094. Figure (31) shows a diagram of the equipment arrangement for this process. The low pass filter shown is to eliminate the effects of aliasing on the final spectral estimate as discussed in Section 3.2.1 and in Reference [5]. Figure (32) shows a measured frequency response of the filter with the break frequency set at 25 cps.

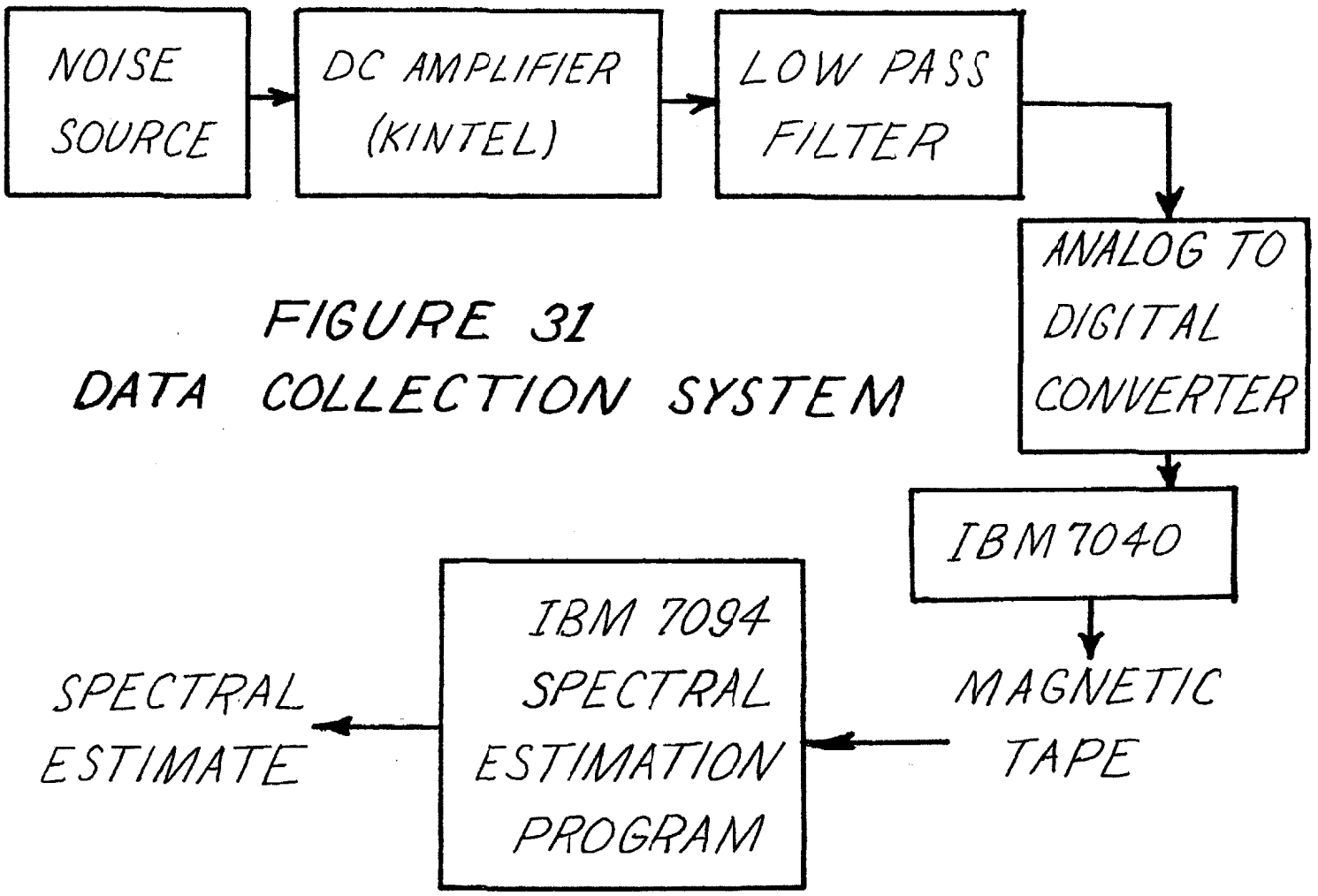

FIGURE 31
DATA COLLECTION SYSTEM

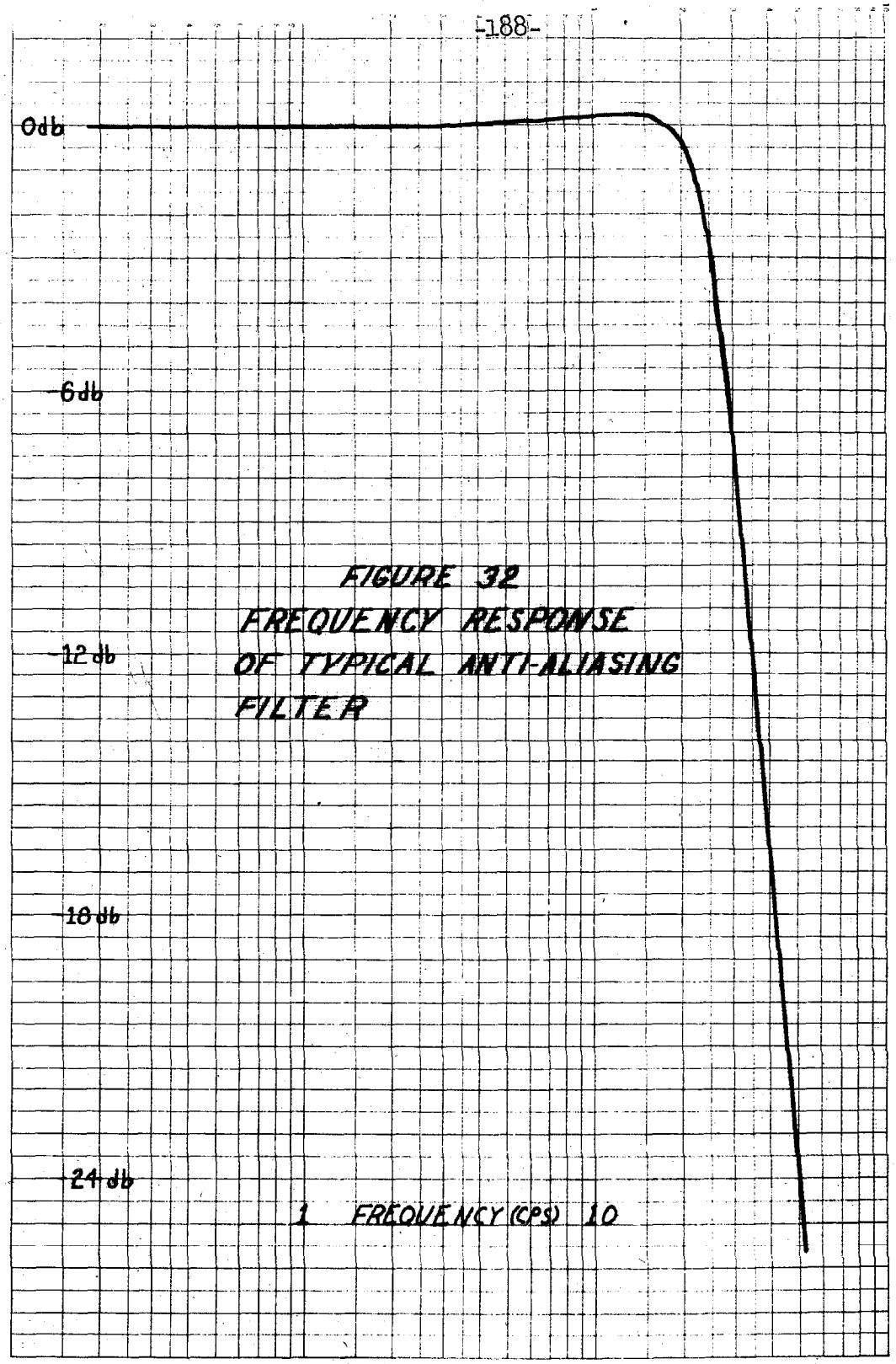

FIGURE 32
FREQUENCY RESPONSE
OF TYPICAL ANTI-ALIASING
FILTER

The second method of obtaining the sampled quantized data was used for low frequencies (i.e., slow sampling rates). This consisted of recording the noise voltage on an Easterline Angus recorder, reading the values at equi-spaced intervals of time and punching these numbers onto IBM cards. These data cards were then entered as input data to the 7094 spectral estimation program which yielded a power spectral density estimate. Figure (33) shows a schematic diagram of this operation.

The third method of data collection used was a somewhat less painful version of the second in which the sampling, quantization and recording of the data was done automatically. The quantization is accomplished through use of a digital voltmeter. The sampling is performed by punching a paper tape with the digital voltmeter's reading at specified times. The paper tape is then read on the paper tape reader unit of Burroughs 220 computer at the CIT computation center. The magnetic tape immage formed in this manner is then decoded by a machinge language program and put onto a FORTRAN DATA tape. This data tape is used as the input to the spectral estimation program. Figure (34) illustrates this data collection and processing scheme.

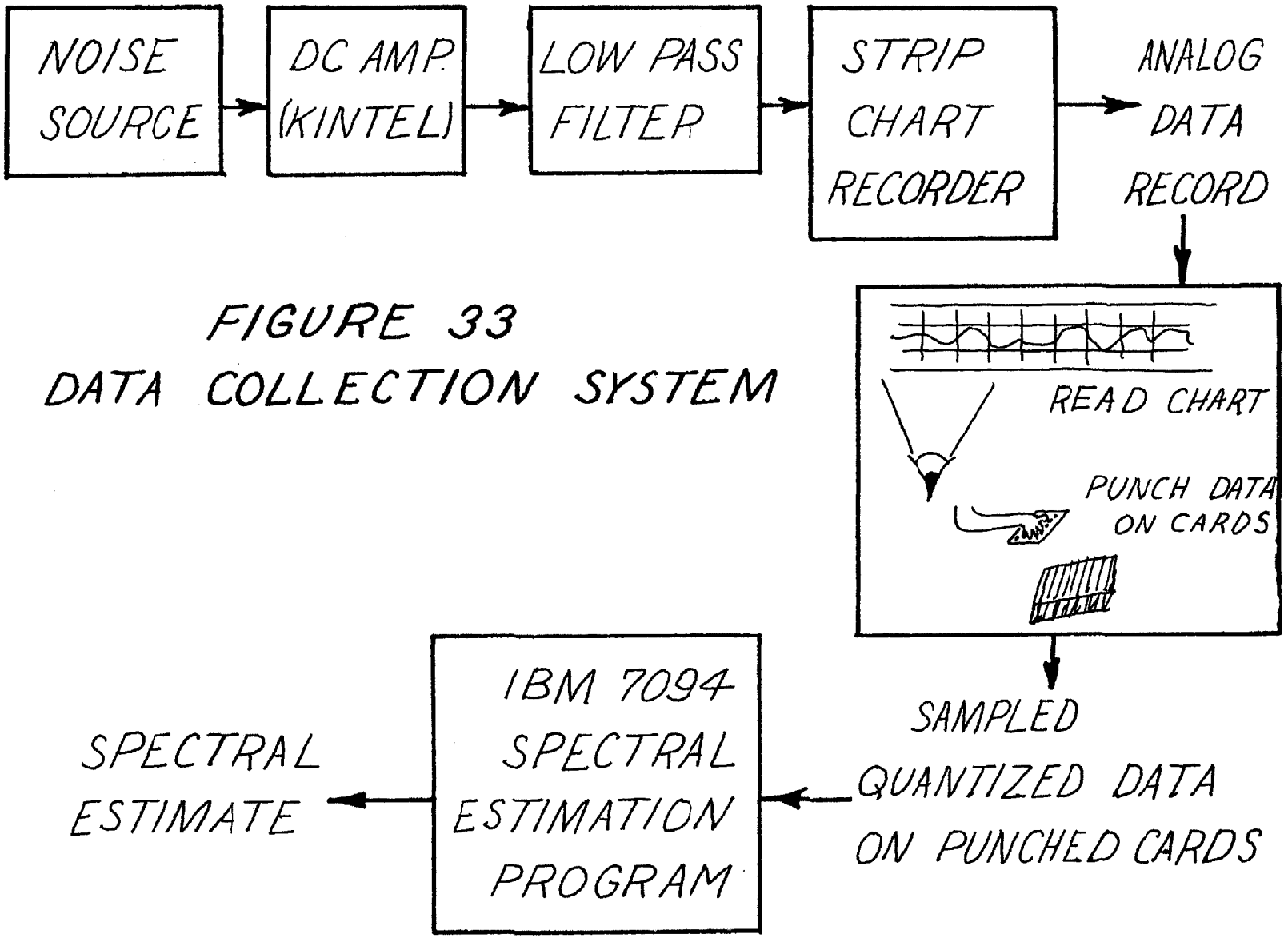

FIGURE 33
DATA COLLECTION SYSTEM

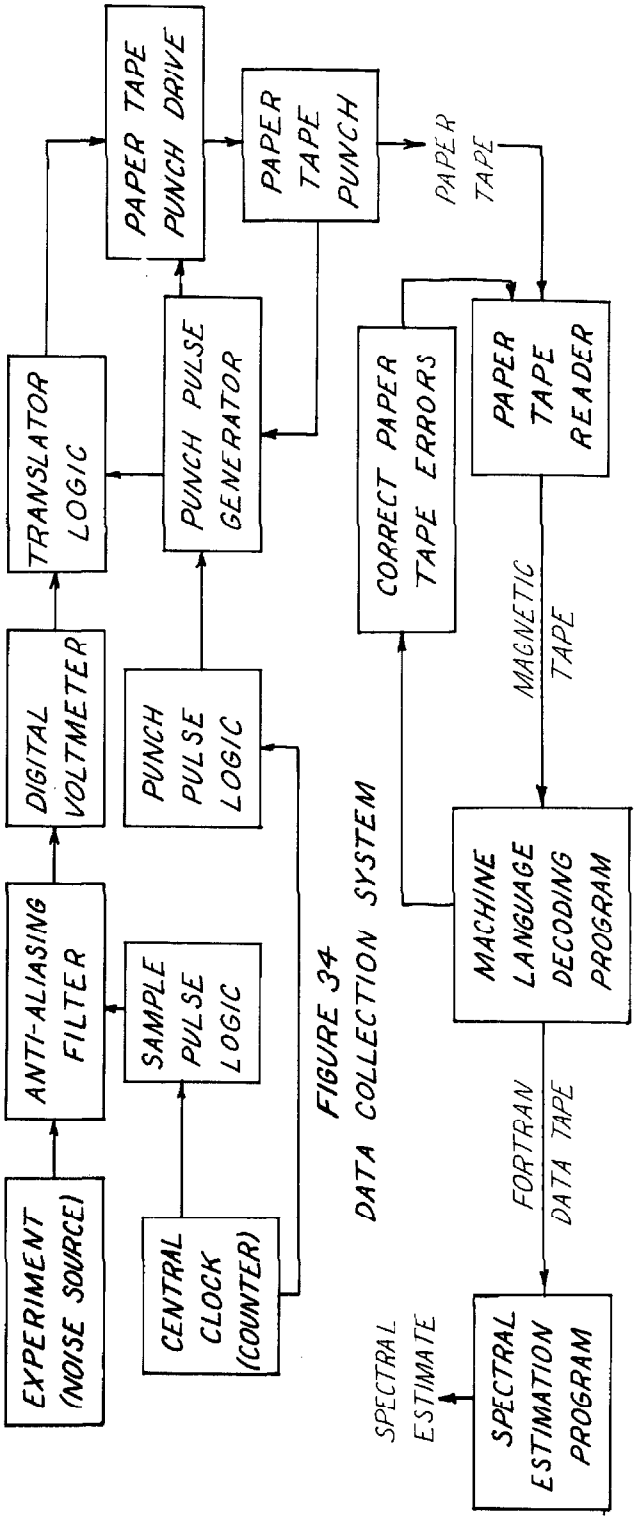

FIGURE 34
DATA COLLECTION SYSTEM

The central clock for the system consists of a Beckman Berkley counter. The outputs of each decimal counting unit are available as four wire binary coded decimal outputs on a plug at the rear of the chassis. These are connected via a cable to binding posts at the front of the relay rack in which most of the equipment is mounted. The appropriate decimal counting unit outputs can then be selected conveniently and fed into the system logic.

The analog to digital conversion was accomplished via a model 3440 Hewlit-Packard digital voltmeter. This meter samples the noise input by counting the time interval required for an internally generated ramp to equal the input voltage.

The digital voltmeter reading is available in a four-wire binary code on a connector at the rear of the instrument. This information is provided in a parallel fashion. The translator logic referred to in Figure (34) converts it to a serial format and changes the code slightly. A schematic of the translator logic circuitry is shown in Figure (35). It is neither clever nor original but was designed for convenience and use of readily available components. The inputs from the digital voltmeter are numbered according to the pin numbers on

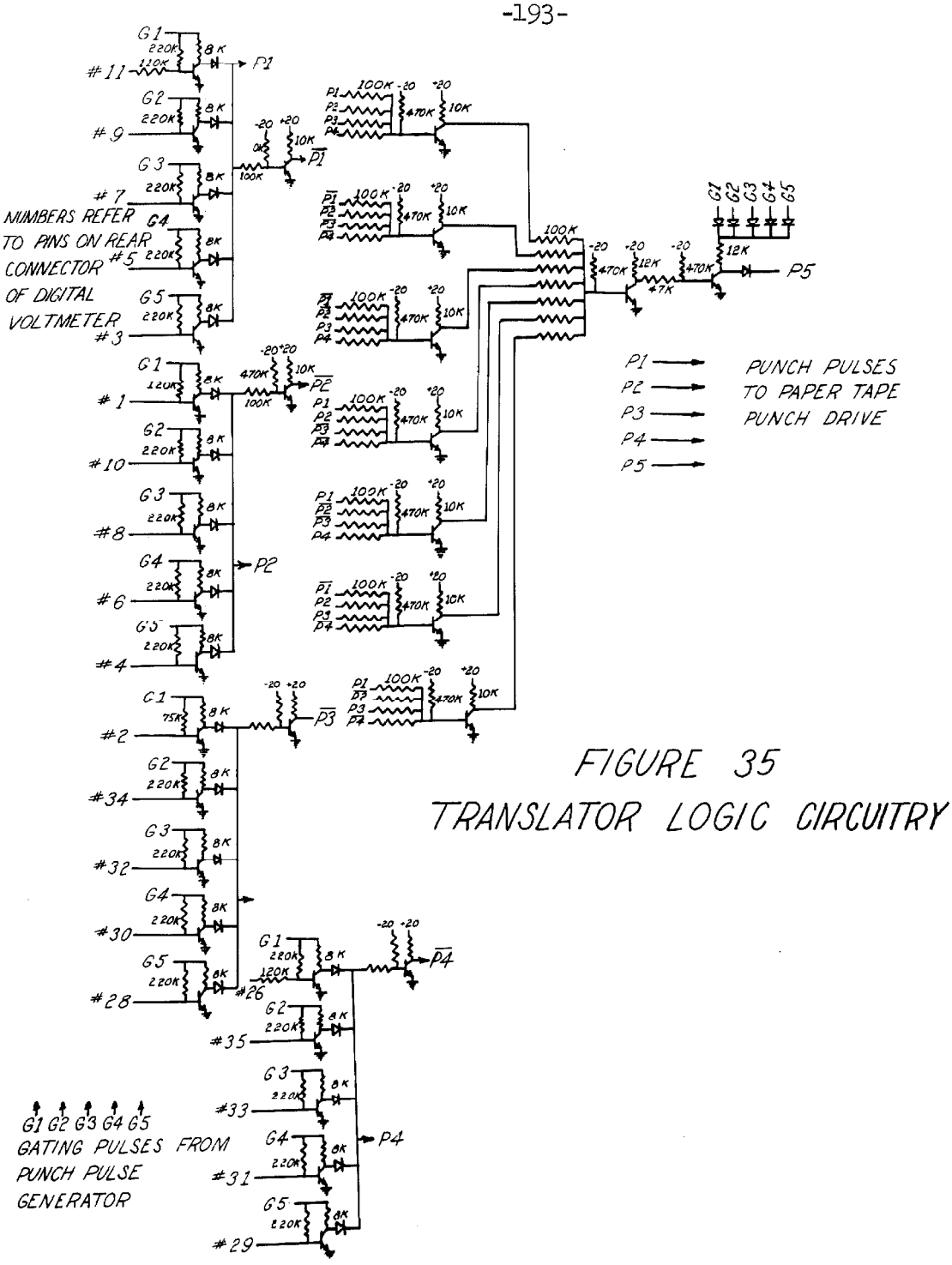

FIGURE 35
TRANSLATOR LOGIC CIRCUITRY

the digital jack at the rear of the digital voltmeter. The punch pulse generator outputs are labled G1, G2, G3, G4, G5 and correspond to the first 5 rows on the paper tape. The sixth pulse is fed directly to the paper tape punch drive circuit which generates the end of word code internally. The outputs from the translator logic appear on five separate lines fed to the paper tape punch magnet drive circuitry and are labeled P1, P2, P3, P4, P5. Most of the circuit complexity is associated with generating a parity bit to be punched on the paper tape. This part of the circuit never did operate entirely without error for any extended period of time. This situation is not without irony in that the part of the circuit which caused the most trouble shooting problems was that designed to make the code error detecting.

The punch pulse circuitry generates pulses at 0.0 and 5.0 to punch the digital voltmeter reading onto the paper tape. The sample pulse circuitry generates pulses at 0.1 and 5.1 which are sent to the digital voltmeters external sample terminal to instigate a new measurement. In this case 4.9 of the 5 seconds between samples are available for the voltmeter to reach a reading. This is long enough to automatic range through the whole set of ranges for the Hp 3440. For other sample times

these values are correspondingly scaled. Figure (36) shows a schematic of the sample and punch pulse circuitry. The Schmitt trigger was required to achieve a fast enough rise time to trigger the digital voltmeter's sample flip-flop.

The punch pulse generator is fed by a synchronizing signal from the shaft of the paper tape punch motor. It generates a series of 6 square pulses each of which eventually generates a row on the paper tape. The sixth is used to generate an end-of-word message and the sequence repeated. Originally, a transistor mechanized scr type circuit was used for this purpose. It was found that small timing errors occurring at various places in the circuit led to false pulses and/or missed pulses. After considerable effort was expended on eliminating this particular version of the digital race problem the circuit was discarded in favor of that shown in Figure (37) This circuit mechanizes the ripple shift register via a 3 stage binary counter and output gating. On receipt of a clock input pulse the circuit puts out the six required pulses at the next available shaft rotation (synch pulse).

The paper tape punch drive generates the currents necessary to drive the magnetic in the paper tape punch and generates a feed pulse to step the paper tape forward. This circuit uses

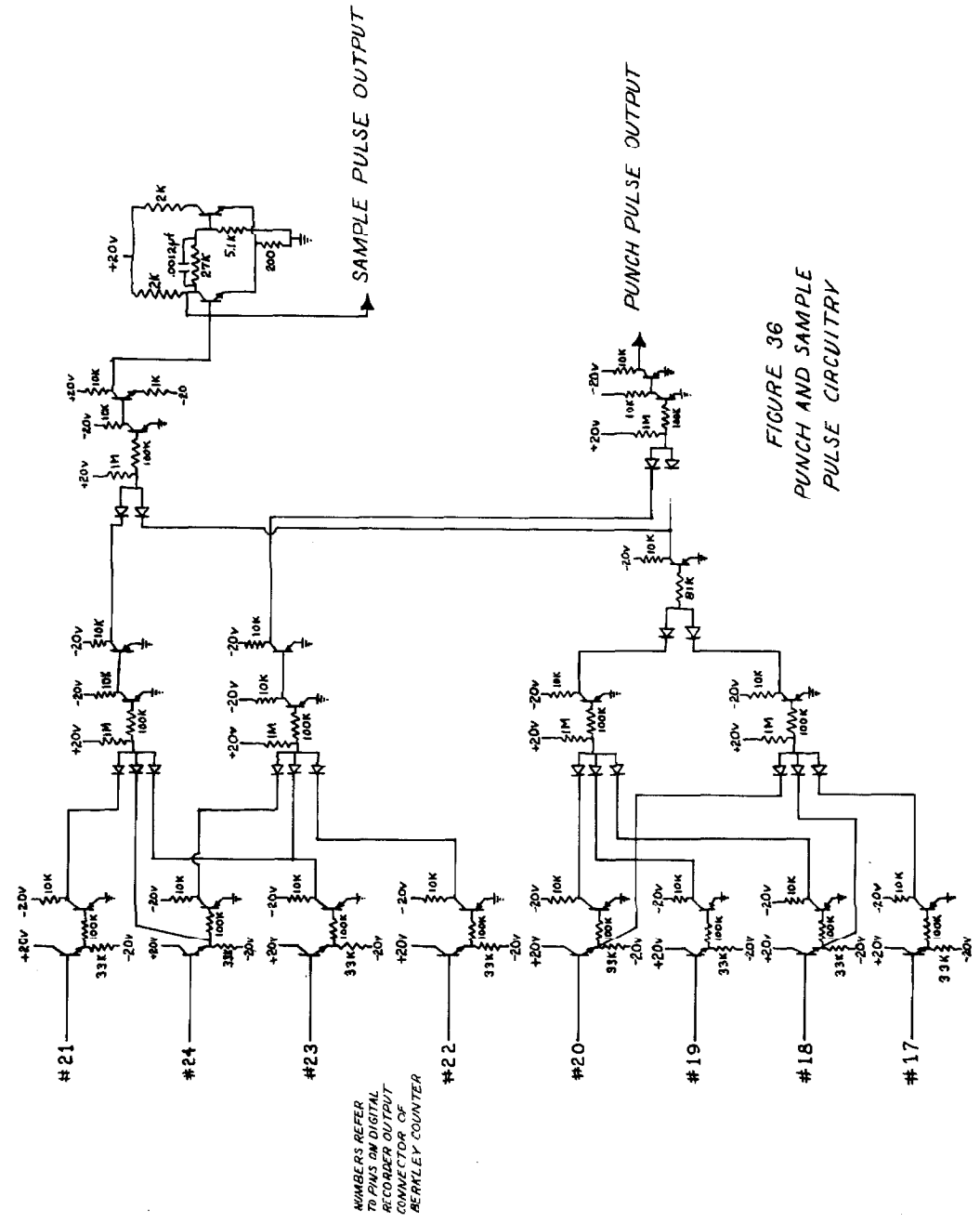

FIGURE 36
PUNCH AND SAMPLE
PULSE CIRCUITRY

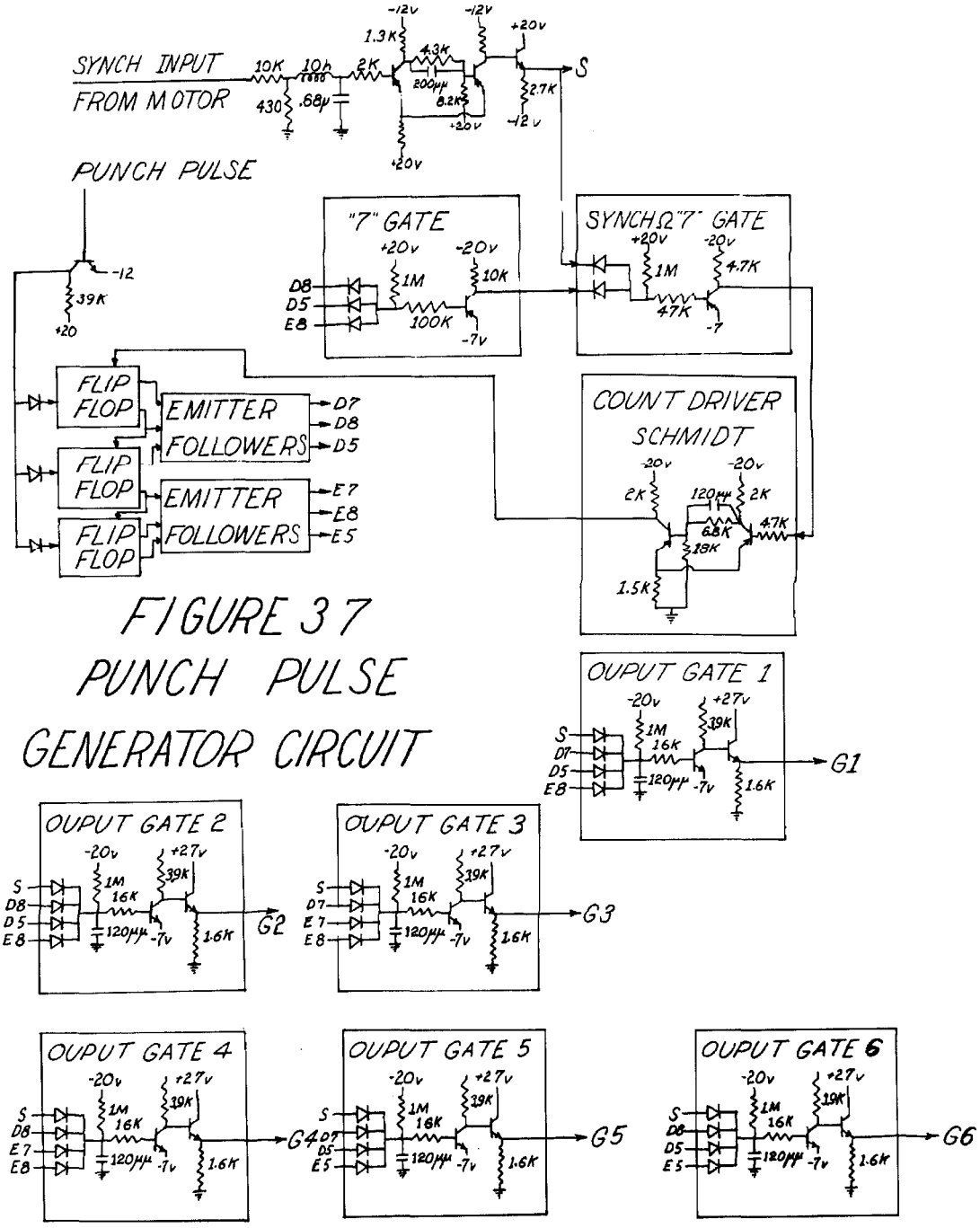

FIGURE 37
PUNCH PULSE
GENERATOR CIRCUIT

silicon controlled rectifiers fed by emitter followers and was designed and contructed by H. C. Martel

After a magnetic tape image of a given paper tape has been formed, the machine language program* attempts to form a FORTRAN DATA tape. If disallowed characters or data words of improper length are found they are printed out. Most simple kinds of errors can be corrected by hand on the paper tape which must then be reread onto magnetic tape.

* This program was originally written by J. K. Lo and later revised by J. Hughes both of the CIT Computation Center.

4.4 Line Voltage Noise

One of the noise processes investigated at very low frequencies was the amplitude fluctuations in the 60 cycle power line. Suppose we consider the 60~ line voltage to have an amplitude which is a constant plus a zero mean, stationary random process. Then it is interesting to ask, "What is the spectrum of these fluctuations in line voltage?" As well as being of academic interest the results are useful in calculating the effects of line voltage "noise" on any given place of experimental equipment operating in the laboratory. Given the performance specifications for the instrument relative to line voltage variations one could then make a more intelligent decision about whether or not a regulated supply should be employed.

All of the power spectral densities obtained for the line voltage experiment were calculated from data hand punched onto IBM cards from analog Easterline Angus Strip Chart recordings. A sketch of the experimental setup used to obtain

the raw data is shown in Figure (38). The simple average reading power supply circuit whose schematic is shown in Figure (39) was utilized. This choice is motivated by the desire to measure the low frequency "dc" fluctuations in line voltage amplitude. This circuit is followed by an amplifier to drive the Easterline Angus recorder. No anti-aliasing filter was employed because it was anticipated that we would be dealing with a spectrum decaying at least as fast as $1/f$ and possibly as fast as $1/f^2$.

5. EXPERIMENTAL RESULTS

This section presents the actual results for the various noise processes measured. These include: room temperature fluctuations, Mark I Noise generator, amplitude noise, and line voltage noise. Both raw data and estimates of spectral density are given.

5.1 Room Temperature Measurements

As mentioned above in Section 4.2 the room temperature first became important through being measured inadvertently by the Mark I output voltage. It was therefore necessary to measure and/or control it. The approach taken as indicated above was to control only a small environment immediately adjoining the noise generator.

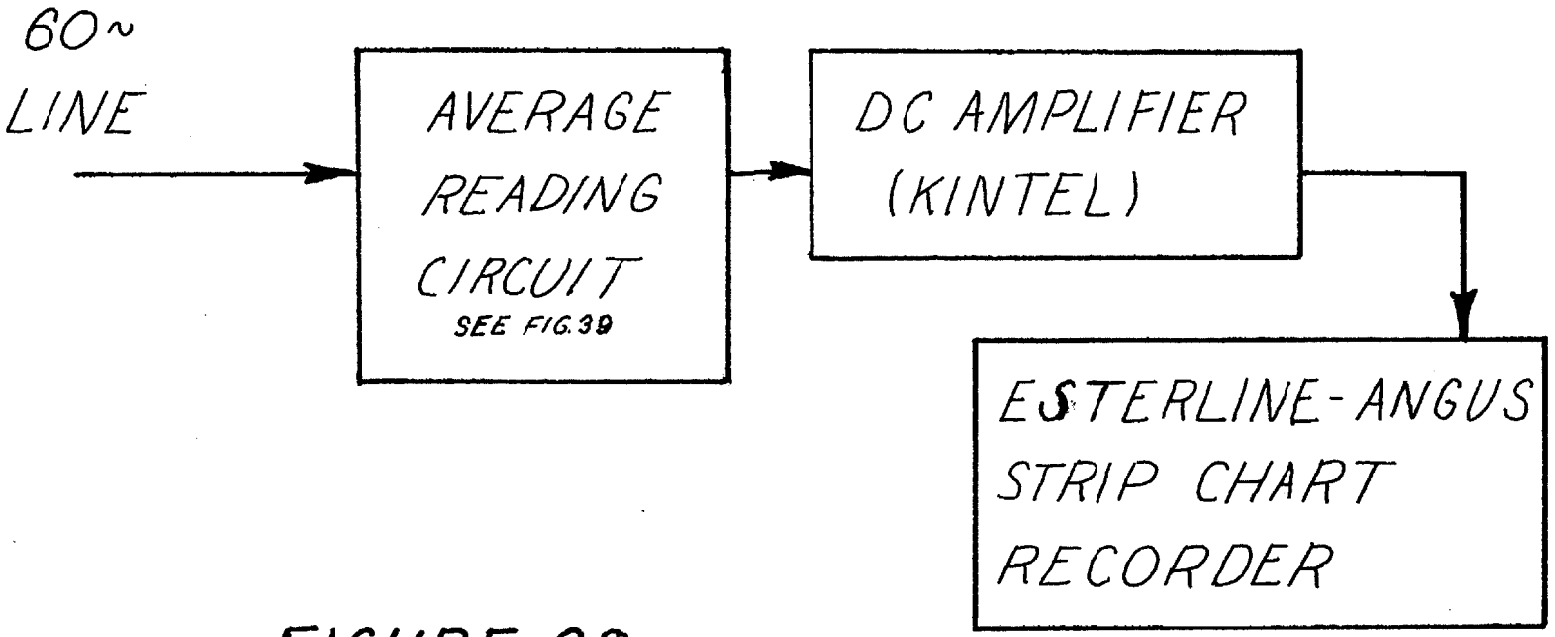

FIGURE 38
LINE VOLTAGE NOISE EQUIPMENT

FIGURE 39

CIRCUIT FOR LINE VOLTAGE EXPERIMENT

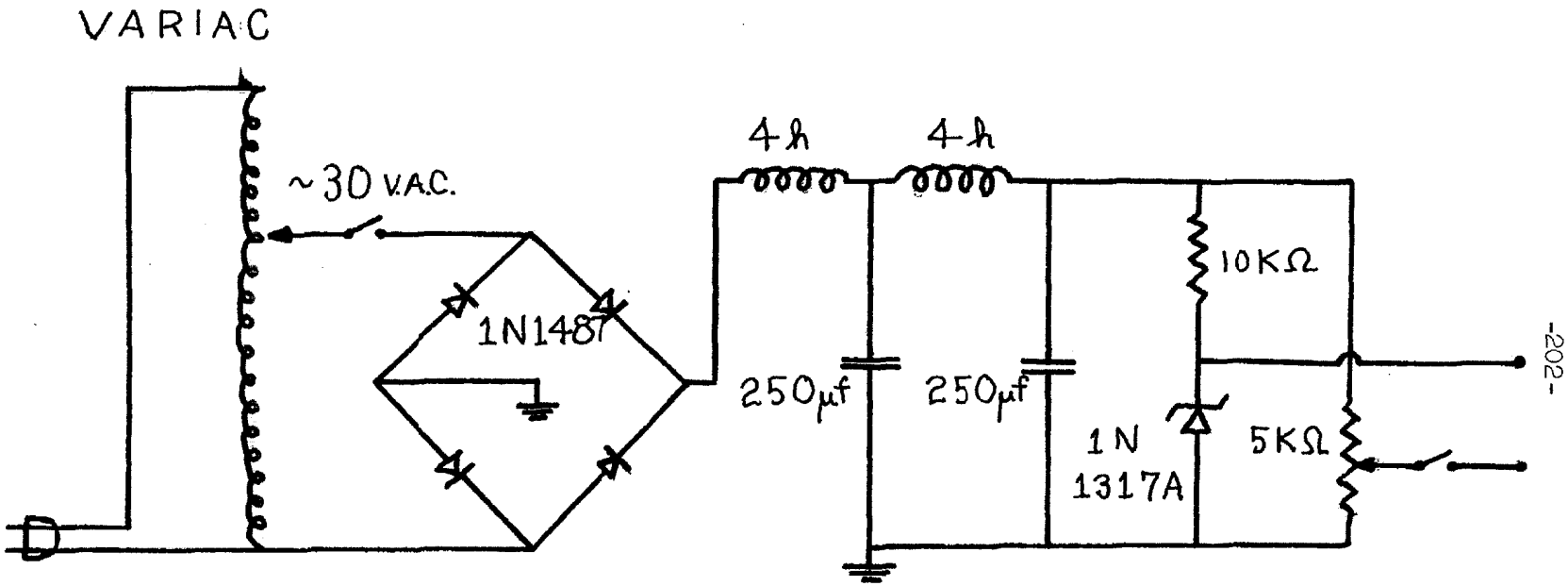

At the same time, however, it was of interest to know if the spectrum of the room temperature was as inferred from Mark I data. In addition, of course, the room temperature was precisely the disturbance a thermal control system for the noise generator environment would have to control against. Thinking of the ambient temperature as a disturbance led naturally to the notion of considering it, like many other disturbances, as a random process.

What does the room temperature do? It gets hotter in the daytime and colder at night, but not by the same amounts every time. This behavior is typical of many processes. Given all the pertinent data on a microscopic scale the process can be calculated exactly. However, on a microscopic scale it can be considered random.

Let us, then, consider the room temperature as a random process. It obviously has a mean value and lots of energy at 24 hrs and its harmonics. But what are the peak excursions? What is the "average" temperature like? Is this process gaussian? What is the "shape" of its spectrum? Does it fall off linearly with increasing frequency or like $1/f^2$? We shall estimate the power spectral density of this random process. The results will be useful in the design of our thermal control system (see Section 4.2 above) and also applicable to a large number of laboratory experiments in which the temperature is not controlled. For instance, suppose the drift in the output

of a solid-state regulated power supply is dominated by the temperature dependence of one or more components. Knowledge of typical spectra for laboratory room temperatures enables a statistically meaningful prediction of the rms value of the drift.

In order to measure and record the temperature electrically, a scheme exactly like that used to measure the oil bath temperature was employed. A complete discussion of the system and its design was presented above in Section 4.2. The setup implemented to monitor room temperature differed only in that a thermometer with a range of 15° - 35°C was used. Its calibrated resolution is $.1^{\circ}$C and it can be read easily to $.01^{\circ}$C. A diagram of the experimental setup is shown in Figure (40).

Appendix C contains a tentative error analysis of the temperature sensing system. It is expected that the resultant overall temperature sensor will have an accuracy on the order of $\pm$ $.1^{\circ}$C. A calibration curve obtained by cycling the temperature in a short period of time will, of course, be somewhat better than this. It will not include long-term drift effects of any of the components. However, this is not the appropriate information for our purposes since we are interested in the accuracy of the temperature sensor over many months. For this reason, it was decided to calibrate the whole temperature sensing system intermittantly over the full length of the experiment. This was accomplished by measuring and

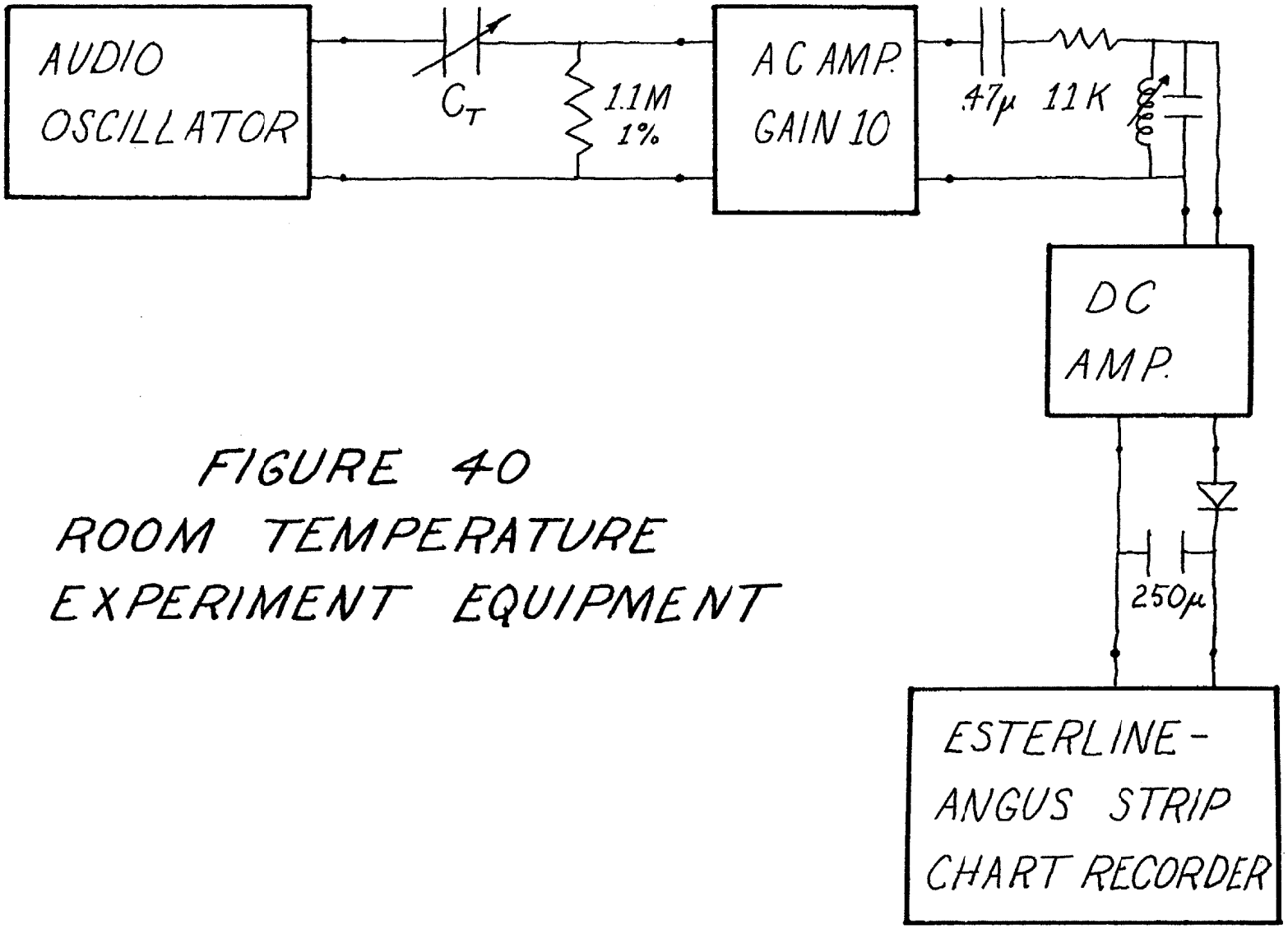

FIGURE 40
ROOM TEMPERATURE
EXPERIMENT EQUIPMENT

recording the actual temperature, the voltage sensed as temperature, the oscillator voltage output, and the recording chart reading intermittantly at arbitrary times. The result is a composite calibration curve for the whole temperature sensing system for the experiment. Figure (41) shows this data and indicates that the system is in fact accurate to something on the order of $\pm .1^{\circ}C$. The line shown is described by

$$V_T = \hat{a}(T - \hat{b}) \tag{130}$$

where $\hat{a}$ and $\hat{b}$ are the minimum variance estimates assuming that the data is actually from a process whereby

$$V_T = a(T - b) + n(t)$$

and $n(t)$ is white noise. One can use the estimated variance for $n(t)$ to calculate an error in the measured spectrum of the room temperature. However, such sophistication is hardly worthwhile in this case. The quantization error due to the visual reading at the recordings is much larger than $n(t)$. Therefore, to the extent that this quantization noise is negligible in the final spectral estimate the temperature sensing is exact.

The room temperature measured is for Room 223 Spaulding from March 17, 1965 through March 9, 1966. It is asserted that this is typical behavior for an air-cooled laboratory with some amount of equipment operating continuously.

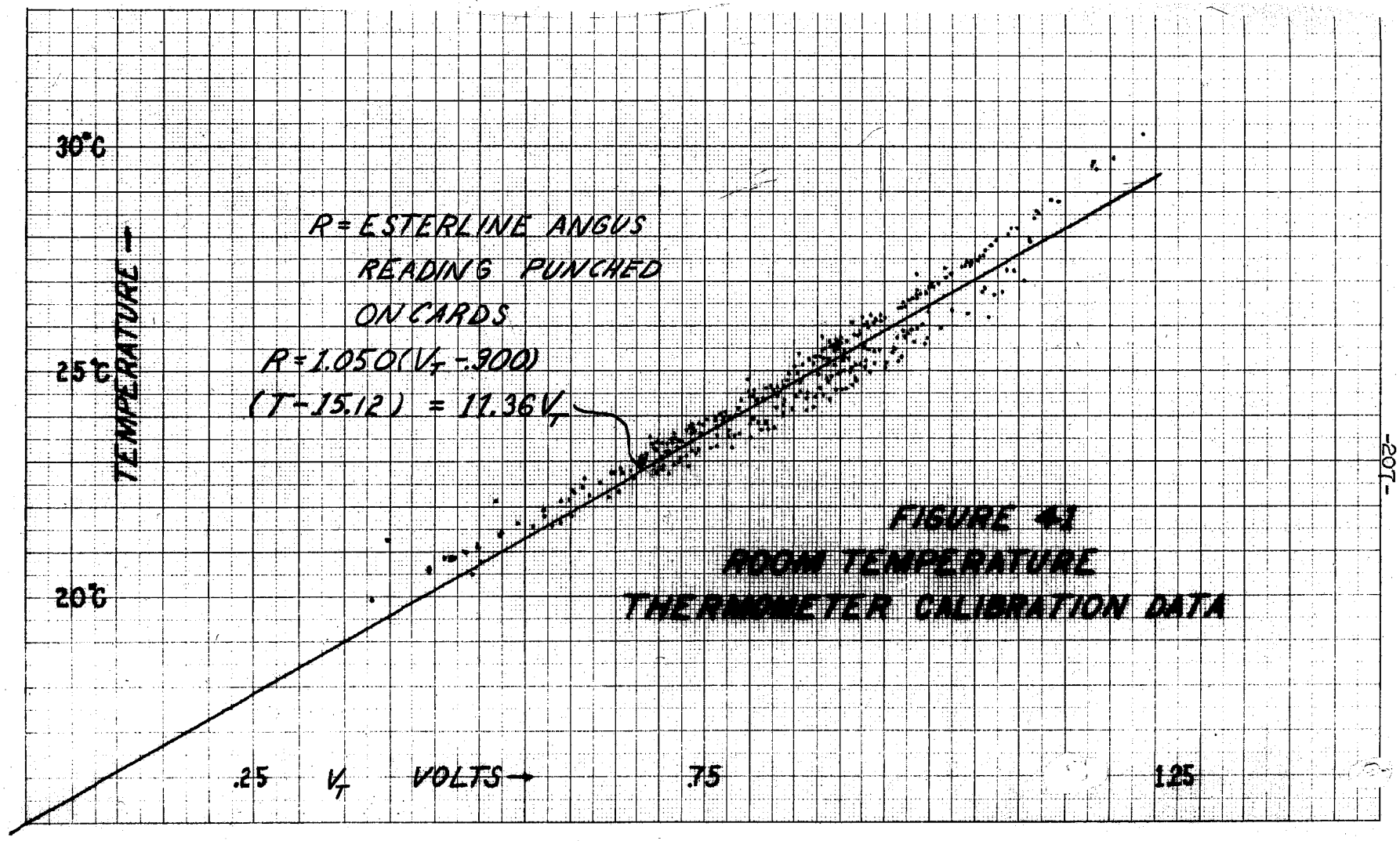

FIGURE 4.1
ROOM TEMPERATURE
THERMOMETER CALIBRATION DATA

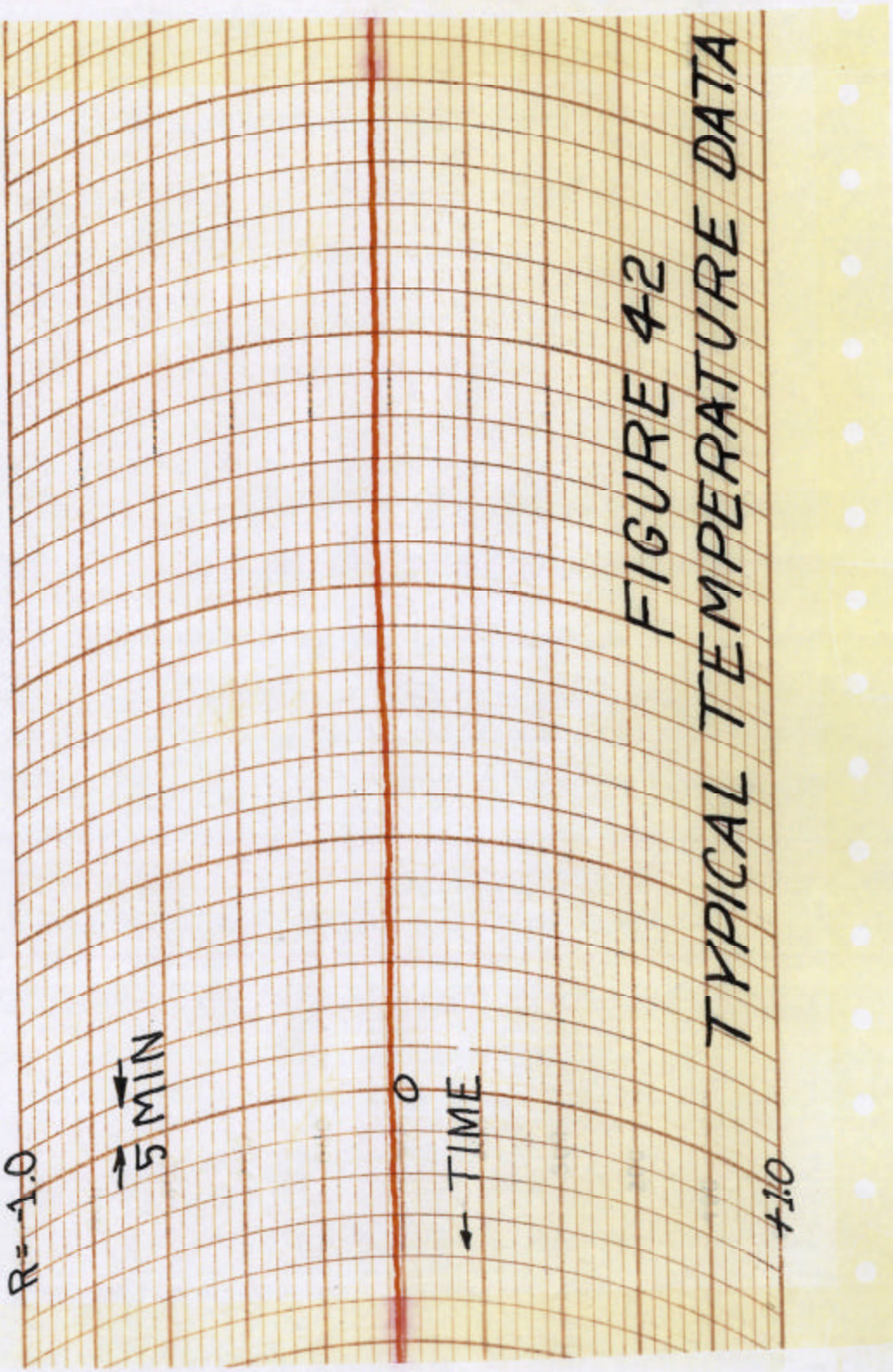

FIGURE 42
TYPICAL TEMPERATURE DATA

In an examination of the experimental results regarding room temperature, it is perhaps most instructive to start with the raw data. Figure (42) shows a typical section of Easterline Angus chart from which the lowest frequency raw data was taken. As indicated on the figure the time scale is such that a sample is taken every 5 minutes and the vertical scale is ± 1 volt full scale with zero at the center. This figure is full size. The quantization level is .01 volts which corresponds to reading four levels between each line shown on the chart. This data is available for the time period 3-17-65 through 3-9-66. As is obvious from the figure, not much information about the random process is obtained by examining the raw data on this scale.

The first level of condensation is more informative and is represented by Figure (43a) and (43b). The time scale is such that each curve covers 5 days. At this scale 52 sheets of graph paper are required just to cover the period from 6-26-65 to 3-9-66. A few typical sections were chosen and 8 of these are presented, 4 on each figure. If it is sensible to make such a characterization when dealing with random processes, these samples represent the various "types" of behavior exhibited in the composite data. The time period represented by each curve is shown on the figures and the vertical scale is ± 1 volt; that at which the data was read from the Easterline Angus Chart. Down on these graphs

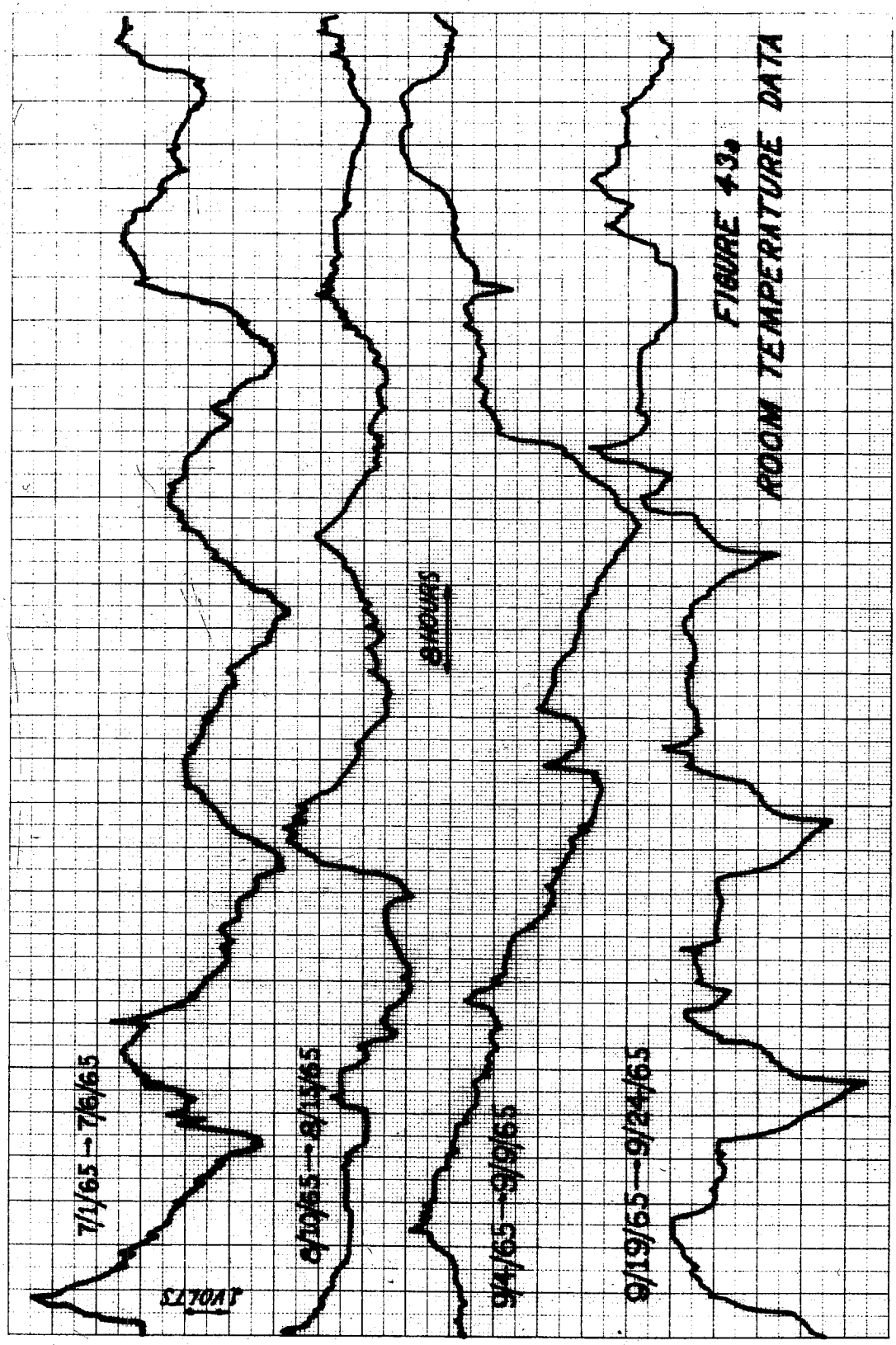

FIGURE 43.
ROOM TEMPERATURE DATA

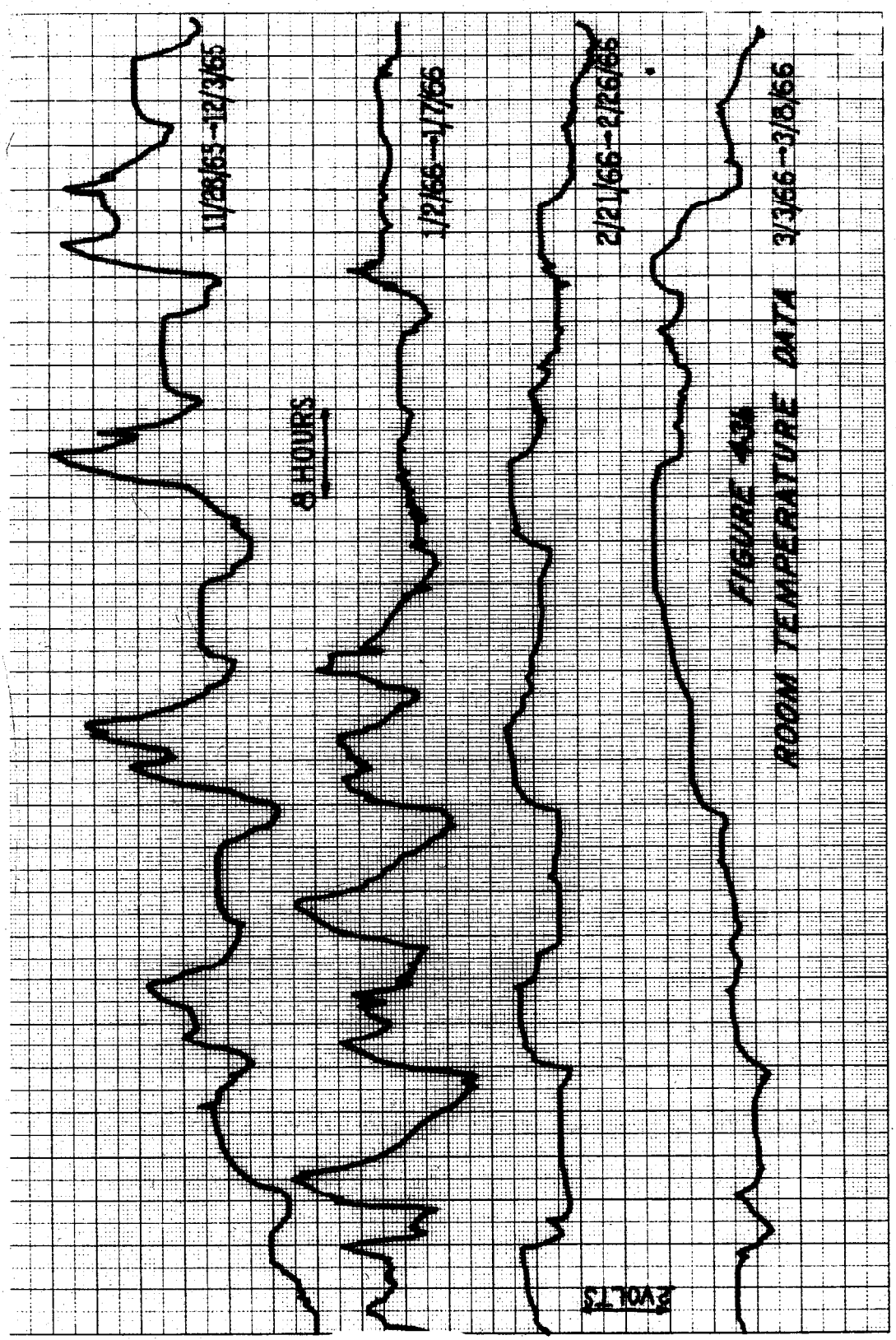

FIGURE 43A
ROOM TEMPERATURE DATA

corresponds to lower temperatures and vice-versa. The scale of conversion from volts to degrees centrigrade is given by Equation (130). In general, the bottom most excursions run to something like 20°C and the top most to something like 30°C. The first curve on Figure (43a) (i.e., uppermost) indicates very clearly the dominant feature of the room temperature, namely its 24 hour cycle. However, the second and succeeding curves indicate that the story is nowhere near so simple. The waveforms are strange enough to indicate that there must be a considerable amount of energy at higher harmonic frequencies. The third curve on Figure (43a) is an example of the behavior tending to indicate that there is also considerable energy at frequencies below 1 cycle per day. The first curve on Figure (43b) indicates a very common type of behavior which illustrates the comment made above about the non-randomness of the room temperature "noise" when viewed on a microscopic scale. The flat portions show that between about 2 AM and 8 AM the temperature in the room is very constant. During this time the room is rarely entered and the fans are off in the air circulating system for the building. The temperature characteristically decayed in the morning (8 AM) when the fans come on and decreased until somewhere around noon. Because no extra equipment was being operated during the mornings in

this period, the room temperature didn't begin rising until afternoon. It then rose due to equipment operation and other independent building phenomena through 10 PM or so. At 10 PM, the fans were once more turned off and the temperature decayed back to "steady state" with no excitation for the 2 AM to 8 AM period (actually "small" is more proper since some equipment was operating on a 24 hour basis). This situation does not always occur due to both internal and external conditions changing as the other curves indicate. However, it or some version of it occurs frequently enough to merit discussion. The very smooth behavior appearing in the last two curves is believed to be a result of operating a great deal of equipment in the room on a 24 hour basis. The paper tape punch data collecting system was obtaining a large portion of the Mark I data during this time. If one considers the air conditioning system for this room to have a volume flow saturation then one expects the resultant temperature to be higher and more regulated, which is apparently what occurred.

Leaving aside for the moment all cause and effect relationships, the data on this time scale does not seem to be very "random"; or does it? The character certainly changes from time to time. Is it perhaps best regarded as a non-stationary random process? This is not clear, since

one could, by applying a little Yankee ingenuity, invent an ensemble for which this data would make a reasonable sample function. In any case an idea of the amount, in some sense, of non-stationarity present is given by estimating spectra from these eight pieces of data separately. Figures (44a) and (44b) show these estimated spectra labled 1 through 8 in the order in which the raw data appears in Figures (43a) and (43b). The minimum frequency resolution on these plots is 8.33×10^{-5} cps and they are Q_2 estimates prewhitened for a $1/f^2$ spectrum The fact that these spectra do not differ more violently is consistent with the fact that their minimum resolution corresponds to a period of ≈ 3 hours. To obtain reasonable variance estimates with greater resolution, one has to look at longer sections of data. This will be done shortly. The power spectral density of room temperature variations can be modeled fairly accurately as $1/f^2$ for this region (8.33×10^{-5} cps to 1.667×10^{-3} cps). The quantization noise for this data calculated from the $\Delta\epsilon = .01$ step size is -26 db. The smooth variance approximation yields 1σ bands of $\pm$ 11.8% or (+.48 db, -.54 db).

The next level of condensation is again more informative in that it provides a still broader view. Looking at the data on more and more condensed time scales allows the human eye and brain to extract lower and lower frequency information.

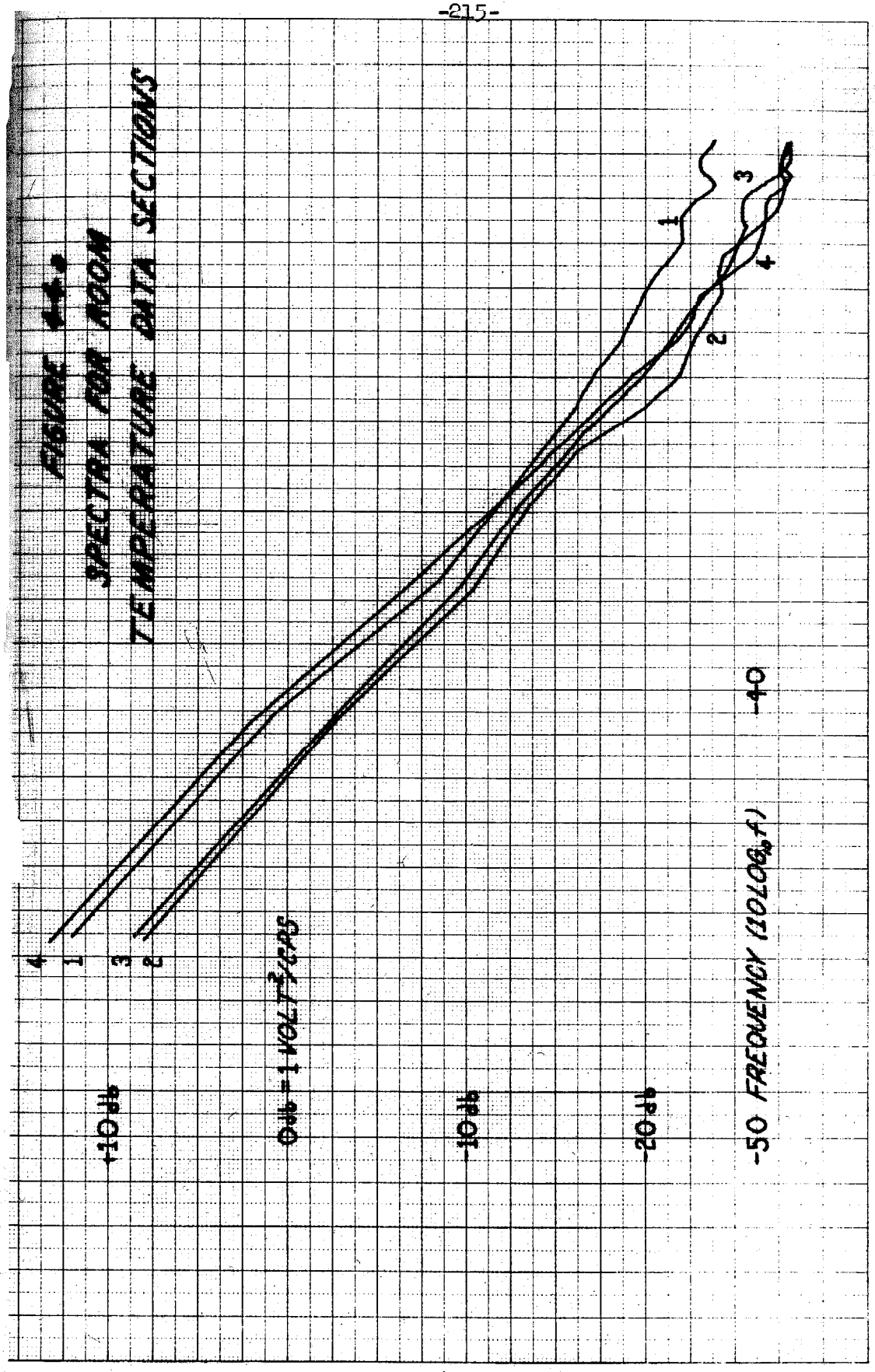
FIGURE 4.3
SPECTRA FOR ROOM TEMPERATURE DATA SECTIONS
+10 db
0 db = 1 VOLT²/cps
-10 db
-20 db
-50
-40
FREQUENCY (10LOG₁₀f)
1
2
3
4

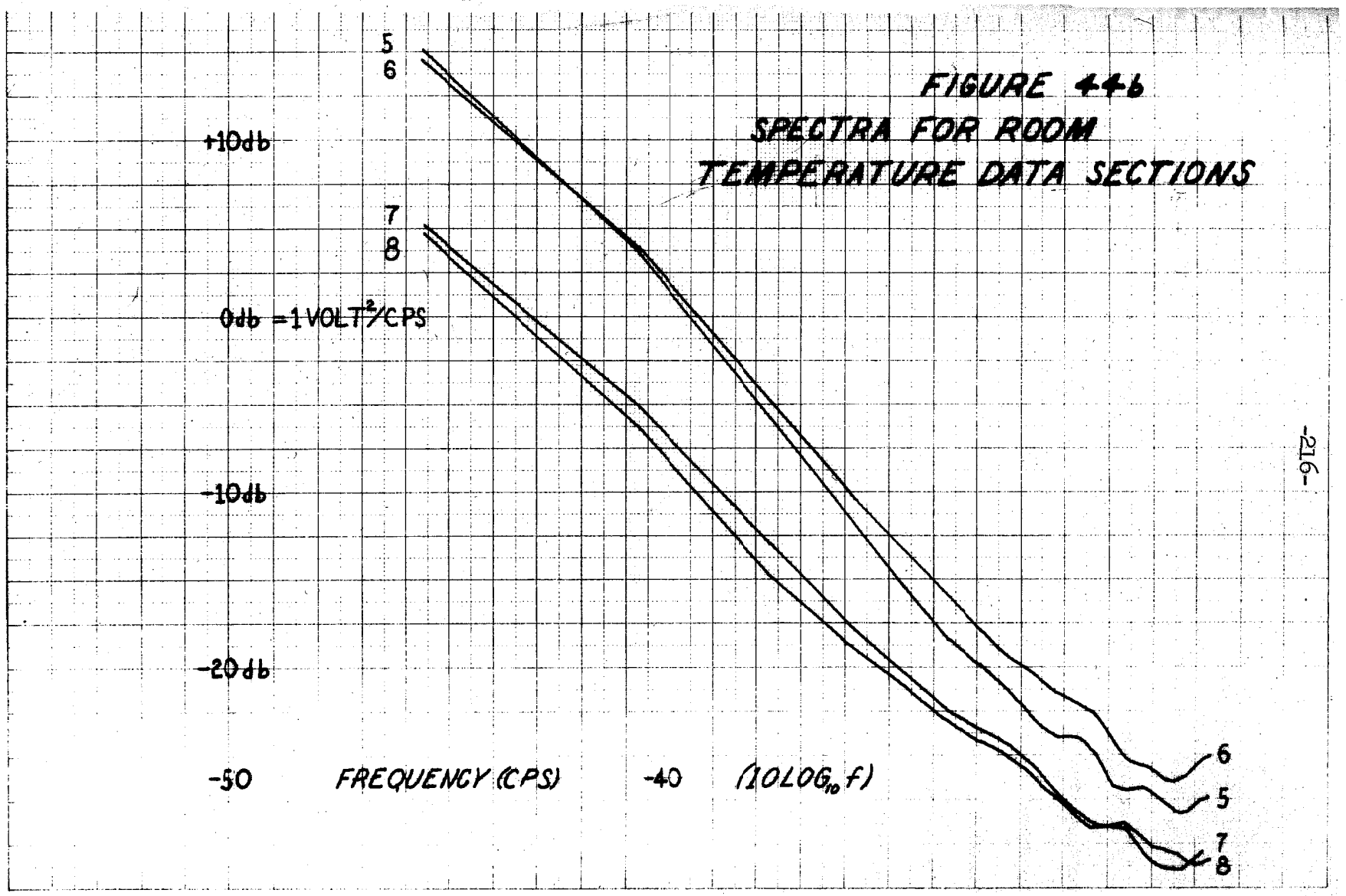

FIGURE 44b
SPECTRA FOR ROOM
TEMPERATURE DATA SECTIONS

Figures (45a,b,c,d,e,f,g,h) show all of the room temperature data (a years worth) on a still more condensed scale. The vertical scale now extends only ± .6 volt and the time scale is 30 days per sheet. Another feature of the noise process becomes more obvious. There exists what might be called a "week end fluctuation." Figure (45h) illustrates it in a most pronounced fashion and has the days of the week labled. It seems to be present in almost all cases to some extent. The activity in the room is naturally somewhat different on weekends. This is combined with a different schedule for the building's air circulating and heating/cooling system. These figures show the daily cycle in very pronounced form but also indicate that there is a considerable energy at still lower frequencies. An informative exercise is to time scale mentally by 9 decades so that 24 hours becomes roughly 10Kc. Then imagine a narrow band noise signal with a center frequency at 10Kc. How would the narrow band noise waveform as viewed on an oscilloscope differ from the scaled up room temperature waveform? It would, in general, not have the slower wiggles seen in the temperature data. If RC noise were viewed in the same way it would appear more similar in the slower wiggles but less in the faster ones. In this sense one expects intuitively that the room temperature spectrum should be roughly $1/f^2$ type (RC or first order) noise with an excess of energy at 24 hours and its harmonics.

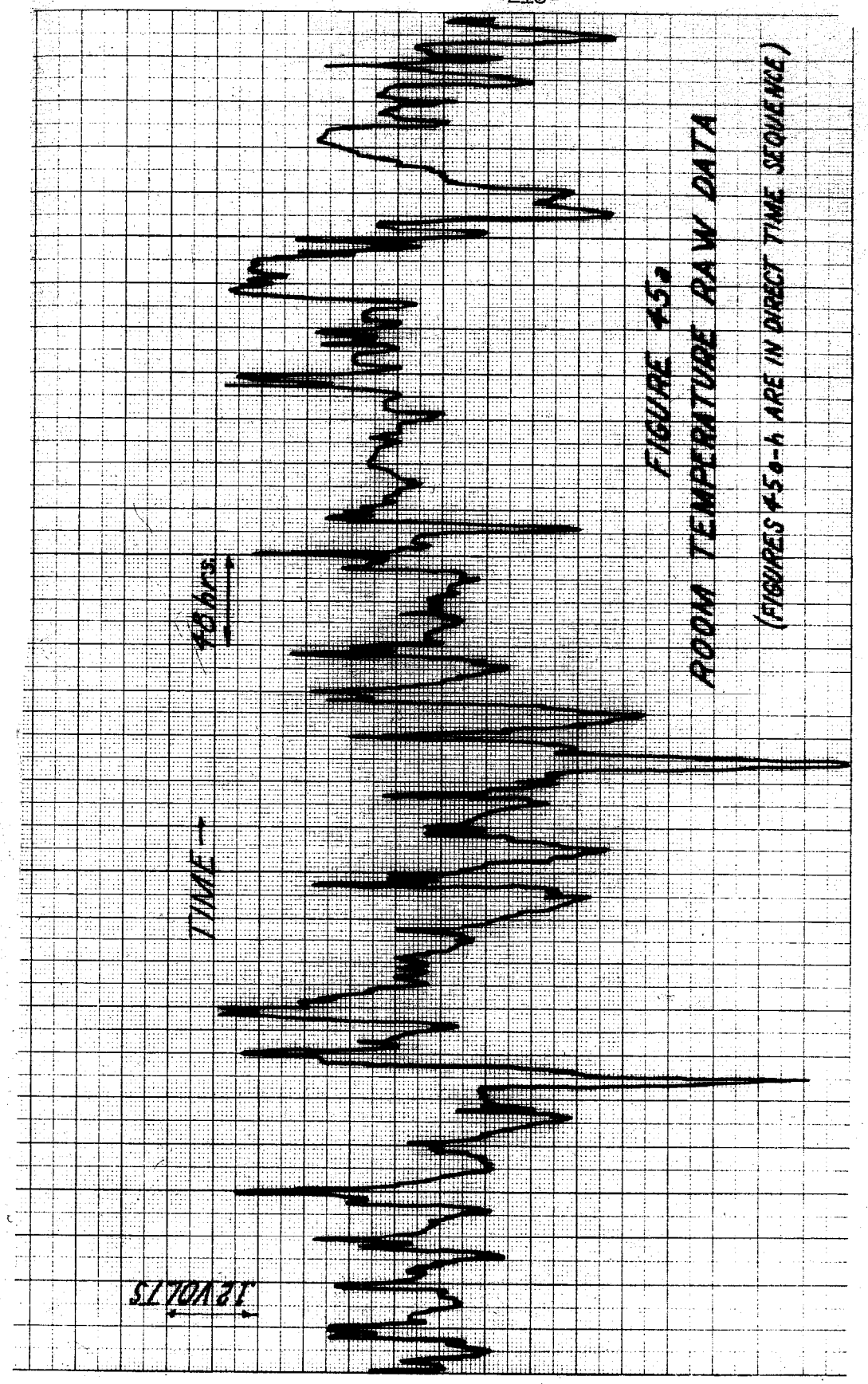

FIGURE 45a
ROOM TEMPERATURE RAW DATA
(FIGURES 45a-h ARE IN DIRECT TIME SEQUENCE)

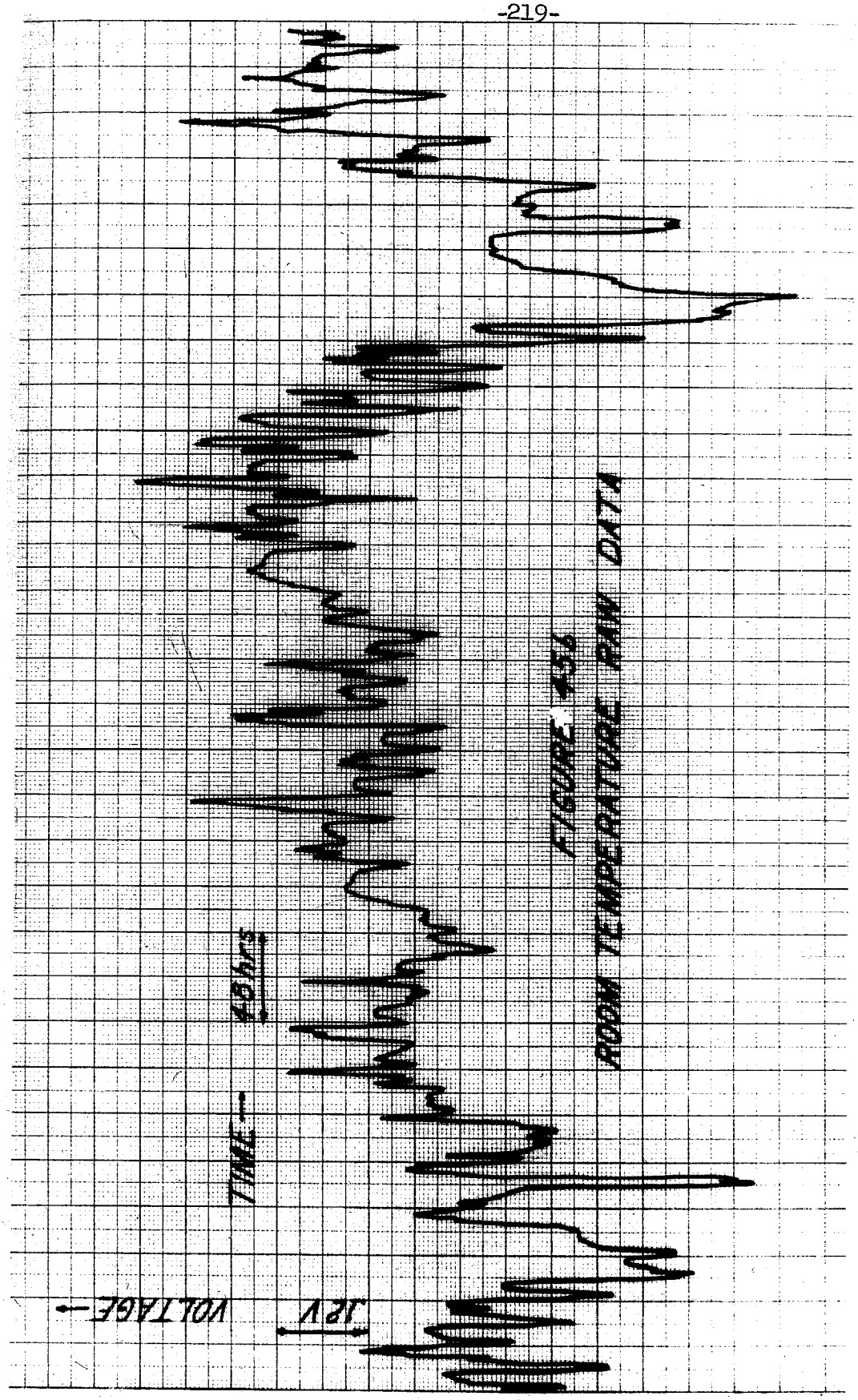

FIGURE 45
ROOM TEMPERATURE RAW DATA

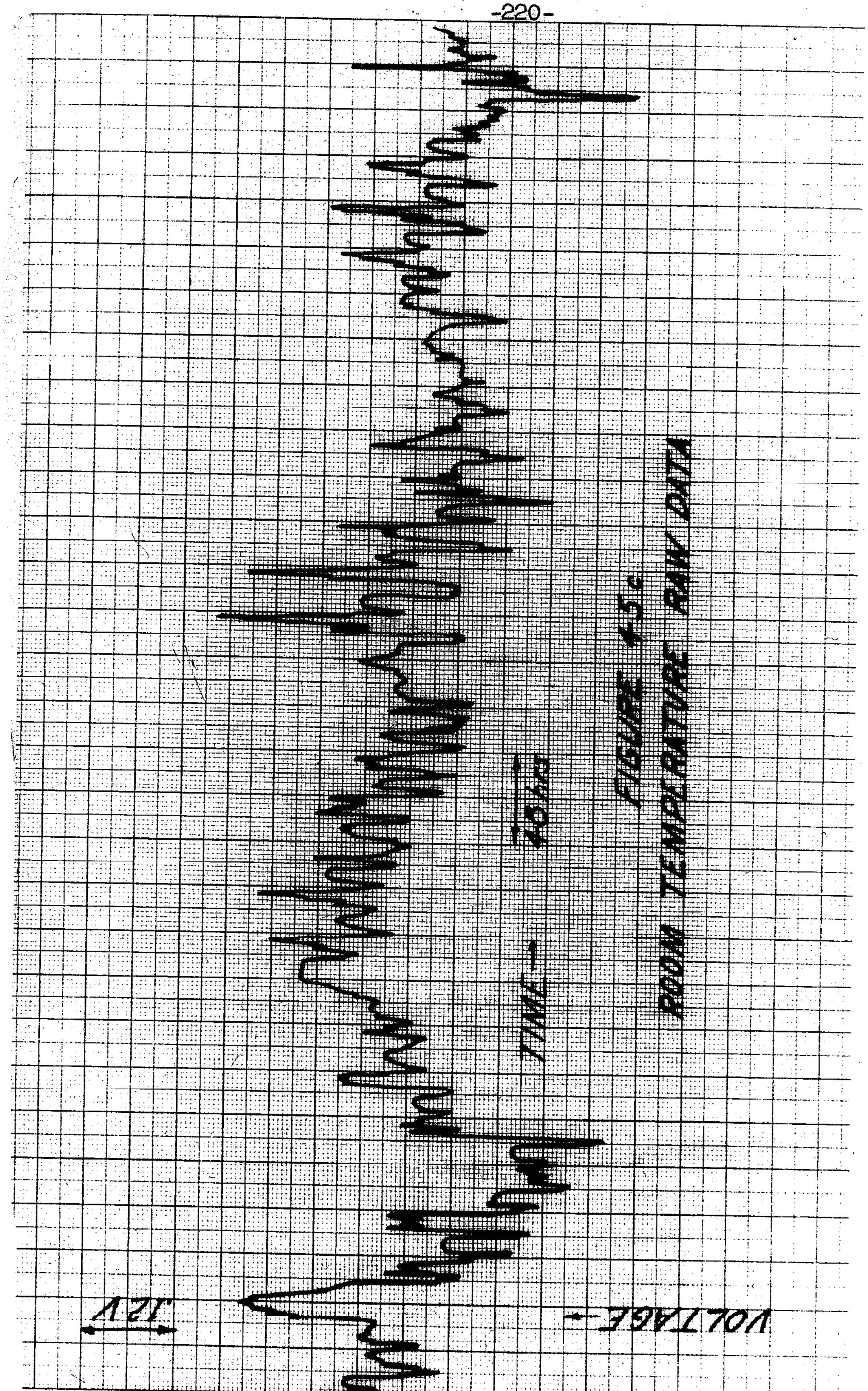

FIGURE 4-5c
ROOM TEMPERATURE RAW DATA

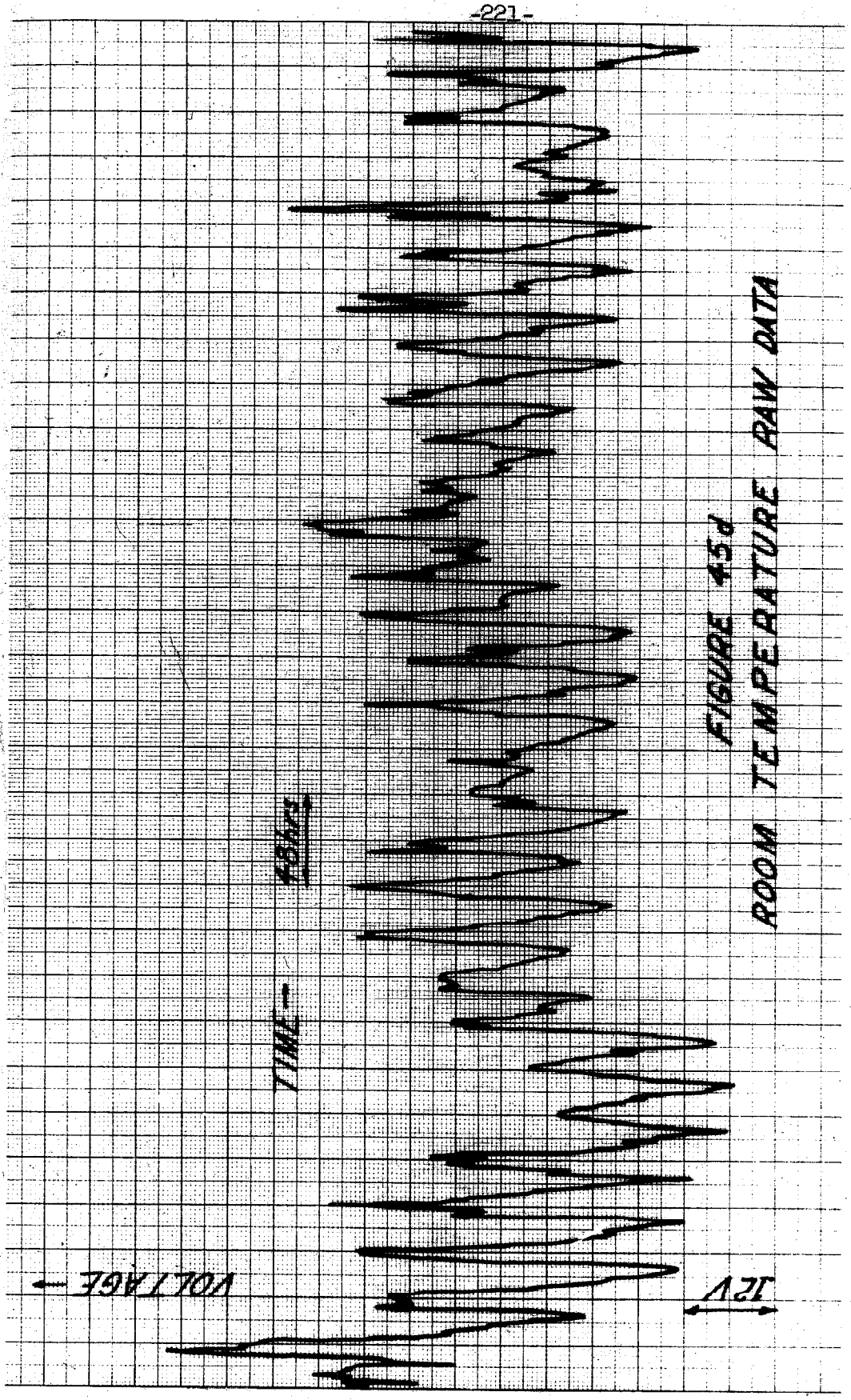

FIGURE 45d
ROOM TEMPERATURE RAW DATA

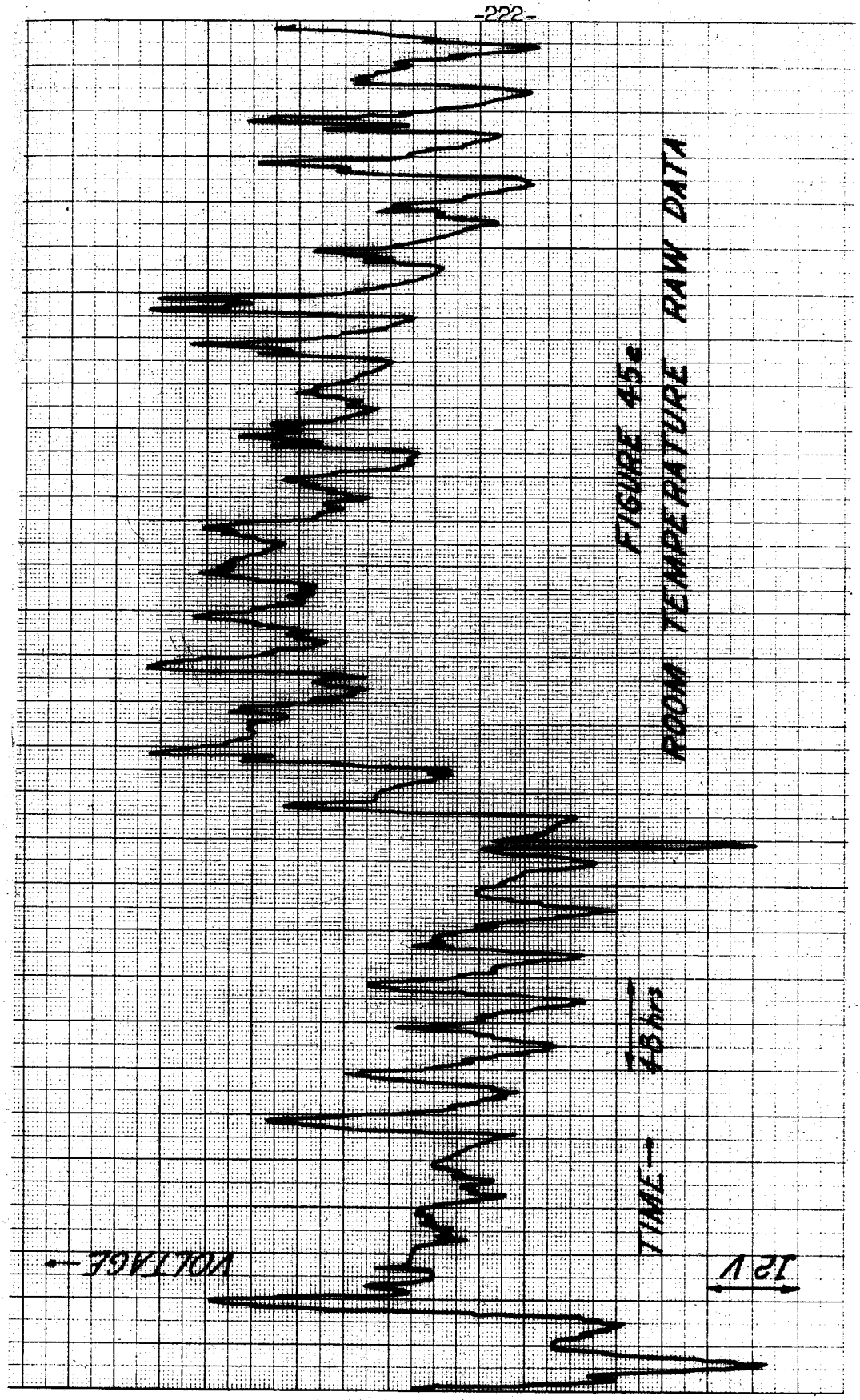

FIGURE 45e ROOM TEMPERATURE RAW DATA

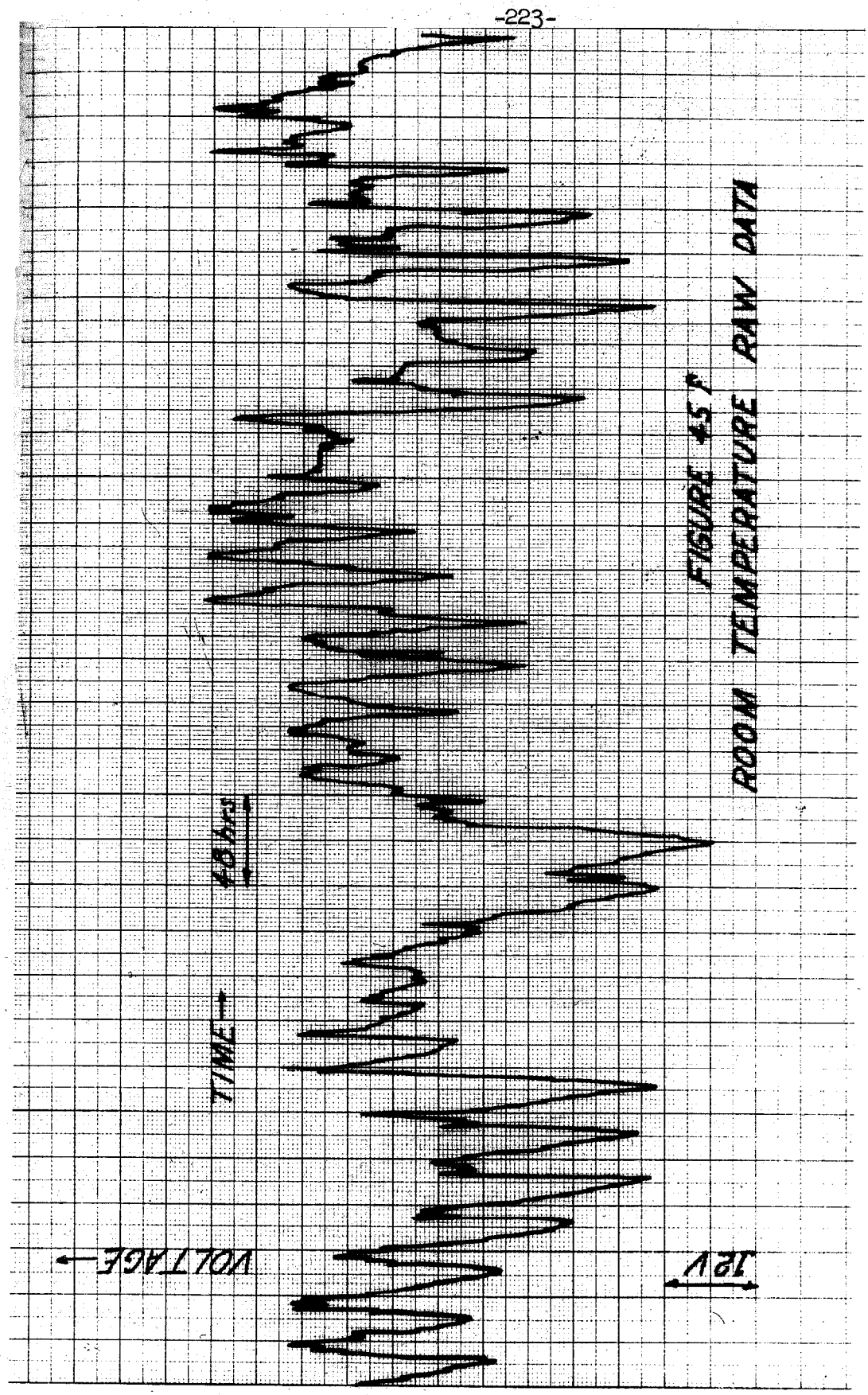

FIGURE 45 ROOM TEMPERATURE RAW DATA

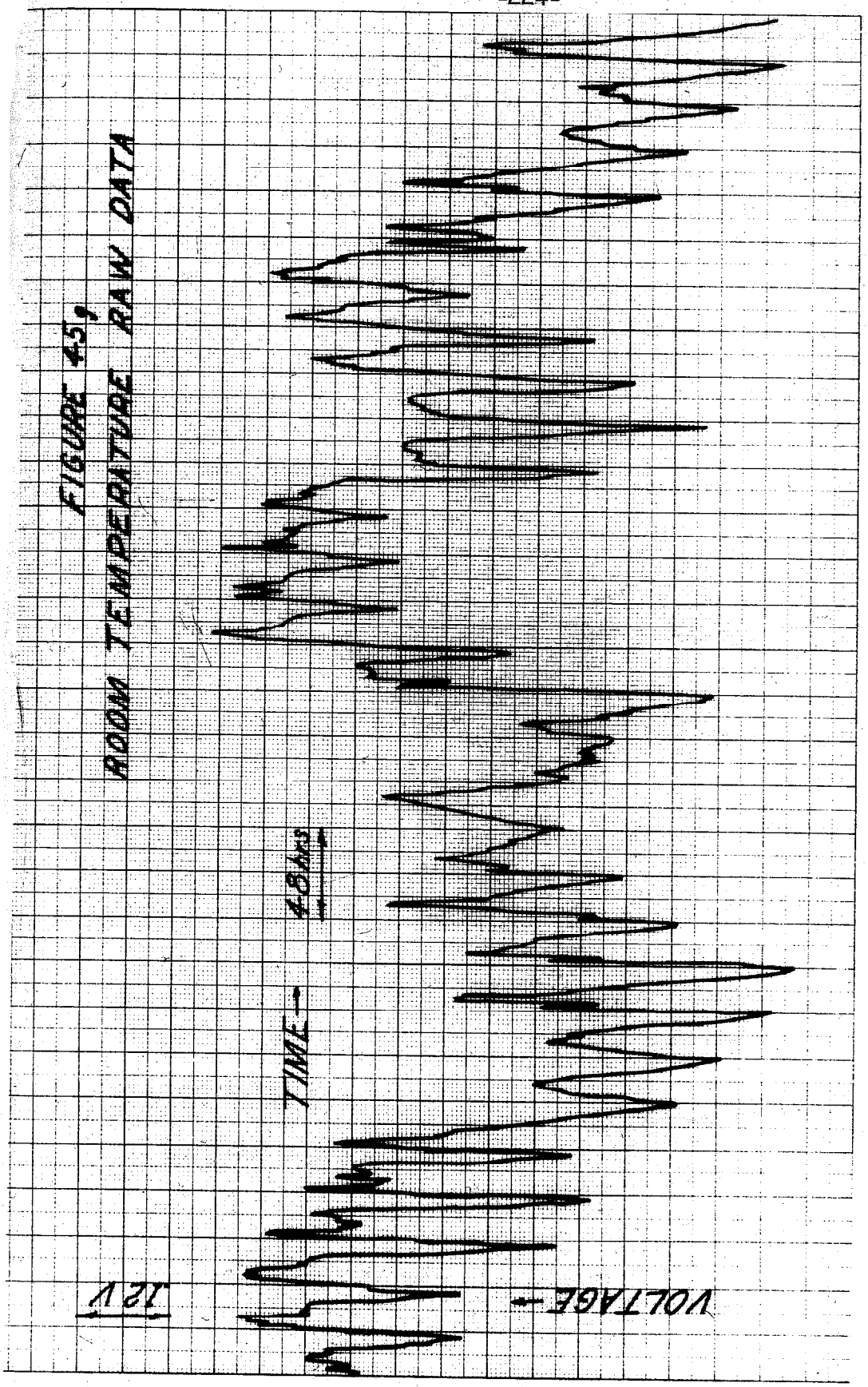

FIGURE 45, ROOM TEMPERATURE RAW DATA

FIGURE 45b
ROOM TEMPERATURE RAW DATA
12V VOLTAGE
24HRS TIME
M Tu W Th F S S M Tu W Th F S FRIDAY S M Tu W Th F Sun M Tu W Th F S S M Tu W Th F

With the data available on this time scale (Figures 45a through h) the non-stationarity aspects discussed above become even more apparent. For instance, compare the section of small amplitude behavior of Figure (45c) with the larger amplitude behavior in Figure (45d) or the even larger amplitude behavior of Figures (45 f,g) and the beginning of Figure (45h). In addition, there are sections of the data where it seems to be much sharper and therefore presumably contains relatively more energy at higher frequencies. This feature may be merely the bias of the human eye to large amplitudes. In any case, as before, we can obtain at least a semiquantative measure of the difference by estimating spectra separately for representative sections of the data. Three sections were chosen; the last part of Figure(45c)which exemplifies the small amplitude behavior, Figure (45d)which is a nominal or "regular" section most resembling narrowband noise, and the last part of Figure (45g)which typify the large amplitude behavior. The estimated spectra are shown in Figures 46a, 46b, and 46c . Here again in order to obtain a reasonable variance the minimum frequency resolution available is 1.67×10^{-5} cps so that the energy at 24 hours (1.158×10^{-5} cps) is smeared out over the first few points. Therefore, the differences in "amplitude" of the three sets of data only show up as a general rise in the level of the spectra. These are Q_2

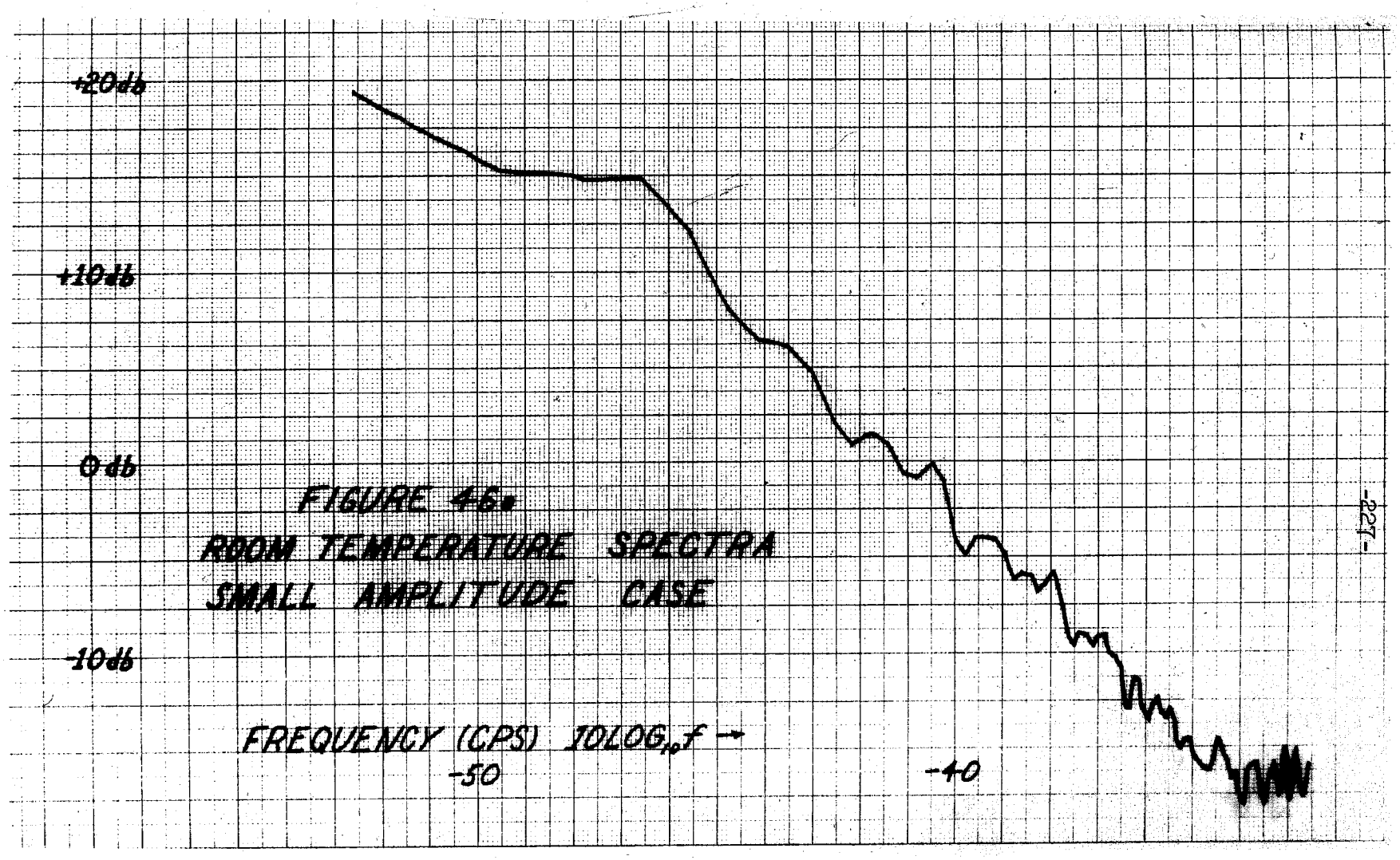

FIGURE 46.
ROOM TEMPERATURE SPECTRA
SMALL AMPLITUDE CASE

FREQUENCY (CPS) $10\log_{10} f \rightarrow$

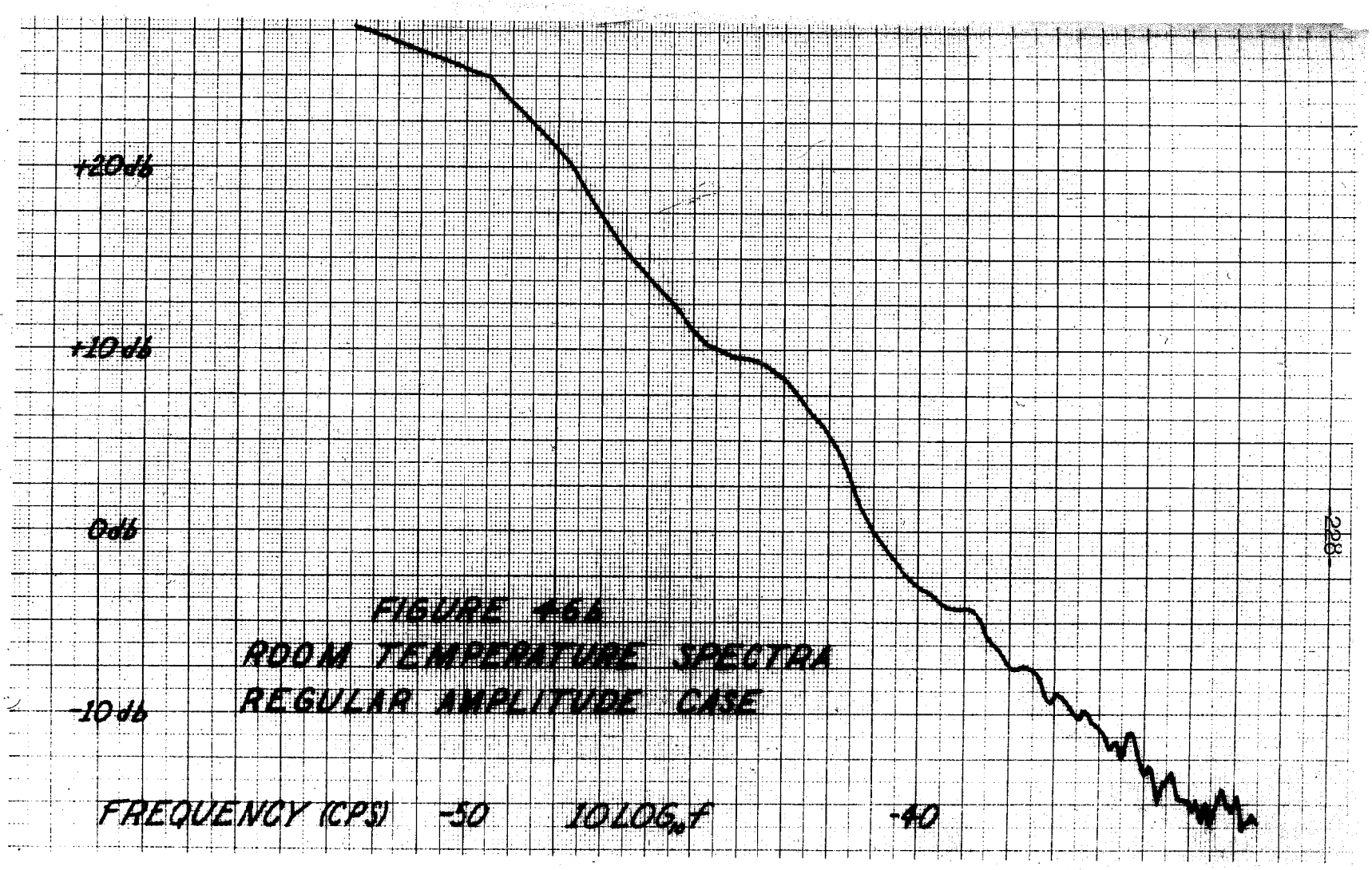

FIGURE 46b
ROOM TEMPERATURE SPECTRA
REGULAR AMPLITUDE CASE

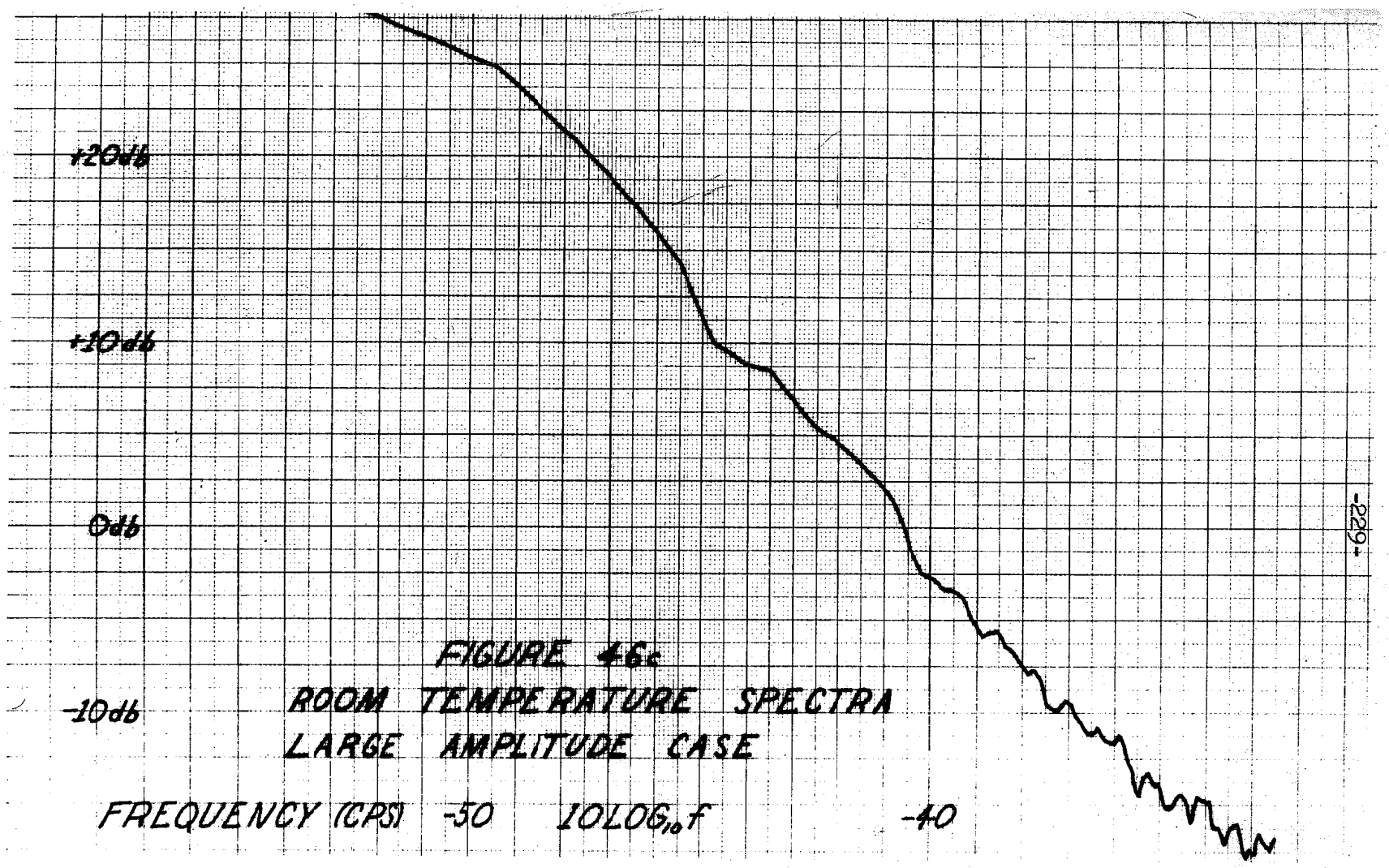

FIGURE 46c
ROOM TEMPERATURE SPECTRA
LARGE AMPLITUDE CASE

estimates from data prewhitened for a $1/f^2$ spectrum The quantization noise level has remained unchanged and the 1σ variance bands are: + .81 db, - .99 db; + .75 db, - .90 db; + .58 db, - .67 db, respectively. The energy at the harmonics of 24 hours is more evident. For comparison if the three spectra were plotted on the same graph, the lowest frequency points would differ by 5 db with the middle one .1 below the upper one. If we put this in the time domain it is a factor of 3 difference in "gain." Here again though the overall picture is clearly one of roughly $1/f^2$ noise with extra energy in some bands.

A final level of contraction is shown in Figure (47)

This shows all of the data on a scale where the 24 hour cycles have almost disappeared into the line widths. The sections of small and large amplitude behavior are apparent, but the general appearance is now much more like noise as we generally think of it. Once again there appear to be slow wiggles which imply sizeable energy at still lower frequencies. With respect to this aspect the data seems surprisingly stationary. No matter on which time scale you examine the data, excluding the 24 hour components, it always appears to have an appreciable amount of energy at still lower frequencies. Figure (48) shows an estimated spectrum for all of the data using only every 30th point. This is one sample every $2\frac{1}{2}$ hours. Aliasing causes no serious difficulty in this case

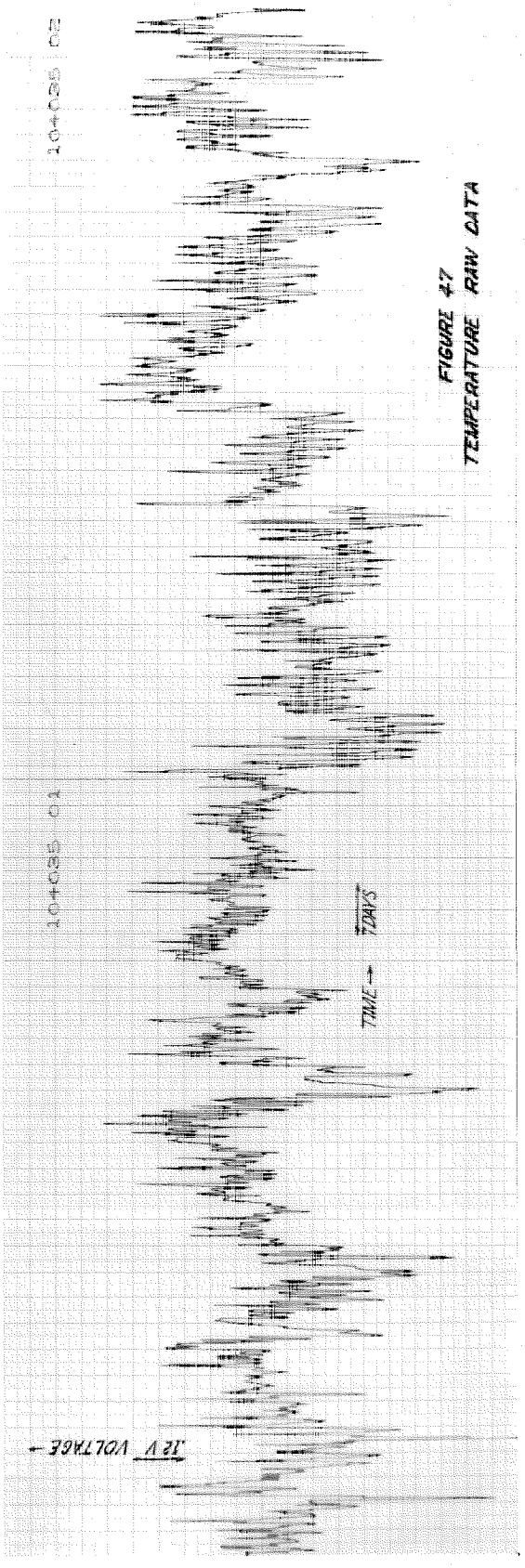

FIGURE 4.7
TEMPERATURE RAW DATA

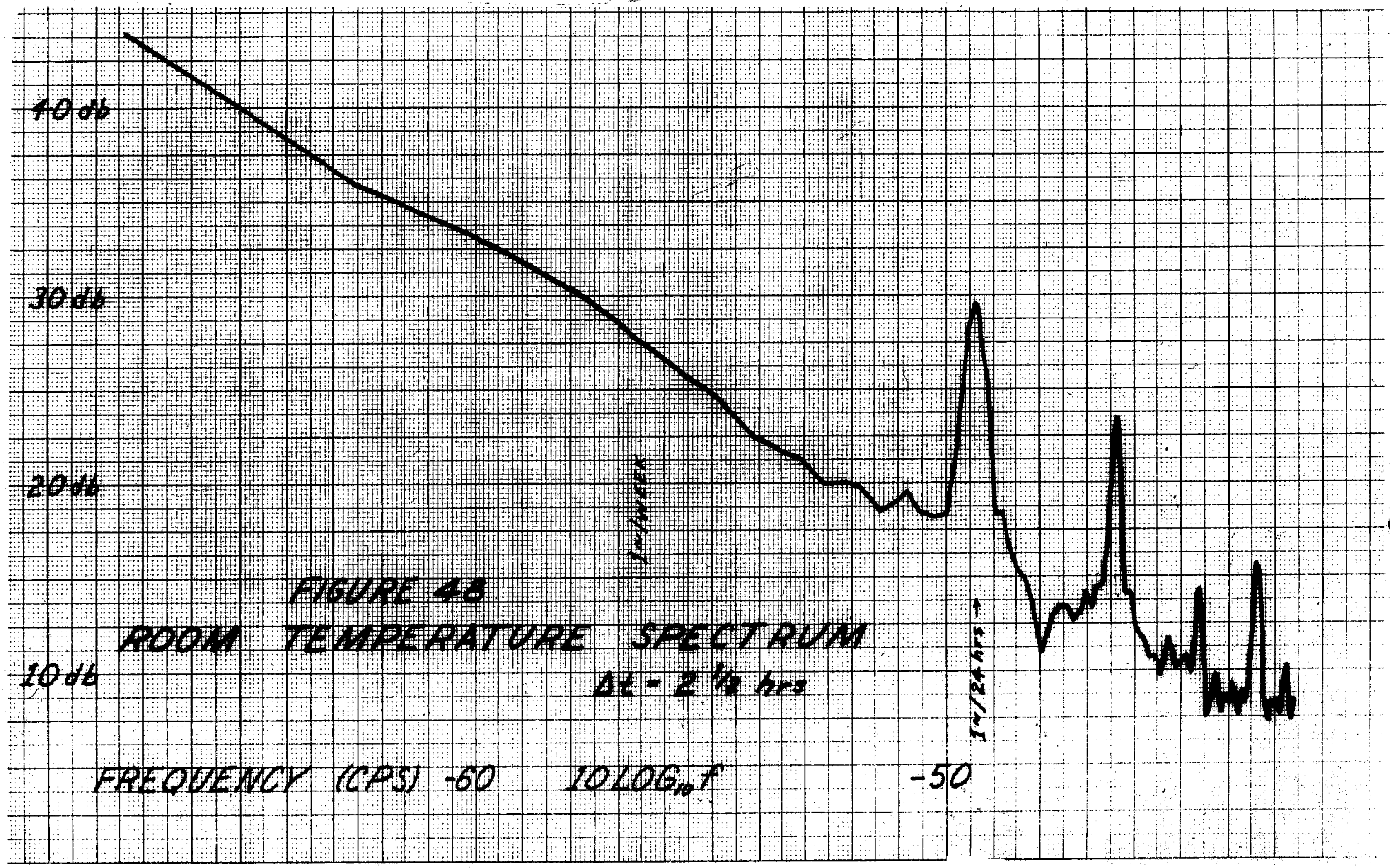

FIGURE 4.8
ROOM TEMPERATURE SPECTRUM
Δt = 2 1/12 hrs

because the spectrum is falling off as the square of the frequency. The minimum resolution on this scale is 5.556×10^{-7} cps or about $\frac{1}{2}$ of a microcycle. The 1σ variance bands are $\pm$ 17.45% or (+ .70 db, - .83 db). These are Q_2 estimates where the data was prewhitened for a $1/f^2$ spectrum. As shown above in Section 3.1.3 the estimator's properties are undesirable when estimating a line. Therefore, one could estimate the spectral density in the vicinity of the 24 hour frequency and its harmonics better by prewhitening with a notch type filter. However, this refinement was felt to be rather ambitious when the raw data itself clearly indicates, as mentioned above, that the amount of 24 hour energy varies from time to time. This estimated spectrum (Figure 48) does, however, illustrate very nicely the daily cycle and its harmonics. Again they appear superimposed on a generally rising spectrum which obeys approximately a $1/f^2$ law. Here the weekly cycle as in the case of the daily cycle before, is not very visible due to the lack of sufficient resolution. It is interesting to note the width of the 24 hour line and its harmonics has decreased each time the spectral resolution was increased. This is exactly in keeping with the discussion of Section 3.1.3 regarding estimating a spectrum containing a delta function. The width and shape which the line appears to have, (i.e., on the average) is just that of the window utilized for the estimation.

At the price of sacrificing statistical properties of the estimate, both bias and variance, one can obtain one more decade of resolution from this data. There are now only 331 data points so that the 1σ smooth approximation variance bands are ± 55.2% or (+ 1.91 db, - 3.49 db) and the smooth approximation is undoubtedly less valid. In addition, significant aliasing will occur at the high frequency end due to the 24 hour spike folding back on the spectrum. This could be eliminated via low pass filtering but since the purpose of this exercise is to investigate the low frequencies it will be acceptable to merely increase the time between samples once more. The result of such an operation is the spectrum shown in Figure (49) . It has the anticipated difficulties but resolves the new spectral component at a week and retains the basic $1/f^2$ background shape. The minimum frequency resolution is 5.556×10^{-8} cps which has a period of about 7 months. This set of data should not be taken too seriously. It serves only as an indication. The 5 db 1σ variance band does not seem very severe, especially on a logarithmic scale. But this is an illusion. The $\frac{M}{N}$ fractional variance approximation itself is questionable in this case. If it is off even by a small amount the estimated spectra for a fair fraction of samples from the ensemble could have negative estimated spectra at a

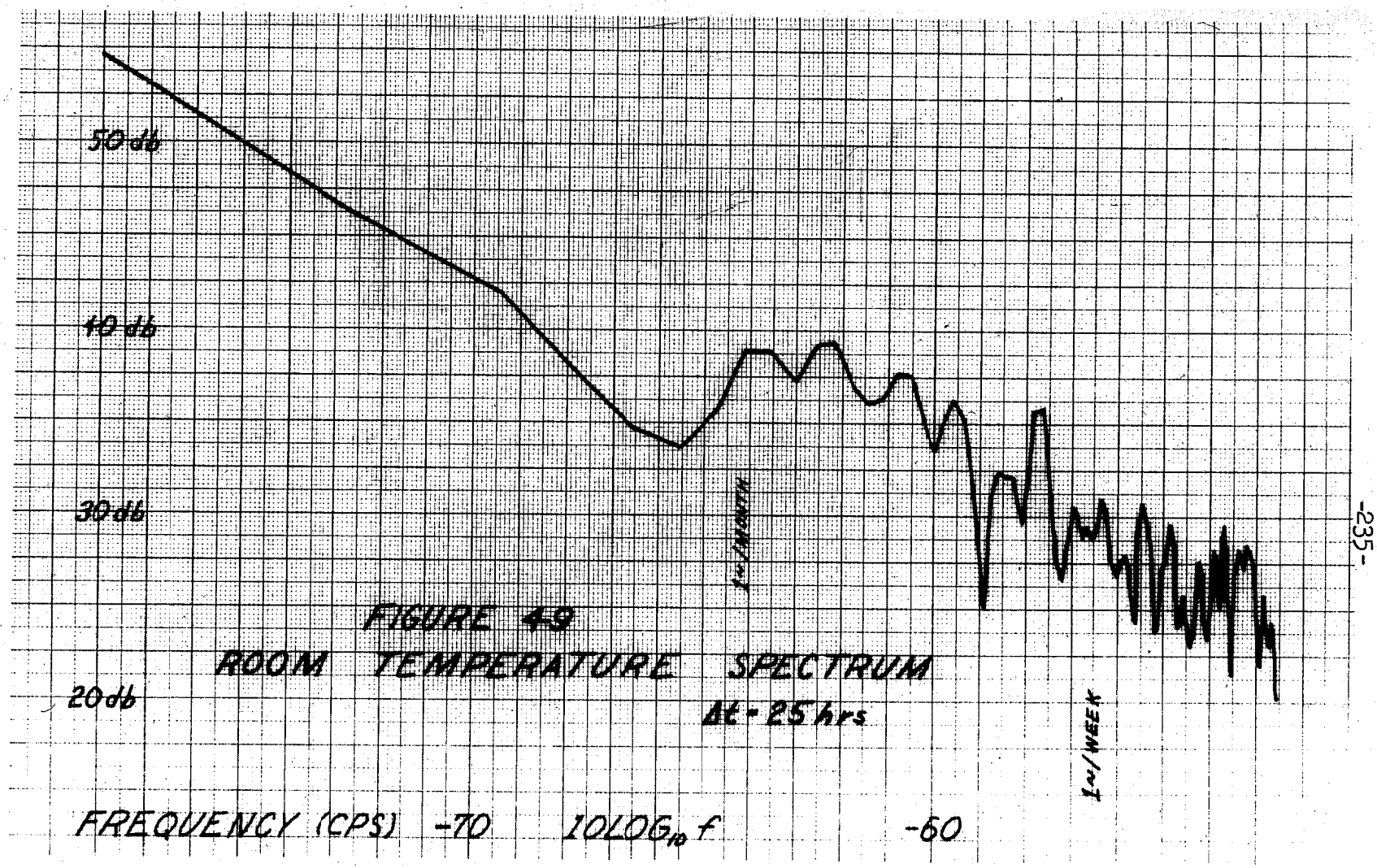

FIGURE 49
ROOM TEMPERATURE SPECTRUM
Δt - 25 hrs

considerable number of points. Such a situation has already been shown to exist for 1/f type spectra in the absence of prewhitening.

A composite view of the room temperature variation spectra is given by Figure (50) . This is a collection and replotting of the results presented in this section. Where more than one run was available over a given frequency range the average was taken although in most cases the differences are so small as to be hardly visible on this scale. Two high frequency runs corresponding to sampling times of 5 seconds and 50 seconds have been included. This data was taken via the paper tape punch technique and the spectra estimated using $1/f^2$ prewhitening. If forced to model the total results in a simple form it seems that a reasonable choice would be

$$S_T(f) = \frac{K_T}{f^2 + f_T^2} + \sum_{n=1}^{k} A_n^2 \, \delta(f - nf_d) \qquad (131)$$

where f_T represents the basic RC noise break frequency, K_T sets its RMS value, the A_n represents the amplitudes of the daily cycle and its harmonics, k is the number of harmonics included, and f_d is the 24 hour frequency, 1.158×10^{-5} cps.

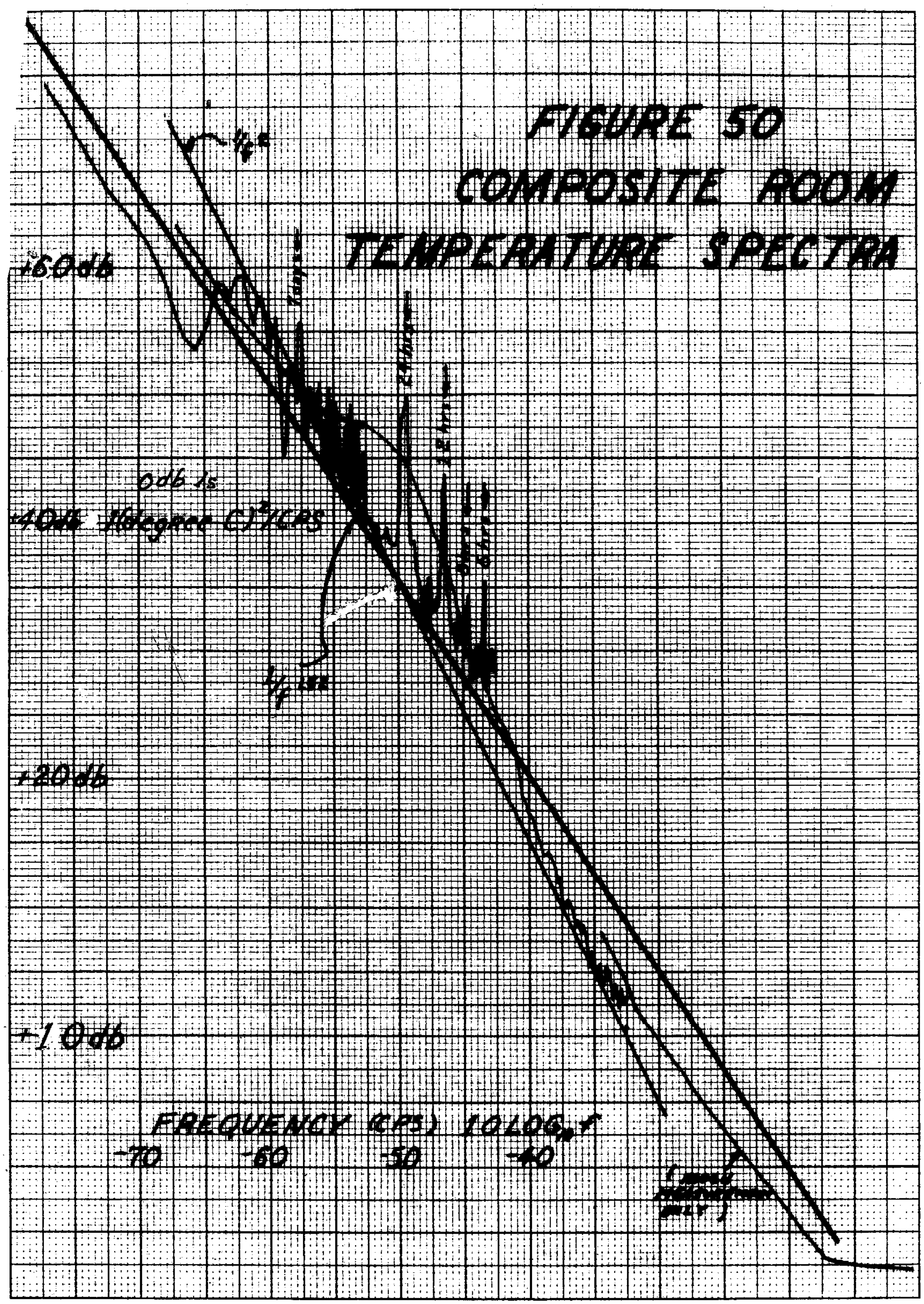
FIGURE 50
COMPOSITE ROOM
TEMPERATURE SPECTRA
+60db
+40db
0db is
1(degree C)²/CPS
+20db
+10db
FREQUENCY (CPS) 10LOG₁₀f
-70
-60
-50
-40

The correlation function corresponding to the model is

$$R_T(\tau) = \frac{K_T \pi}{f_t} e^{-2\pi f_T |\tau|} + \tau_d \sum_{n=1}^{k} A_n^2 \delta(\tau - \frac{\tau_d}{n})$$

Then calculating a limited bandwidth rms from the data of Figure (5), yields

.872°C from RC noise to 1μ cycle

.20 °C @ 7 days

.33 °C @ 24 hrs .17°C @ 12 hrs.

.055°C @ 8 hrs

.063°C @ 6 hrs

5.2 1/f Noise

The experimental results for 1/f Noise were obtained using the Mark I noise generator described in Section 4.1 The raw data was collected via the three methods described in Section 4. As discussed in Section 4.2 the first approach taken toward inhibiting the temperature dependence of the Mark I output was an attempt at thermal isolation. A complete set of data using this approach was taken during May through July 1964. The first set of 7 runs were made utilizing the A-D conversion equipment at the CIT Computation Center on May 25, 1964. Six different sampling rates varying in decades from 10Kc ($\Delta t = 10^{-4}$ sec) to .1 cps (Δt = 10 sec) were used. At least 10000 points were taken at each rate, so that the total time required was about 30 hours. The Mark I noise generator was then removed to Room 223 Spaulding and its output was recorded on an Easterline Angus strip chart. These runs were eventually terminated because of a battery failure by the batteries which were supplying power to the noise generator. Two sets of data were punched onto cards from these strip charts.

Power spectral densities were estimated from these 8 runs with M = 100 and 1/f prewhitening. The composite results are shown in Figure (51). This figure is a photographic reduction

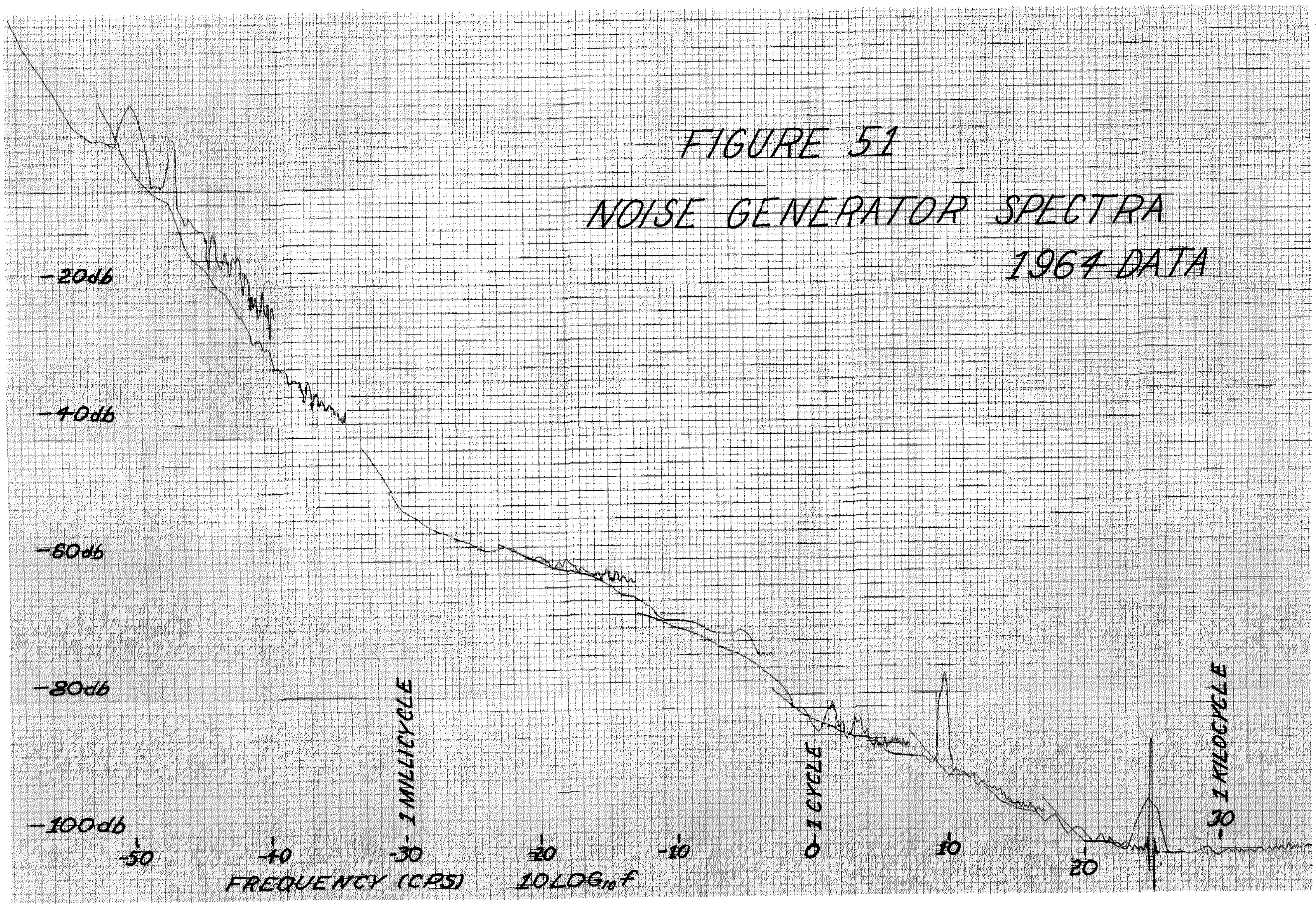

FIGURE 51
NOISE GENERATOR SPECTRA
1964 DATA

of the original plot whose 800 points cover 6 sheets of 11"x 15" graph paper. Most of the significant details are still visible but some sections will be expanded to demonstrate particular points. The vertical scale on Figure (51) runs from - 110 db to + 20 db referred to the output of the Mark I noise generator where 0 db is 1 volt^2/cps. The horizontal scale runs logarithmically from a microcycle to 10 kilocycles. The two lowest frequency spectral lines are at frequencies corresponding to 24 hrs and 12 hours, respectively. They were presumed to be the direct reflection of room temperature on the Mark I output as discussed in Section 4.2. The two spectral lines near the high frequency end are located near 91 cps and 309 cps. These are believed to have been due to extraneous voltages present somewhere in the A-D conversion equipment at the time of data collection. They are not attributed to the noise generator output.

The section around the spectral line at 309 cps is informative when examined in datail. Figure (52) shows this area in detail. There are four curves plotted. The one which shows the δ function in most resolution is for a sampling time of $\Delta t = 10^{-3}$ sec. The other three are spectra estimated from the $\Delta t = 10^{-4}$ sec data. They have M = 100, 30, 10 and

FIGURE 52
PARTIAL $1/f$ NOISE SPECTRA

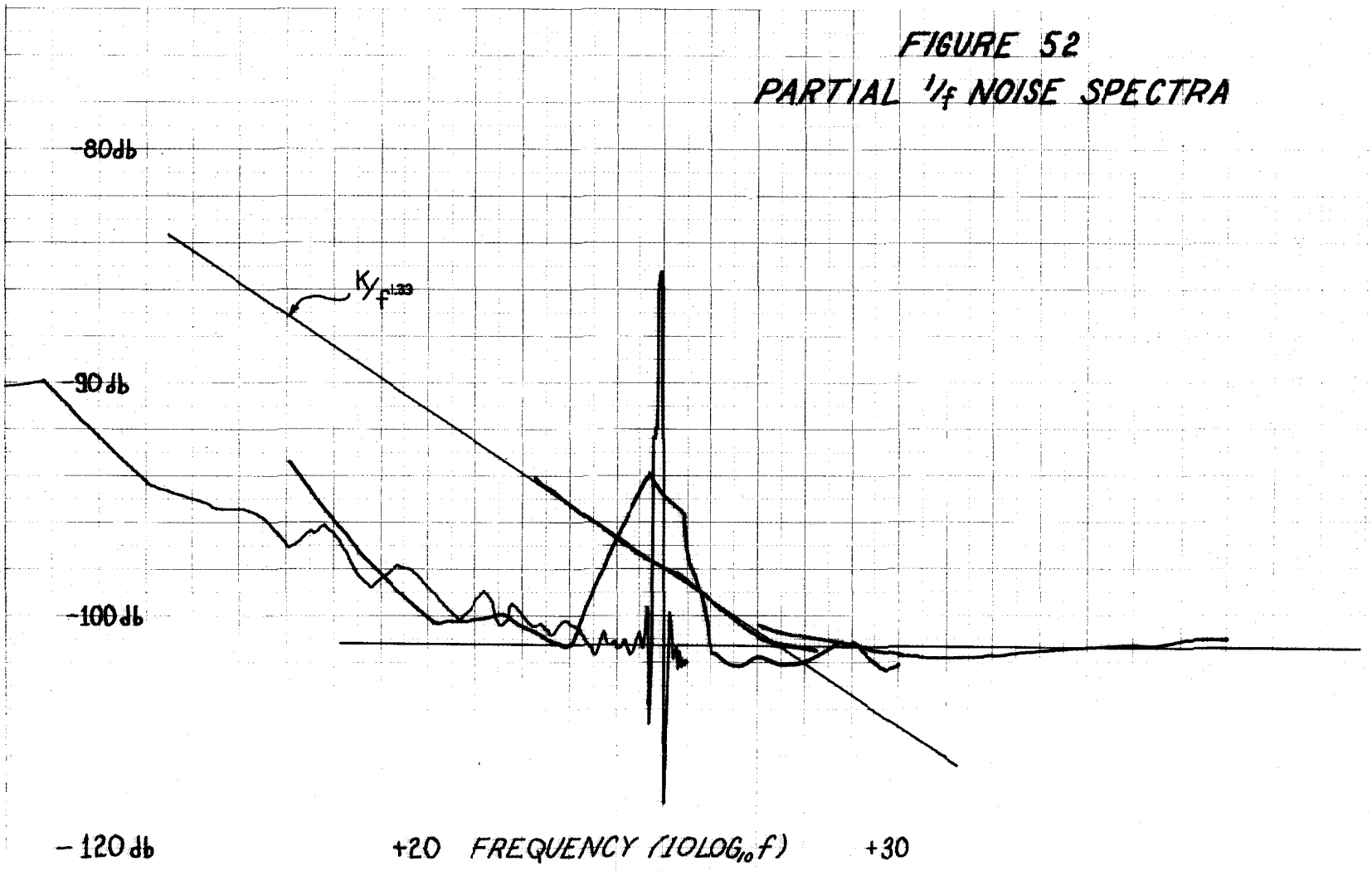

correspondingly decreased resolution. Several points discussed in Section 3.1.3 concerning estimating a spectaum containing a spectral line are illustrated here. First the line is resolved in proportion to the minimum resolution available from the Q_2 window for a given M. Notice that if we examined merely the M = 30 result for this case (thin line) we would come to the conclusion that the spectrum broke at 188 cps and obeyed a $\frac{1}{f}$ 1.33 power law. In addition, this conclusion, looking only at the M = 30 case, would appear to be supported by the empiricial variance which would be consistent with the $\frac{M}{N}$ approximation. Bias is a very sneaky error because it makes you wrong on the average but when discovered is terribly obvious. At the high frequencies where the spectrum is in fact smooth the smaller M estimates do in fact have smaller variance. The more oscillatory higher M estimates are not plotted in this region. We are really not interested in all the wiggles once we know they are small. Regarding the same data it is interesting to observe how poor a spectral estimator the human eyeball turns out to be. All the fancy digital processing of the data apparently has accomplished something. For instance, Figures (53) and (54) show typical sections of the $\Delta t = 10^{-4}$ sec and $\Delta t = 10^{-3}$ sec data, respectively. The vertical scale is the

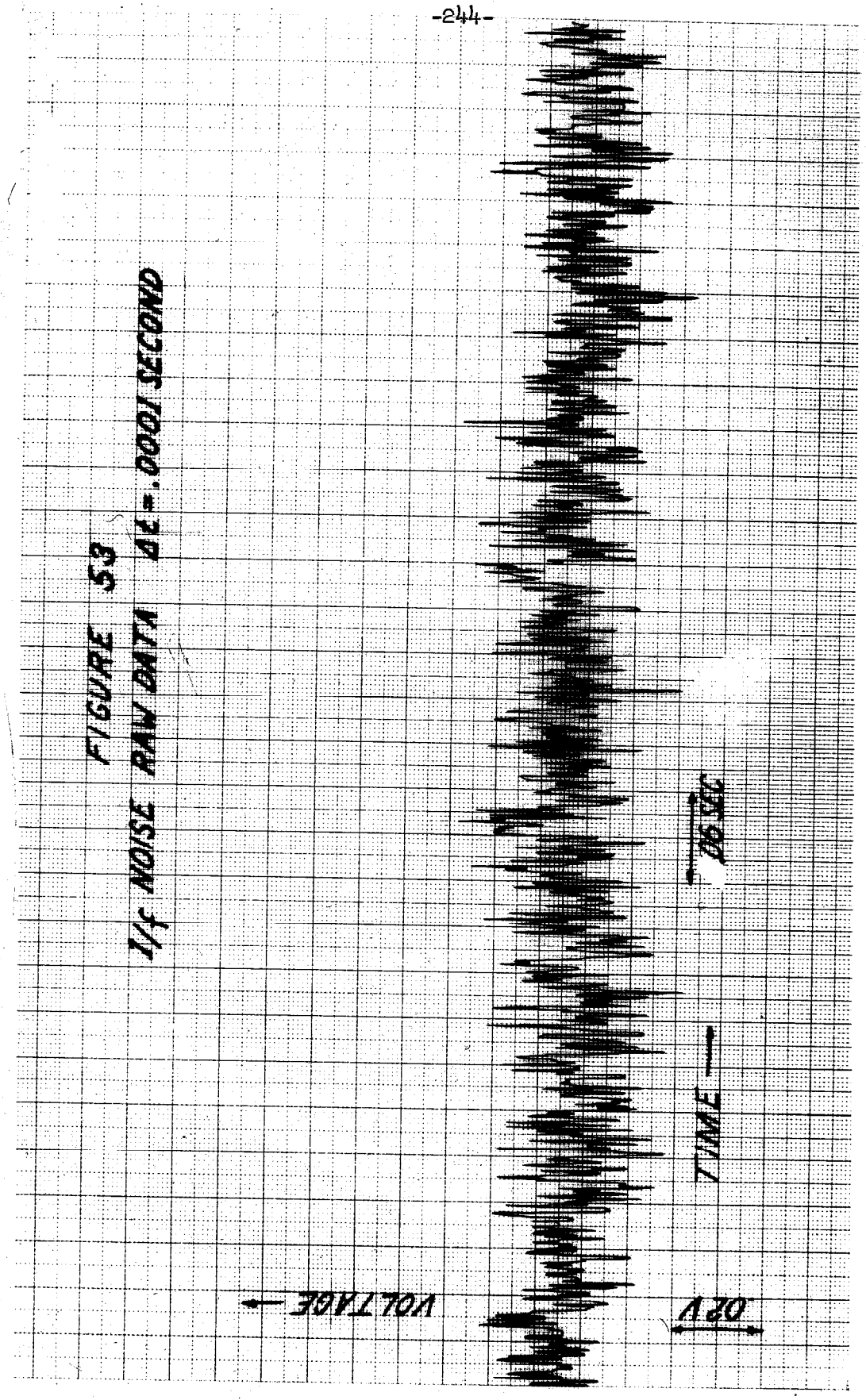

FIGURE 53
1/f NOISE RAW DATA Δt = .0001 SECOND

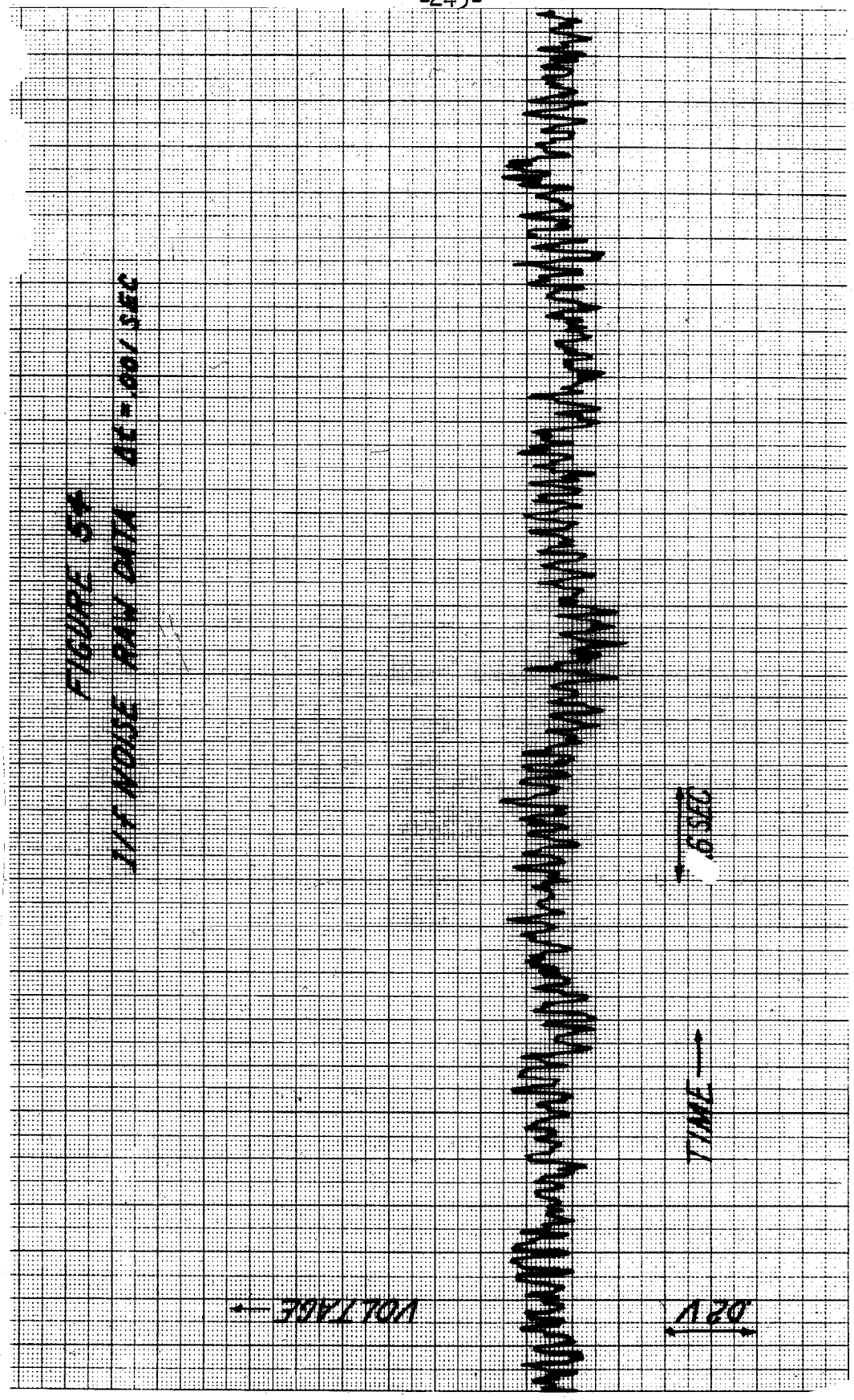

FIGURE 54
WHITE NOISE AND DATA AT .001 SEC

same in both cases. Each graph contains 900 points or about 1/11 of the total data. A 309 cycle sine wave would have about 27 cycles on Figure (53) or 270 on Figure (54). The eye seems to be able to imagine this in the data only with difficulty. Figure (54) for $\Delta t = 10^{-3}$ sec appears to contain relatively less high frequency energy compared to Figure (53) for $\Delta t = 10^{-4}$ sec. Each was low pass filtered similarly and the time scale on the plots is such that this comparison can be made directly. The estimated spectra, of course, yield this conclusion in a much more quantitative fashion. Figure (55) is a plot of $1/11^{th}$ of the $\Delta t = 10^{-2}$ sec raw data on the same vertical scale. Again there seems to be an increasing amount of energy at low frequencies. For all three of these sets of data, $\Delta t = 10^{-4}$, 10^{-3}, 10^{-2} sec, the raw data selections are very typical in that none of the other portions of the data look any different. In other words, the process appears to be stationary. This situation changes abrubtly for the next batch of data.

Let us now examine the $\Delta t = .1$ data. There are again 10000 data points. Suppose we plot the first 9900 points, 900 to a sheet on 11 sheets of graph paper. Figure (56) shows

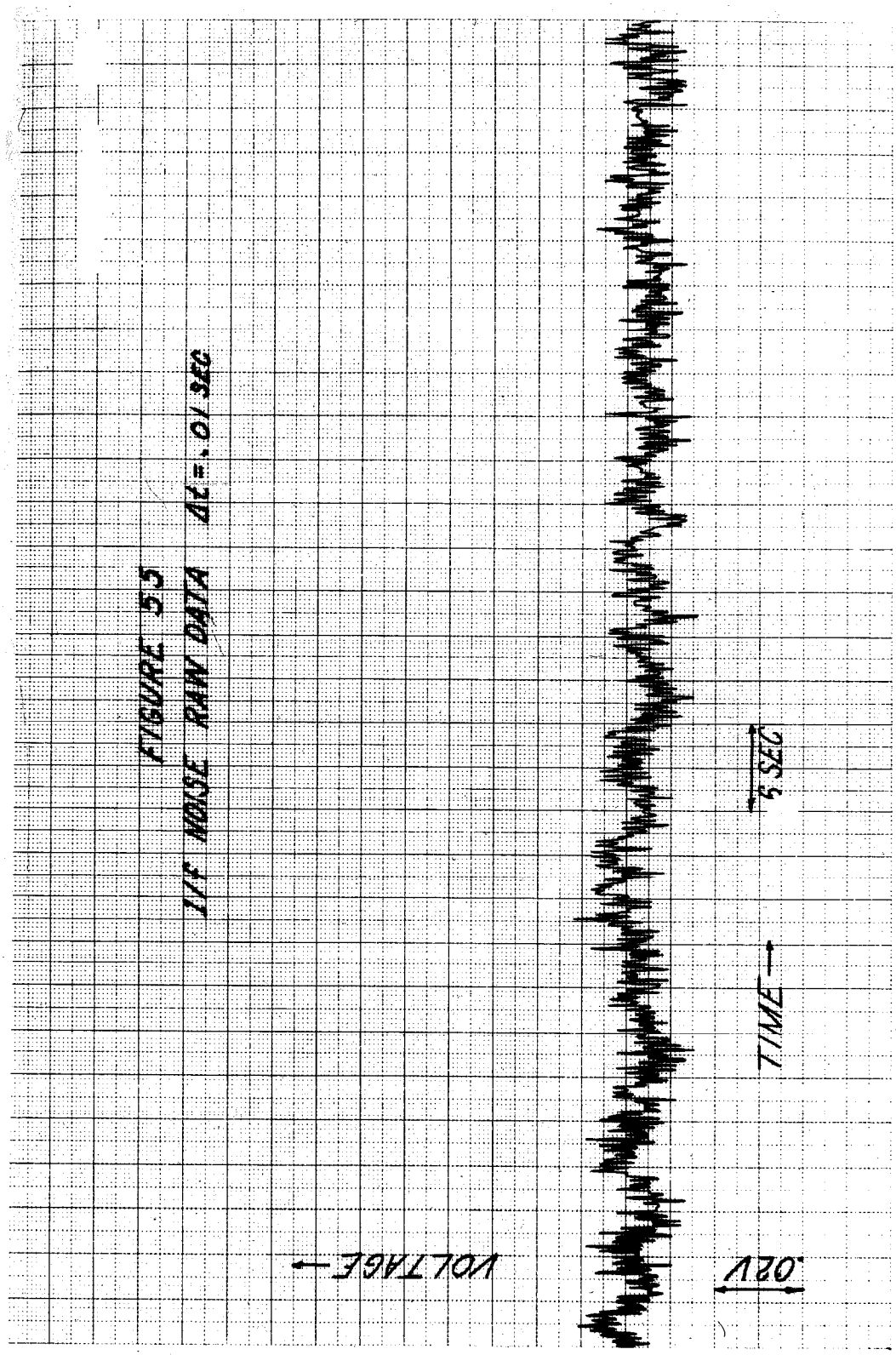
FIGURE 55
1/f NOISE RAW DATA Δt = .01 SEC
VOLTAGE →
.02V
5 SEC
TIME →

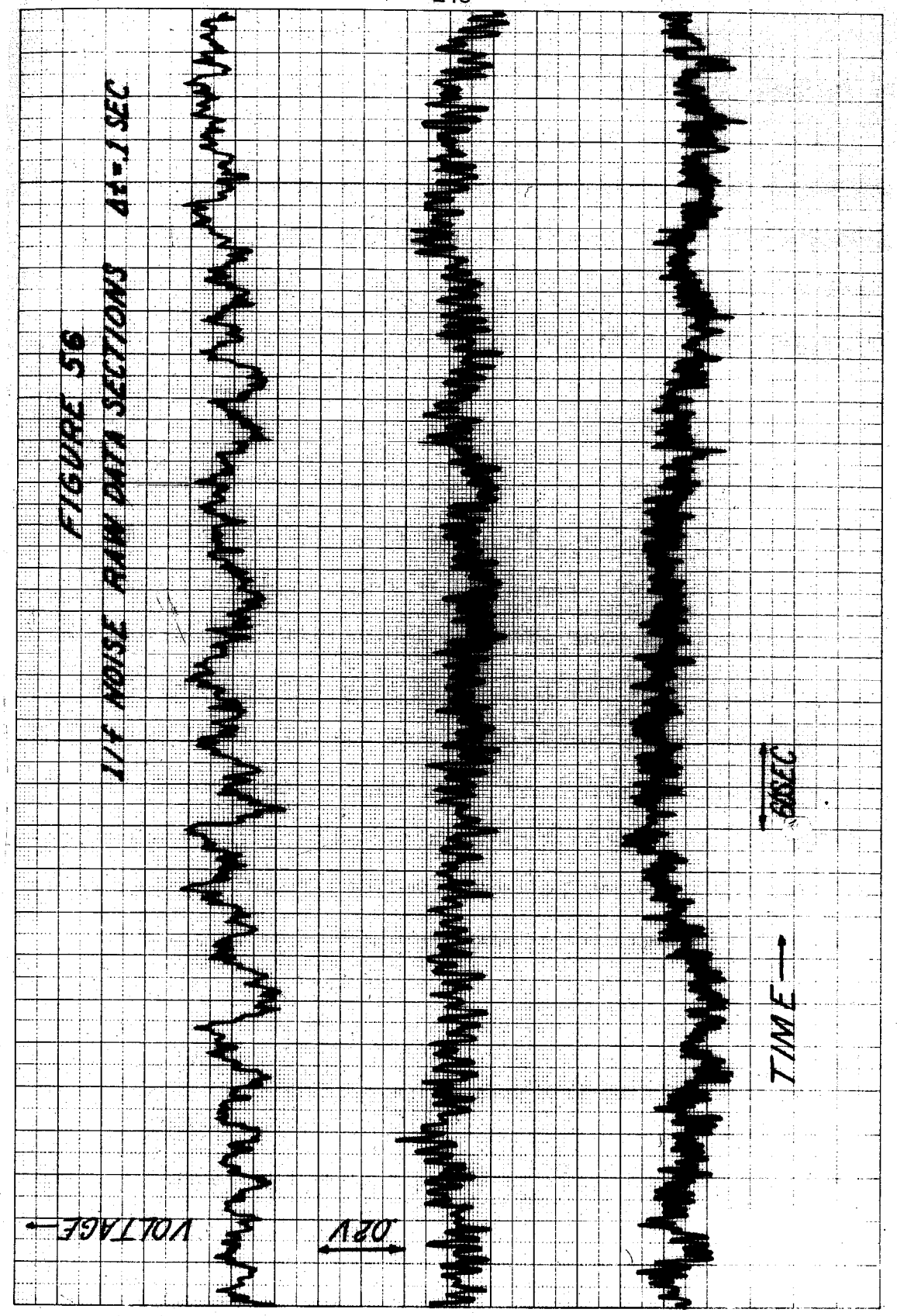

FIGURE 56
1/f NOISE RMS WITH SECTIONS Δt = 1 SEC

sheets 2, 8, and 11 superimposed on the same page. They are not alike. The data seems to exhibit a marked non-stationarity. Figure (57) which is a plot of sheet number 9 shows an additional difficulty. There were apparently violent transients somewhere in the experiment or data collection system. For all of these reasons the spectrum estimated from this data is not felt to be very reliable.

The particular problem of different "kinds" of behavior is illustrated further by the Δt = 1 sec data of which Figure (58) shows a typical section.* Now we have returned to a case where all the sections look alike. However, a close examination of this figure shows the three types of behavior illustrated by the three traces of higher frequency data on Figure (56). Let us get an idea of time scale here. The Δt = 1 sec data run takes about 3 hrs total and the sheet shown in Figure (58) represents about 15 minutes. It now seems less surprising that the estimated spectra between .1 cps and 3 cps don't appear to be consistent within the expected 1 db variance band.

The Δt = 10 sec data required a total of about 30 hrs to collect. It does not seem to show different types of behavior.

---

* The vertical scale is slightly reduced compared to the previous raw data graphs. This scale is + .1 volt to + .4 volts compared to +.0 to .2 volts before.

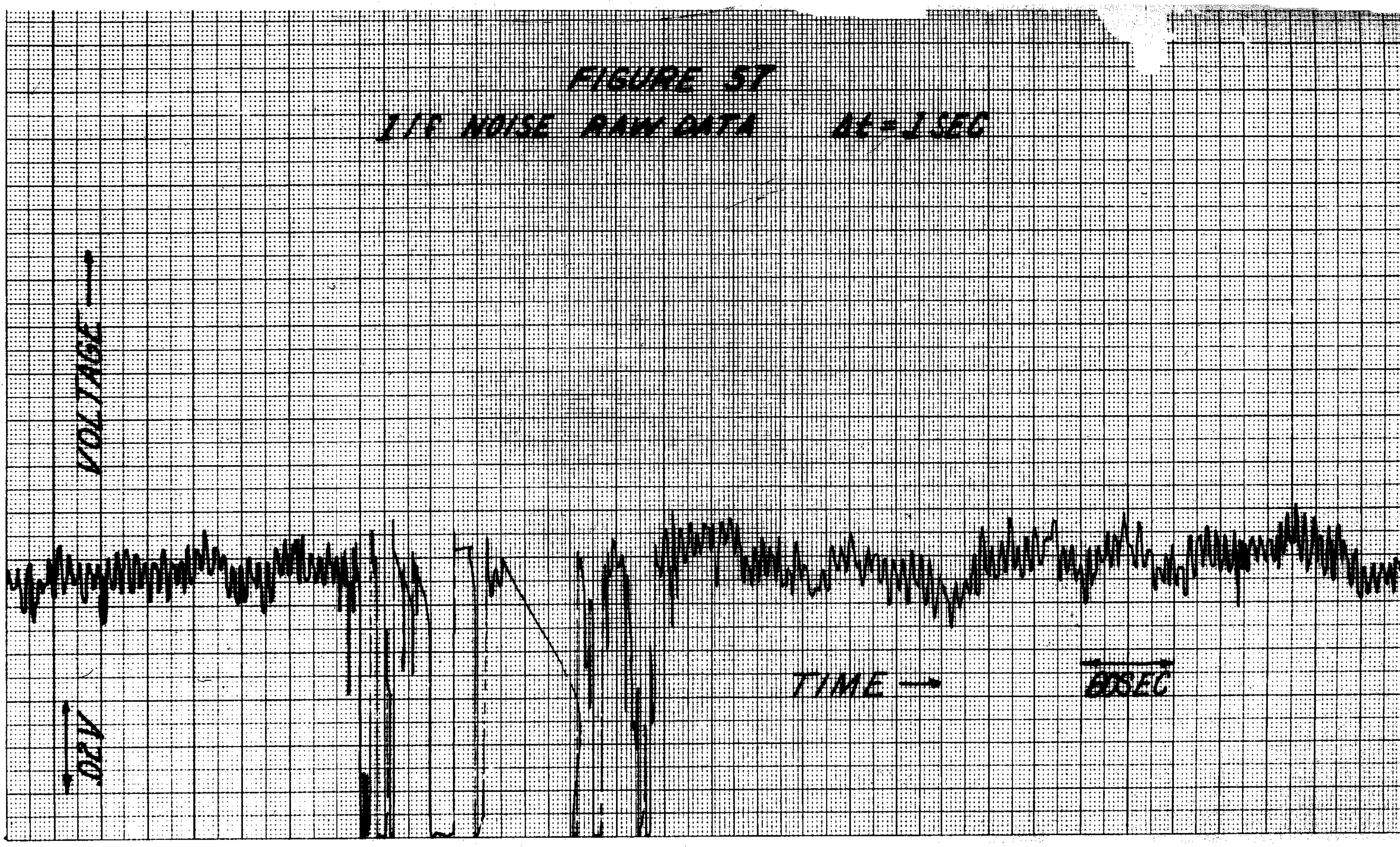

FIGURE 57

1/f NOISE RAW DATA $\Delta t = 1$ SEC

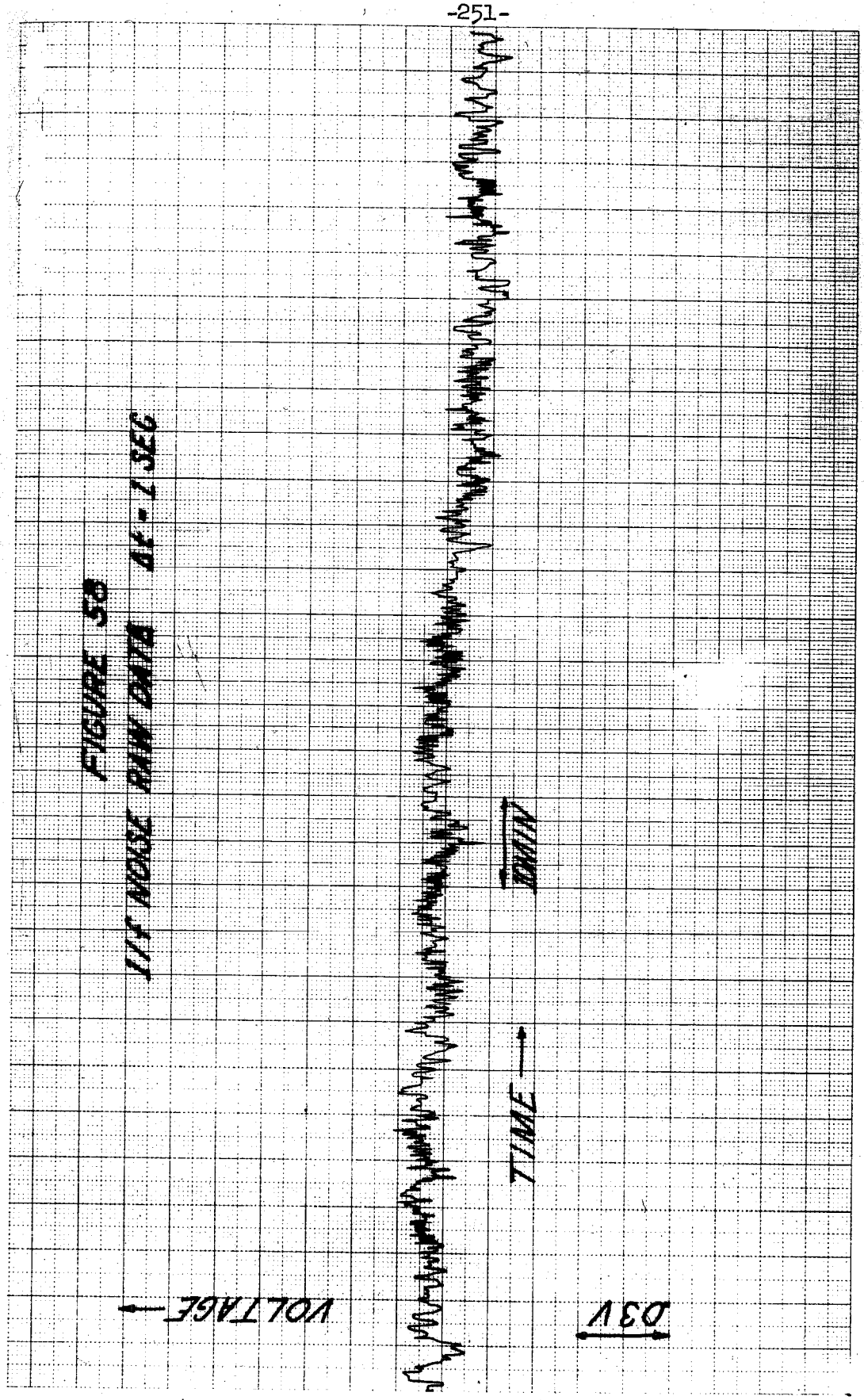

FIGURE 58
I/f NOISE RMS DATA Δf = 1 SEC

It does, however, have what appears to be a strong temperature component in the output. Figures (59) and (60) show two typical sheets of data illustrating this phenomenon. Each sheet represents about $2\frac{1}{2}$ hours of total time. There are such steps in the data at about 12 hr intervals, and this data was taken on a Saturday - Sunday so that they could be direct results of the air conditioning system. All of these latter results concerning the examination of the time domain data are in the nature of hind-sight, in that, they were not uncovered until March 1966.

The next step in the experimental program was to control the temperature environment of the noise source. Section 4.2 discusses the thermal control in detail while we shall present here only the experimental results. The primary interest was in the low frequency behavior. It was felt that the three highest frequency runs of Figure (51) were relatively unaffected by temperature. There was no strange behavior in the time domain data and the estimated spectra are reasonably consistent. Therefore, it was planned to proceed down in frequency from $\Delta t = 5$ sec with Mark I in the oil bath. Unfortunately, over the intermediate period the output of the noise generator was inadvertently shorted. The two emmitter follower transistors (see Figure (17)) were subsequently replaced. The three

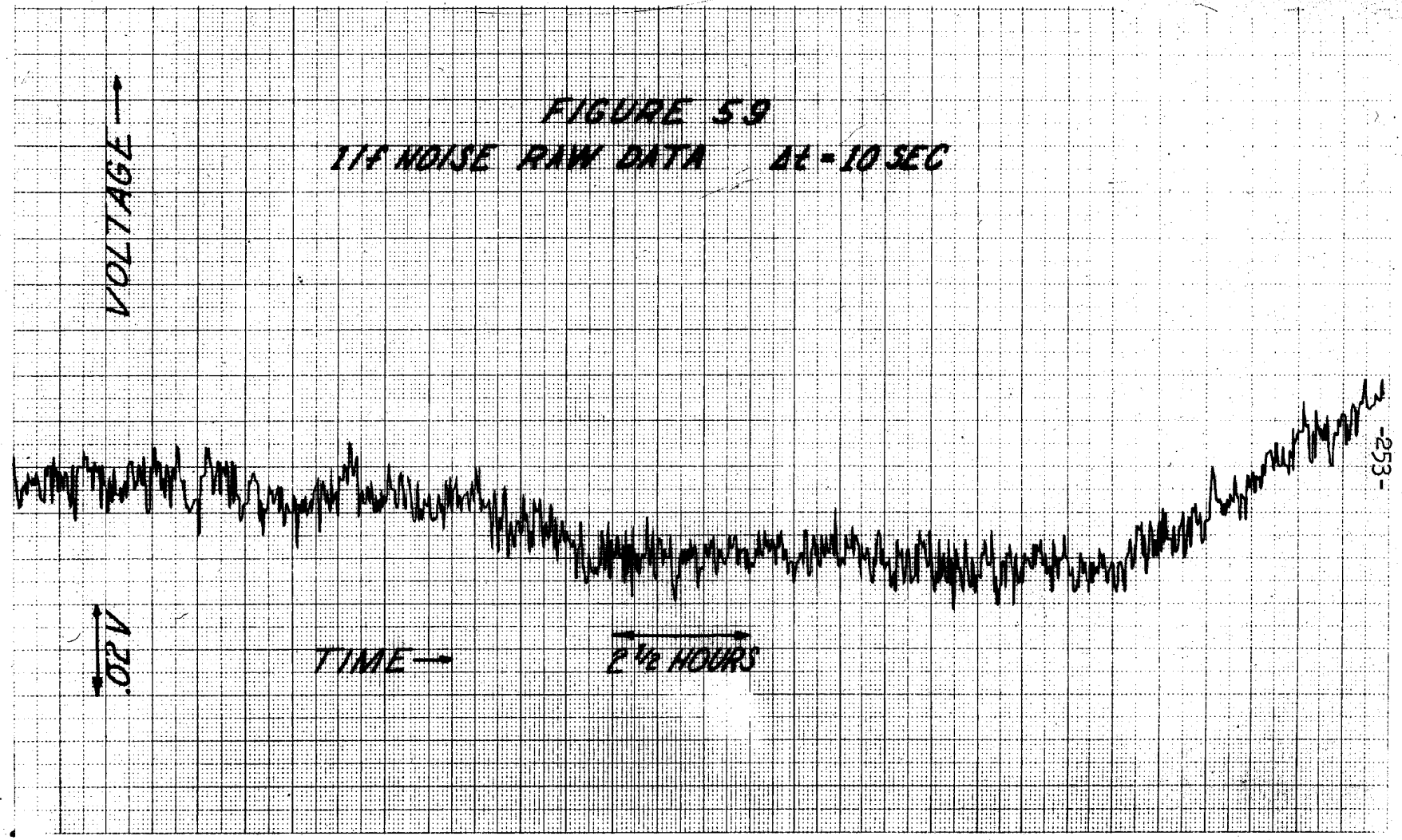

FIGURE 59
I/f NOISE RAW DATA Δt = 10 SEC

FIGURE 60

1/f NOISE RAW DATA Δt=10 SEC

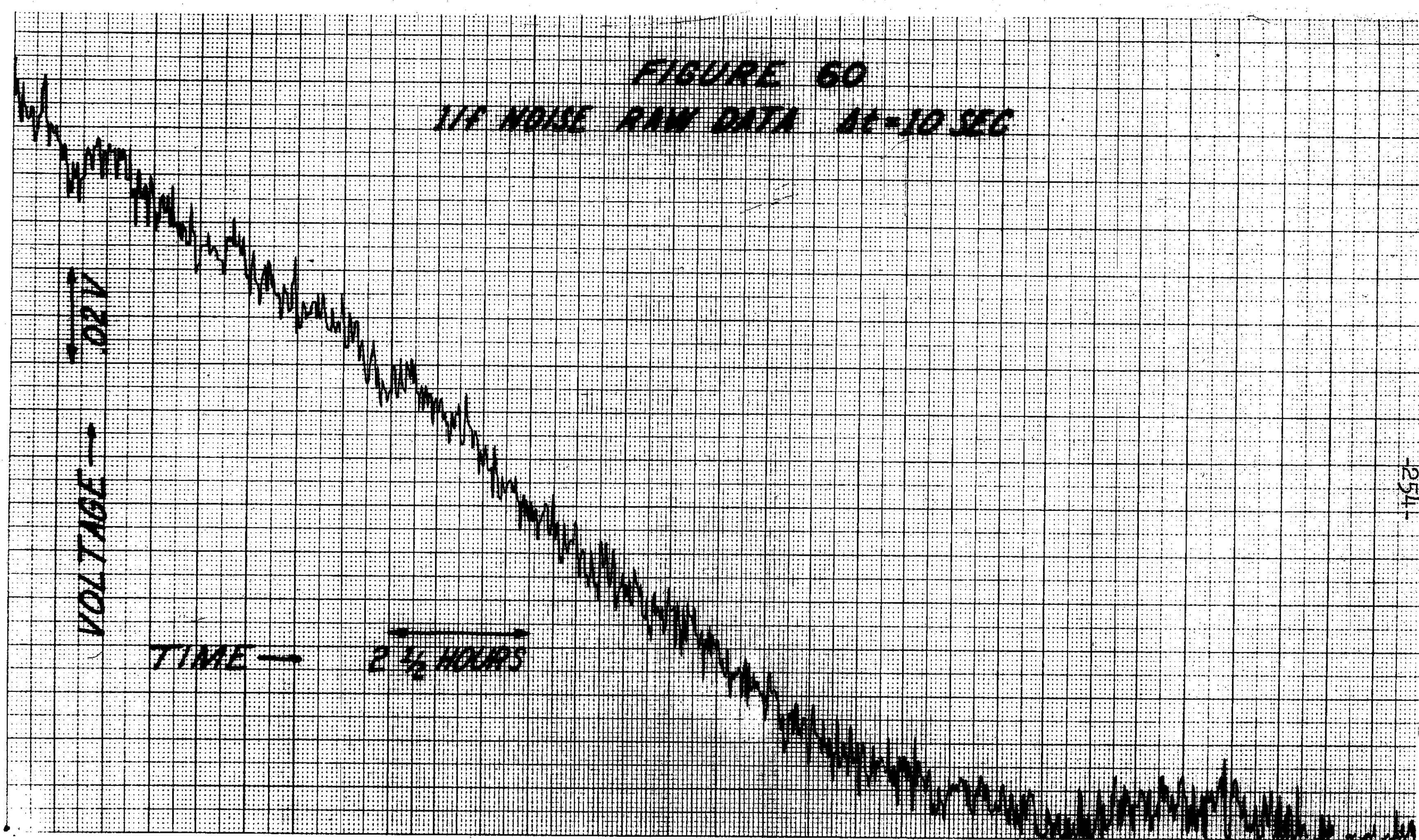

highest frequency runs were then repeated to verify that the noise generator's properties had not been altered substantially. The three highest frequency curves in Figure (61) present this data, which was taken in August 1965. Again there are apparently extraneous frequencies present in the A-D conversion equipment. In addition, there appears to be a significant low frequency bias in the highest frequency run. This data was taken with the noise generator in the aluminum block but not enclosed in the temperature isolation aluminum box (see the beginning of Section 4.2). The low frequency points are thus presumably biased by room temperature to a greater extent than the comparable previous results of Figure (51). Comparison of the level of the high frequency white noise asymptote for the 1964 data and the 1965 data indicates that this aspect of the noise generator did not change a great deal. After allowance for the gains of all the amplifiers and filters following the Mark I output, these levels are within about 2 db of each other.

The other major portion of the Mark I environment which it was felt required control for the second series of measurements was the power supply. The 1964 data of Figure (51) was taken with 4 "D" cells as the power supply. As batteries discharge their voltage does not decay smoothly, but in small

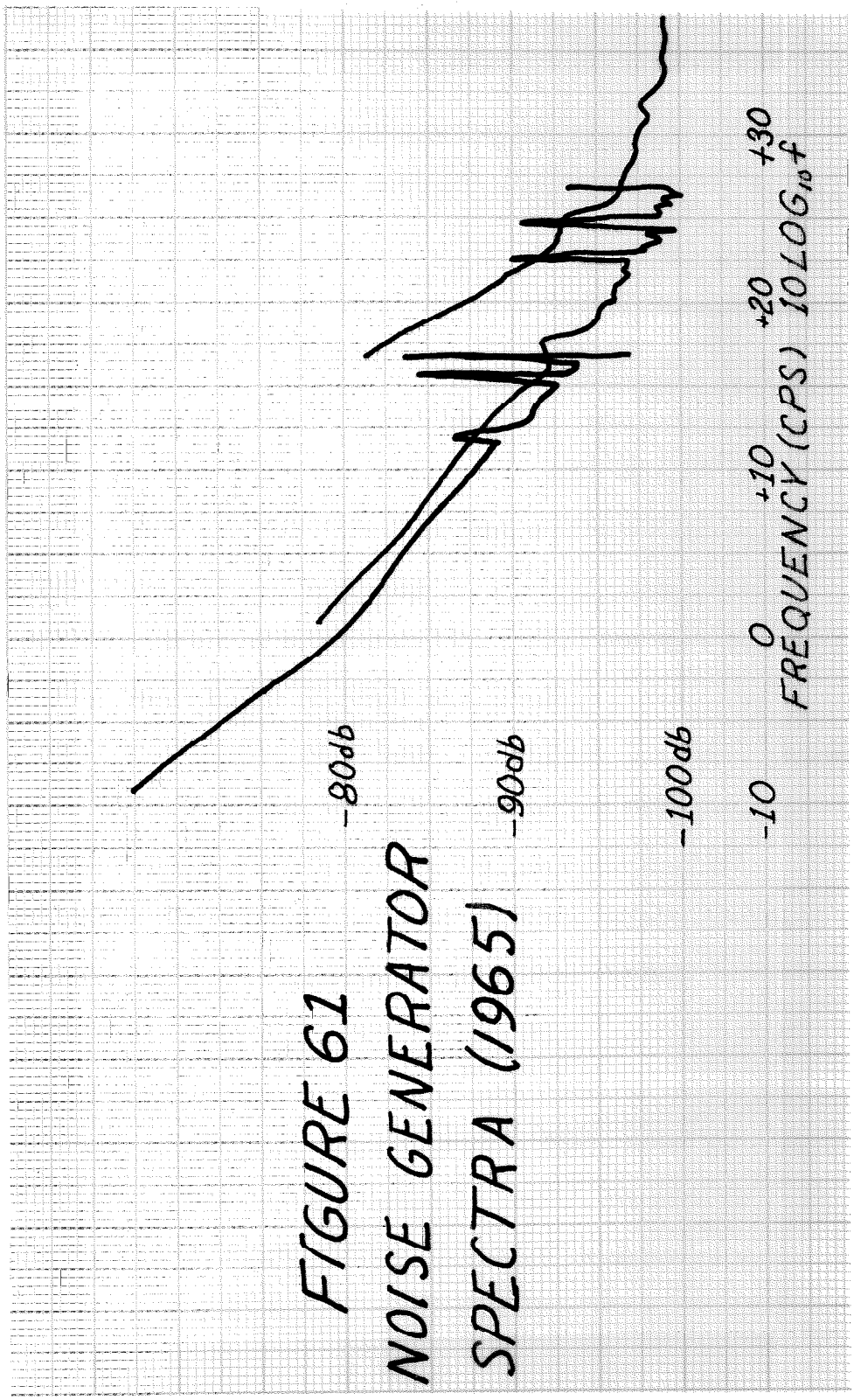

FIGURE 61
NOISE GENERATOR
SPECTRA (1965)

discontinuous teps. Mark I is a differential mode device and its power supply batteries discharge independently. It is possible that such a phenomenon might be the explanation for the non-stationarity effects noticed in the raw data, particularly some long-term linear trend effects noticeable in the lowest frequency data. A scheme employing continuously charged Nickle Cadmium cells was utilized initially but proved unsatisfactory. Eventually, the solid-state regulated power supply discussed in Section 4.1 was constructed. With the aid of hindsight this choice seems to have been a mixed blessing. Long-term decay effects were reduced but short-term (daily) temperature response effects were increased. The most intensive set of data taken in the oil bath was for $\Delta t = 5$ sec. Ten independent sets of data were taken in February and March of 1966. Each run lasts about 12hrs. Initially spectra run directly from the raw data seemed to contain too much variability. They were 1/f prewhitened spectra so that the smooth spectra $\frac{M}{N}$ variance formula was expected to hold. On further investigation it turned out that the raw data contained small steps of arbitrary times which biased the spectral estimates considerably (see Section 3.3.3). Figure (62) shows an example of such a step. The vertical scale is from + .55 volt to + .25 volt at the Mark I output and the step size is about .1 volt.

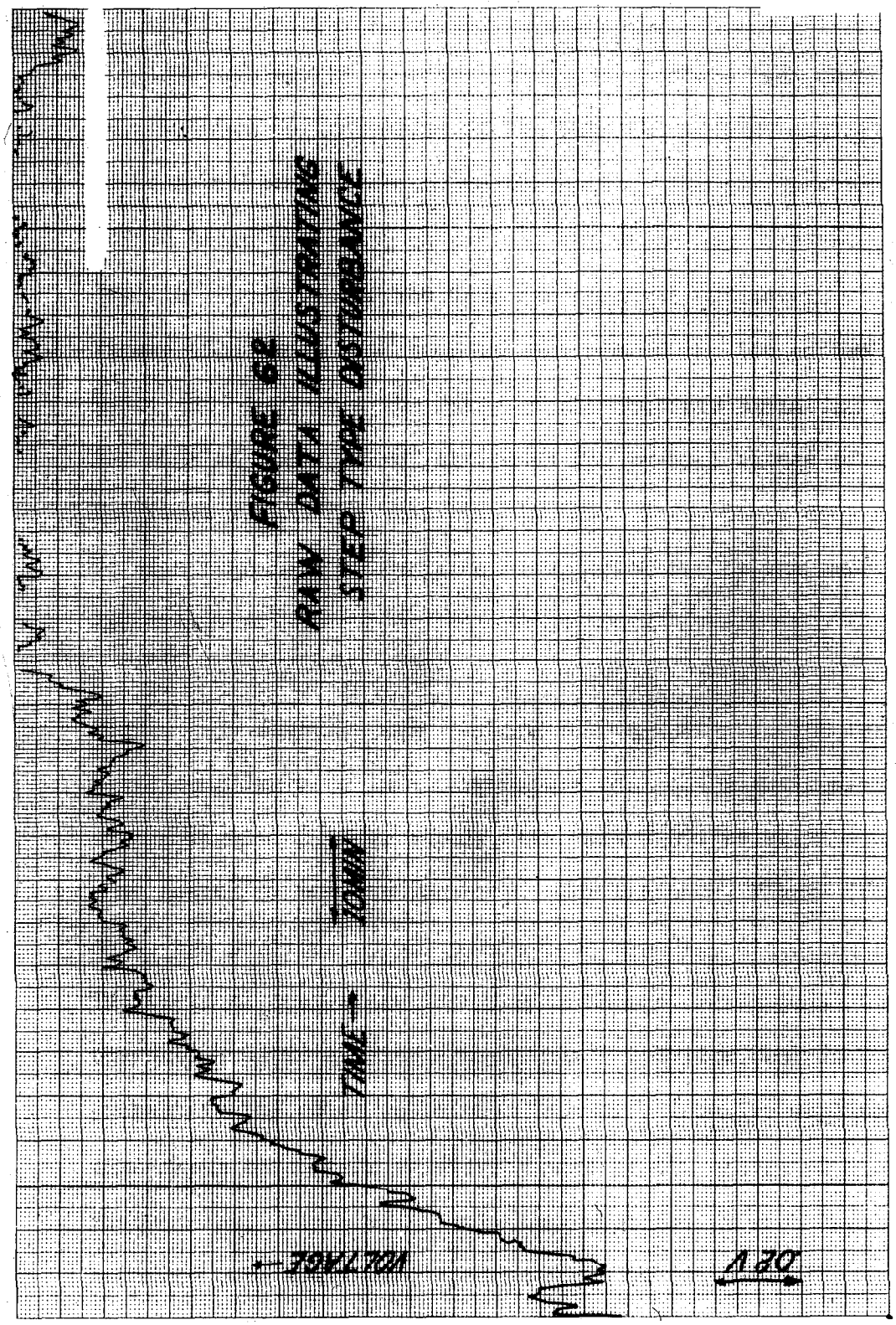

FIGURE 62
RAW DATA ILLUSTRATING
STEP TYPE DISTURBANCE

The approach adopted for analyzing this data is that such steps were related to influences of the external environment and not to be attributed to semiconductor noise. The raw data was edited where necessary to exclude the steps and utilize only "smooth" portions of the data for spectral estimates.* Figure (63) shows a plot of the average of the ten edited runs. Table (10) indicates the ratio of the standard deviation to the mean of the spectral estimates for several values of R. The ideal result for this data is 10%. Thus, there does seem to be a component of variance unaccounted for by the smooth approximation.

Unfortunately, displaying the average behavior as in Figure (63) obscures some perhaps relevant detail. At the 5 sec sampling rate in a temperature controlled environment, with a regulated power supply, the Mark I output still exhibits some degree of non-stationarity. For instance, Figure (64) shows two sections of 900 points each from two different runs. The vertical scales are identical although overlapped. One seems to exhibit a "large amplitude" behavior that is not present in the other while the "normal" (smaller amplitude) case seems to contain relatively more of its energy at higher frequencies. Since relatively long sections of each type of behavior were available, spectra could be estimated for each separately. Figure (65) indicates that the process, at least as

* 3 complete runs contained no steps at all.

R	$\frac{1}{N-1}\sum_{i=1}^{N}\frac{\sqrt{(S_i - \bar{S})^2}}{\bar{S}}$
0	68.58%
1	67.95%
2	68.94%
3	62.55%
4	49.52%
5	43.67%
6	40.18%
7	36.37%
8	31.69%
9	22.55%
10	16.78%
11	13.69%
12	13.94%
13	13.57%
14	10.40%
15	11.64%
16	14.38%
17	12.84%
18	12.57%
19	15.81%
20	13.856%
21	13.77%
22	10.93%
23	14.50%
24	9.22%
25	7.66%
26	11.20%
27	10.66%
28	7.67%
29	7.22%
30	7.67%

Table (10)

Empirical Standard Deviation to Mean Ratios

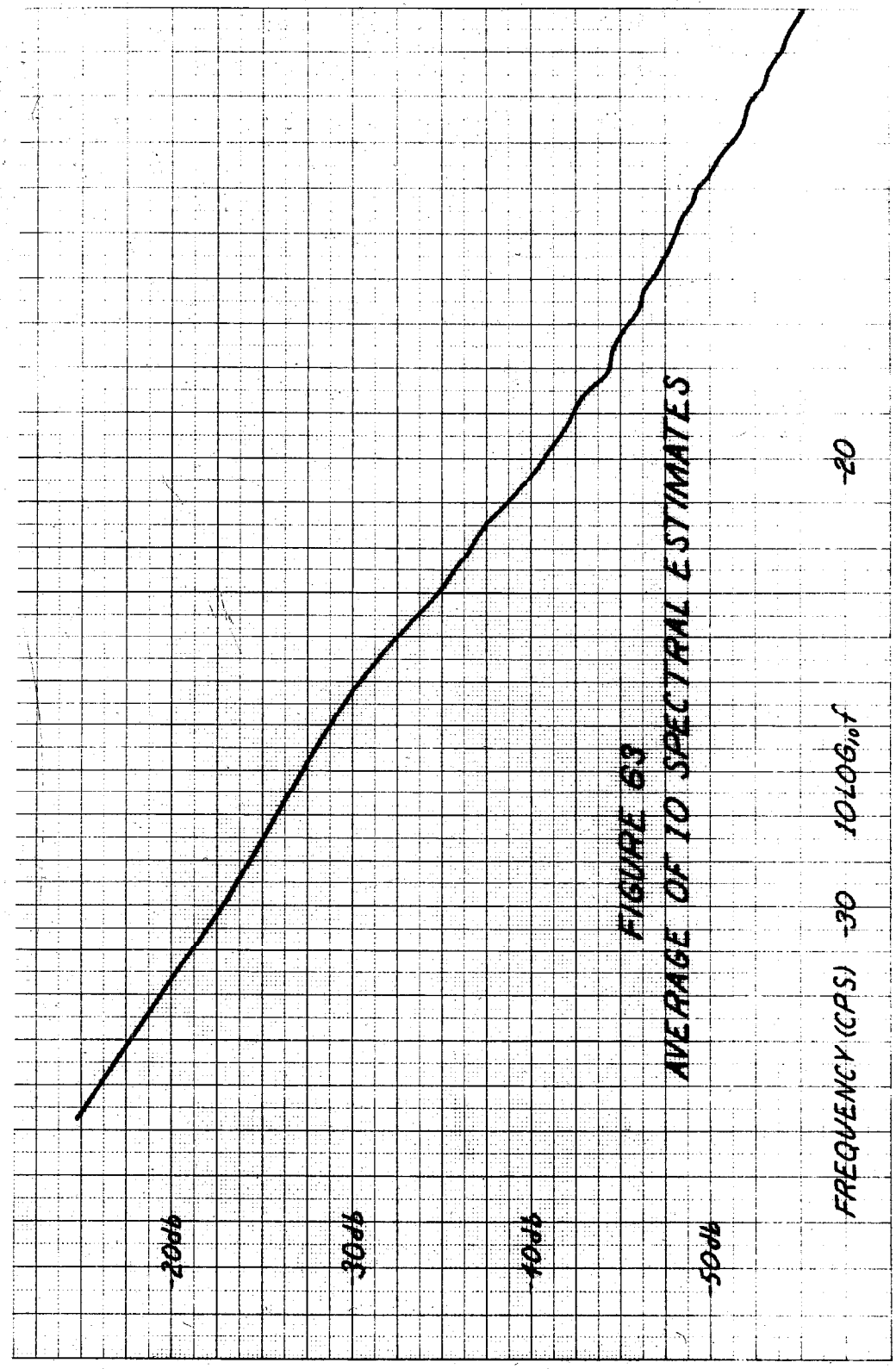

FIGURE 63
AVERAGE OF 10 SPECTRAL ESTIMATES

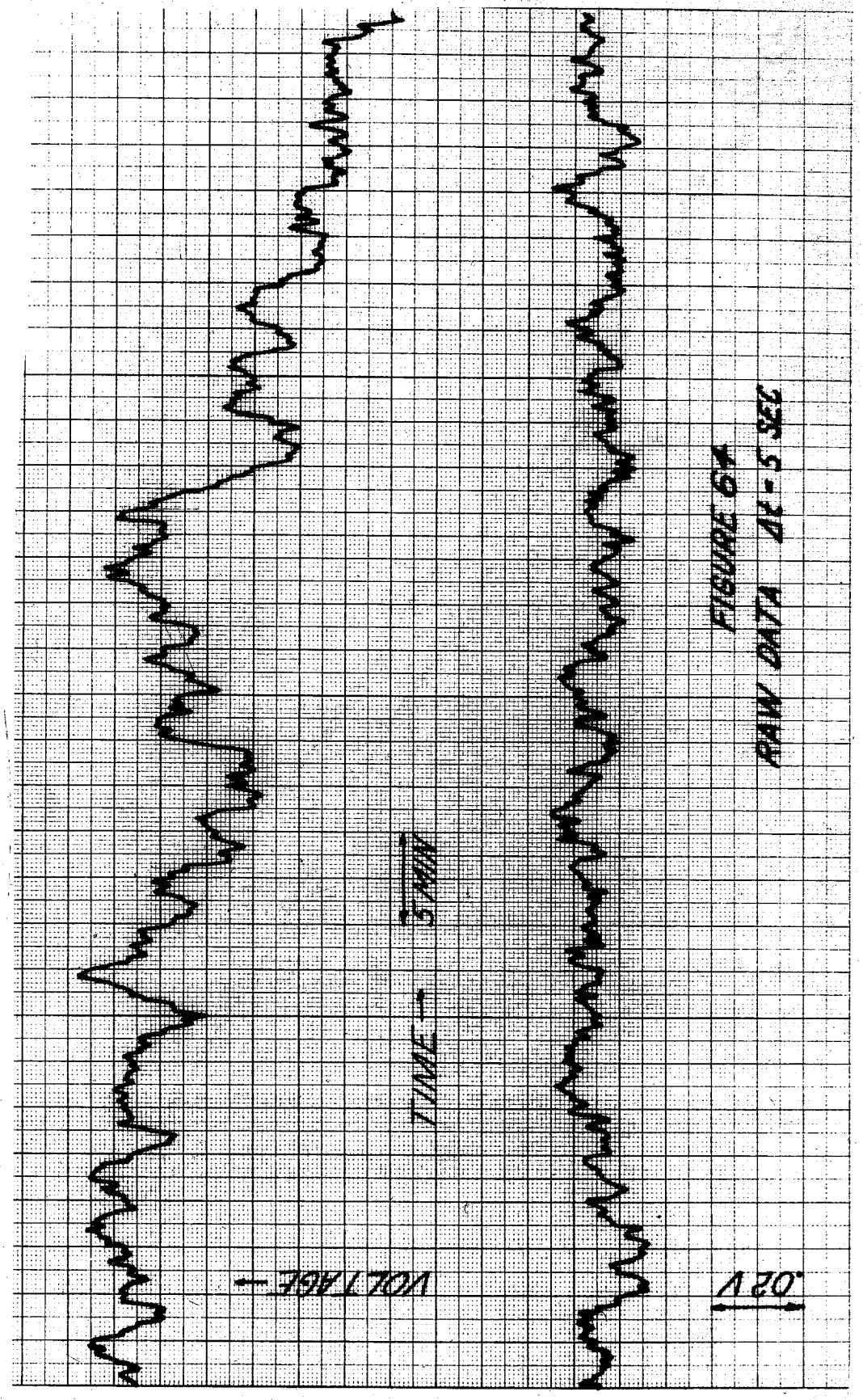

FIGURE 64
RAW DATA Δt - 5 SEC

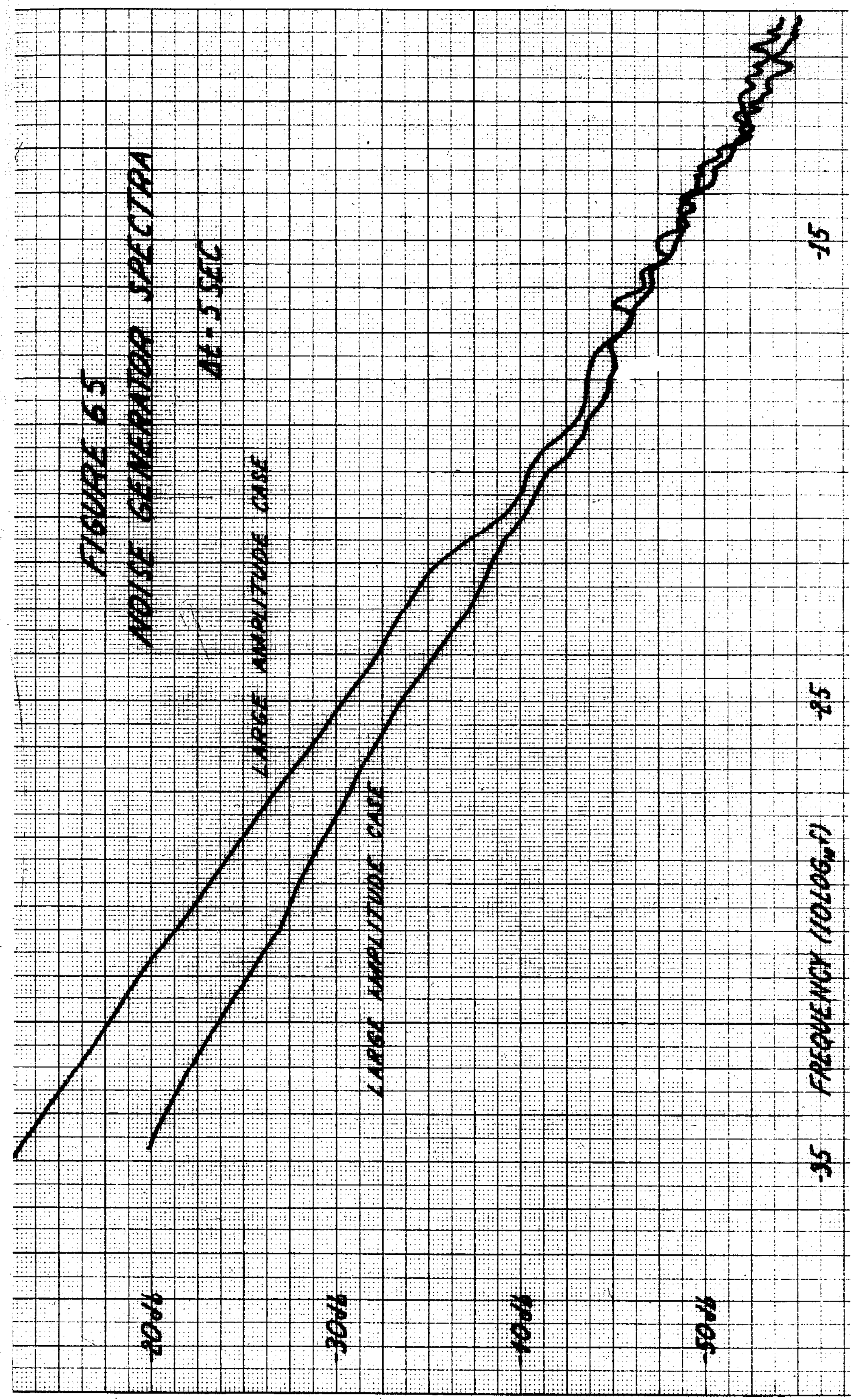
FIGURE 65
NOISE GENERATOR SPECTRA
ΔE - .5 SEC
LARGE AMPLITUDE CASE
LARGE AMPLITUDE CASE
-20db
-30db
-40db
-50db
-35
-25
-15
FREQUENCY (10LOG10 f)

measured here, does not contain much "large amplitude" type behavior since the "normal" estimated spectrum is very close to that for the average of the 10 runs.

The raw data for $\Delta t = 50$ sec run is very similar with respect to the occurrence of steps. Figure (66a) shows a typical section of smooth data while Figure (66b) illustrates a section containing a step. These particular steps occur at about 2:30 AM and 7:00 AM which is very reminiscent of the room temperature behavior in Figure (43b) discussed in Section 5.1. Again the approach of editing the data (in the sense of selecting sections for which no steps occurred) was chosen to obtain meaningful spectral estimates. Figure (67) shows the spectral estimate for the smooth ("normal") part of the $\Delta t = 50$ sec data.

The lowest frequency data available for the Mark I noise generator was read from Easterline Angus Strip Charts at 5 minute intervals (i.e., $\Delta t = 300$ seconds). It is similar to the room temperature raw data in almost all respects. Thus, most of the discussion of Section 5.1 is pertinent concerning the 24 hr components and the manner in which the raw data is most informatively displayed. Figure (68) shows 4 sections of raw data each 5 days in length. Despite the temperature control and special power supply, some of the previously observed non-stationarity effects appear to still be present. Steps

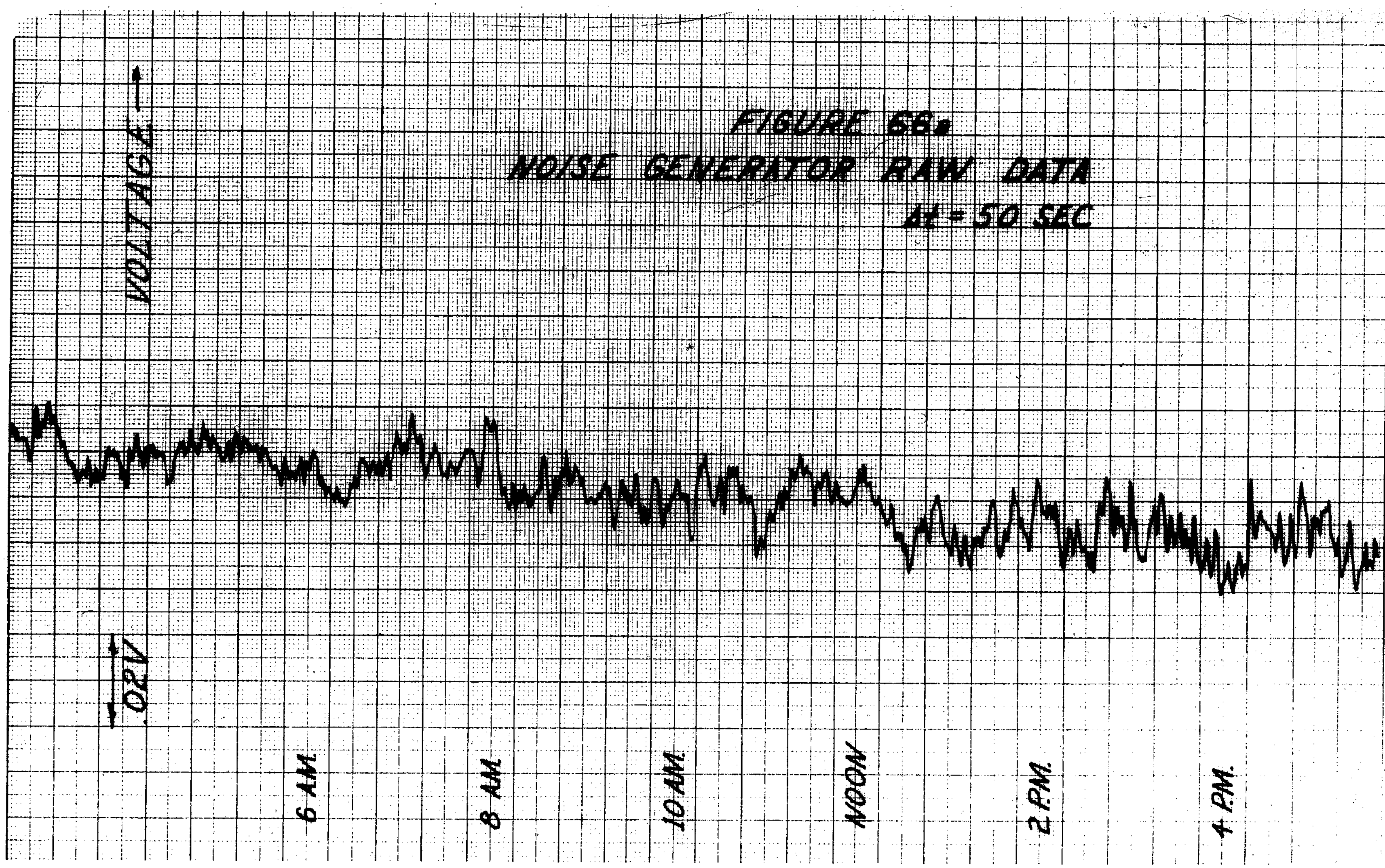

FIGURE 68.
NOISE GENERATOR RAW DATA
Δt = 50 SEC

FIGURE 66b
NOISE GENERATOR RAW DATA
Δt = 50 SEC
VOLTAGE
.02V
TIME
MIDNIGHT
2 AM
FRIDAY
4 AM
6 AM
8 AM

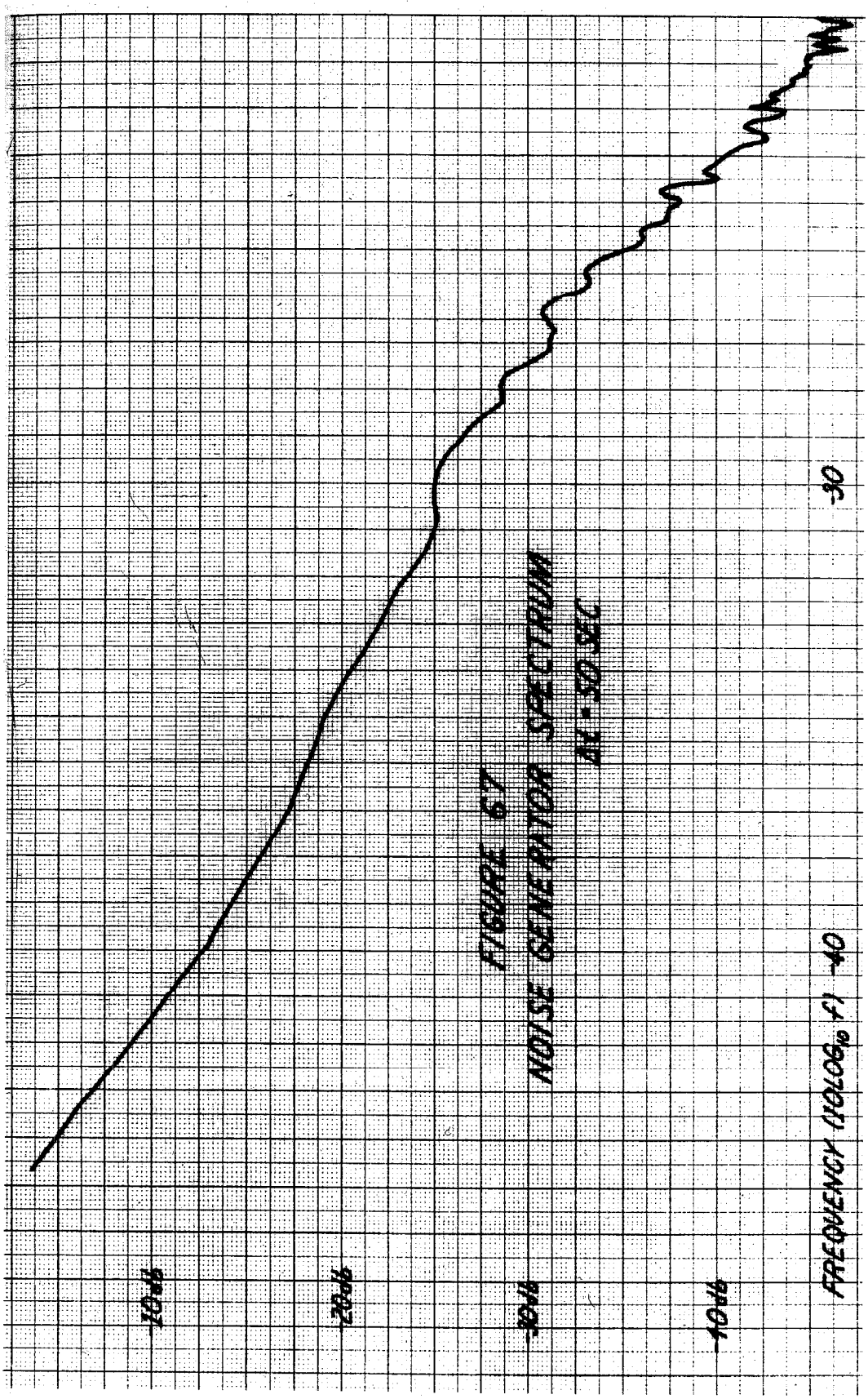

FIGURE 67
NOISE GENERATOR SPECTRUM
M = 50 SEC

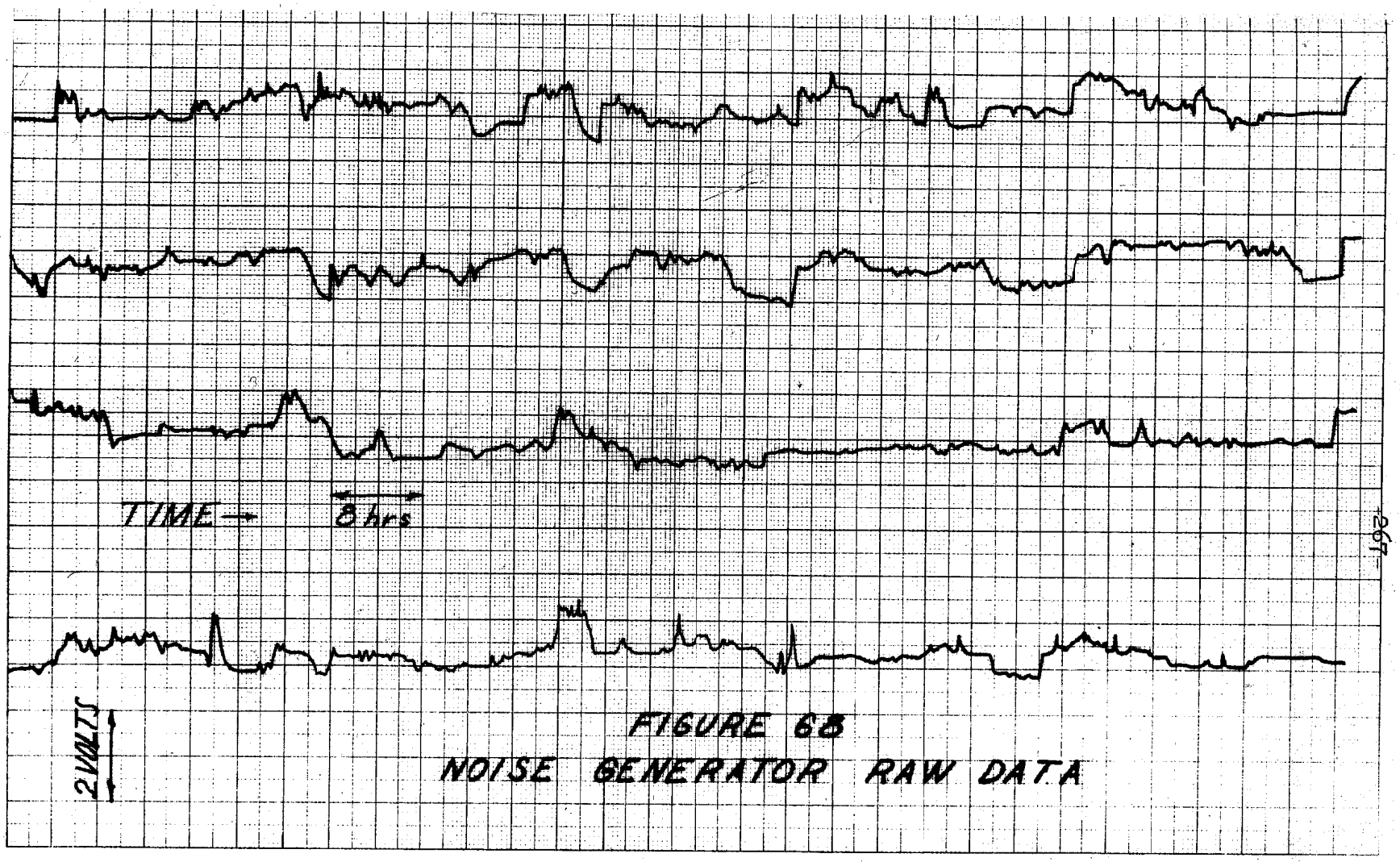

FIGURE 68
NOISE GENERATOR RAW DATA

seem to occur often and last varying lengths of time. At the next level of aggregation the three traces of Figure (69) give an indication of the diversity of behavior that is present here. . Again spectra were estimated from different representative sections of the data in an attempt to ascertain the seriousness of the non-stationarity. The first section chosen is marked on the top trace of Figure (69) and will be referred to as the "small amplitude" case. The other section is the last part of the second trace and the first part of the third (these pieces of data are continuous in time) and will be referred to as the "normal amplitude" case. Figure (70) shows the spectra estimated from these two data sections. The variability is higher for the "small amplitude" case because the M is 100 for both estimates but the total number of data points in this section is smaller than in the normal amplitude section. The spectra differ by as much as 10 db at low frequencies. This indicates a change by a factor of 3 in the corresponding time domain amplitude of the random process which is an appreciable indication of non-stationarity. An additional feature whose presence it is important to recognize is illustrated by Figure (71) which shows

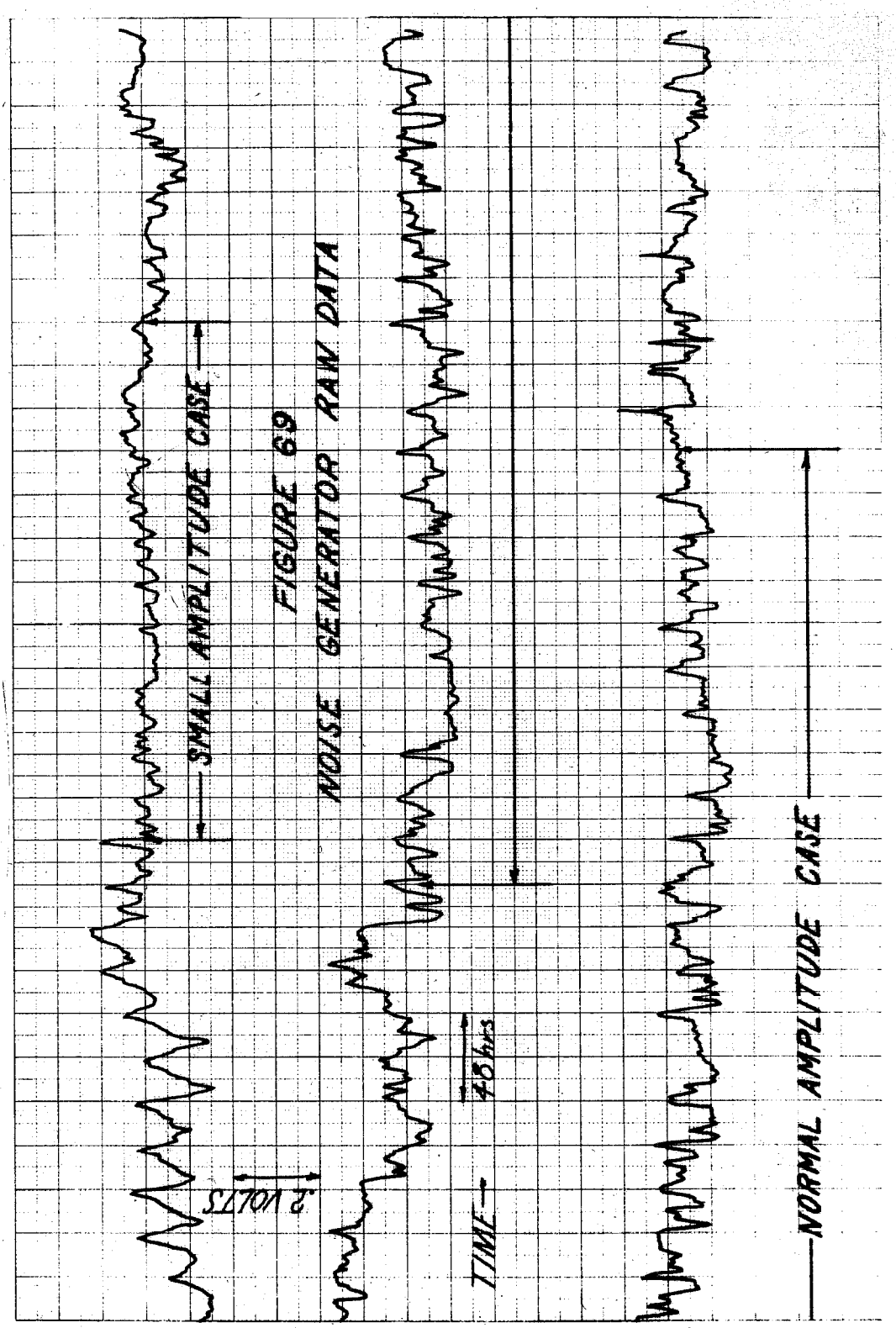

FIGURE 69
NOISE GENERATOR RAW DATA

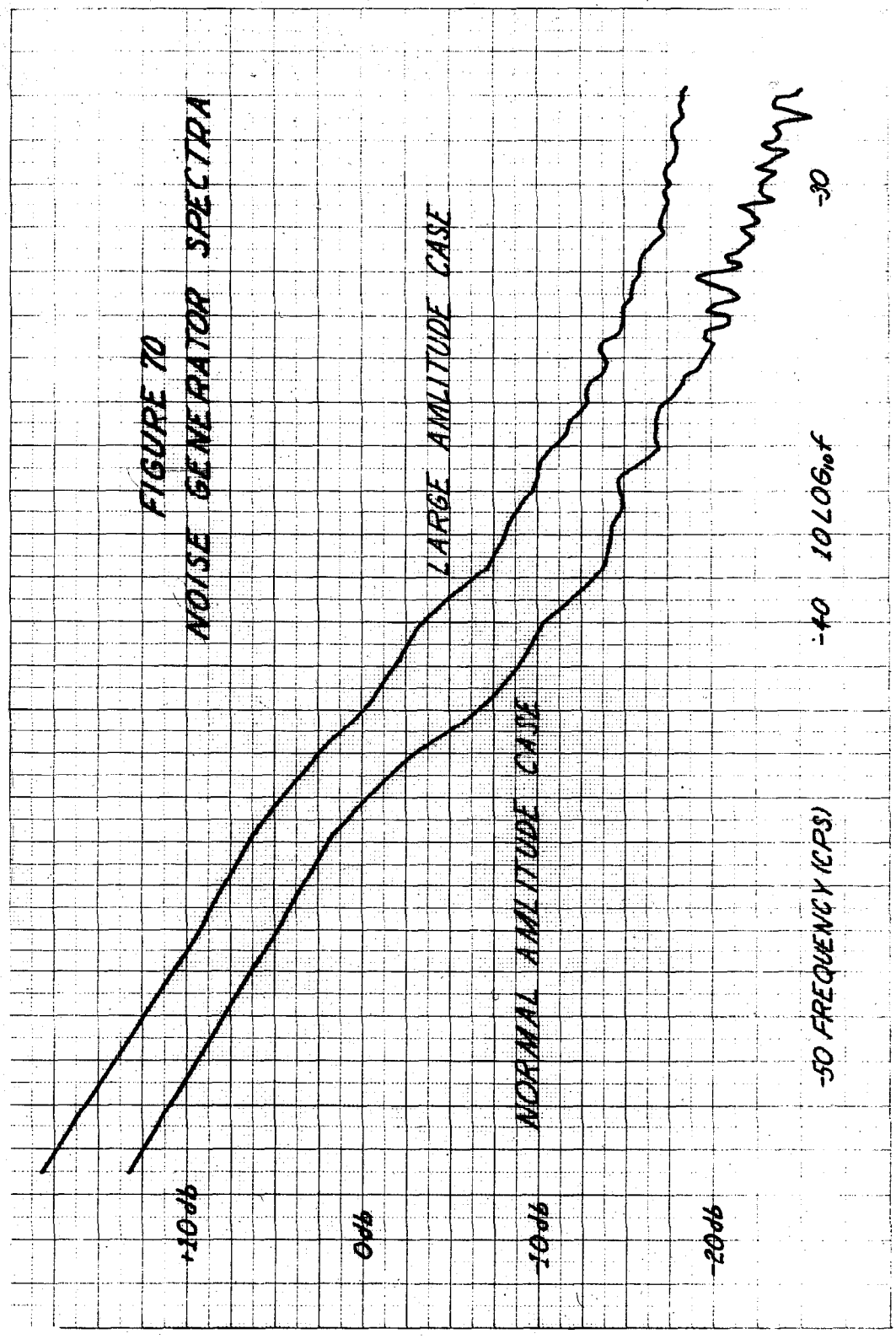
FIGURE 70
NOISE GENERATOR SPECTRA
LARGE AMPLITUDE CASE
NORMAL AMPLITUDE CASE
+10db
0db
-10db
-20db
-40 10LOG10f
-30
-50 FREQUENCY (CPS)

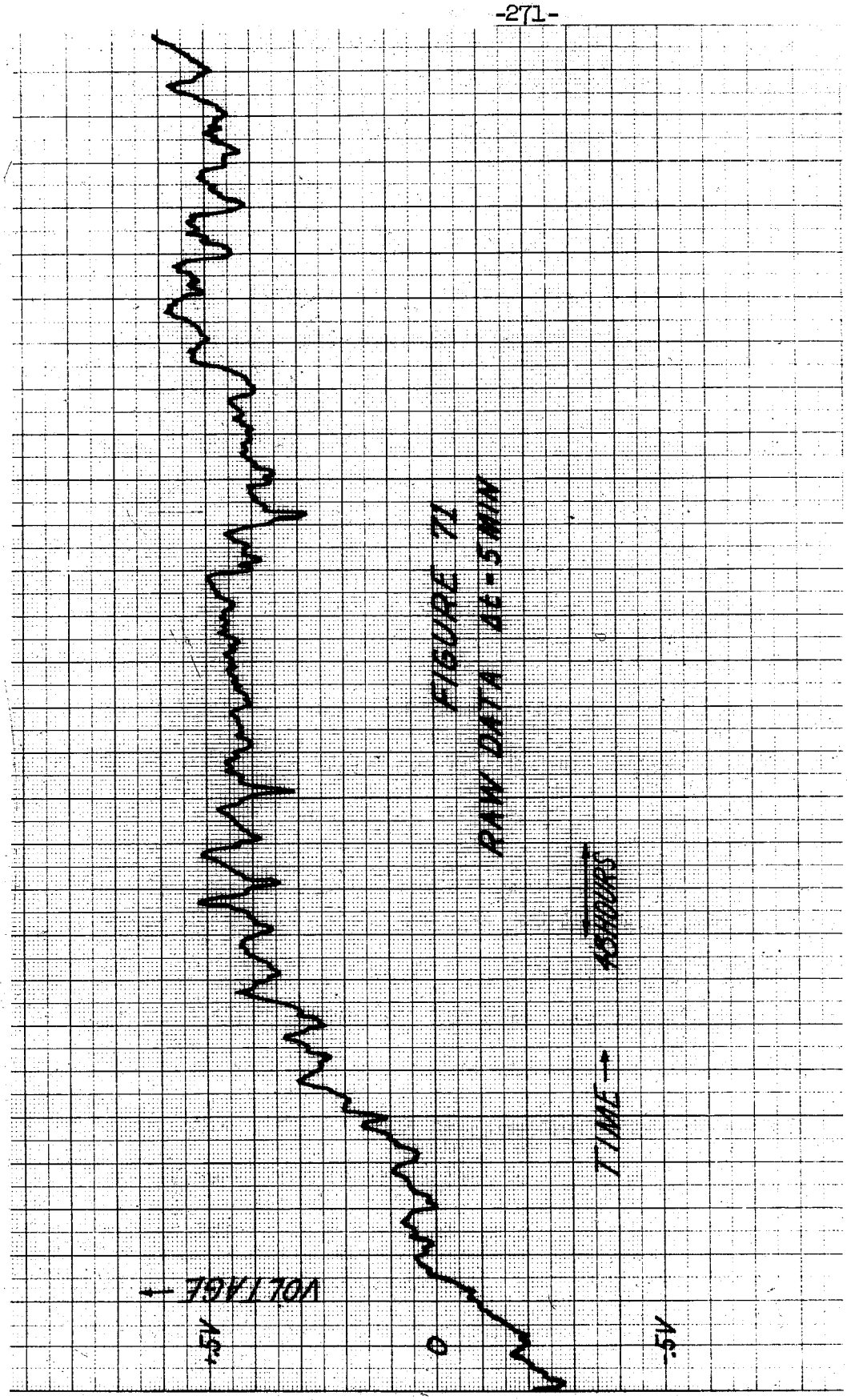

FIGURE 71
RAW DATA AT 5 MM

the first 1296 data points on a -1 v to + 1 v vertical scale. Some kind of warmup phenomenon is apparently occurring which lasts about 10 days.

Evident in all this data, of course, is the 24 hr cycle. It is very significant to note that on this scale, 30 days per page, and the previous one, 5 days per page, the Mark I 24 hr cycles do not correlate with the roomtemperature very closely. Figure (72) illustrates this point by showing the Mark I output (top) and the corresponding room temperature (bottom) on the same time scale (5 days per sheet). There may be some statistical correlation between these two waveforms but is certainly not as high as for the comparison made earlier in Figure (21) and described in Section 4.2. When the Mark I noise generator is responding to temperature its response is definite and immediate. Suppose the oil temperature control system is operating approximately according to the mathematical model of Section 4.2. Then we should expect the oil temperature response to a 24 hr input to look like an attenuated, lagged version of the room temperature. If this were the dominating factor in the Mark I output it would be expected to be highly correlated with the room temperature. Thus, it appears that the attempt at thermal control has been at least partially successful in that the room temperature is no longer directly sensed by the noise generator.

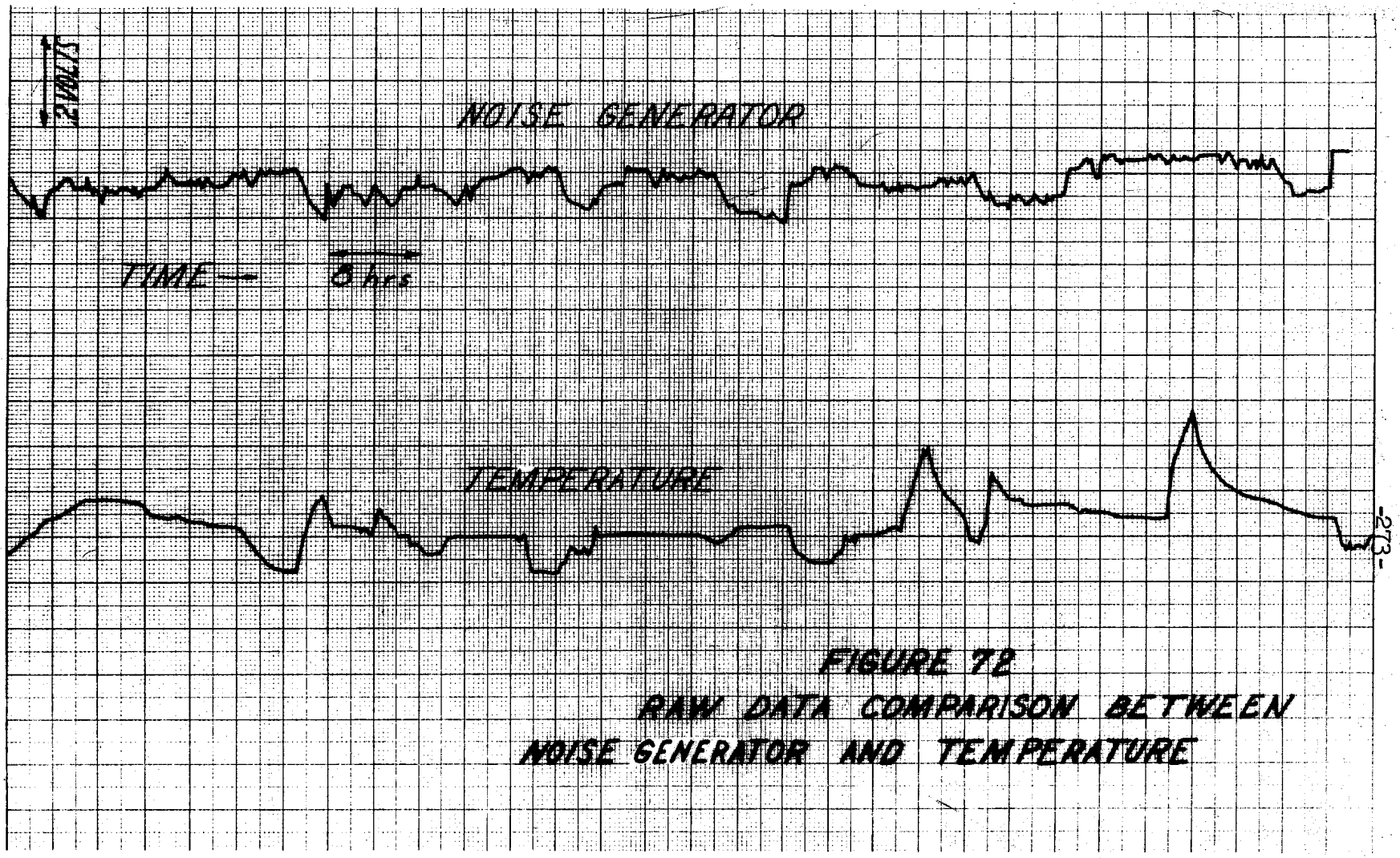

FIGURE 72
RAW DATA COMPARISON BETWEEN
NOISE GENERATOR AND TEMPERATURE

But the Mark I output certainly does have a strong 24 hr component. Some additional light is shed on the subject by Figure (73) which is the final condensation of the Mark I data on an expanded vertical scale. The first portion of the warmup period illustrated in Figure (71) has been excluded to utilize a vertical scale of + .35 to + .95 volts. The horizontal scale was about 7 days per inch on the original graph so that after the photographic reduction the daily cycles are barely visible. This is about the same scale as Figure (47) above for the room temperature. If the corresponding time sections of these two figures are compared, one finds that the large and small amplitude behavior regions of each function correspond. Thus, it seems clear that Mark I must in fact be measuring the room temperature by some intermediate variable or combination of variables.* This composite view of the Mark I output also indicates vividly the existence of a considerable amount of energy in a weekly cycle. Also evident is the fact that the latter portion is most smooth and would be most attractive for eliminating low frequency biases. This latter portion was in fact used for the lowest frequency spectral estimations. There are some fairly plausible

* It is now believed that the most likely candidate for the indirect temperature influence is the Mark I power supplies. Monitoring these power supplies shows changes in excess of the expected amounts calculated in Section 4.1. The power supplies appear to vary something on the order of ± 15 mv over the daily cycle although the data is not precise enough at this time to correlate the changes directly with the room temperature variations.

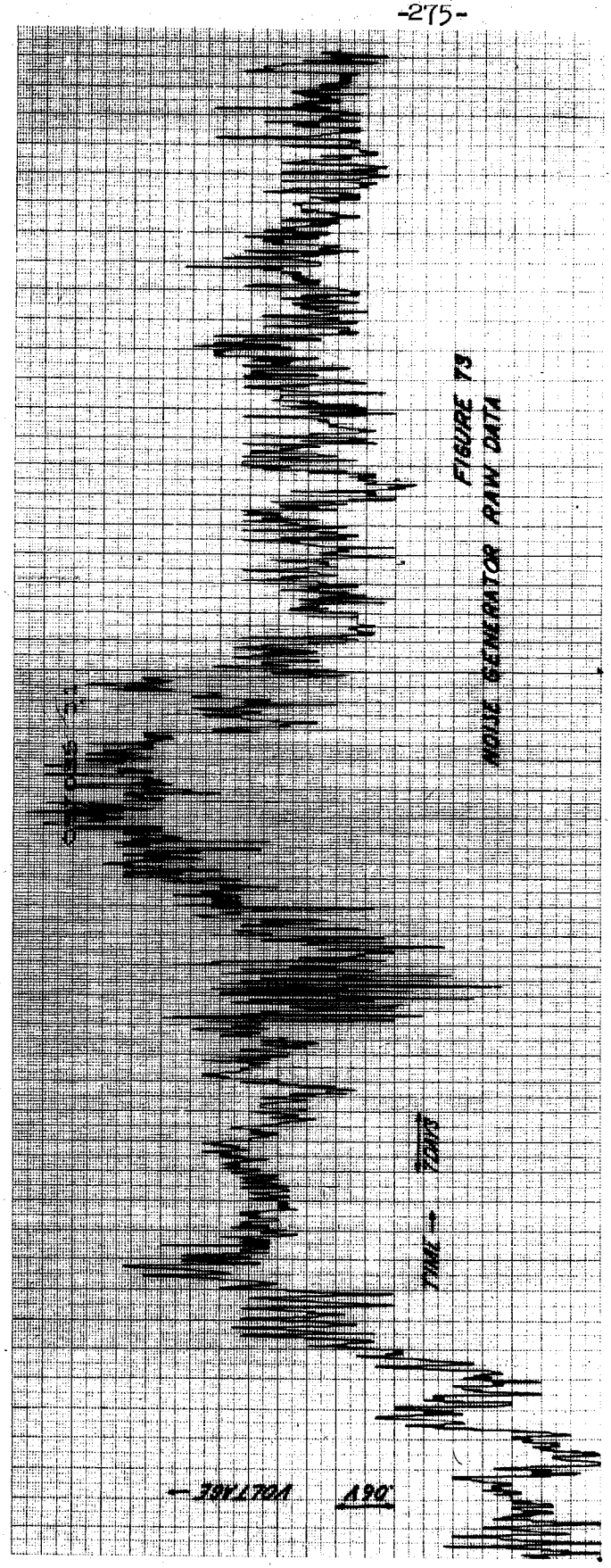

FIGURE 73
NOISE GENERATOR RAW DATA

physical reasons for this behavior. No changes in power supply, reference cell batteries, low pass filters, steady heating current, or other parameters of the thermal control system were made during this period. Each of these parameters was adjusted at least once during the earlier part of the run.

The spectrum estimated from this edited lowest frequency data is shown in Figure (74). Plotted for comparison of the low frequency end is the same spectrum estimated from all the Mark I data shown in Figure (73) . Considering that the latter includes: warmup transient, the switchover from rechargeable batteries to a regulated power supply, and the adjustment of the thermal control system parameters, the differences are surprisingly small.

Collecting our best estimate of the Mark I noise generator's spectrum over the whole range of estimation now yields the spectrum of Figure (75). Only selected points have been plotted. Some of the minor statistical variation has been smoothed and the extraneous high frequency lines have been ignored. The 24 hr and harmonic lines have been retained because it has not been established with enough certainty that they are not, in fact, intrinsic to the noise process.

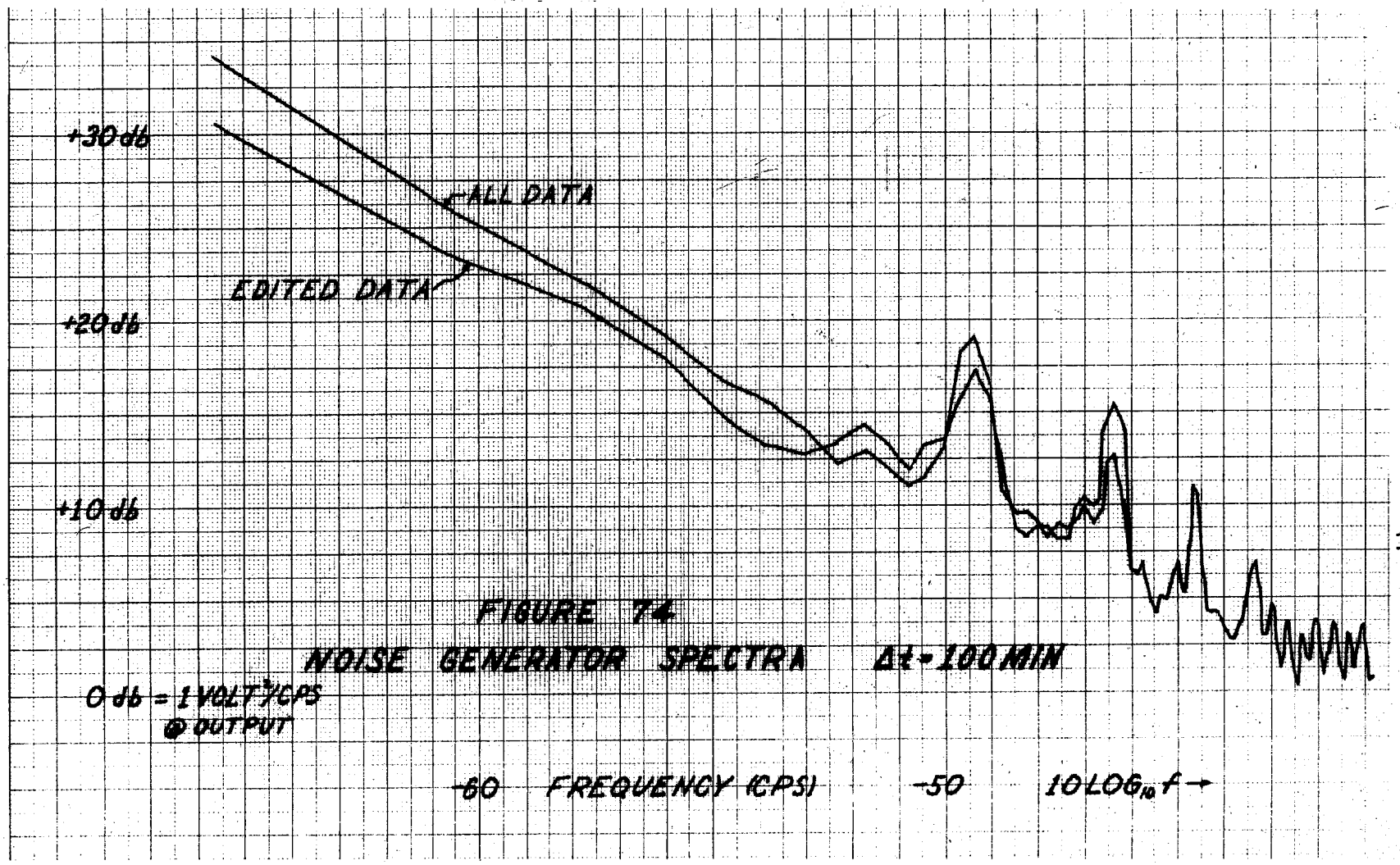

FIGURE 74
NOISE GENERATOR SPECTRA Δt = 100 MIN

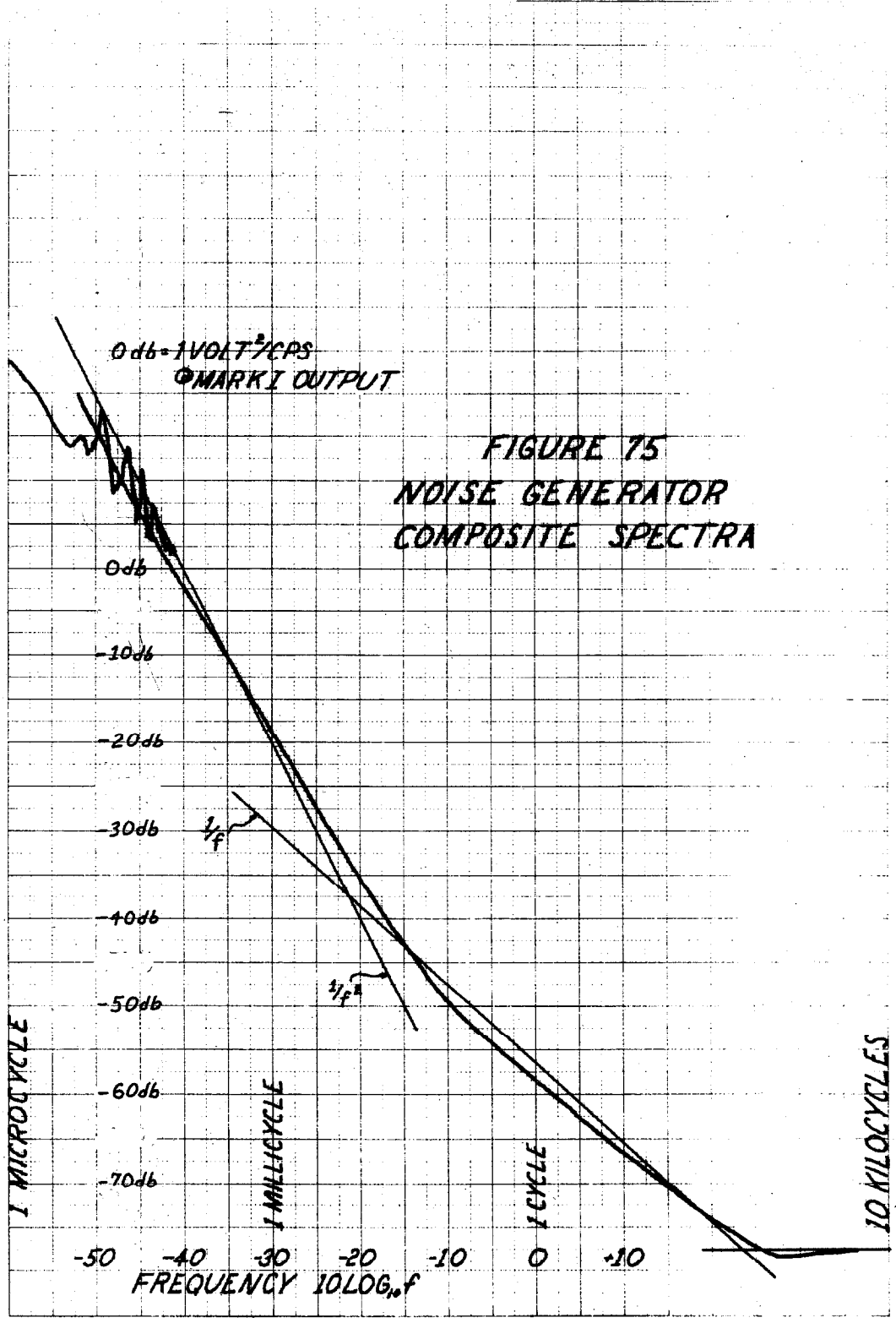

FIGURE 75
NOISE GENERATOR
COMPOSITE SPECTRA

It is significant to note that the lowest sampling rate for which we were able to obtain "smooth" data, $\Delta t = 50$ sec, the estimated spectrum lies somewhat below the two lower frequency runs. These were obtained from the 5 min data which is definitely not smooth.

One could now proceed as in the case of room temperature noise to construct a crude mathematical model for the overall noise behavior. The simplest model would be $1/f^2$ noise (RC noise with very low break frequency) plus excess noise at 24 hrs and harmonics plus 1/f noise plus white noise. If the parameters are picked to correspond to the asymptotes shown in Figure (75) we would have

$$S(f) = \frac{K_2}{f^2 + f_2^2} + \frac{K_1}{|f|} + \sum_{n=-k}^{k} A_n^2 \, \delta(f - nf_d) + N_o$$

with

$K_2 = 8.92 \times 10^{-9}$ $\qquad$ $A_1 = .00724$

$K_1 = 2.63 \times 10^{-7}$ $\qquad$ $A_2 = .00437$

$f_2 < 10^{-7}$ cps $\qquad$ $A_3 = .00335$

$f_d = 1.15 \times 10^{-5}$ cps $\qquad$ $A_4 = .00207$

$N_o = 1.78 \times 10^{-8}$

referred to the output of Mark I. This model should not be taken too seriously in view of the obvious non-stationarities

in the data discussed above. Also the real data appears to move smoothly from $1/f$ behavior to $1/f^2$ behavior. Thus, a polynomial or other more complicated fit to the data is probably better. However, it seems fruitless at this point to fit more sophisticated models to such crude data.

In conclusion let us suppose that this simple model holds and that we wish to compute an RMS value for the "drift" of Mark I over the limited band from 1μ to 10Kc . We would find a value of approximately 18 millivolts referred to the output.* Utilizing a differential mode gain of 8700 (see Section 4.1) yields an input RMS drift over this band of about $1\frac{1}{2}$ microvolts. On the other hand, if we calculate an RMS value based on the data (as opposed to the model) we arrive at 11 mv referred to the output, which yields an equivalent input drift of 1.3 μv.

* This excludes the 24 hr and harmonic energy.

5.3 Amplifier Noise

Low frequency noise measurements were also made on operational amplifiers. First of all it was necessary to establish that the operational amplifiers used in other experiments were not contributing significantly to the measured output. Secondly, it was desirable to know their "drift" properties for comparison with the Mark I measurements.

The particular unit measured was a Kaylab 110A dc amplifier. The two higher frequency sets of runs were made via the digital voltmeter-paper tape scheme and the lowest frequency data was taken from Easterline Angus Strip Chart recordings. These data collection schemes are just those described in Section 4.3 above. All of the raw data was taken with the unit operating open in the ordinary room environment. No attempt was made to control either the temperature environment seen by the amplifier or the line voltage from which it is operated. In other words, these results are expected to be representative of reasonable laboratory conditions.

For the highest frequency data the sampling time was 5 seconds which yields a highest estimation frequency of .1 cps. Spectra at higher frequencies for amplifiers are fairly well known. The primary interest here was the low frequency or "drift" properties. The power spectral density

from the 5 sec data is shown in Figure (76). The vertical scale extends from - 140 db to - 90 db where 0 db corresponds to 1 volt^2/cps. This spectrum is referred back to the input of the amplifier through its gain. The horizontal scale represents logarithmic frequency from 10^{-4} to 10^{-1} cps.

By this time it should come as no great shock that the result is basically a "1/f type" spectrum This data was taken with the digital voltmeter fixed at 10 volts full scale and another intermediate amplifier of gain 100. Therefore, the quantization level is 1/100th of a millivolt at the output. In the notation of Section 3.2.4 this is $\Delta\epsilon = 10^{-5}$ which implies a quantization noise level of 4.166×10^{-9} at the ouput or - 164 db referred to the input. There is clearly no problem here for this data. The spectrum shown was estimated from prewhitened data so that the M/N approximation is probably a reasonable estimate of the expected relative variability. There were 7658 total data points and an M of 100 was used for this estimation. Thus, we would expect about an + 11% 1σ estimator. This is (+ .573 db, - .528 db) which is approximately a 1 db band. The small section with lines enclosing the estimates shows a 1 db band. A plateau seems to occur at the R = 4, 5, 6 points. To the right of R = 6 point (6×10^{-3} cps) the results seem to be consistent with a 1 db 1σ band about a line, i.e., power law. The lowest

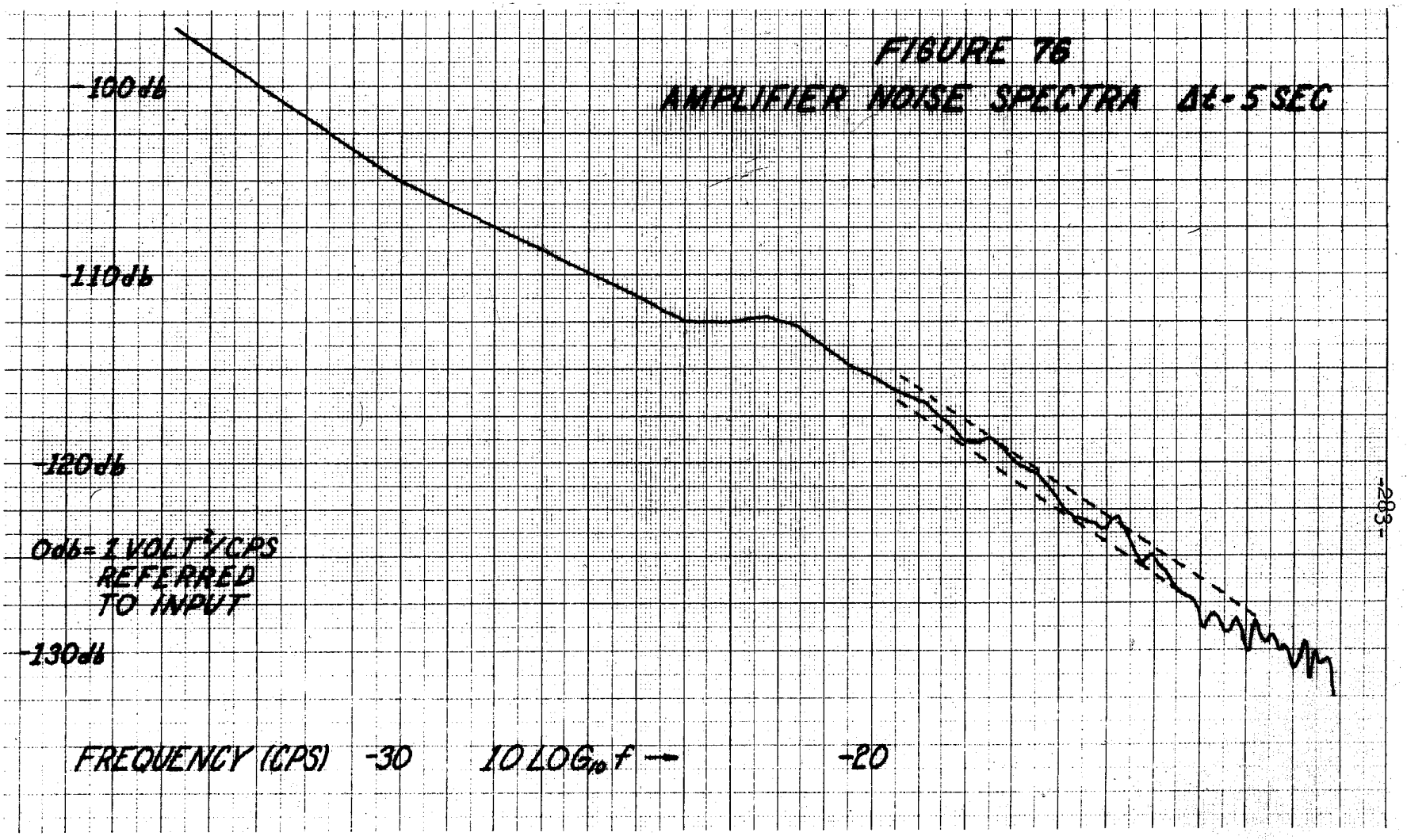
FIGURE 76
AMPLIFIER NOISE SPECTRA Δt - 5 SEC
-100db
-110db
-120db
0db = 1 VOLT²/CPS REFERRED TO INPUT
-130db
FREQUENCY (CPS) -30
10 LOG10 f —
-20

frequency data was read from the Easterline Angus Charts at a sampling rate of once every 5 minutes. Figure (77) shows a typical section of raw data. There were a total of N = 4840 data points and an M = 100 spectral estimation was performed yielding a minimum frequency resolution of 1.67×10^{-5} cps. The data was prewhitened for a $1/f^2$ spectrum and the 1σ variance bands are $\pm$ 14.4% or + .58 db, - .68 db. Figure (78) presents this spectrum. The vertical scale is - 120 db to - 70 db where once again 0 db is 1 $volt^2/cps$ referred to the input and the horizontal scale is $10 log_{10}(f)$ from - 55 to - 25 which corresponds to 3.16×10^{-6} cps to 3.16×10^{-3} cps. A composite spectrum can now be assembled. The lowest frequency spectrum is obtained by taking every 10^{th} sample of the 5 minute data and has 1σ variance bands of (+ 1.63 db, - 2.64 db). Figure (79) shows the three spectra plotted together. All are prewhitened $1/f^2$ estimates. As with the room temperature and Mark I spectra there is excess energy at 24 hrs and its harmonics. Despite the prewhitening, the lowest frequency points on each curve seem biased upward. As in the Mark I data case fitting a power law to this data is a significant oversimplification as the line shown on Figure (79) indicates. This line is $K/_f 1.32$ where $K = 2.17 \times 10^{-14}$ $volts^2/cps$. It is not at all a good fit to

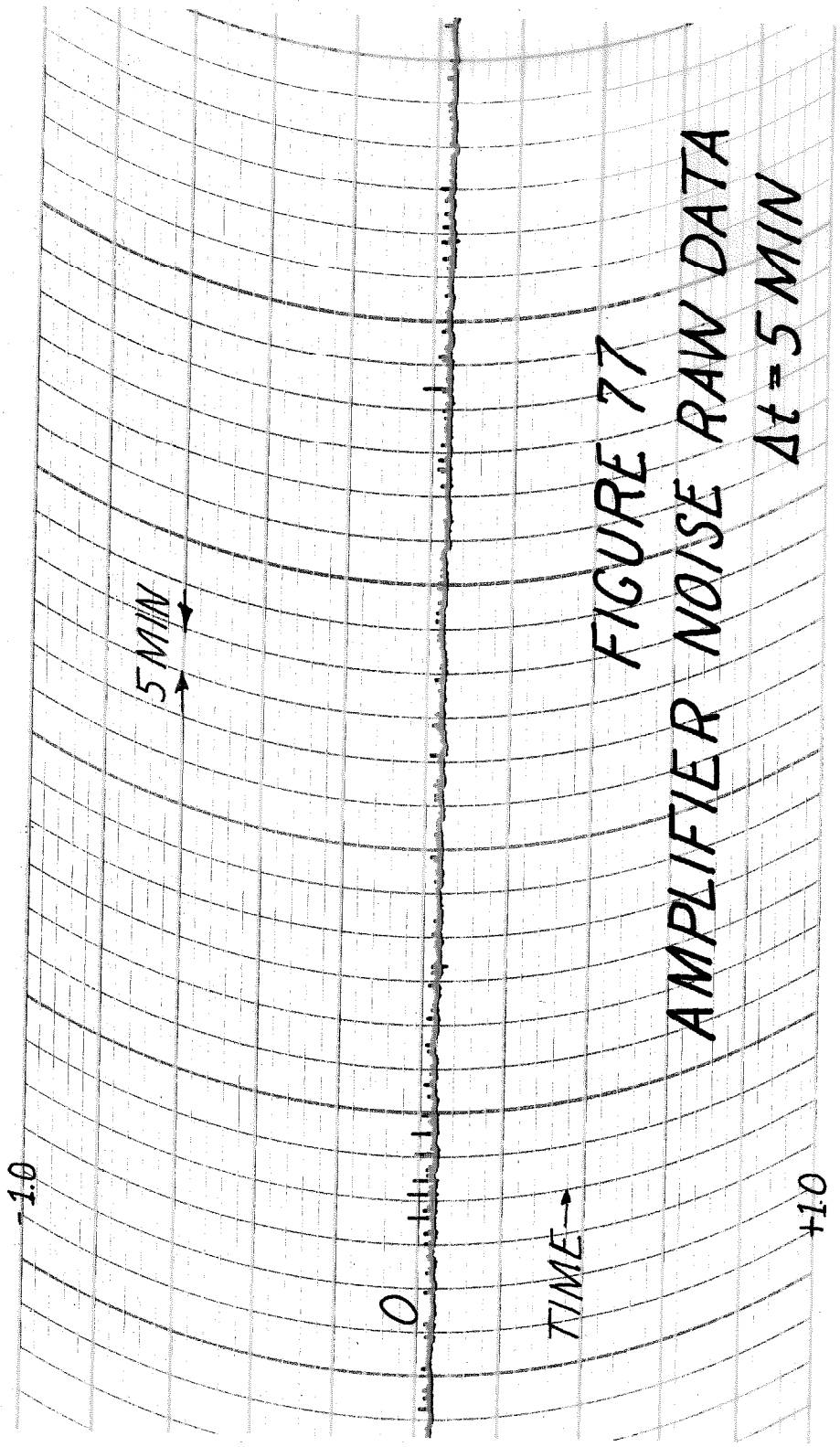

FIGURE 77
AMPLIFIER NOISE RAW DATA
$\Delta t = 5$ MIN

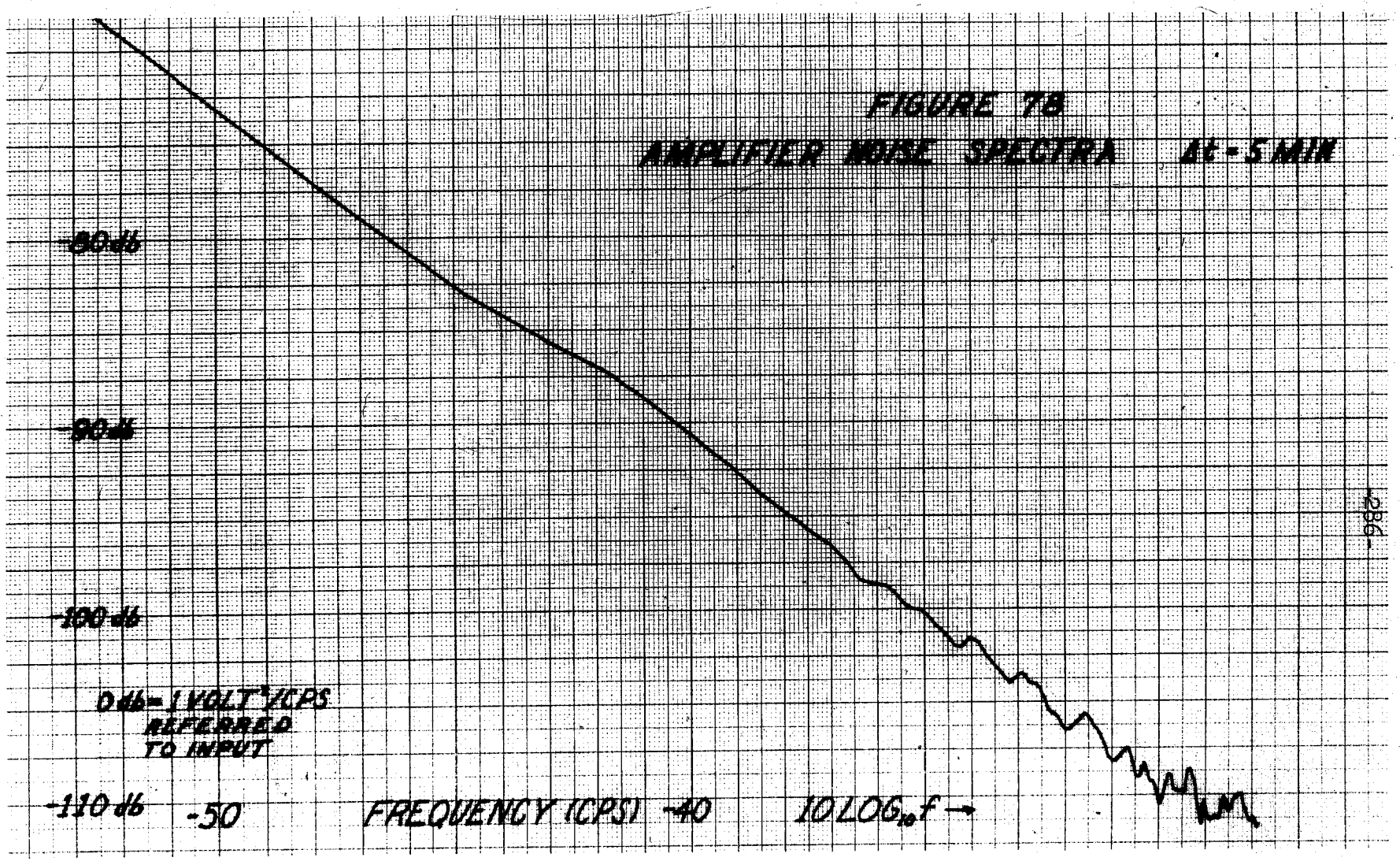
FIGURE 7B
AMPLIFIER NOISE SPECTRA Δt = 5 MIN
-80 db
-90 db
-100 db
0 db = 1 VOLT²/CPS REFERRED TO INPUT
-110 db
-50
FREQUENCY (CPS)
-40
10 LOG10 f →
2961

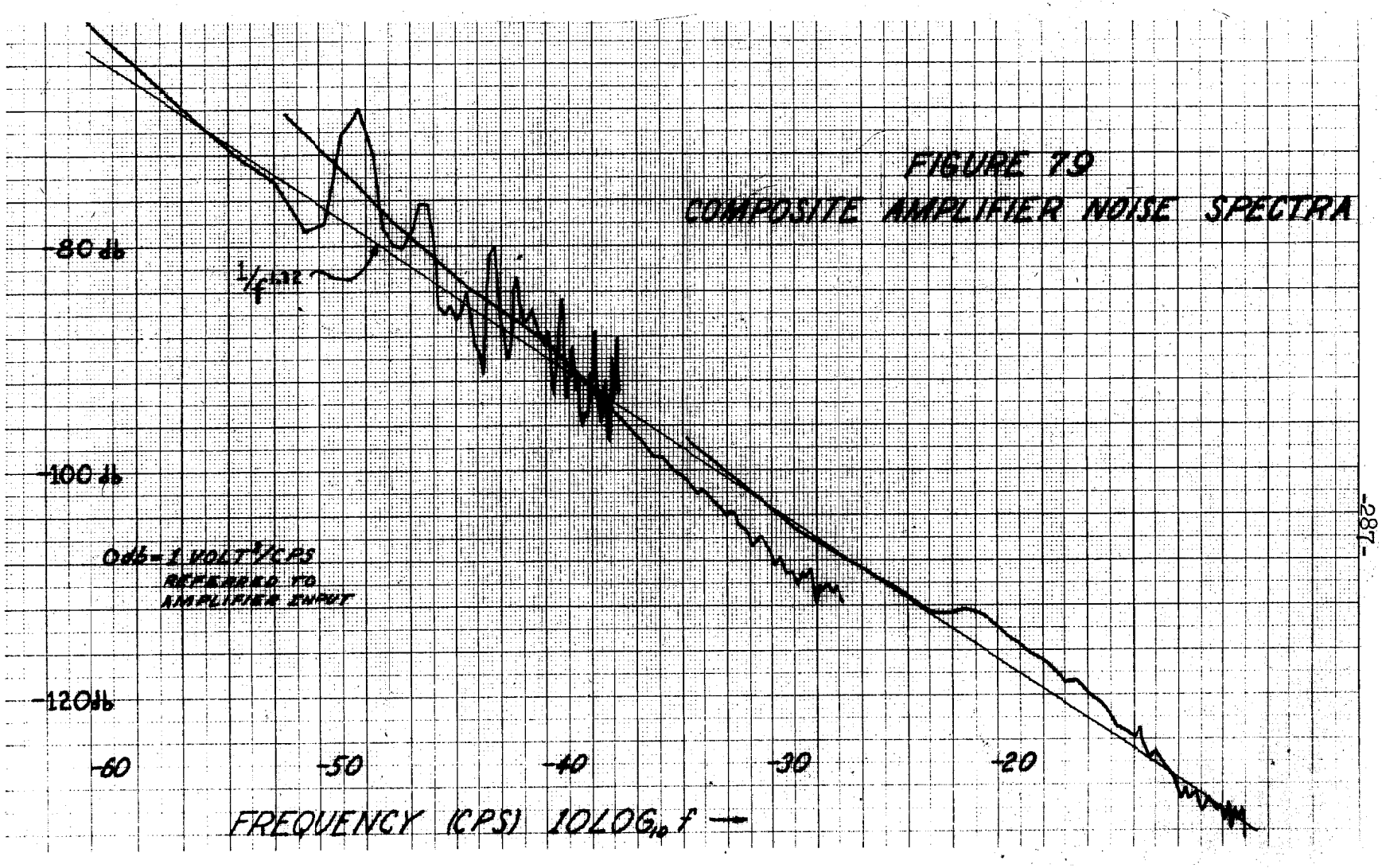

FIGURE 79
COMPOSITE AMPLIFIER NOISE SPECTRA

the middle run data. However, we can use this form to calculate a crude limited bandwidth RMS value for the region from 1 microcycle to 1 cycle. The result is RMS = 1.1×10^{-6} or about 1μ volt. This is an extremely interesting result because it implies that the instrument's RMS "drift" is really quite low, almost a decade lower than its specification guarantees. This calculation is, of course, inaccurate. The model itself doesn't really match the data because it does not include the 24 hr energy peaks. We could eliminate this difficulty by including these as additional narrow band noises as done for room temperature (see Section 5.1).

There is an additional feature of operational amplifier noise which indicates clearly that we still do not fully understand the phenomenon of drift. Data was also taken at a 50 sec sampling rate via the paper tape punch scheme. While none of the above spectra are from this data the raw data itself is extremely interesting. There were 10000 data points available and these were plotted 900 to a sheet. Figures (80) shows two typical sections of data. The vertical scale is ± 10μ volts full scale referred to the input. There seem to be two distinct processes with violently different RMS values and different mean values. The times between state changes are long, on the order of 12 hrs. It is possible that the different states are related to room

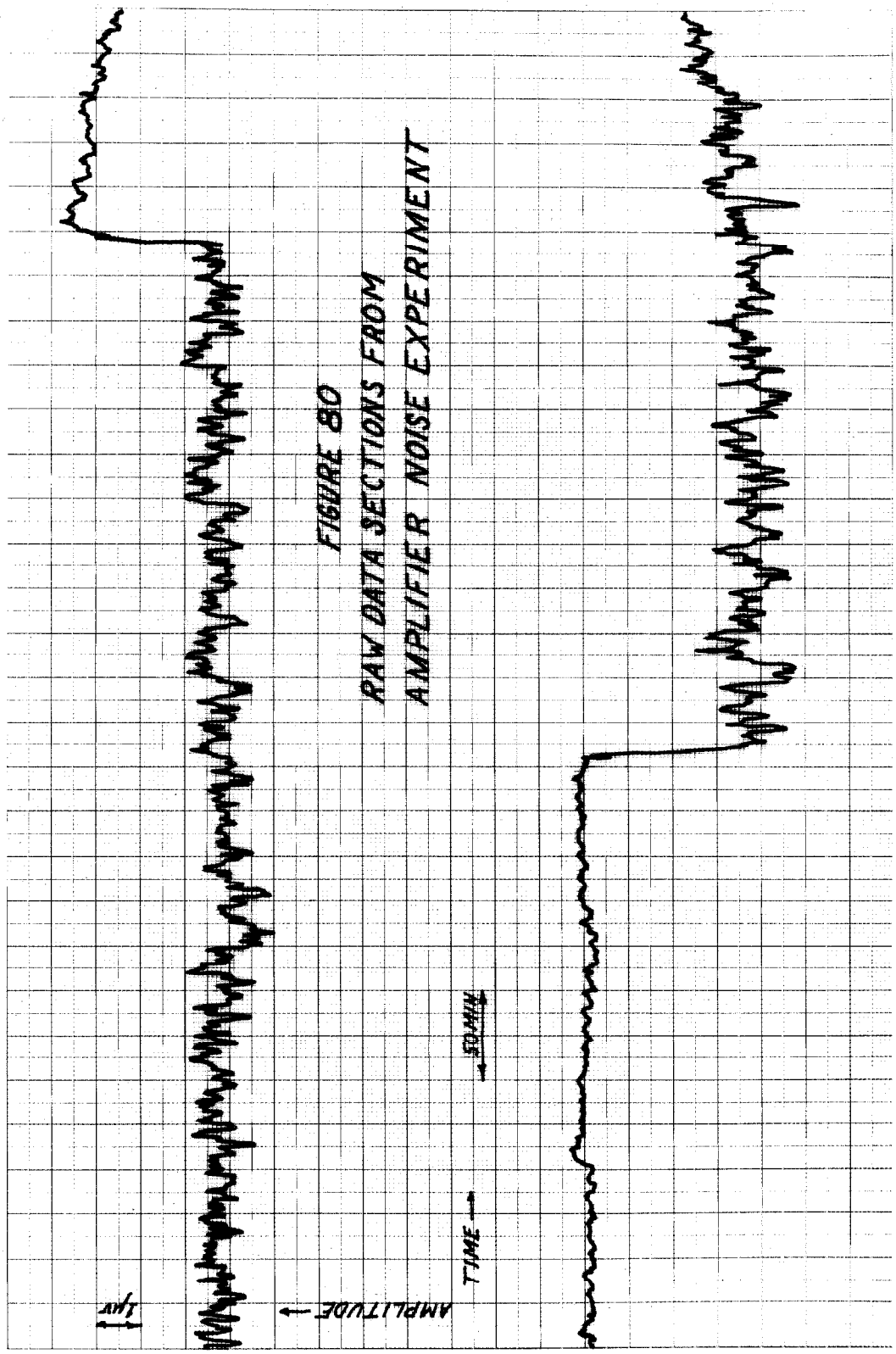

FIGURE 80
RAW DATA SECTIONS FROM
AMPLIFIER NOISE EXPERIMENT

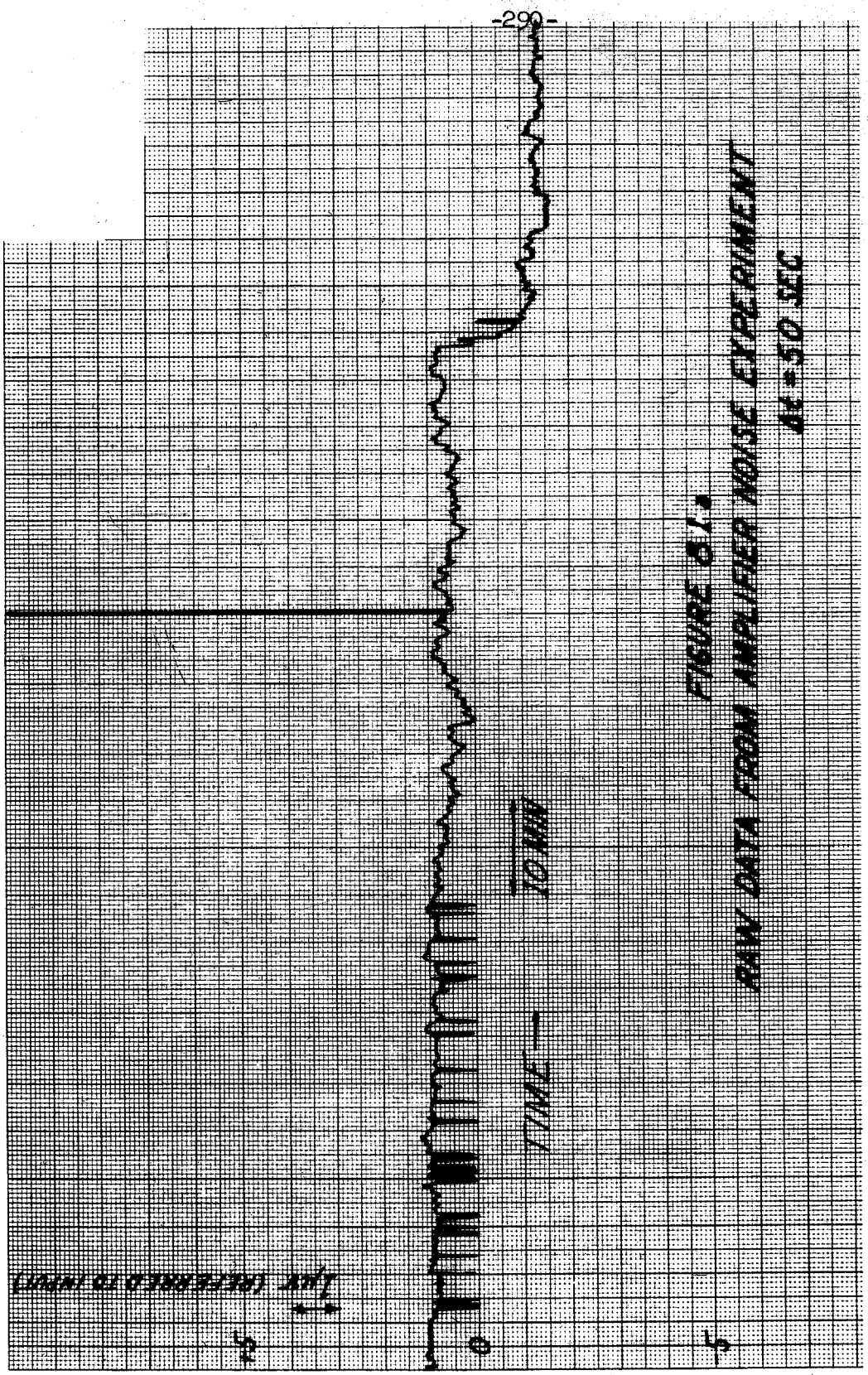

FIGURE 6.1
RAW DATA FROM AMPLIFIED NOISE EXPERIMENT
$\Delta t = 50$ SEC

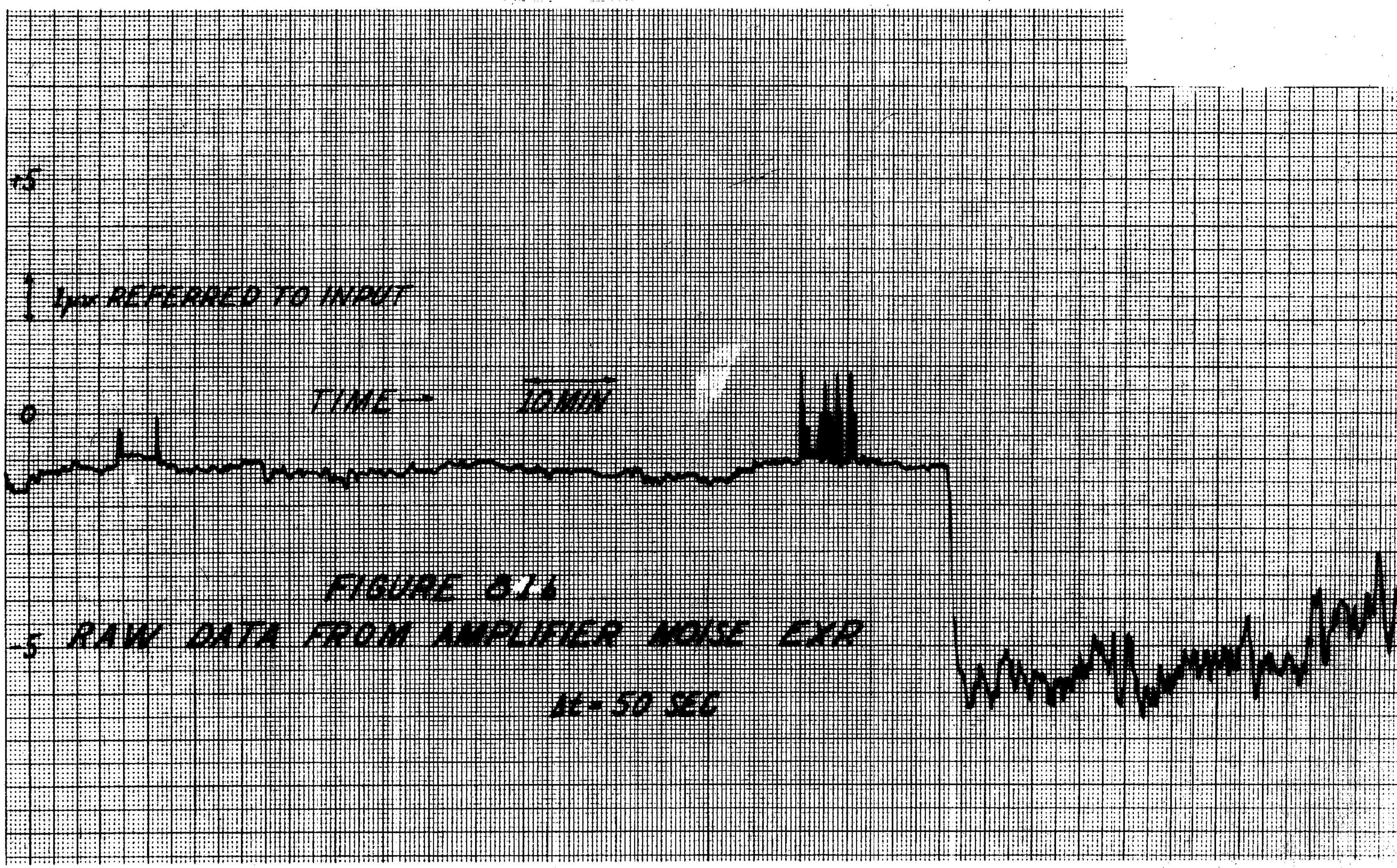
+5
1μv REFERRED TO INPUT
0
TIME→
10 MIN
-5
FIGURE 6.1b
RAW DATA FROM AMPLIFIER NOISE EXP
Δt = 50 SEC

temperature. However, this speculation looks doubtful when the whole sequence of data is examined (6 days total) because the switch times do not appear to be regular or particularly correlated with the time of day. Another possibility is that the building's line voltage changes periodically leading to a different behavior for the amplifier. Or perhaps the electromechanical chopper in this operational amplifier really does have two distinct noise states. Figures (81a) and (81b)illustrate that the situation is even more complicated. They are also pieces of the same 50 sec sampling rate data. They also indicate the existence of the two states but in addition show two other kinds of behavior. The vertical scale is $\pm$ 10μ volts zero center (referred to the amplifier input) so that the sharp transients in Figure(81a) are indications that the output was going to zero. This tends to make one suspicious of circuit failure type errors. In addition, this figure illustrates another of the pitfalls of practical spectral estimation. The large point at about the horizontal midpoint of the data appears to be due to an error in either the paper tape coding circuit or the translating program. If a spectrum were estimated from this data it would be very nearly white because of the influence of this bad point as discussed in Section 3.3.3. This figure is also the only

point in the entire data run of 6 days length when more than two distinct mean levels were observed. Here there seem to be two levels of low RMS behavior rather than just one. Figure (8b) shows in addition some transients which increase in voltage to further confuse the situation.

In general, it seems that the noise properties of this electromechanical chopper stabilized dc amplifier are in one sense an extension of those of the Mark I noise generator. The two state phenomenon is more accentuated and the RMS values in the two states differ more for the amplifier noise. But the general characteristics of the spectra are very similar.

5.4 Line Voltage Results

As described in Section 4.4 the mechanization chosen was to measure the average value of the rectified 60~ line and record these "dc" fluctuations. Power spectral density estimates obtained from this data are then presumed to reflect the spectrum of line voltage amplitude variations. When the experiments were planned it was anticipated that the major contributor to the line voltage fluctuation spectrum would be temperature and that the resultant spectra should increase with decreasing frequency, possibly like $1/f$ or $1/f^2$. Therefore, it was felt to be unnecessary to go to the trouble of mechanizing very low frequency antialiasing filters. This expectation was justified by the results. Three different sets of runs were made with sampling times, Δt, of 1.25 sec, 30 sec, and 5 min. Figures (82a), (82b), and (82c) show short segments of typical raw data for the three different sampling times. It is obvious from this data that there will be trouble with the lowest frequency runs. When a large transient occurs near a sample time the actual amplitude at the sampling instant is uncertain. From the raw data it appears that the error might be characterized as a quantization problem. The line voltage amplitude variations apparently have a very non-gaussian probability density. The line "sags" much more often than anything else and generally in response to transients. For instance, a small fraction of time and the large transient type behavior exhibited in Figure (82c) was found to be directly

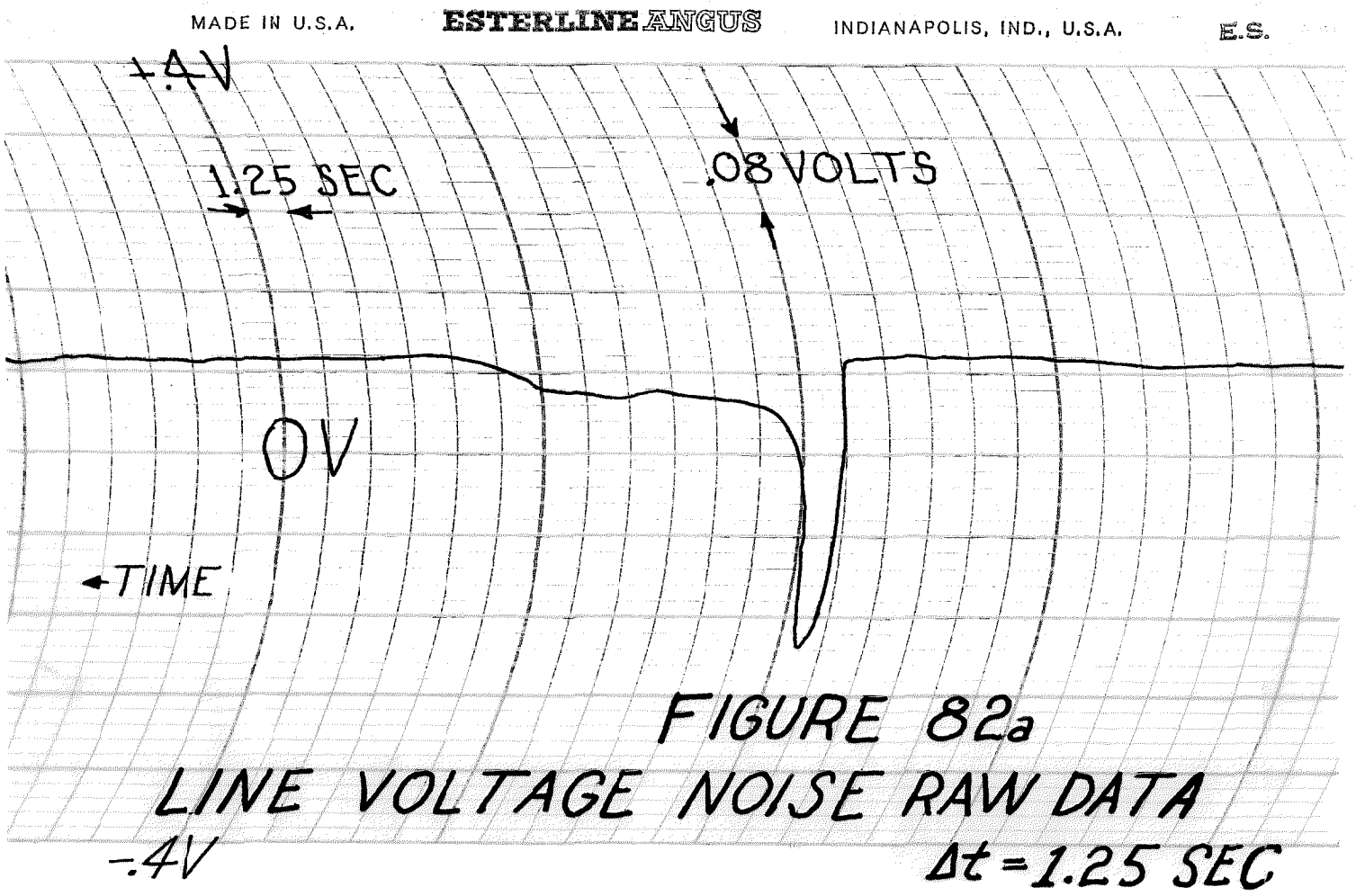

FIGURE 82a

LINE VOLTAGE NOISE RAW DATA

$\Delta t = 1.25$ SEC

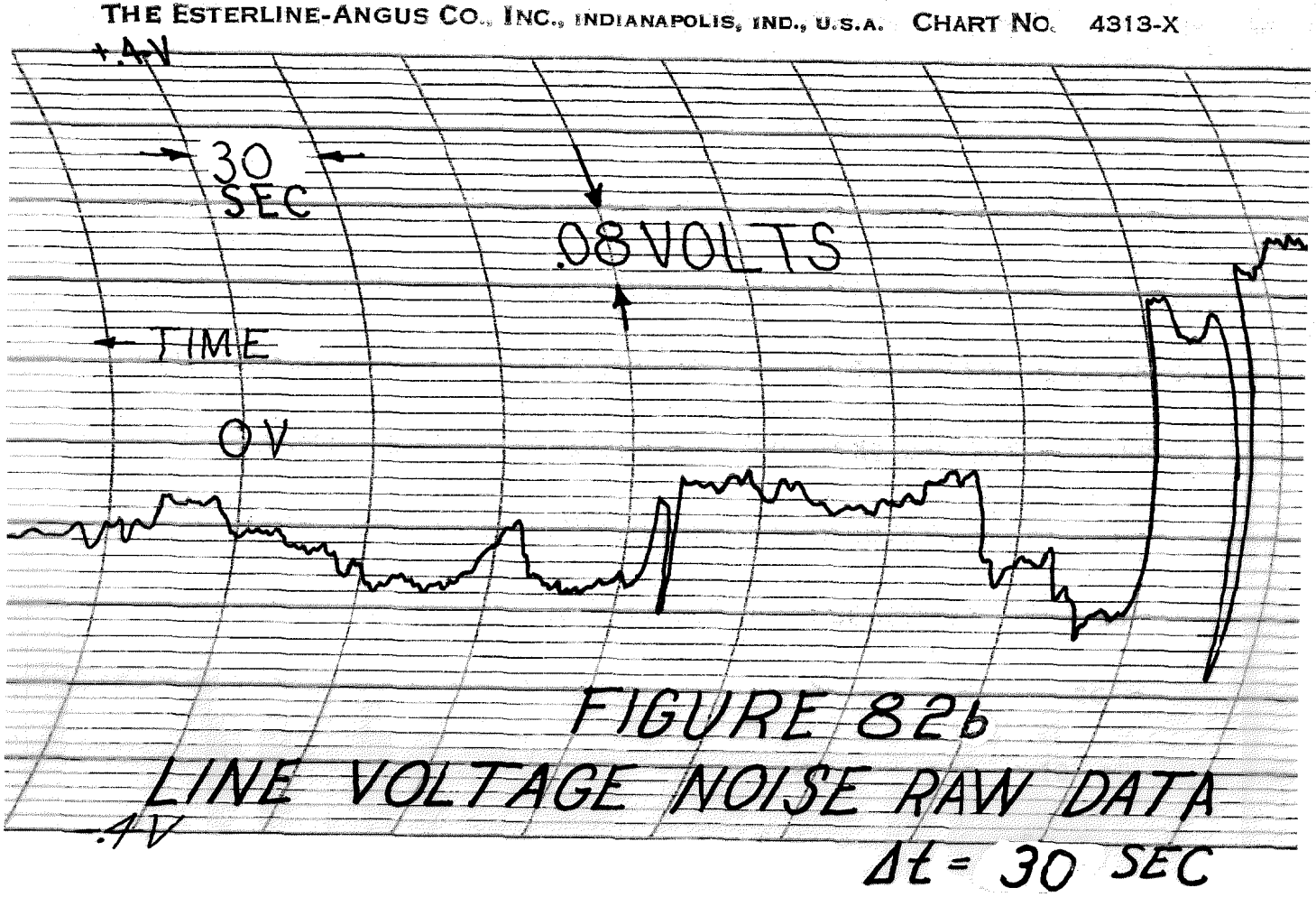

FIGURE 82b

LINE VOLTAGE NOISE RAW DATA

Δt = 30 SEC

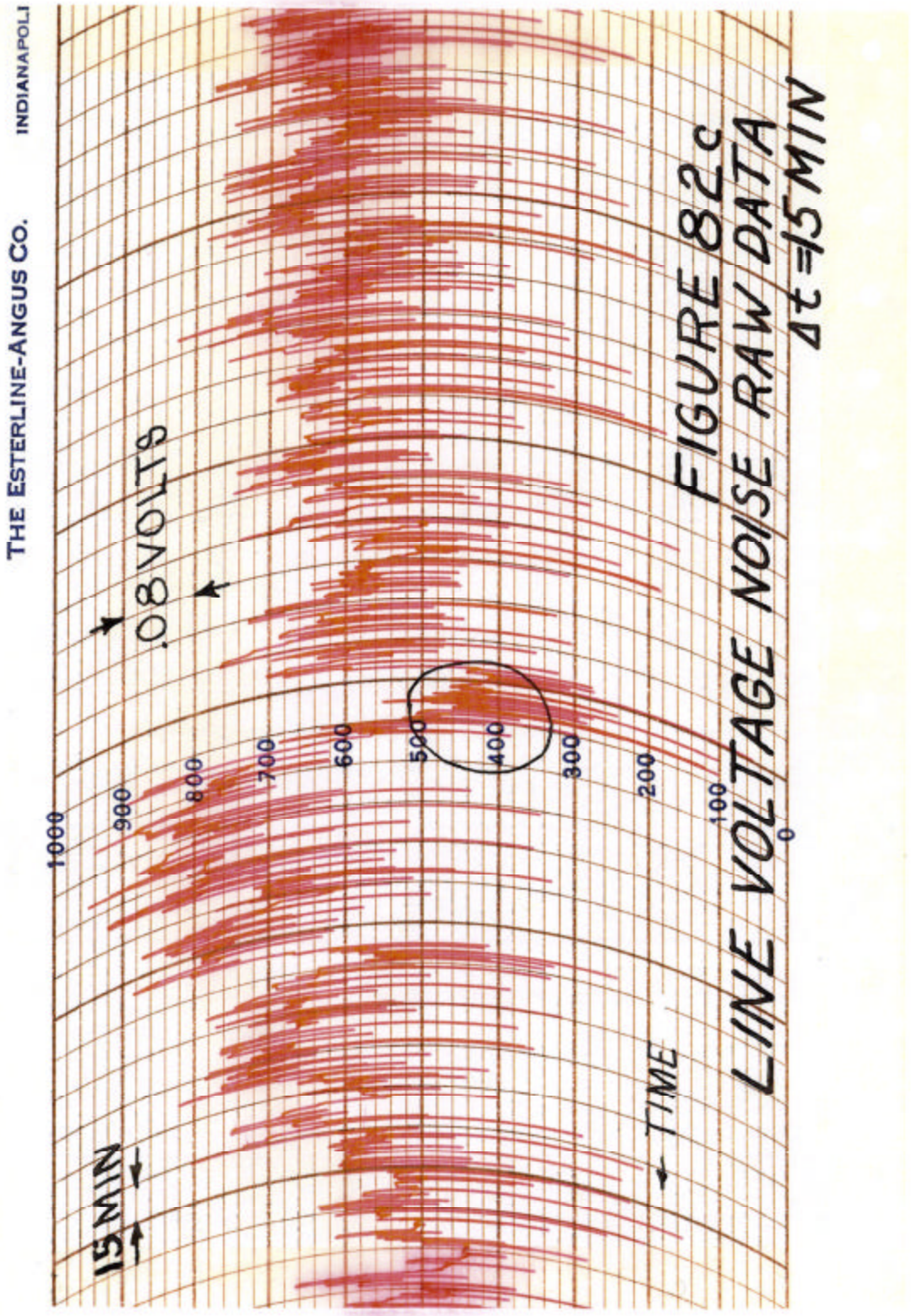
THE ESTERLINE-ANGUS CO. INDIANAPOLI
15 MIN
.08 VOLTS
1000
900
800
700
600
500
400
300
200
100
0
TIME
LINE VOLTAGE NOISE RAW DATA
Δt = 15 MIN

FIGURE 82c

correlated with the operation of the elevator in the building when the apparatus was located. When a large transient happens to coincide with a sampling time (for instance see circled area in Figure (82c)) then one may consider that a large quantization error is present in that particular sample, (for instance $\approx$ .16 volts for the example from Figure (82c)). Since this event does not occur for every sample the discussion of Section 3.2.4 regarding quantization is not directly applicable. If we, however, use it as an approximation it indicates that a white noise level of about

$$\frac{\Delta t \Delta E^2}{12} = \frac{(900)}{12} \quad \frac{(.16)^2}{} = 2.8 \text{ db}$$

would be present due to the quantization.

Figures (83a) , and (83b), and (83c) present the spectra for the three sets of data runs Δt = 1.25 sec, 30 sec, 900 sec, respectively. These are Q_2 estimates (hanning window). The estimation was done utilizing prewhitening for $1/f^2$. Alternatively, a linear trend was removed from the lowest frequency run with the only difference being at the R = 0,1 points which are plotted for the trend removed estimations. The whitening of the lowest frequency run at its high frequency end seems to be adequately explained via the approximate quantization argument made above. Each run has been antialiased under the assumption that the straight line shown in Figure (84) is the correct result.

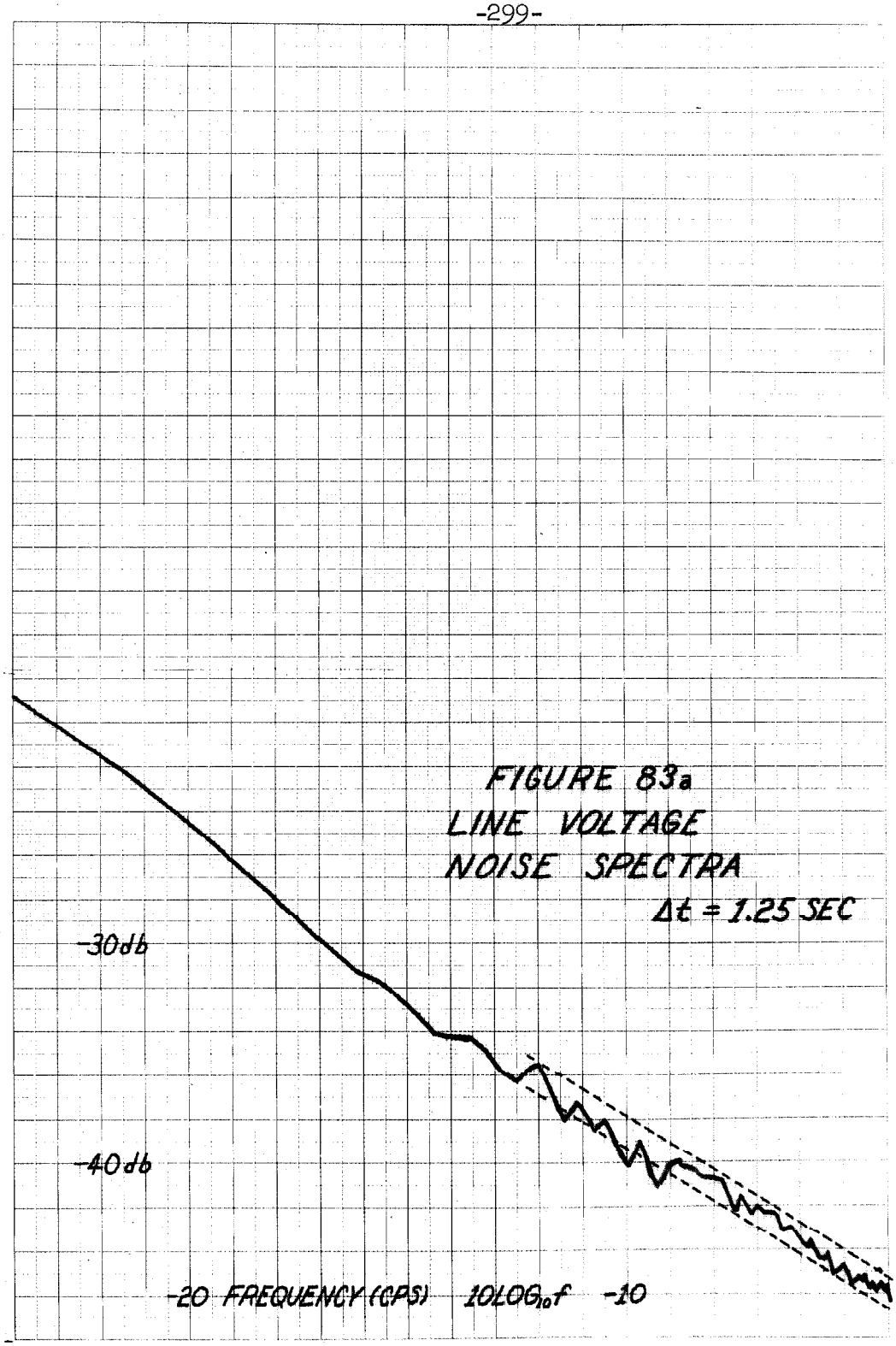

FIGURE 83a
LINE VOLTAGE
NOISE SPECTRA
$\Delta t = 1.25$ SEC

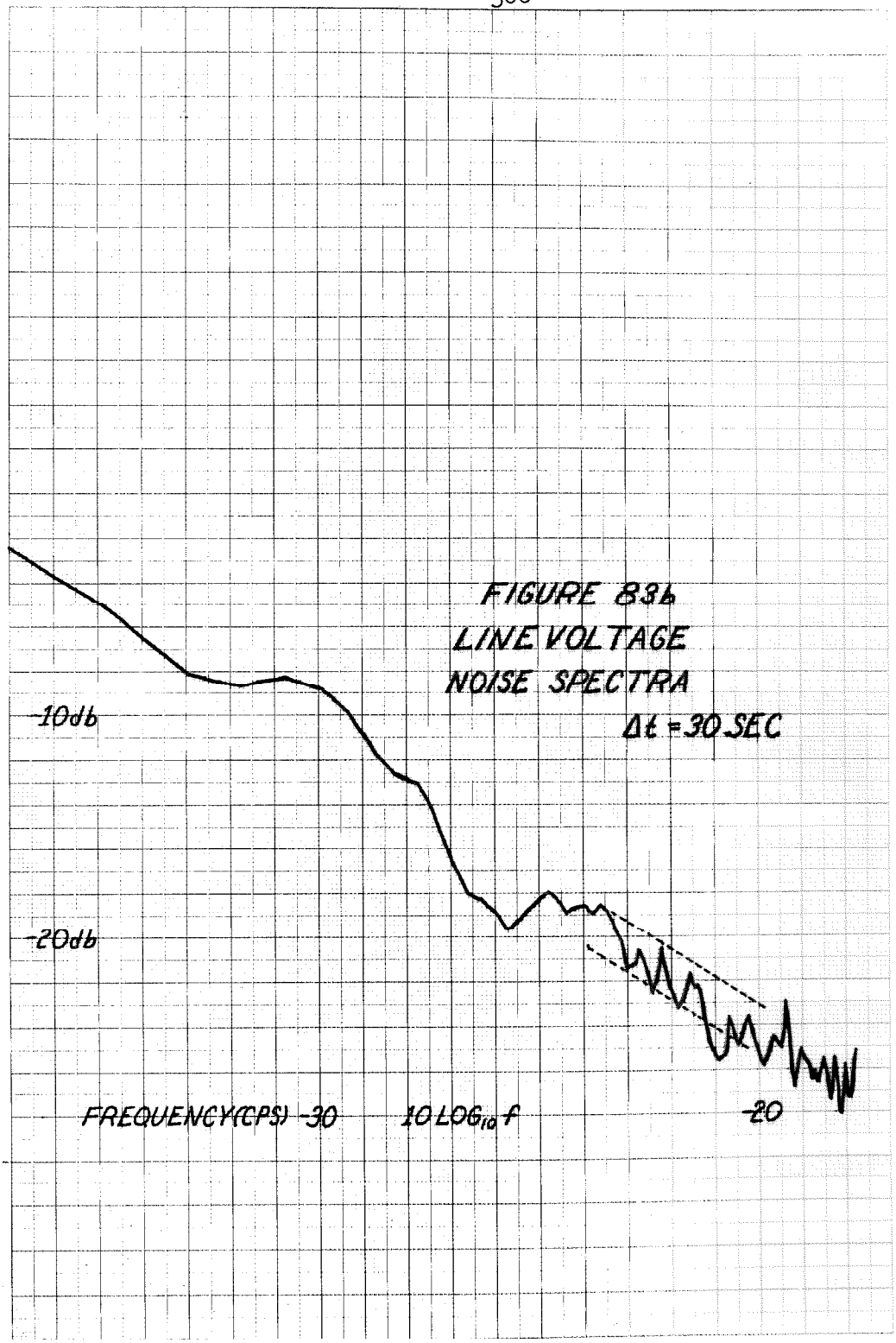
FIGURE 83b
LINE VOLTAGE
NOISE SPECTRA
Δt = 30 SEC
-10db
-20db
FREQUENCY(CPS) -30
10 LOG10 f
-20

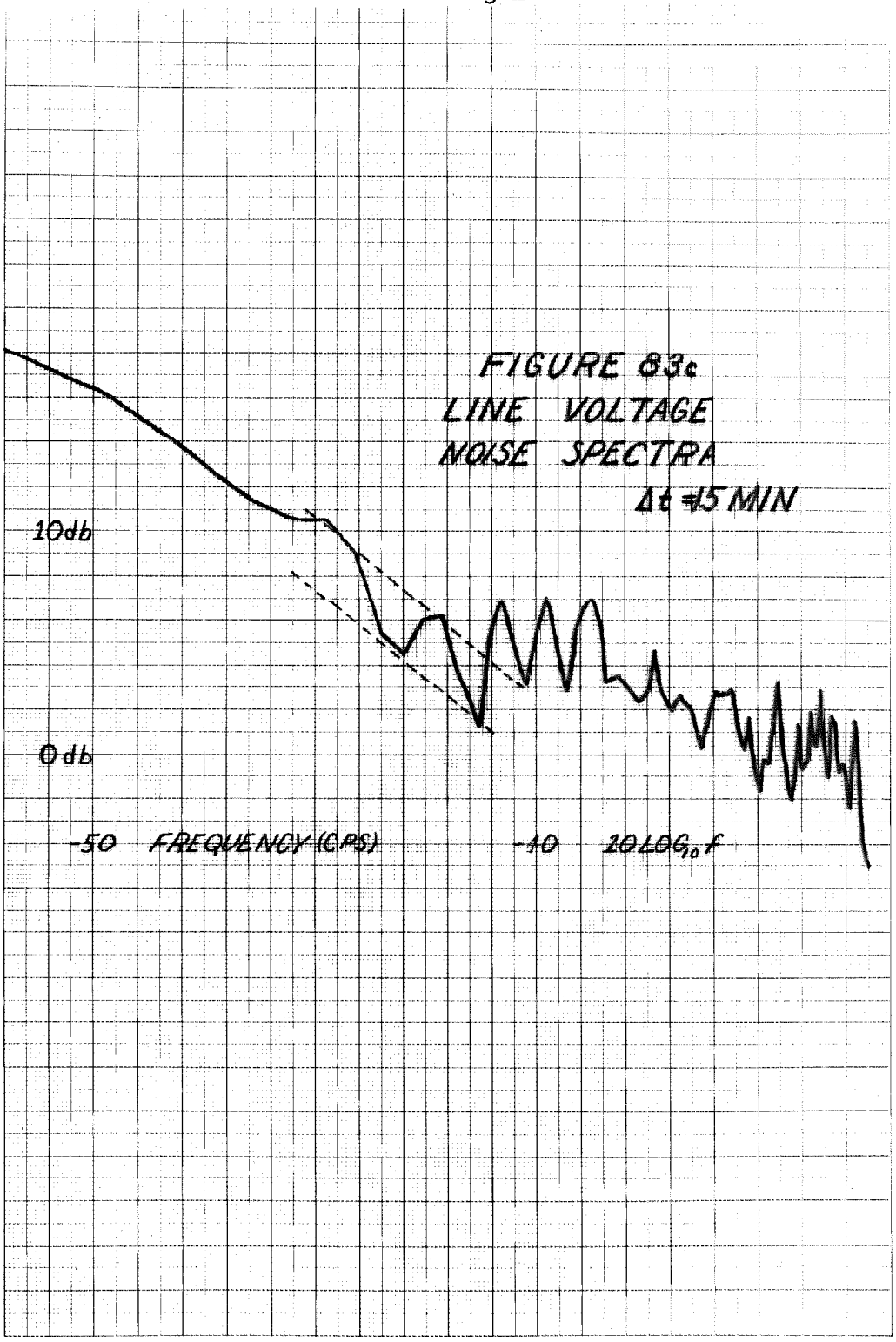
FIGURE 83c
LINE VOLTAGE
NOISE SPECTRA
Δt = 15 MIN
10db
0 db
-50
FREQUENCY (CPS)
-10
10 LOG10 f

The variance of the estimates for each run is different increasing with decreasing frequency. M is 100 for each set but N is 3920, 1550, and 790, 1σ so that under the smooth approximation these would be 16%, 25%, and 36% estimations, respectively. These yield 1σ various bands of (+ .64 db - .76 db), (+ .98 db, - 1.26 db), (+ 1.32 db, - 1.91 db), respectively, which are shown on the figures as dotted lines for a short segment to indicate their size. It appears to be a reasonable statement to say the estimated spectral density lies roughly within those bands about 2/3 of the time. Since those estimates are prewhitened one expects this smooth approximation to yield reasonable agreement with the empirical result with the possible exception of the very lowest frequency points. It should be kept in mind that putting equi-spaced data on a logarithmic scale tends to reduce the visual variability in the low frequency points.

Figure (84) is a composite of the total results. The horizontal scale on this graph covers six decades in frequency from 1 microcycle (10^{-6} cps) to 1 cycle (1 cps). Based on past experience we tend to be very suspicious of simple power law modeling for spectral densities. However, we can fit a $1/(f)^a$ curve to the sloping portion of the results. This yields a value for the line shown on the figure of a = 1.33.

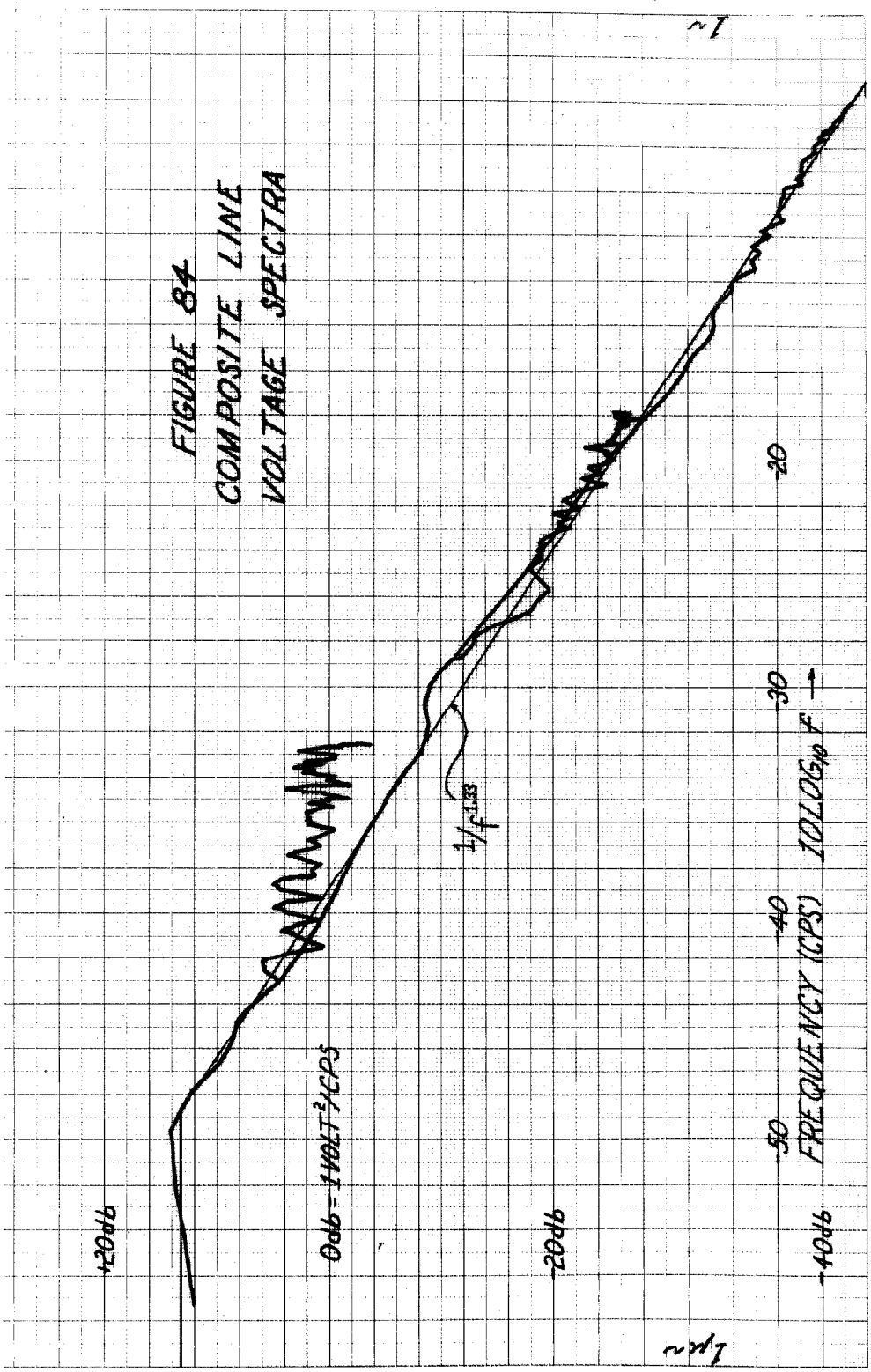
FIGURE 84
COMPOSITE LINE
VOLTAGE SPECTRA
0db = 1 VOLT²/CPS
1/f^1.33
+20db
-20db
-40db
10
20
30
40
50
FREQUENCY (CPS) 10LOG₁₀ f →

If we claim that the spectrum is indeed flat at the lower frequencies we obtain as a model

$$S_L(f) = \left\{ \begin{array}{ll} \dfrac{K_L}{|f_L|^a} & |f| < f_L \\ \dfrac{K_L}{|f|^a} & f_c > |f| > f_L \\ 0 & |f| > f_c \end{array} \right\} \qquad (132)$$

where $K = 8.36 \times 10^{-9}$, volt^2/cps, $f_L = 2 \times 10^{-5}$cps, $a = 1.33$, $f_c = 1$ cps. The reason we are so cautious in claiming this as a valid representation of the true result is related to how many times during the course of the Mark I noise studies similar conjectures were proposed for its "true" spectrum which turned out to be erroneous.

In any case if one takes the position that these results are representative then the total RMS value

$$\sqrt{\frac{2K_L}{f_L^{\,a}} + \frac{2K_L}{(a-1)}\left(\frac{1}{f_L^{\,a-1}} - \frac{1}{f_c^{\,a-1}}\right)} = 36 \text{ millivolts}$$

can be taken as the 1σ fluctuations expected from low frequency line voltage amplitude fluctuations in a typical air conditioned laboratory.

6. FURTHER WORK

Because of the exhorbitantly long data records required, it is unlikely that power spectral densities can be estimated at much lower frequencies than those presented above. All of the equipment problems discussed above compound as the desired data lengths grow. Indeed, there is considerable question as to whether power spectral density is a useful concept in the context of "yearly" etc., fluctuations. Consequently, information pertaining to still lower frequencies will have to be obtained indirectly. For instance, hypothesis tests might be constructed to yield information analagous to the lower break frequency in the 1/f case.

One of the most interesting areas for further work pertains to the nature of the sampling scheme. Discrete spectral estimation schemes customarily deal only with equi-spaced samples. There are many cases where non-equispaced samples might be a great deal more convenient.

For instance, suppose it is desired to estimate the spectral density over many decades of frequency from one sample function of the random process.* If a sampling rate is chosen high enough to allow estimation of the highest frequency desired, an extremely large number of samples must be taken if information is to be obtained of the lowest frequency, (i.e., for 7 decades with M = 100, N = 10^4

---

* The situation is somewhat more complicated if aliasing is a serious problem.

as in Figure (51), 10^{11} samples would be required). For this work, the straightforward approach of taking a "reasonable" number ($\approx 10{,}000$*) of samples at a specific sampling rate and then repeating the process at a different rate was employed. Figure (85) depicts such a sampling scheme. This procedure is intuitively unappealing and has the disadvantage that several data "runs" must be made. Several "more efficient" sampling schemes suggest themselves.

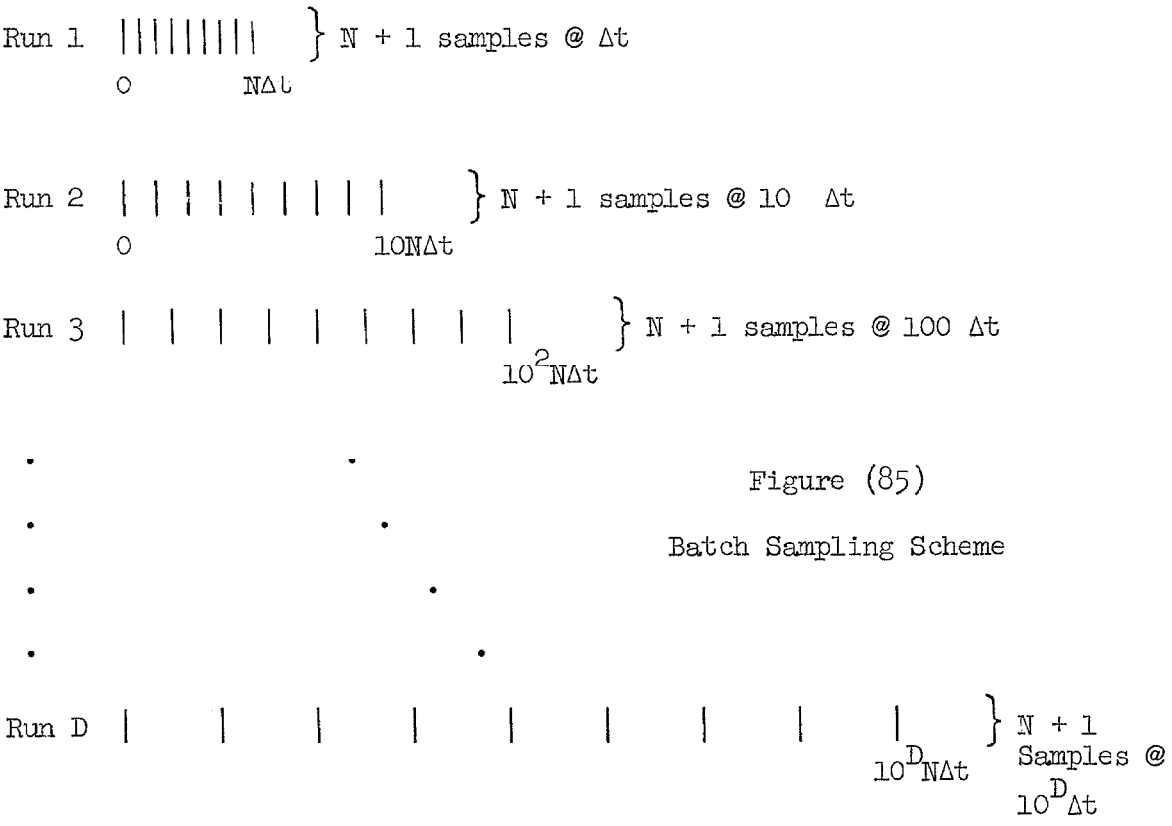

Figure (85)

Batch Sampling Scheme

D "Runs" (ND + D) total samples: yields Spectral Density Estimates over D decades in frequency.

---

* This is strictly a function of the particular equipment available but is probably no longer than 10^7 so that the following arguments will apply.

The first obvious simplification is to collapse this all into one "run," where the sampling rate changes every N samples. Figure (86) illustrates schematically such a scheme. It should be pointed out that the serious effect of aliasing can be removed from the spectral estimates obtained from the batch sampling scheme via different anti-aliasing filters for each "run." But, the nature of the aliasing problem faced with the "decade" sampling scheme is quite different and in fact the author does not know of a way to handle the aliasing problem in this situation. For spectral densities

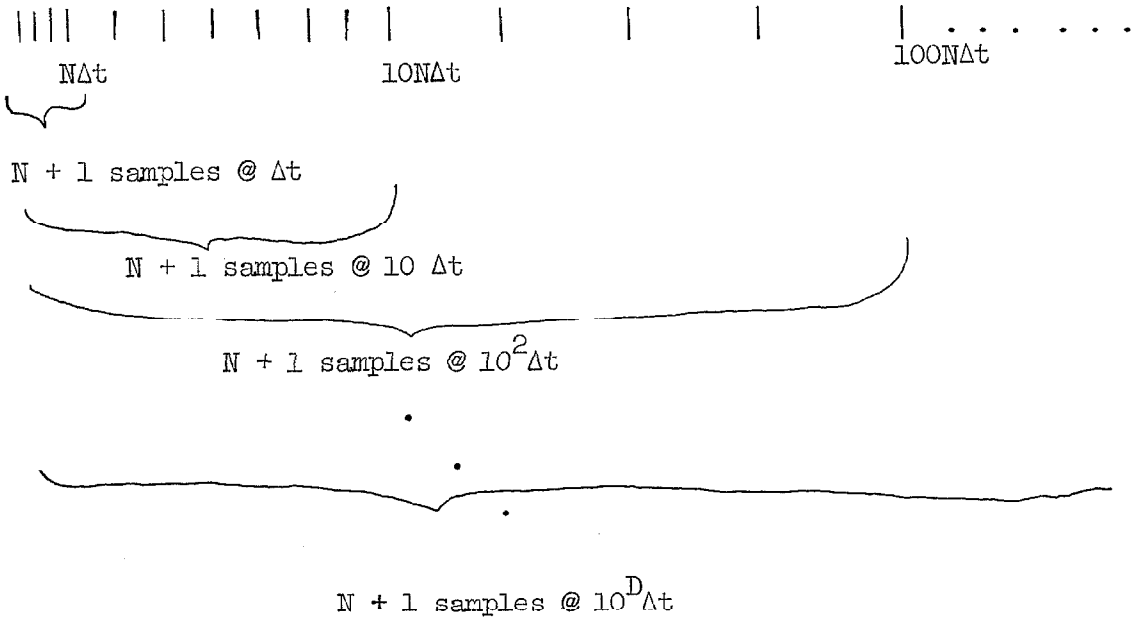

1 Run $(ND + N + 1 - D)$ Total Samples: yields Spectral Density Estimates over D decades in frequency.

Figure (86)

Decade Sampling Scheme

which are of the general 1/f character, neither scheme should experience great difficulty as any reasonable folding of the actual spectrum cannot be too serious.

The most striking appearance characteristic of the low frequency noise data records themselves is their slowly varying nature. There arises naturally out of the fact that a very large part of the energy in the random process is at very low frequencies. This appearance suggests that a suitable sampling scheme might be to record only changes in the noise voltage and the times at which they occur. This could be further simplified to recording only the times at which the noise voltage changes by a pre-specified fixed amount. Two courses of action are then available. One could reconstruct the noise voltage to the pre-determined accuracy on the digital computer and sample it at any desired rate. Alternatively, one could invent a technique for estimating the correlation function or spectral density directly from the switching time data and the sizes of the steps.

A simple technique for obtaining a logarithmic frequency spacing of the spectral estimates could be mechanized utilizing the present correlation function estimator. The window could be applied in the τ domain and the Fourier transform to obtain spectral estimates could simply be evaluated at logarithmically spaced points in the frequency domain. This would be more or less equivalent to using the present scheme and calculating $\hat{S}\left(\frac{R}{2M\Delta t}\right)$ only for selected values of R.

This would be only slightly less expensive from a computational standpoint because the major job is in calculating the mean lagged products from the raw data.

It is perhaps interesting to note that it is not a mathematical necessity that the spectral estimate be biased. In fact, for any spectrum, $S(f)$, for which the window $Q(f)$ is an eigenfunction of $S(f)$ then $\hat{S}(f)$ can be unbiased. One could, in fact, imagine asking the question, "For a given spectrum, for instance $1/f$ noise, what window should I use to make $\hat{S}(f)$ an unbiased estimate?" This line of attack has not been pursued here because it is not of practical interest for the following reason. The window $Q(f)$ must be bandlimited in the τ domain because only a finite data record is available. Therefore, $Q(f)$ cannot be bandlimited in the f domain. Because of aliasing problems the spectrum to be estimated must be bandlimited in the frequency domain. Therefore, $Q(f)$ cannot be an eigenfunction of $S(f)$ since it would have to be bandlimited in f. One could perhaps ask for the "best" approximation to a bandlimited function. The work of Slepian, Landau, and Pollak leading to prolate spheriodal wave functions is then applicable and gives the answer for a particular definition of "best" and the special case of a white spectrum. Alternatively one can notice that the requirement that $S(f)$ be bandlimited to meet aliasing requirements is in fact much too severe. As a practical matter it appears that a spectrum decaying even as fast as $1/f^2$ creates no serious aliasing difficulties. This leaves

considerably more flexibility for finding allowable Q's since they now need not be bandlimited in the frequency domain and can meet that requirement in the τ domain.

Still another approach might be to solve for the eigenfunctions ignoring this constraint and mechanize them approximately in the τ domain by truncation. The resulting effects of this approximation would however be difficult to evaluate.

There are three major features of the spectral estimation techniques employed in this work which appear intuitively unsatisfactory. That is, one would hope to improve upon the scheme of taking data at equi-spaced points in time. First, it seems sort of silly to blindly sample the random process only at equi-spaced specified intervals of time. Secondly, if the interest is in making spectral estimates over more than a decade in frequency, the current scheme is usually quite inconvenient and inefficient because of the linear frequency spacing of the points. A log spacing would be much more appealing. Finally, if a large range of frequency is to be covered from one set of time domain data, some kind of anti-aliasing filtering (low pass) must be done. Again this seems inefficient intuitively. It would seem that a more efficient computational algorithm could improve this situation.

One alternate approach which is very appealing intuitively is to change the basic form of the data available. In other words, let us not ask, "how can we more efficiently process the equi-spaced data to yield a spectral estimate?" But let us go back one step further and ask how could we take the data in a form which might lead to more efficient processing algorithms. The "decade sampling" scheme is one small step in this direction. The "sample at data change times" scheme is a further step. A more basic change which is very appealing intuitively is to sample at random or psuedo-random times.

Suppose one sampled the random process at times t_k distributed according to some density $p(t_k)$. For example, one might easily imagine mechanizing t_k's that were normally distributed (or uniformly distributed etc.) about some set of fixed times (say equispaced). One could then imagine taking an ensemble average over the t_k's either on the estimated correlation function in the τ domain or on the spectrum in the frequency domain. In a manner of speaking then one might have an estimate of $R(\tau)$ "averaged over τ" in some sense.

A slightly different computational scheme which might be utilized for random time sampled data is given by the following. Suppose each pair of data points $x(t_i)$, $x(t_y)$ were used to get an estimate of the correlation function. If the t_k's distributed over a large enough interval this could alleviate the aliasing problem.

The subsequent estimation of the correlation function, $R(\tau)$, will be essentially a scatter diagram. Each point will be unbiased and will have a very large variance given by

$$\mathrm{var}\left\{\hat{R}(t_i-t_j)\right\} = E\left\{\left[x(t_i)\,x(t_j) - R(t_i-t_j)\right]\right\}^2$$

which becomes under a zero mean gaussian assumption for $x(t)$

$$\mathrm{var}\left[\hat{R}(t_j-t_j)\right] = 2\sigma^4$$

This will, of course, be useful only where there is a sufficient concentration of points to reduce this variance considerably. However, it must be kept in mind that there are a very large number of such $R(t_i-t_y')$ points available; something on the order of $N^2/2$ for N data points.

There seem to be a number of special problems associated with data acquisition for very low frequency spectral estimation. They might be categorized generally as "non-stationarities"; i.e., such things as steps, spikes, and very low frequency oscillations in the data. When records many days, or even weeks long, must be dealt with one must take extreme caution to avoid the influence of external conditions. This is, of course, nothing new or startling. One must always be careful about exactly what one is measuring. Its just that on this time scale very few pieces of commercially available equipment have outputs that are in fact independent of their environment. In this respect hindsight is extremely powerful. For the particular

case of low frequency semiconductor noise it is now much more obvious to what extent the environment must be controlled. After the next "round" of experiments it will undoubtedly be found that the experimental conditions must be even more carefully controlled to answer the next round of questions. For instance, "Is 1/f Noise only the reflection of temperature variations at the input through the gain of the device and will it therefore disappear in exact proportion to the amount of temperature control?"

APPENDIX A

ANALYSIS OF A PARTICULAR SPECTRAL ESTIMATOR

1. Mathematical Model

Let us construct a mathematical model intended to correspond to the "photographic playback method" of spectral analysis used by Winston and Firle. At the conclusion of any real experiment we will have a finite piece of, let us say continuous, record of length, T, seconds. We shall immediately form a periodic function x(t) whose T second sections are exact replicas of our data. We shall assume that x(t) is a sample function from a stationary, zero mean gaussian random process whose spectral density is S(f). We note at this point that the only spectral density we can ever hope to estimate is S(f) which is not of course the spectral density of the original random process.

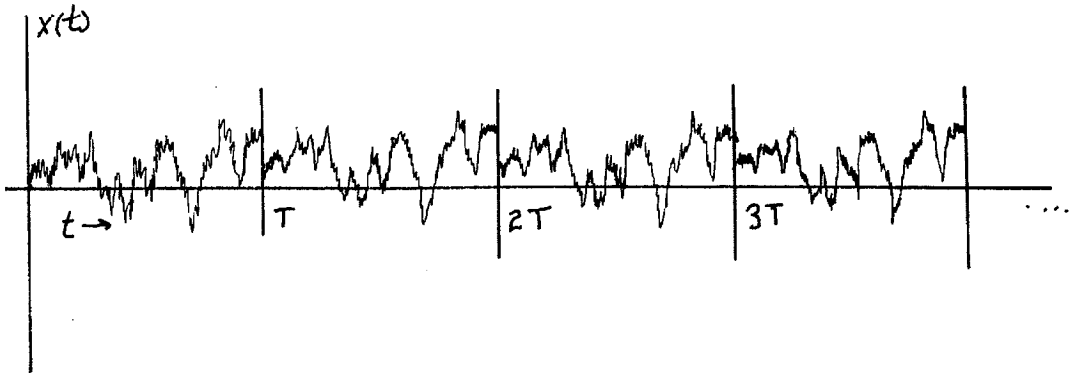

Now let us begin by making a Fourier Series expansion of the periodic waveform $x(t)$. We will have

$$x_p(t) = \text{l.i.m.}\left\{ \sum_{n=1}^{\infty} [a_n \cos n\omega_o t + b_n \sin n\omega_o t] + \frac{a_o}{2} \right\}$$

where the right hand side converges in the limit in the mean sense and

$$\omega_o = 2\pi/T$$

$$a_n = \frac{2}{T} \int_o^T x(t) \cos n\omega_o t \, dt$$

$$b_n = \frac{2}{T} \int_o^T x(t) \sin n\omega_o t \, dt$$

Thinking of $\sqrt{a_n^2 + b_n^2}$ as the magnitude of the complex Fourier coefficient, let us venture the conjecture that it is proportional to the energy in the random process at frequency $n\omega_o$. But

$$z_n = \sqrt{a_n^2 + b_n^2}$$

is incorrect dimensionally to estimate the power spectral density of the random process, $x(t)$. Therefore, let us form as an estimate of $\sqrt{S(f)}$ the quantity

$$\zeta_n = Bz_n$$

In other words let us take

$$\widehat{\sqrt{S(f_n)}} = \widehat{\sqrt{S(nf_o)}} = \widehat{\sqrt{S(\tfrac{n}{T})}} = \zeta_n$$

so that ζ_n will be our estimate of the square root of the spectral density at multiples of the reciprocal of the record length. The constant B, as we shall see presently, can be chosen in such a manner that the estimate will be unbiased if x(t) is white noise. It should be noticed that a fallacy has already been perpetrated since, in general, one has absolutely no guarantee that estimating the square root of a quantity and squaring the result will yield a desirable estimate of the quantity itself.

2. Properties of the Estimator

We have assumed that x(t) is gaussian and zero mean. Therefore, the random variables a_n and b_n will be gaussian and zero mean since they are obtained by integration which is a linear operation. To complete their statistical description, then, we need only find their correlation and variances. We begin the latter task by forming their squares

$$a_n^2 = \frac{4}{T^2}\int_o^T\int_o^T x(t)\, x(t')\cos n\omega_o t \cos n\omega_o t'\, dt\, dt'$$

$$b_n^2 = \frac{4}{T^2}\int_o^T\int_o^T x(t)\, x(t')\sin n\omega_o t \sin n\omega_o t'\, dt\, dt'$$

We then obtain on taking the expected value, interchanging the orders of integration (and expectation), and writing the trigonometric functions as sums and differences that

$$\left\{\begin{matrix}\sigma_{a_n}^2\\ \sigma_{b_n}^2\end{matrix}\right\} = \frac{2}{T^2}\int_o^T\int_o^T R(t-t')[\cos n\omega_o(t-t') \pm \cos n\omega_o(t+t')]\, dt\, dt'$$

where the upper and lower signs refer to the variances of a_n and b_n, respectively and $R(\tau)$ is the correlation function of the random process $x(t)$. We will eventually wish to express this as an integral on the spectral density. As a first step in this direction we see that by changing variables we will be able to perform one of the integrations. To this end, then, let the new variables τ and u be defined by

$$t - t' = \tau$$

$$t + t' = u$$

from which we have immediately that

$$t = \tfrac{1}{2}(u + \tau)$$

$$t' = \tfrac{1}{2}(u - \tau)$$

The Jacobian of the transformation, J, therefore has an absolute value equal to

$$|J| = \left| \begin{vmatrix} \frac{1}{2} & \frac{1}{2} \\ \frac{1}{2} & -\frac{1}{2} \end{vmatrix} \right| = \frac{1}{2}$$

The region of integration in the (t,t') plane was the square region, R

$$R = \{(t,t') : 0 \le t \le T,\ 0 \le t' \le T\}$$

or

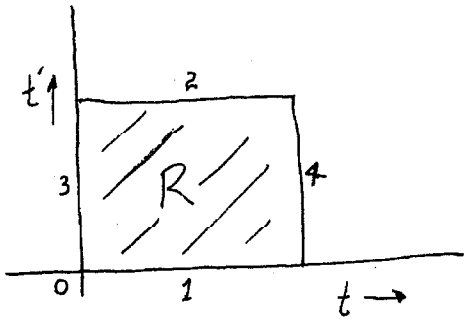

which maps into the (u, τ) plane as the region R' given by

$$R' = \{(t,t'): -\tau \le u \le 2T+\tau,\ -T \le \tau \le 0\} \cup \{(t,t'): \tau \le u \le 2T-\tau,\ 0 \le \tau \le T\}$$

or

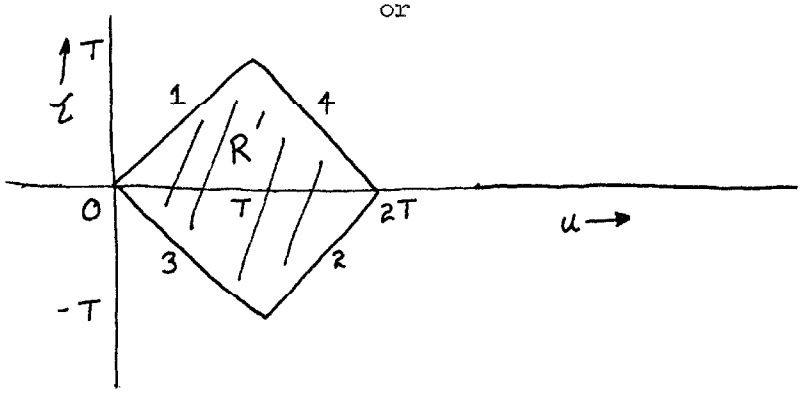

Performing the u integration first, the equation for the variances becomes

$$\begin{Bmatrix} \sigma_{a_n}^2 \\ \sigma_{b_n}^2 \end{Bmatrix} = \frac{1}{T^2}\int_{-T}^{0}\int_{\tau}^{\tau+2T} R(\tau)[\cos n\omega_o\tau \pm \cos n\omega_o u]\, du\, d\tau$$

$$+ \frac{1}{T^2}\int_{0}^{T}\int_{\tau}^{-\tau+2T} R(\tau)[\cos n\omega_o\tau \pm \cos n\omega_o u]\, du\, d\tau$$

Performing the u integration now yields

$$\begin{Bmatrix} \sigma_{a_n}^2 \\ \sigma_{b_n}^2 \end{Bmatrix} = \frac{2}{T}\int_{-T}^{0} R(\tau)\left[\cos(n\omega_o\tau)\left(1+\frac{\tau}{T}\right) \pm \frac{\sin n\omega_o\tau}{n\omega_o T}\right] d\tau$$

$$+ \frac{2}{T}\int_{0}^{T} R(\tau)\left[\cos(n\omega_o\tau)\left(1-\frac{\tau}{T}\right) \mp \left(\frac{\sin n\omega_o\tau}{n\omega_o T}\right)\right] d\tau$$

where use has been made of the fact that $\omega_o = 2\pi/T$ in simplifying trigonometric expressions. Combining terms we have

$$\left\{\begin{matrix}\sigma_{a_n}^2 \\ \\ \sigma_{b_n}^2\end{matrix}\right\} = \frac{2}{T}\int_{-T}^{T} R(\tau)\left[\cos n\omega_o\tau\left(\frac{1-|\tau|}{T}\right) \mp \frac{|\tau|}{T}\cdot\frac{\sin n\omega_o\tau}{n\omega_o\tau}\right] d\tau$$

The contribution from the second term in the brackets is zero since it will be the integral of an odd function over symmetrical limits. Hence, we see already that $\sigma_{a_n}^2 = \sigma_{b_n}^2 = \sigma_n^2$. Writing the cosine in exponential form we then have

$$\sigma_n^2 = \frac{1}{T}\int_{-\infty}^{\infty} R(\tau)\left(e^{+jn\omega_o\tau} + e^{-jn\omega_o\tau}\right) D(\tau)\, d\tau$$

where

$$D(\tau) \triangleq \left\{\begin{matrix}1 - \frac{|\tau|}{T} & |\tau| < T \\ \\ 0 \quad \text{otherwise} & \end{matrix}\right\}$$

i.e.,

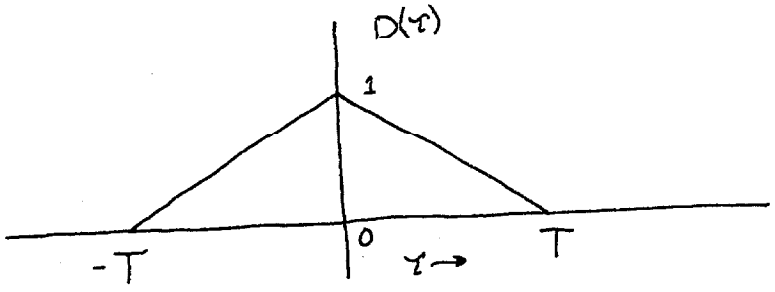

But since both $R(\tau)$ and $D(\tau)$ are even in τ the contribution for each

exponential term is just the Fourier transform of the product $R(\tau)D(\tau)$ evaluated at the frequency nf_o. Hence, the result is equivalent to the convolution of the Fourier transforms in the frequency domain evaluated at this frequency. Thus,

$$\sigma_n^2 = \frac{2}{T}\left[S(f) * Q(f)\right]_{f - nf_o - \frac{n\omega_o}{2\pi}}$$

$$= \frac{2}{T}\int_{-\infty}^{\infty} S(f'-nf_o)\, Q(f')df' = \frac{2}{T}\int_{-\infty}^{\infty} S(f')\, Q(f'-nf_o)df'$$

where $Q(f)$ is the Fourier transform of $D(\tau)$ which is well known to be given by

$$Q(f) = \int_{-\infty}^{\infty} D(\tau)\, e^{-j\omega\tau}\, d\tau = T\left(\frac{\sin \pi fT}{\pi fT}\right)^2$$

Inserting this fact in the above result yields finally

$$\sigma_n^2 = 2\int_{-\infty}^{\infty} S(f')\left[\frac{\sin \pi T(f'-nf_o)}{\pi T(f'-nf_o)}\right] df'$$

$$= 2\int_{-\infty}^{\infty} S(f')\left[\frac{\sin(\pi Tf'-n\pi)}{(\pi Tf'-n\pi)}\right]^2$$

Given a spectral density $S(f)$ this quantity is just a fixed number. In fact, if the spectral density is white or "smooth" the

$(\sin x / x)^2$ acts as a delta function and "samples" the function so that $\sigma_{a_n}^2$ and $\sigma_{b_n}^2$ will be proportional to the real spectral density at the frequency nf_o. i.e.,

$$\sigma_n^2 = \sigma_{a_n}^2 = \sigma_{b_n}^2 \approx 2S(nf_o) \int_{-\infty}^{\infty} \left(\frac{\sin x}{x}\right)^2 \frac{dx}{\pi T} \approx \frac{2}{T} S(nf_o)$$

Thus, there is some hope that the ζ_n defined earlier may be a reasonable estimator of the square root of the power spectral density.

To complete the description of the random variables a_n and b_n we must calculate their correlation $\rho_{a_n b_n}$. Proceeding directly from the definition we obtain

$$\rho_{a_n b_n} = E\{a_n b_n\} = E\left\{\frac{4}{T^2} \int_o^T \int_o^T x(t)\, x(t')\, \cos n\omega_o t \, \sin n\omega_o t' \, dt \, dt'\right\}$$

Again taking the expectation inside the integration, recognizing the correlation function, and expanding the trigonometric function we have

$$\rho_{a_n b_n} = \frac{2}{T^2} \int_o^T \int_o^T R(t-t') \left[\sin n\omega_o(t+t') + \sin n\omega_o(t'-t)\right] dt \, dt'$$

which becomes after the same change of variables used previously

$$\rho_{a_n b_n} = \frac{1}{T^2} \int_{-T}^{o} \int_{\tau}^{\tau+2T} R(\tau)[\sin n\omega_o u + \sin n\omega_o \tau] \, du \, d\tau$$

$$+ \frac{1}{T^2} \int_o^T \int_{\tau}^{-\tau+2T} R(\tau)[\sin n\omega_o u + \sin n\omega_o \tau] \, du \, d\tau$$

On performing the u integration we obtain

$$\rho_{a_n b_n} = \frac{1}{T^2} \int_{-T}^{0} R(\tau) \left[(2\tau+2T) \sin n\omega_o \tau - \left(\frac{\cos n\omega_o u}{n\omega_o} \right) \Bigg|_{-\tau}^{\tau+2T} \right] d\tau$$

$$+ \frac{1}{T^2} \int_{0}^{T} R(\tau) \left[(2T-2\tau) \sin n\omega_o \tau - \left(\frac{\cos n\omega_o u}{n\omega_o} \right) \Bigg|_{\tau}^{2T-\tau} \right] d\tau$$

But because $\omega_o = \frac{2\pi}{T}$ we see that

$$\rho_{a_n b_n} = \frac{2}{T} \int_{-T}^{T} R(\tau) \left(1 - \frac{|\tau|}{T} \right) \sin n\omega_o \tau \, d\tau$$

which is identically zero since $R(\tau)$ and $\left(1 - \frac{|\tau|}{T} \right)$ are even while the sine is odd. Thus,

$$\rho_{a_n b_n} = 0$$

so that the Fourier coefficients are uncorrealted to each other (and hence independent since gaussian) for the same n.

Now because a_n and b_n are equal variance uncorrelated gaussian variables we know that

$$z_n = \sqrt{a_n^2 + b_n^2}$$

will be Rayleigh distributed, i.e., that the probability density function for z_n will be given by

$$p(z_n) = \begin{cases} \frac{z_n}{\sigma_n^2} e^{-\frac{z_n^2}{2\sigma_n^2}} & z_n \geq 0 \\ 0 & z_n < 0 \end{cases}$$

Then because of the definition of ζ_n we will have

$$p(\zeta_n) = \begin{cases} \frac{1}{B^2} \frac{\zeta_n}{\sigma_n^2} e^{-\frac{\zeta_n^2}{2B^2\sigma_n^2}} & \zeta_n \geq 0 \\ 0 & \text{otherwise} \end{cases}$$

from which we can calculate the mean and variance of our estimator ζ_n. The mean will be given by

$$\zeta_n = \frac{1}{B^2\sigma_n^2} \int_0^\infty \zeta_n^2 e^{-\frac{\zeta_n^2}{2B^2\sigma_n^2}} d\zeta_n$$

$$= \sqrt{\frac{\pi}{2}}\, \sigma_n B$$

Suppose $x(t)$ has a spectral density which is white:

$$S(f) = N_o$$

Then to have our estimator be unbiased in this case we must clearly have

$$\overline{\zeta_n} = \sqrt{N_o}.$$

We have already seen above that for x(t) white

$$\sigma_n = \sqrt{\frac{2}{T} N_o}$$

from which we see that

$$\sqrt{N_o} = \sqrt{\frac{\pi}{2}} \sqrt{\frac{2}{T} N_o B}$$

and thus we should choose

$$B = \sqrt{\frac{T}{\pi}} .$$

This will guarantee an unbiased estimate for white noise and presumably a nearly unbiased estimate at f = n/T for any case where the spectral density is relatively constant in the neighborhood of $\frac{n}{T}$ cycles. Fixing B at this value we will have

$$\overline{\zeta_n} = \sqrt{\frac{T}{2}} \sigma_n$$

We now calculate the second moment of our estimate as follows:

$$\overline{\zeta_n^2} = E\{\zeta_n^2\} = \frac{1}{B^2 \sigma_n^2} \int_o^\infty \zeta_n^3 \, e^{-\frac{\zeta_n^2}{2\sigma_n^2 B^2}} \, d\zeta_n$$

$$= 2B^2 \sigma_n^2$$

But on utilizing the value for B chosen above this becomes

$$\zeta_n^2 = \frac{2T}{\pi} \sigma_n^2$$

from which we obtain the variance as

$$\text{var } \zeta_n = \overline{\zeta_n^2} - (\overline{\zeta_n})^2 = \frac{2T}{\pi} \sigma_n^2 \left(1 - \frac{\pi}{4}\right)$$

One of the frequently employed measures of the usefulness of the spectral estimator is the ratio of its variance to the square of its mean. For the estimator considered we find that

$$\frac{\text{var } \zeta_n}{(\text{mean } \zeta_n)^2} = \frac{2\sigma_n^2 (T/\pi)(1 - \pi/4)}{(T/2)\sigma_n^2}$$

$$= \frac{4}{\pi} - 1 \approx .285$$

It is particularly significant to notice that this important result is independent of σ_n and hence independent of the particular spectral density being estimated. In other words in estimating (the square root of) any power spectral density whatsoever by this technique only 68% of the time will the estimate fall within 53.4% of its own average value (which itself may be biased in any particular case). The fractional variability formula also is independent of T. The frequencies over which the estimate is made thus depends on the record length but not the relative accuracy of the results.

3. Specific Example: RC Noise

In this section and the next we shall examine our model of the photographic playback method estimator in two specific examples, RC Noise and 1/f Noise in that order. We should like to obtain some

idea of how bad its bias is likely to be in these particular cases.

Suppose then that we are attempting to estimate the spectral density of a random process, x(t), whose spectral density, S(f) is given by

$$S(f) = \frac{K}{1 + \left(\frac{f}{a}\right)^2}$$

where K is the value at very low frequencies and a is the "break frequency" in cps.

Utilizing the results of Section 2 we will then have for the variance of the Fourier coefficients

$$\sigma_n^2 = 2 \int_{-\infty}^{\infty} \frac{K}{1 + \left(\frac{f}{a}\right)^2} \left[\frac{\sin(\pi fT - n\pi)}{(\pi fT - n\pi)}\right]^2 df$$

which becomes on letting $x = \pi Tf$

$$\sigma_n^2 = 2Ka^2\pi T \int_{-\infty}^{\infty} \left(\frac{\sin(x-n\pi)}{(x-n\pi)}\right)^2 \frac{dx}{x^2 + (a\pi T)^2}$$

This integral can be evaluated by integrating the product of the Fourier transforms of the two factors in the integrand. Appendix D carries out this calculation with the result

$$\int_{-\infty}^{\infty} \left[\frac{\sin(x-n\pi)}{(x-n\pi)}\right]^2 \frac{dx}{a^2 + x^2} = \frac{\pi}{a^2 + (n\pi)^2} \left[1 - \frac{a}{a^2 + (n\pi)^2}\right] + \frac{\pi a e^{-2a}}{[a^2 + (n\pi)^2]^2}$$

which when inserted in the above expression and simplified yields

$$\sigma_n^2 = \frac{2}{T}\left\{\frac{K}{1+\left(\frac{n}{aT}\right)^2}\left[1 - \frac{1}{\pi aT\left[1+\left(\frac{n}{aT}\right)^2\right]}\right] + \frac{K}{\pi aT}\,\frac{e^{-2a\pi T}}{\left[1+\left(\frac{n}{aT}\right)^2\right]^2}\right\}$$

Now since the average value of our estimate is given by

$$\zeta_n = \sqrt{\frac{T}{2}}\,\sigma_n$$

we have

$$\bar{\zeta}_n = \sqrt{K}\left\{\frac{1}{1+\left(\frac{n}{aT}\right)^2}\left[1 - \frac{1}{\pi aT\left[1+\left(\frac{n}{aT}\right)^2\right]}\right] + \frac{e^{-2a\pi T}}{\pi aT\left[1+\left(\frac{n}{aT}\right)^2\right]^2}\right\}^{\frac{1}{2}}$$

This is to be compared with the square root of the true spectral density at frequencies of n/T which will be

$$\sqrt{S\left(\frac{n}{T}\right)} = \sqrt{K}\left\{\frac{1}{1+\left(\frac{n}{aT}\right)^2}\right\}^{\frac{1}{2}}$$

For the case where $aT \gg 1$ we have to first order in (aT) that*

$$\bar{\zeta}_n \approx \sqrt{K}\left\{\left[\frac{1}{1+\left(\frac{n}{aT}\right)^2}\right]\left[1 - \frac{1}{\pi aT} + \cdots\right]\right\}^{\frac{1}{2}}$$

or

$$\bar{\zeta}_n \approx \sqrt{S\left(\frac{n}{T}\right)}\left[1 - \frac{1}{2\pi aT}\right]$$

* We assume n is sufficiently small such that the inequality need not be written $aT \gg n$.

which is to be expected since this corresponds to the case where the record is of sufficient length to expose many cycles of the noise at its break frequency. Another way of phrasing this would be that we are estimating the spectral density only at such low frequencies that it is essentially white. Hence, the first order error term does not depend on h and the estimate is not badly biased in this case.

On the other hand when $aT \ll 1$ we obtain in a similar fashion

$$\overline{\zeta}_n \approx \sqrt{S\left(\frac{n}{T}\right)} \left[1 - \left(\frac{aT}{n}\right)^2 + \cdots\right]$$

so that again the estimate is not badly biased. Here we are estimating at very high frequencies compared to the break frequency of the noise. Again note that the first order error term (zero) is independent of n.

Thus, it appears that the only significant bias is for cases where $\frac{1}{T}$ is on the order of the break frequency of the noise, a. For the case $aT = 1$, Figure 1 shows $\overline{\zeta}_n$ and $\sqrt{S\left(\frac{r}{T}\right)}$ with $K = 1$ and $a = 1$. As expected the bias is only significant near the break frequency but it is interesting to note its irregular nature.

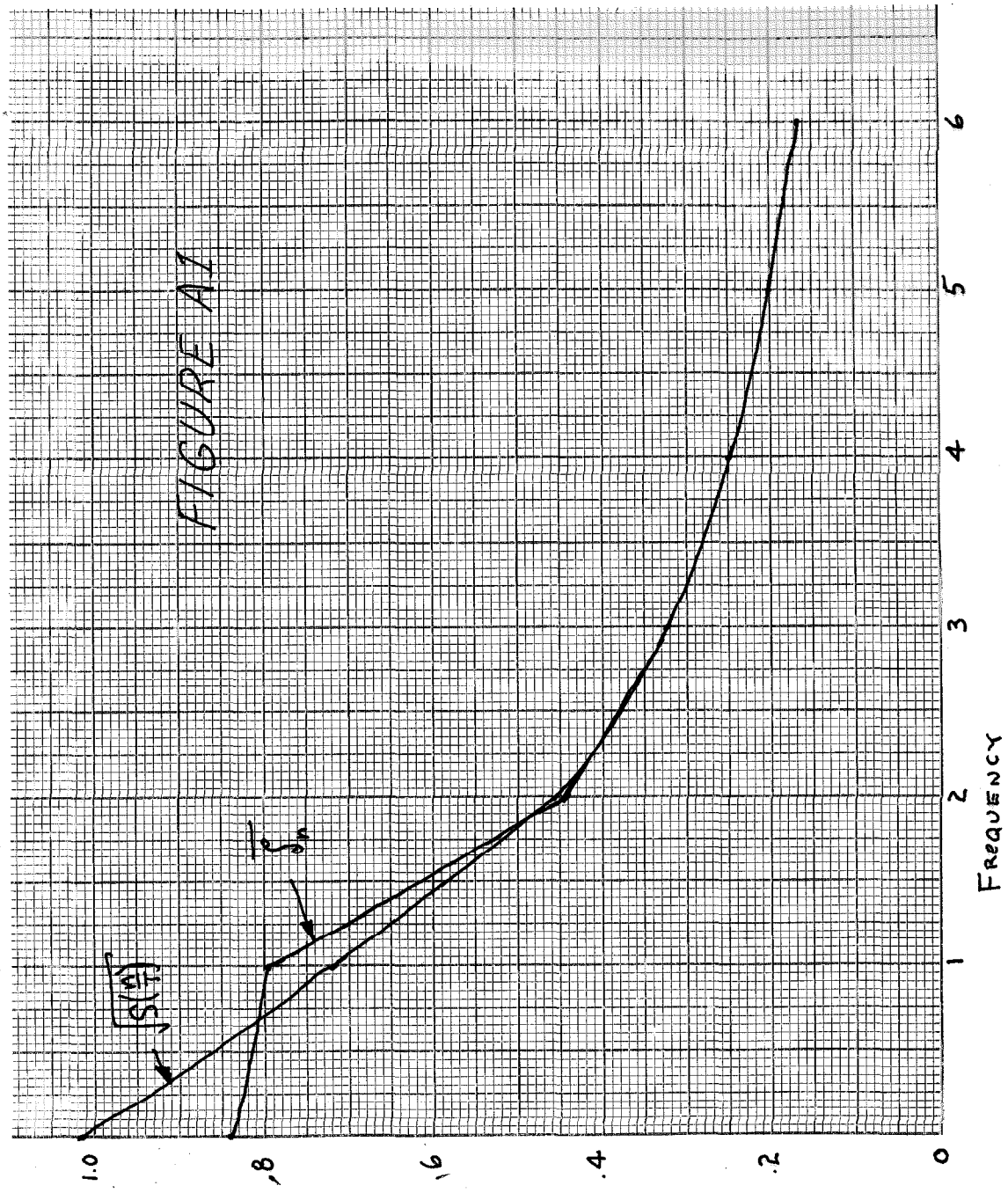
FIGURE A1
1.0
.8
.6
.4
.2
0
1
2
3
4
5
6
FREQUENCY

4. Specific Example: 1/f Noise

In this case we shall suppose that we are attempting to estimate the power spectral density,

$$S(f) = K/|f|^{a}$$

where K is a constant and a is in the vicinity of unity.

Applying the results of Section 2 we will have for the variance of the Fourier coefficients

$$\sigma_n^2 = 2 \int_{-\infty}^{\infty} \frac{K}{|f|^{a}} \left[\frac{\sin(\pi Tf-n\pi)}{(\pi Tf-n\pi)}\right]^2 df$$

Letting $x = \pi Tf$ we will obtain:

$$\sigma_n^2 = 2K(\pi T)^{a-1} \int_{-\infty}^{\infty} \left[\frac{\sin(x-n\pi)}{(x-n\pi)}\right]^2 \frac{dx}{|x|^{a}}$$

$$= 2K(\pi T)^{a-1} I(n,a)$$

where

$$I(n,a) = \int_{-\infty}^{\infty} \left[\frac{\sin(x-n\pi)}{(x-n\pi)}\right]^2 \frac{dx}{|x|^{a}} \qquad 0 < a < 2$$

Initially, it appears that the integral might not converge. This is, however, not the case as will be shown. The integrand does not have a singularity at the origin because the origin is a zero of $\left[\frac{\sin(x-n\pi)}{(x-n\pi)}\right]^2$. It can be seen from a Taylor Series expansion of

this function about this zero that it approaches zero quadratically. Hence, since $a < 2$ the integrand does not have a singularity at this point but indeed has a zero. Since the integrand is bounded in the region $-n\pi < x < n\pi$ where $N >> n$ and is less than $\frac{\sin(x-n\pi)}{(x-n\pi)}^2$ outside this region it will be integrable and $I(n,a)$ will exist.

Since $I(n,a)$ will be calculated by numerical integration it will be useful to bound the error made in taking the integration limits to be finite. Appendix B derives the following formula:

$$I(n,1) - XINT(N,1) - \frac{3}{2A^2} + \frac{\sin 2A}{2A^3}$$

$$- \frac{1}{4A^4} [3 \cos 2A + 5(n\pi)^2] + \mathcal{O}\left(\frac{1}{A^4}\right)$$

where the first term is just the finite integral defined by

$$XINT(N,1) = \int_{-A}^{A} \left[\frac{\sin(x-n\pi)}{(x-n\pi)}\right]^2 \frac{dx}{|X|}$$

and the last term approaches zero at a rate faster than A^{-4}.

If we now choose

$A = 4n\pi$

we see that for $n = 1$

$$\frac{-3}{2A^2} \approx .0095$$

and we make less than a 1% error in taking

$I(1,1) = XINT(1,1)$

The approximation improves as n increases and similar results are expected to hold for $a \neq 1$.

We now have for the average value of the estimator

$$\bar{\zeta}_n = \sqrt{\frac{T}{2}}\,\sigma_n$$

$$= \sqrt{K}\;\pi^{\frac{a-1}{2}}\,T^{\frac{a}{2}}\sqrt{XINT(N,a)}$$

which is to be compared with the correct result

$$\sqrt{S(f)}\Big|_{f=\frac{n}{T}} = \sqrt{K}\left(\frac{T}{N}\right)^{\frac{a}{2}}$$

A convenient way to present the comparison is to normalize with respect to K and T. To examine the bias we can then compare $\sqrt{\pi^{a-1}\,X\,INT(N,a)}$ with $N^{-\frac{a}{2}}$. Figure A2 shows such a comparison. The values for the integral were obtained by numerical integration using a digital computer. The curve of N^{-a} is, of course, a straight line since the paper is logarithmic in both directions and is indistinguishable from the computed integral on the graphs.

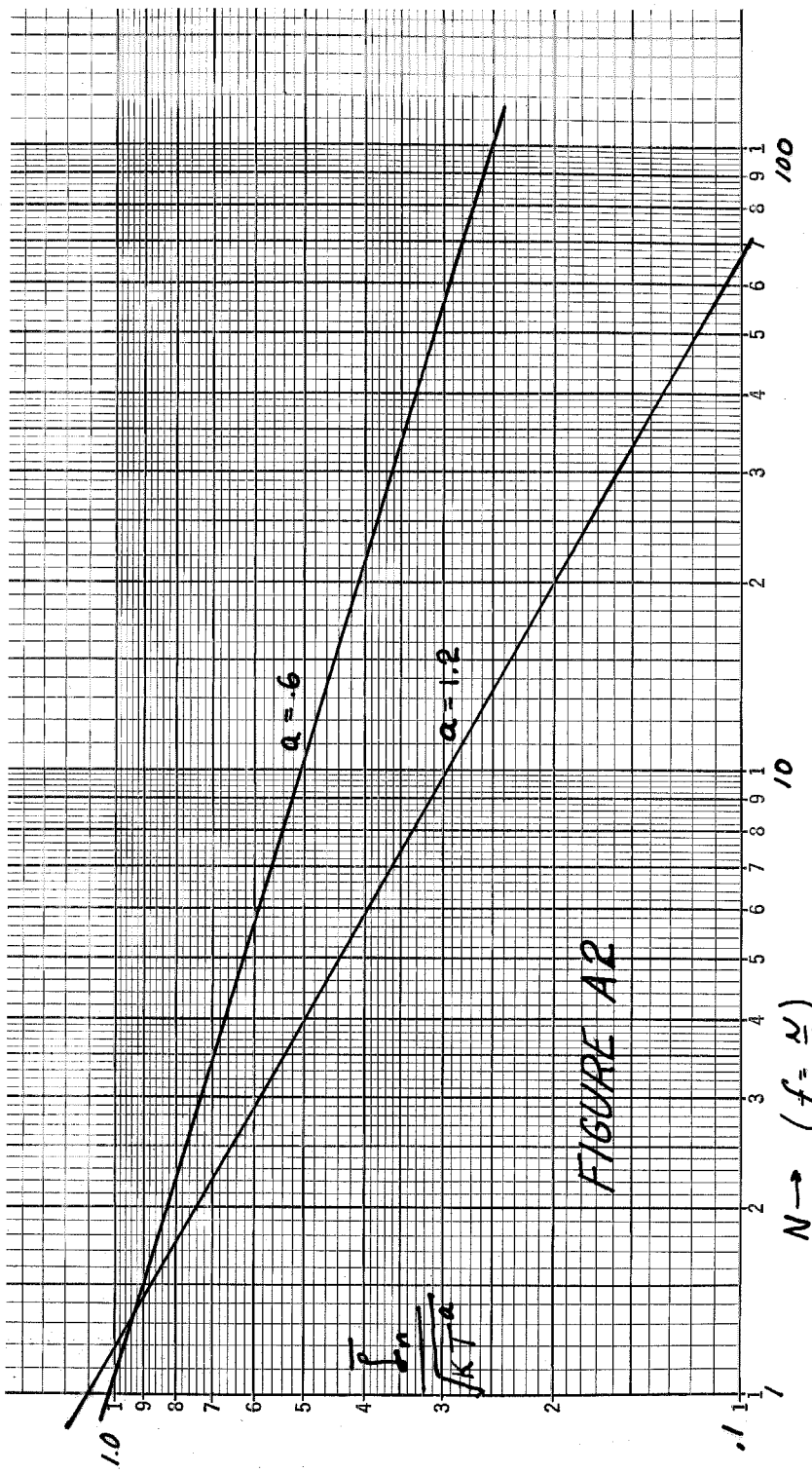

FIGURE A2

APPENDIX B

SPECTRAL ESTIMATION PROGRAM

A listing of the FORTRAN program used for obtaining the spectral estimates of this thesis is given below in Table B1. Similar programs to compute power spectral density estimates are available at a large number of places throughout the country. This one is presented only because it has a few features not generally available. First, the ability to prewhiten the data (i.e., perform any linear filtering operation) before spectral estimation is incorporated directly into the program. Second, some amount of effort has been exerted to render the output format both serviceable and convenient to read. A number of intermediate results are presented which are not often printed out. Among these are: the estimated correlation function, the magnitude squared of the prewhitening filter's transfer function, the actual spectral densities estimated from the prewhitened data, the Q_o windowed estimates, and the logarithmic frequency. Table B2 shows a typical output from the program with M = 30. The first page gives the first 400 raw data points while the second gives the estimated spectrum.

```
      SUBROUTINE SPEEST
C  CODE 1 INITIAL RUN - READ CONSTANTS, DATA
C  CODE 1 REPEAT THE WHOLE SHOW - READ  ALL NEW CONSTANTS, DATA
C  CODE 2 REPEAT WITH NEW DATA ONLY - READ NEW ID,JBATCH,DELT,N,NSTART,SOURCE
C  CODE 3 REPEAT WITH NEW  M  ONLY - READ NEW M
C  G(F) = Y(F) MAGNITUDE  SQUARED
      DIMENSION X(10000), AO(1), A(100), DO(1), D(10), CO(1), C(100),
     1  VO(1), V(100), UO(1), U(100), BO(1), B(100), YO(1), Y(100),
     2  COO(1), CO(200), DBSO(1), DBS(100), SO(1), S(100), Z(10000),
     3  UWSO(1), UWS(100), DBUWSO(1), DBUWS(100),F(100), FLOG(100),
     4 FMT(12)
      COMMON X,AO,A,DO,D,CO,C,VO,V,UO,U,BO,B,YO,Y,COO,CO,DBSO,DBS,SO,S,
     1 UWSO,UWS,DBUWSO,DBUWS,F,FLOG,M
      EQUIVALENCE(X,Z)
  500 FORMAT(3XI7, A6)
  501 FORMAT(7XI3, 5X, 4E15.7/ (5E15.7))
  502 FORMAT(2A6, 6XI2, 5F10.7/(7F10.7))
  992 FORMAT(9XI1)
  503 FORMAT(A6, I4, F10.2, I10, I10, A4)
  504 FORMAT (5XI1)
  508 FORMAT(1H1129X51HSPECTRAL DENSITY ESTIMATION ON DATA FROM EXPERIMEN
     1T 5XA6, 3X5HBATCH 1XI2/ 30X 73(1H*))
  510 FORMAT(/ 1X30HTOTAL NUMBER OF SAMPLES = N = I6,2X27HSTARTING WITH
     1SAMPLE NUMBER I6, 3X15HOF DATA RECORD.  17X20HNUMBER OF LAGS = M =
     2I4,1H. //1X29HSAMPLING INTERVAL = DELTA T = 1PE14.7, 2X8HSECONDS.
     313X31HFREQUENCY RESOLUTION = 1/2MDT = E14.7,2X18HCYCLES PER SECOND
     4.)
  512 FORMAT(/1X16HNO PREWHITENING. 3X5HK = 0 10X 6HA(0) = F10.7,
     1  10X 6HB(0) = F10.7)
  514 FORMAT(/1X18HPREWHITENED WITH A I4, 2X27HTERM MOVING LINEAR AVERAG
     1E.3X3HK =I3,1H.21X42HNUMBER OF PREWHITENED SAMPLES = N' = N-K =
     2  I6, 1H. /5X33HPREWHITENING FILTER COEFFICIENTS  A1     /2(7X5(3X
     32HA(I1,3H) = 1PE15.7, A1)/),18(7X5(2X2HA(I2,3H) = E15.7, A1)/),(7X
     45(1X2HA(I3,3H) = E15.7, A1)))
  516 FORMAT(5X33HPOSTGREENING FILTER COEFFICIENTS A1/2(7X5(3X
     12HB(I1,3H) = 1PE15.7, A1)/),18(7X5(2X2HB(I2,3H) = E15.7, A1)/),(7X
     25(1X2HB(I3,3H) = E15.7, A1)))
  520 FORMAT(/1X2A6, 3X4HL = I2, A4, 5(3X2HD(I1,3H) = F11.8, A1)/ 26X
     15(3X2HD(I1,3H) = F11.8, A1)/ (26X 5(2X2HD(I2,3H) = F11.8, A1)))
  522  FORMAT(/1X17HDETRENDED FOR   (,1PE11.4,7H)  +  (,1PE11.4,22H)T   S
     1AMPLE AVERAGE = ,1PE13.6,4X25HSAMPLE AVERAGE SQUARED = ,1PE13.6/
     25X19HFIRST THIRD MEAN = ,1PE13.6,8X20HSECOND THIRD MEAN = ,
     31PE13.6,8X18HLAST THIRD MEAN = ,1PE13.6//)
  600 FORMAT (12A6)
  610 FORMAT(1H1 41X46HFIRST 480 RAW DATA POINTS - READ DOWN BY COLUMNS
     1 // (1X1P8E16.7))
  700 FORMAT(//10X4HMEAN22X3HRAW8X8HWINDOWED4X50H******** FINAL SPECTRAL
     1 DENSITY ESTIMATES ******** /9X6HLAGGED 4X12HPREWHITENING 3X8HSPEC
     2TRAL5X8HSPECTRAL5X9HQD WINDOW4XA6,A3,5X9HQD WINDOW4XA6,A3,5X17H***
     3 FREQUENCY ***/1X5HINDEX 2X8HPRODUCTS 6X6HFILTER 6X8HESTIMATE 5X
     4 8HESTIMATE 33X8HDECIBELS 5X8HDECIBELS  8X3HCPS /
     5 3X1HR 5X6HC(ROT)8X4HG(F)9X4HV(F)9X4HU(F)9X4HS(F)9X4HS(F)9X7HDB S(
     6F)6X7HDB S(F)10X1HF6X7H10LOG F)
  702 FORMAT(/1X13,1X1P5E13.5, 1H* 1PE12.5, 1H*0PF11.3, 1H*F12.3, 1H*
     1  9X 1HO  9X3HINF)
```

TABLE B1

```
          EXTERNAL FORMULA NUMBER  -  SOURCE STATEMENT  -  INTERNAL FORMULA NUMBER(S)

  704 FORMAT(3( 1D(/1XI3,1X1P6E13.5,0PF12.3, F13.3, 1PE15.3,0PF9.2)/)1H1
     1 2X1HR 5X6HC(RDT)8X4HG(F)9X4HV(F)9X4HU(F)9X4HS(F)9X4HS(F)9X7HDB S(
     2F)6X7HDB S(F)10X1HF6X7H10LOG F
     3       5(/1D(/1XI3,1X1P6E13.5,0PF12.3, F13.3, 1PE15.3,0PF9.2))/1H1
     4 2X1HR 5X6HC(RDT)8X4HG(F)9X4HV(F)9X4HU(F)9X4HS(F)9X4HS(F)9X7HDB S(
     5F)6X7HDB S(F)10X1HF6X7H10LOG F
     6       5(/1D(/1XI3,1X1P6E13.5,0PF12.3, F13.3, 1PE15.3,0PF9.2)))
  706 FORMAT( 1X13,1X1P5E13.5, 1H* 1PE12.5, 1H*0PF11.3, 1H*F12.3, 1H*
     1 1PE14.3, 0PF9.2//)
  708 FORMAT(/1X63H*FIRST AND LAST FINAL SPECTRAL DENSITY ESTIMATES POST
     1GREENED AT
     2  /10X7HR = 1/3 7X3HF = 1PE10.3, 5X9H10LOG F =0PF7.2,5X6HG(F) =
     3 1PE12.5/ 10X4HR = I3, 4H 2/3 3X3HF = 1PE10.3, 5X9H10LOG F =
     4 0PF7.2, 5X6HG(F) = 1PE12.5)
C  READ M, BLANKS, THEN K, A'S (E15 FORMAT), THEN L, D'S (F10 FORMAT),ER
       MOLD = 0                                                          ,1
    10 READ (5,504) ICODE                                                ,2    ,3    ,4
       IF(ICODE.EQ.0) GO TO 999                                          ,5    ,6    ,7
       GO TO (11, 20, 11),ICODE                                          ,8
    11 READ (5,500) M, BLANKS                                            ,9    ,10   ,11   ,12
       INTEGER ZERO,R,SOURCE,TAPE,CARD,ER,KLUG
       ZERO = 0                                                          ,13
       MX2 = M + M                                                       ,14
       MLES1 = M - 1                                                     ,15
       CM = M
C  FORM COSINE TABLE                                                     ,16
       IF (M.EQ.MOLD) GO TO 15                                           ,17   ,18   ,19
       PIM = 3.14159265/CM                                               ,20
       CO(ZERO) = +1.0                                                   ,21
       CO(M) = - 1.0                                                     ,22
       MHALF = M/2                                                       ,23
       DO  80 I = 1, MHALF                                               ,24
       CI = I                                                            ,25
       CO(I) = COSICI * PIM)                                             ,26
       I2 = M - I                                                        ,27
       CO(I2) = - CO(I)                                                  ,28
       I3 = M + I                                                        ,29
       CO(I3) = - CO(I)                                                  ,30
       I4 = MX2 - I                                                      ,31
    80 CO(I4) = + CO(I)
C POST  GREENING FILTER COEFFICIENTS                                     ,32   ,33
       IF (ICODE.EQ.3) GO TO 17                                          ,34   ,35   ,36
    15 READ (5,501) K, (A(I), I = ZERO, K)                               ,37   ,38   ,39   ,40   ,41   ,42

       READ (5,502) WIND1, WIND2, L, (D(I), I = ZERO,L)                  ,43   ,44   ,45   ,46   ,47   ,48

       READ(5,992) ER                                                    ,49   ,50   ,51
       DO 180 I = ZERO, K                                                ,52
       B(I) = 0.0                                                        ,53
       DO 170 J = I, K                                                   ,54
       JLESI = J - I                                                     ,55
   170 B(I) = B(I) + A(JLESI) * A(J)                                     ,56   ,57
   180 CONTINUE
C  WHITENING FILTER                                                      ,58   ,59
    17 DO 200 I = ZERO, M                                                ,60
       IXJ = 0                                                           ,61
```

```
      EXTERNAL FORMULA NUMBER  -  SOURCE STATEMENT  -  INTERNAL FORMULA NUMBER(S)

      Y(I) = 0.0                                                    ,62
      DO 190 J = 1, K                                               ,63
      IXJ = IXJ + I                                                 ,64
      IF (IXJ.GE.MX2)  IXJ = IXJ - MX2                              ,65   ,66   ,67
  190 Y(I) = Y(I) + B(J) * CO(IXJ)                                  ,68   ,69
  200 Y(I) = B(ZERO) + 2.0 * Y(I)                                   ,70   ,71
      CSIGN = - 1.0                                                 ,72
      Y13 = 0.0                                                     ,73
      YM3 = 0.0                                                     ,74
      DO 202  I = 1, K                                              ,75
      CI = I                                                        ,76
      TEMP = B(I) * COS(CI*PIM/3.0)                                 ,77
      Y13 = Y13 + TEMP                                              ,78
      YM3 = YM3 + CSIGN*TEMP                                        ,79
  202 CSIGN = - CSIGN                                               ,80   ,81
      Y13 = B(ZERO) + 2.0 * Y13                                     ,82
      YM3 = B(ZERO) + 2.0 * YM3
C  READ N, NSTART, THEN DATA                                         ,83
      IF(ICODE.EQ.3) GO TO 105                                      ,84   ,85   ,86
   20 READ (5,503)  ID,JBATCH,DELT, N, NSTART, SOURCE               ,87   ,88   ,89   ,90   ,91   ,92
                                                                    ,93
      IF(NSTART.EQ.0) NSTART = 1                                    ,94   ,95   ,96
      DATA TAPE,CARD,KLUG/ 4HTAPE,4HCARD,4HKLUG/
      IF(SOURCE.EQ.CARD) GO TO 21                                   ,97   ,98   ,99
      IF(SOURCE.EQ.KLUG) GO TO 22                                   ,100  ,101  ,102
      IF(SOURCE.NE.TAPE) GO TO 999
C  READ STATEMENT FOR TAPES GENERATED BY HUGHES PROGRAM               ,103  ,104  ,105
      READ(15)(X(I),I=1,N)                                          ,106  ,107  ,108  ,109  ,110
      REWIND 15                                                     ,111
      GO TO 30
C  READ STATMENT FIR A/D TAPES                                        ,112
   22 CALL AD(0,ID,JBATCH,X,NSTART,N,JRET)                          ,113
      IF(JRET.NE.N) GO TO 23                                        ,114  ,115  ,116
      GO TO 30                                                      ,117
   23 WRITE(6,24) JRET                                              ,118  ,119  ,120
   24 FORMAT(/6HJRET= ,I6)
    21 READ(5,600)(FMT(I), I = 1, 12)                               ,121  ,122  ,123  ,124  ,125
      READ(5,FMT) (X(I), I = 1, N)                                  ,126  ,127  ,128  ,129  ,130
    30 WRITE(6,610) (X(I),X(I+60),X(I+120),X(I+180),X(I+240),X(I+300),
     1 X(I+360),X(I+420),I = 1, 60)
C  PREWHITEN   DATA Z(I) AND FIND ZBAR                               ,131  ,132  ,133  ,134  ,135
  666 NLESK = N - K                                                 ,136
      N3=NLESK/3                                                    ,137
      ZBR1=0.0                                                      ,138
      DO 100 I=1,N3                                                 ,139
      ZI = 0.                                                       ,140
      DO 90 J = ZERO, K                                             ,141
      IPLUSJ = I + J                                                ,142
   90 ZI = ZI + A(J) * X(IPLUSJ)                                    ,143  ,144
      Z(I) = ZI                                                     ,145
  100 ZBR1=ZBR1+Z(I)                                                ,146  ,147
      CN3=N3                                                        ,148
      ZBR1=ZBR1/CN3                                                 ,149
      ZBR2=0.0                                                      ,150
      N3P1= N3+1                                                    ,151
      ITN3=2*N3                                                     ,152
```

EXTERNAL FORMULA NUMBER - SOURCE STATEMENT - INTERNAL FORMULA NUMBER(S)

```
      DO 998 I=N3P1,ITN3                                                  ,153
      ZI=0.                                                               ,154
      DO 997 J=ZERO,K                                                     ,155
      IPLUSJ=I+J                                                          ,156
 997  ZI=ZI+A(J)*X(IPLUSJ)                                                ,157  ,158
      Z(I)=ZI                                                             ,159
 998  ZBR2=ZBR2+Z(I)                                                      ,160  ,161
      ZBR2=ZBR2/CN3                                                       ,162
      ZBR3=0.0                                                            ,163
      ITN3P1=ITN3+1                                                       ,164
      DO 996 I=ITN3P1,NLESK                                               ,165
      ZI=0.                                                               ,166
      DO 995 J=ZERO,K                                                     ,167
      IPLUSJ=I+J                                                          ,168
 995  ZI=ZI+A(J)*X(IPLUSJ)                                                ,169  ,170
      Z(I)=ZI                                                             ,171
 996  ZBR3=ZBR3+Z(I)                                                      ,172  ,173
      CNLESK=NLESK                                                        ,174
      XTN3=ITN3                                                           ,175
      ZBR3=ZBR3/(CNLESK-XTN3)                                             ,176
      ZBAR = (ZBR1*CN3 + ZBR2*CN3 + ZBR3*     (CNLESK-2.*CN3))/CNLESK     ,177
      ZBARSQ=ZBAR**2
C  MEAN LAGGED PRODUCTS                                                   ,178
  105 DO 120 I = ZERO, M                                                  ,179
      C(I) = 0.0                                                          ,180
 6    NKR=NLESK - I                                                       ,181
      DO 110 J = 1, NKR                                                   ,182
      JPLUSI = J + I                                                      ,183
  110 C(I) = C(I) + Z(J) * Z(JPLUSI)                                      ,184  ,185
      CNKR=NKR                                                            ,186
      IF(IER.EQ.0) GO TO 994                                              ,187  ,188  ,189
      IF(IER.EQ.1) GO TO 993                                              ,190  ,191  ,192
      GO TO 999                                                           ,193
 993  XKR=1-1/(NLESK**2) -2*I/NLESK -I*I**2/NLESK**2                      ,194
      E=ZBARSQ+(3./16.)*XKR*((ZBR3-ZBR1)**2)                              ,195
      TREND=(ZBR3-ZBR1)*3./CNLESK                                         ,196
      GO TO 120                                                           ,197
 994  E=ZBARSQ                                                            ,198
      TREND = 0.                                                          ,199
 120  C(I)=C(I)/CNKR -E
C RAW SPECTRAL ESTIMATE V(R)                                              ,200  ,201
      CSIGN = +1.0                                                        ,202
      DO 140 I = ZERO, M                                                  ,203
      IXJ = 0                                                             ,204
      V(I) = 0.0                                                          ,205
      DO 130 J = 1, MLES1                                                 ,206
      IXJ = IXJ + I                                                       ,207
      IF(IXJ.GE.MX2)  IXJ = IXJ - MX2                                     ,208  ,209  ,210
  130 V(I) = V(I) + C(J) * CO(IXJ)                                        ,211  ,212
      V(I) = DELT * (C(ZERO) + 2.0 * V(I) + CSIGN * C(M))                 ,213
  140 CSIGN = - CSIGN
C WINDOWED ESTIMATE U(R)                                                  ,214  ,215
      DO 160  I = ZERO, M                                                 ,216
      U(I) = D(ZERO) * V(I)                                               ,217
      DO 150  J = 1, L                                                    ,218
      ILESJ = IABS(I-J)                                                   ,219
```

EXTERNAL FORMULA NUMBER - SOURCE STATEMENT - INTERNAL FORMULA NUMBER(S)

```
      IPLUSJ = M - IABS(M - (I+J))                                    ,220
  150 U(I) = U(I) + D(J) * (V(ILESJ) + V(IPLUSJ))                     ,221  ,222
  160 CONTINUE
C FINAL ESTIMATE (POST-GREENED) S(R)                                  ,223  ,224
      DO 210  I = 1, MLES1                                            ,225
      S(I) = U(I) / Y(I)                                              ,226
      UWS(I) = V(I)/Y(I)                                              ,227
      DBUWS(I) =  10.0*ALOG10(UWS(I))                                 ,228
  210 DBS(I) = 10.0*ALOG10(S(I))                                      ,229  ,230
      S(ZERO) = (CNLESK/(CNLESK - CM)) * U(ZERO)/Y13                   ,231
      S(M) = U(M) / YM3                                               ,232
      DBS(ZERO) = 10.0 * ALOG10(S(ZERO))                              ,233
      DBS(M) = 10.0 * ALOG10(S(M))                                    ,234
      UWS(ZERO) = (CNLESK/(CNLESK - CM)) * V(ZERO)/Y13                ,235
      UWS(M) = V(M)/YM3                                               ,236
      DBUWS(ZERO) = 10.0 * ALOG10(UWS(ZERO))                          ,237
      DBUWS(M) = 10.0 * ALOG10(UWS(M))
C  FREQUENCY TABLE                                                    ,238
      DM2 = .5 / (CM*DELT)                                            ,239
      DO 300 I = 1, M                                                 ,240
      CI = I                                                          ,241
      F(I) = CI * DM2                                                 ,242
  300 FLOG(I) = 10.0*ALOG10(F(I))                                     ,243  ,244
      F13 = DM2/3.0                                                   ,245
      FLOG13 = 10.0*ALOG10(F13)                                       ,246
      FM3 = DM2 * (CM-0.333333333)                                    ,247
      FLOGM3 = 10.0*ALOG10(FM3)
C OUTPUT                                                              ,248
      WRITE (6,508) ID,JBATCH                                         ,249  ,250  ,251
      WRITE (6,510) N, NSTART, M, DELT, DM2                           ,252  ,253  ,254
      KTEMP = K + 1                                                   ,255
      IF(K.EQ.0) WRITE(6,512) A(ZERO), B(ZERO)                        ,256  ,257  ,258  ,259  ,260
      IF(K.NE.0) WRITE(6,514) KTEMP, K, NLESK, (BLANKS,I,A(I),I=ZERO,K)  ,261  ,262  ,263  ,264  ,265  ,266
                                                                      ,267  ,268
      IF(K.NE.0) WRITE (6,516) (BLANKS, I, B(I), I = ZERO,K)          ,269  ,270  ,271  ,272  ,273  ,274
                                                                      ,275
      WRITE (6,520) WIND1, WIND2, L, (BLANKS, I, D(I), I = ZERO,L)    ,276  ,277  ,278  ,279  ,280  ,281

      WRITE(6,522) ZBAR,TREND,ZBAR,ZBARSQ,ZBR1,ZBR2,ZBR3              ,282  ,283  ,284
      WRITE(6,700) WIND1, WIND2, WIND1, WIND2                         ,285  ,286  ,287
      WRITE(6,702) ZERO, C(ZERO), Y(ZERO), V(ZERO), U(ZERO), UWS(ZERO),
     1 S(ZERO), DBUWS(ZERO), DBS(ZERO)                                ,288  ,289  ,290
      WRITE(6,704) (R, C(R), Y(R), V(R), U(R), UWS(R), S(R), DBUWS(R),
     1 DBS(R), F(R), FLOG(R), R = 1, MLES1)                           ,291  ,292  ,293  ,294  ,295
      WRITE(6,706) M, C(M), Y(M), V(M), U(M), UWS(M), S(M), DBUWS(M),
     1 DBS(M), F(M), FLOG(M)                                          ,296  ,297  ,298
      WRITE(6,708) F13, FLOG13, Y13, MLES1, FM3, FLOGM3, YM3          ,299  ,300  ,301
      MOLD = M                                                        ,302
      GO TO 10                                                        ,303
  999 RETURN                                                          ,304
      END                                                             ,305
```

Table B2

FIRST 480 RAW DATA POINTS - READ DOWN BY COLUMNS

1.2000000E-01	1.4000000E-01	6.9999999E-02	7.9999999E-02	1.0000000E-01	1.2000000E-01	1.5000000E-01	1.4000000E-01
1.2000000E-01	1.4000000E-01	6.9999999E-02	8.9999999E-02	1.0000000E-01	1.2000000E-01	1.5000000E-01	1.4000000E-01
1.2000000E-01	1.4000000E-01	6.9999999E-02	7.9999999E-02	1.0000000E-01	1.2000000E-01	1.5000000E-01	1.5000000E-01
1.2000000E-01	1.4000000E-01	7.9999999E-02	7.9999999E-02	1.0000000E-01	1.2000000E-01	1.5000000E-01	1.5000000E-01
1.2000000E-01	1.4000000E-01	7.9999999E-02	7.9999999E-02	1.0000000E-01	1.2000000E-01	1.5000000E-01	1.5000000E-01
1.2000000E-01	1.4000000E-01	7.9999999E-02	8.9999999E-02	1.0000000E-01	1.2000000E-01	1.5000000E-01	1.5000000E-01
1.2000000E-01	1.4000000E-01	7.9999999E-02	8.9999999E-02	1.0000000E-01	1.2000000E-01	1.5000000E-01	1.5000000E-01
1.3000000E-01	1.4000000E-01	7.9999999E-02	8.9999999E-02	1.0000000E-01	1.3000000E-01	1.5000000E-01	1.5000000E-01
1.3000000E-01	1.4000000E-01	7.9999999E-02	8.9999999E-02	1.0000000E-01	1.3000000E-01	1.5000000E-01	1.5000000E-01
1.3000000E-01	1.4000000E-01	8.9999999E-02	8.9999999E-02	1.0000000E-01	1.3000000E-01	1.5000000E-01	1.5000000E-01
1.3000000E-01	1.4000000E-01	8.9999999E-02	8.9999999E-02	1.0000000E-01	1.3000000E-01	1.5000000E-01	1.5000000E-01
1.3000000E-01	1.4000000E-01	1.0000000E-01	8.9999999E-02	1.0000000E-01	1.3000000E-01	1.5000000E-01	1.5000000E-01
1.3000000E-01	1.4000000E-01	1.0000000E-01	8.9999999E-02	1.0000000E-01	1.3000000E-01	1.5000000E-01	1.5000000E-01
1.3000000E-01	1.3000000E-01	1.0000000E-01	8.9999999E-02	1.0000000E-01	1.3000000E-01	1.6000000E-01	1.5000000E-01
1.3000000E-01	1.3000000E-01	1.0000000E-01	8.9999999E-02	1.0000000E-01	1.3000000E-01	1.6000000E-01	1.5000000E-01
1.4000000E-01	1.3000000E-01	1.0000000E-01	8.9999999E-02	8.9999999E-02	1.4000000E-01	1.6000000E-01	1.4000000E-01
1.4000000E-01	1.3000000E-01	1.1000000E-01	8.9999999E-02	8.9999999E-02	1.4000000E-01	1.5000000E-01	1.4000000E-01
1.4000000E-01	1.3000000E-01	1.1000000E-01	8.9999999E-02	8.9999999E-02	1.4000000E-01	1.4000000E-01	1.3000000E-01
1.4000000E-01	1.3000000E-01	1.1000000E-01	8.9999999E-02	8.9999999E-02	1.4000000E-01	1.4000000E-01	1.3000000E-01
1.4000000E-01	1.3000000E-01	1.1000000E-01	8.9999999E-02	8.9999999E-02	1.4000000E-01	1.4000000E-01	1.3000000E-01
1.4000000E-01	1.3000000E-01	1.1000000E-01	8.9999999E-02	8.9999999E-02	1.4000000E-01	1.4000000E-01	1.3000000E-01
1.4000000E-01	1.3000000E-01	1.1000000E-01	8.9999999E-02	8.9999999E-02	1.4000000E-01	1.4000000E-01	1.3000000E-01
1.4000000E-01	1.3000000E-01	1.1000000E-01	8.9999999E-02	8.9999999E-02	1.4000000E-01	1.4000000E-01	1.3000000E-01
1.4000000E-01	1.2000000E-01	1.2000000E-01	8.9999999E-02	8.9999999E-02	1.4000000E-01	1.4000000E-01	1.3000000E-01
1.4000000E-01	1.2000000E-01	1.2000000E-01	8.9999999E-02	7.9999999E-02	1.4000000E-01	1.4000000E-01	1.3000000E-01
1.4000000E-01	1.2000000E-01	1.2000000E-01	8.9999999E-02	7.9999999E-02	1.4000000E-01	1.4000000E-01	1.3000000E-01
1.4000000E-01	1.2000000E-01	1.2000000E-01	8.9999999E-02	7.9999999E-02	1.4000000E-01	1.4000000E-01	1.3000000E-01
1.4000000E-01	1.2000000E-01	1.2000000E-01	8.9999999E-02	7.9999999E-02	1.4000000E-01	1.4000000E-01	1.3000000E-01
1.4000000E-01	1.2000000E-01	1.2000000E-01	8.9999999E-02	7.9999999E-02	1.4000000E-01	1.4000000E-01	1.3000000E-01
1.4000000E-01	1.2000000E-01	1.3000000E-01	8.9999999E-02	7.9999999E-02	1.4000000E-01	1.4000000E-01	1.3000000E-01
1.4000000E-01	1.3000000E-01	1.3000000E-01	8.9999999E-02	7.9999999E-02	1.4000000E-01	1.4000000E-01	1.3000000E-01
1.4000000E-01	1.4000000E-01	1.3000000E-01	1.0000000E-01	7.9999999E-02	1.4000000E-01	1.4000000E-01	1.3000000E-01
1.4000000E-01	1.3000000E-01	1.3000000E-01	1.0000000E-01	7.9999999E-02	1.4000000E-01	1.4000000E-01	1.3000000E-01
1.4000000E-01	1.2000000E-01	1.3000000E-01	1.0000000E-01	7.9999999E-02	1.4000000E-01	1.4000000E-01	1.3000000E-01
1.4000000E-01	1.2000000E-01	1.4000000E-01	1.0000000E-01	7.9999999E-02	1.4000000E-01	1.4000000E-01	1.3000000E-01
1.4000000E-01	1.1000000E-01	1.4000000E-01	1.0000000E-01	7.9999999E-02	1.4000000E-01	1.4000000E-01	1.3000000E-01
1.4000000E-01	1.1000000E-01	1.4000000E-01	1.0000000E-01	6.9999999E-02	1.4000000E-01	1.4000000E-01	1.4000000E-01
1.4000000E-01	1.1000000E-01	1.3000000E-01	1.0000000E-01	6.9999999E-02	1.4000000E-01	1.3000000E-01	1.4000000E-01
1.4000000E-01	1.0000000E-01	1.2000000E-01	1.0000000E-01	6.9999999E-02	1.4000000E-01	1.3000000E-01	1.4000000E-01
1.4000000E-01	8.9999999E-02	1.2000000E-01	1.0000000E-01	6.9999999E-02	1.4000000E-01	1.3000000E-01	1.4000000E-01
1.4000000E-01	8.9999999E-02	1.2000000E-01	1.0000000E-01	7.9999999E-02	1.5000000E-01	1.3000000E-01	1.4000000E-01
1.4000000E-01	8.9999999E-02	1.2000000E-01	1.0000000E-01	6.9999999E-02	1.5000000E-01	1.3000000E-01	1.4000000E-01
1.4000000E-01	7.9999999E-02	1.1000000E-01	1.0000000E-01	5.9999999E-02	1.5000000E-01	1.3000000E-01	1.4000000E-01
1.4000000E-01	7.9999999E-02	1.1000000E-01	1.0000000E-01	5.9999999E-02	1.5000000E-01	1.3000000E-01	1.4000000E-01
1.4000000E-01	7.9999999E-02	1.1000000E-01	1.0000000E-01	5.9999999E-02	1.5000000E-01	1.3000000E-01	1.4000000E-01
1.4000000E-01	7.9999999E-02	1.0000000E-01	1.0000000E-01	5.9999999E-02	1.5000000E-01	1.3000000E-01	1.4000000E-01
1.4000000E-01	7.9999999E-02	1.0000000E-01	1.0000000E-01	6.9999999E-02	1.5000000E-01	1.3000000E-01	1.4000000E-01
1.4000000E-01	7.9999999E-02	8.9999999E-02	1.0000000E-01	6.9999999E-02	1.5000000E-01	1.3000000E-01	1.4000000E-01
1.4000000E-01	7.9999999E-02	8.9999999E-02	1.0000000E-01	6.9999999E-02	1.5000000E-01	1.3000000E-01	1.4000000E-01
1.4000000E-01	6.9999999E-02	8.9999999E-02	1.0000000E-01	7.9999999E-02	1.5000000E-01	1.3000000E-01	1.4000000E-01
1.4000000E-01	6.9999999E-02	8.9999999E-02	1.0000000E-01	7.9999999E-02	1.5000000E-01	1.3000000E-01	1.4000000E-01
1.4000000E-01	6.9999999E-02	8.9999999E-02	1.0000000E-01	7.9999999E-02	1.5000000E-01	1.3000000E-01	1.4000000E-01
1.4000000E-01	6.9999999E-02	8.9999999E-02	1.0000000E-01	7.9999999E-02	1.5000000E-01	1.3000000E-01	1.4000000E-01
1.4000000E-01	5.9999999E-02	8.9999999E-02	1.0000000E-01	7.9999999E-02	1.5000000E-01	1.3000000E-01	1.4000000E-01
1.4000000E-01	5.9999999E-02	8.9999999E-02	1.0000000E-01	7.9999999E-02	1.5000000E-01	1.3000000E-01	1.4000000E-01
1.4000000E-01	5.9999999E-02	8.9999999E-02	1.0000000E-01	8.9999999E-02	1.5000000E-01	1.3000000E-01	1.4000000E-01
1.4000000E-01	5.9999999E-02	8.9999999E-02	1.0000000E-01	1.0000000E-01	1.5000000E-01	1.4000000E-01	1.4000000E-01
1.4000000E-01	5.9999999E-02	8.9999999E-02	1.0000000E-01	1.0000000E-01	1.5000000E-01	1.4000000E-01	1.4000000E-01
1.4000000E-01	5.9999999E-02	8.9999999E-02	1.0000000E-01	1.1000000E-01	1.5000000E-01	1.4000000E-01	1.4000000E-01
1.4000000E-01	5.9999999E-02	8.9999999E-02	1.0000000E-01	1.1000000E-01	1.5000000E-01	1.4000000E-01	1.4000000E-01

Table B2

SPECTRAL DENSITY ESTIMATION ON DATA FROM EXPERIMENT DJBRP8 BATCH 8

TOTAL NUMBER OF SAMPLES = N = 1440 STARTING WITH SAMPLE NUMBER 1 OF DATA RECORD. NUMBER OF LAGS = M = 20.

SAMPLING INTERVAL = DELTA T = 3.0000000E 02 SECONDS. FREQUENCY RESOLUTION = 1/2MDT = 8.3333331E-05 CYCLES PER SECOND.

PREWHITENED WITH A 8 TERM MOVING LINEAR AVERAGE. K = 7. NUMBER OF PREWHITENED SAMPLES = N' = N-K = 1433.

PREWHITENING FILTER COEFFICIENTS

A(0) = 8.5900590E-01 A(1) = -9.3806539E-01 A(2) = 1.8554991E-01 A(3) = -8.6138682E-02 A(4) = 3.1371808E-02

A(5) = -3.4452610E-02 A(6) = 6.3926556E-03 A(7) = -2.3757884E-02

POSTGREENING FILTER COEFFICIENTS

B(0) = 1.6624829E 00 B(1) = -9.9999994E-01 B(2) = 2.4999999E-01 B(3) = -1.1111110E-01 B(4) = 6.2499998E-02

B(5) = -3.9999997E-02 B(6) = 2.7777777E-02 B(7) = -2.0408162E-02

Q2 WINDOW L = 1 D(0) = 0.50000000 D(1) = 0.25000000

DETRENDED FOR (8.8884E-06) + (0.)T SAMPLE AVERAGE = 8.888419E-06 SAMPLE AVERAGE SQUARED = 7.900399E-11

FIRST THIRD MEAN = -5.395997E-05 SECOND THIRD MEAN = -3.529567E-04 LAST THIRD MEAN = 4.318087E-04

INDEX R	MEAN LAGGED PRODUCTS C(RDT)	PREWHITENING FILTER G(F)	RAW SPECTRAL ESTIMATE V(F)	WINDOWED SPECTRAL ESTIMATE U(F)	******** FINAL SPECTRAL DENSITY ESTIMATES ******** Q0 WINDOW S(F)	Q2 WINDOW S(F)	Q0 WINDOW DECIBELS DB S(F)	Q2 WINDOW DECIBELS DB S(F)	*** FREQUENCY *** CPS F	10LOG F
0	9.08240E-06	4.47035E-08	1.09999E-02	7.92459E-03	4.09504E 00*	2.95017E 00*	6.123*	4.698*	0	INF
1	-5.50527E-08	2.33163E-02	4.84928E-03	5.64514E-03	2.07978E-01	2.42111E-01	-6.820	-6.160	8.333E-05	-40.79
2	1.89991E-06	7.97103E-02	1.88208E-03	2.74950E-03	2.36115E-02	3.44936E-02	-16.269	-14.623	1.667E-04	-37.78
3	1.14995E-06	1.45018E-01	2.38455E-03	2.04435E-03	1.64431E-02	1.40972E-02	-17.840	-18.509	2.500E-04	-36.02
4	1.21907E-06	2.14168E-01	1.52620E-03	1.76735E-03	7.12619E-03	8.25216E-03	-21.471	-20.834	3.333E-04	-34.77
5	1.05268E-06	3.08111E-01	1.63245E-03	1.58461E-03	5.29824E-03	5.14297E-03	-22.759	-22.888	4.167E-04	-33.80
6	1.28896E-06	4.48750E-01	1.54733E-03	1.71391E-03	3.44808E-03	3.81931E-03	-24.624	-24.180	5.000E-04	-33.01
7	6.93310E-07	6.31351E-01	2.12856E-03	1.96163E-03	3.37144E-03	3.10704E-03	-24.722	-25.077	5.833E-04	-32.34
8	6.05045E-07	8.28538E-01	2.04208E-03	1.97928E-03	2.46468E-03	2.38889E-03	-26.082	-26.218	6.667E-04	-31.76
9	9.10265E-07	1.02324E 00	1.70441E-03	1.90114E-03	1.66570E-03	1.85796E-03	-27.784	-27.310	7.500E-04	-31.25
10	7.62570E-07	1.23193E 00	2.15367E-03	1.83696E-03	1.74821E-03	1.49113E-03	-27.574	-28.265	8.333E-04	-30.79
11	5.63905E-07	1.48761E 00	1.33610E-03	1.82917E-03	8.98150E-04	1.22961E-03	-30.467	-29.102	9.167E-04	-30.38
12	9.43166E-07	1.79900E 00	2.49083E-03	2.26365E-03	1.38456E-03	1.25828E-03	-28.587	-29.002	10.000E-04	-30.00
13	5.33516E-07	2.13425E 00	2.73685E-03	2.78865E-03	1.28235E-03	1.30662E-03	-28.920	-28.839	1.083E-03	-29.65
14	4.39403E-07	2.45484E 00	3.19008E-03	2.82092E-03	1.29951E-03	1.14913E-03	-28.862	-29.396	1.167E-03	-29.33
15	4.88799E-07	2.76685E 00	2.16668E-03	2.68379E-03	7.83084E-04	9.69979E-04	-31.062	-30.132	1.250E-03	-29.03
16	5.05853E-07	3.12767E 00	3.21172E-03	2.89730E-03	1.02687E-03	9.26344E-04	-29.885	-30.332	1.333E-03	-28.75
17	4.70926E-07	3.58481E 00	2.99906E-03	3.18609E-03	8.36604E-04	8.88776E-04	-30.775	-30.512	1.417E-03	-28.49
18	1.57971E-07	4.09719E 00	3.53451E-03	3.35845E-03	8.62667E-04	8.19696E-04	-30.642	-30.863	1.500E-03	-28.24
19	-1.62206E-07	4.52027E 00	3.36572E-03	3.62264E-03	7.44585E-04	8.01421E-04	-31.281	-30.961	1.583E-03	-28.00
20	6.47849E-07	4.68608E 00	4.22459E-03	3.79516E-03	9.05210E-04*	8.13195E-04*	-30.433*	-30.898*	1.667E-03	-27.78

*FIRST AND LAST FINAL SPECTRAL DENSITY ESTIMATES POSTGREENED AT

R = 1/3 F = 2.778E-05 10LOG F = -45.56 G(F) = 2.72417E-03

R = 19 2/3 F = 1.639E-03 10LOG F = -27.85 G(F) = 4.66697E 00

ONE SHEET HAS BEEN POINT PLOTTED. 103001 1

Q0 RT8 RT3 PAGE16P (8) 5 MINUTE SAMPLES PREWHITENED 1/F**2

THE X COORDINATE IS SCALED FROM -5.500E 01 TO -2.500E 01

THE Y COORDINATE IS SCALED FROM -3.000E 01 TO 2.000E 01

APPENDIX C

ERROR ANALYSIS OF TEMPERATURE SENSOR

Let us examine what kinds of errors are generated in the temperature sensor due to various non-ideal components in the circuit. For an approximate first order analysis we shall consider only the new factors represented in Figure C 1 . They are: the non-zero output impedance of the audio oscillator, R_s; the non-infinite input impedance of the AC amplifier, R ; the leakage capacitance between the input and output, C_2; the leakage capacitance between the input and ground, C_3; the stray capacitance of the mercury column to ground, C_4; and the capacitance between the output and ground, C_1. The elements previously discussed, C_T, C_B, and R are also included. If we define V_g and V_s as the voltages at the internal nodes as shown

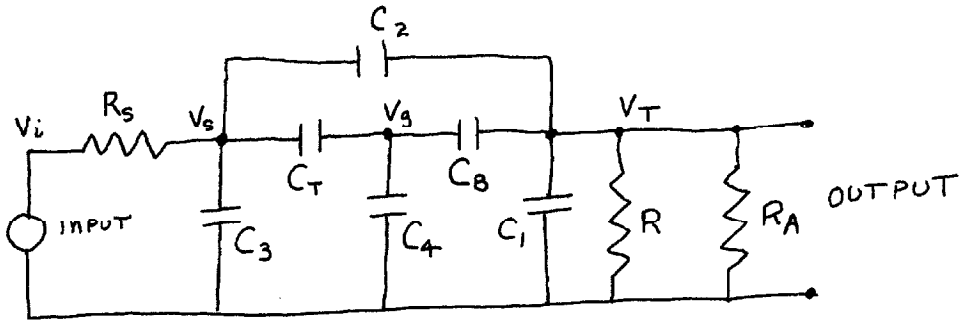

Figure (C1)

Temperature Sensing Circuit Model

and R_L as the parallel combination of R and R_A we can write

$$\begin{pmatrix} \frac{V_i}{R_s} \\ 0 \\ 0 \end{pmatrix} = A \begin{pmatrix} V_s \\ V_g \\ V_T \end{pmatrix}$$

for the circuit equations in the Laplace domain where the Matrix A is given by

$$A = \begin{pmatrix} s(C_3+C_2+C_T) + \frac{1}{R_s} & -sC_T & -sC_2 \\ -sC_T & s(C_4+C_B+C_T) & -sC_B \\ -sC_2 & -sC_B & s(C_1+C_B+C_2) + \frac{1}{R_L} \end{pmatrix}$$

The solution of this set of equations for the output voltage in terms of the input is given by

$$V_T = \frac{V_i}{R_s} \frac{s^2(C_TC_B+C_2C_4+C_2C_B+C_2C_T)}{|A|}$$

where $|A|$ is the determinent of the matrix A.

Physically we expect to be operating under conditions where $C_B \gg C_T$, C_1, C_2, C_3, C_4 because the bottom mercury reservoir of the thermometer is separated from the painted outside covering only be a thin layer of glass.

For the case of the fine differential thermometer used as the thermal control system sensor our nominal operating point will be in the middle of its range so that we will also have

$C_T \gg C_1, C_2, C_3, C_4$.

For the case of the larger range thermometer used to measure room temperature the capillarly tube is much larger in diameter and the glass cnvolope is smaller in diameter. Thus, C_T is much larger so that the above approximations would be expected to hold until the temperature reached say 20°C (the range of the thermometer is 15°C - 35°C). In addition, we expect the oscillators output impedance to be small so that

$R_s \ll R_L$

Utilizing these approximations we have to first order that the transfer function becomes

$$\frac{V_T}{V_i} \approx \frac{s(C_T+C_2)R_L}{1 + s R_L(C_1 + C_T) + s^2 C_T C_1 R_s R_L}$$

In Section 4.2 we ignored these denominator poles. They are much higher frequency than the pole due to the the thermal lag in the glass mercury bulb itself. The significant first order error term seems to be C_2 the input-output capactiance. If C_T is proporitonal to temperature, T, as

$C_T = a + bT$

where a $\ll$ b then the major contribution of C_2 will be to increase a, but will not effect the linearity of the sensor. For the differential thermometer $C_T \approx .4\mu\mu f$ at the operating point. Hence, a stray capacitance between input and output of a few hundredths of a micro-microfared will lead to an appreciable offset in the temperature sensor. However, for use as a small range linear sensor about a fixed operating point this dc bias will be unimportant. For the long range room temperature measuring thermometer C_T is much larger while C_2 is probably on the same order. Thus, the dc bias is smaller. The magnitude of the first order error in the linearity of the sensor will be

$$\omega R_L C_T$$

compared to unity. For the differential thermometer with $C_T \approx .4\mu\mu f$, $R_L \approx 1$ MΩ, and an operating frequency of 10Kc we will have a first order linearity error of about 3%. For the room temperature thermometer C_T is larger and the situation is slightly worse with possibly a linearity on the order of 10%.

APPENDIX D

1. Calculation of $\int_{-\infty}^{\infty} \left(\frac{\sin(x-n\pi}{(x-n\pi)}\right)^2 \frac{dx}{a^2 + x^2}$

Consider the integral

$$I = \int_{-\infty}^{\infty} \left[\frac{\sin(x-n\pi)}{(x-n\pi)}\right]^2 \frac{dx}{a^2 + x^2}$$

Because of the generalized version of Parseval's Theorem, this integral is equivalent to the integral of the Fourier Transforms of the factors of the integrand in the corresponding domain. Thus

$$I = \int_{-\infty}^{\infty} F\left\{\left[\frac{\sin(x-n\pi)}{(x-n\pi)}\right]^2\right\} F\left\{\frac{1}{a^2 + x^2}\right\} dy$$

where $F\{f(x)\} = \int_{-\infty}^{\infty} f(x)\, e^{-j2\pi yx}\, dx$ denotes the Fourier transform of $f(x)$. The Fourier transform of the second factor is well known to be

$$F\left\{\frac{1}{a^2 + x^2}\right\} = \frac{\pi}{a}\, e^{-2\pi a|y|}$$

The Fourier transform of the first factor can be easily obtained as follows:

$$F\left\{\left[\frac{\sin(x-n\pi)}{(x-n\pi)}\right]^2\right\} = \int_{-\infty}^{\infty} \left[\frac{\sin(x-n\pi)}{(x-n\pi)}\right]^2 e^{-j2\pi xy}\, dx$$

$$= e^{-j2\pi yn\pi}\, F\left\{\left(\frac{\sin x}{x}\right)^2\right\}$$

But the latter transform is well known so that we have finally

$$F\left\{\left[\frac{\sin(x-n\pi)}{(x-n\pi)}\right]^2\right\} = e^{-j2\pi yn\pi} \begin{cases} \pi^2\left(\frac{1}{\pi} - |y|\right) & |y| < \frac{1}{\pi} \\ 0 & \text{otherwise} \end{cases}$$

Inserting these results above yields

$$I = \int_{-\frac{1}{\pi}}^{\frac{1}{\pi}} e^{-j2\pi yn\pi}\, \pi^2 \left[\frac{1}{\pi} - |y|\right] \frac{\pi}{a} e^{-2\pi a|y|}\, dy$$

which becomes after simplifcation

$$I = \frac{\pi}{2a} \int_0^2 (2 - x) \cos n\pi x\, e^{-ax}\, dx$$

Writing this latter integral as two integrals I_1 and I_2, respectively, we have

$$I = I_1 + I_2$$

where

$$I_1 = \frac{\pi}{a} \int_0^2 \cos n\pi x\, e^{-ax}\, dx$$

$$I_2 = -\frac{\pi}{2a} \int_0^2 x \cos n\pi x\, e^{-ax}\, dx$$

The first of these can be evaluated immediately DW 576.1 yielding

$$I_1 = \frac{\pi}{a^2 + (n\pi)^2} (1 - e^{-2a})$$

Noting that

$$I_2 = \tfrac{1}{2} \frac{dI_1}{da}$$

we have by differentiation that

$$I_2 = \frac{-\pi a}{[a^2 + (n\pi)^2]^2} + \frac{\pi e^{-2a}}{a^2 + (n\pi)^2} \left[1 + \frac{a}{a^2 + (n\pi)^2}\right]$$

Combining these two results yields

$$I = I_1 + I_2 = \frac{\pi}{a^2 + (n\pi)^2} \left[1 - \frac{a}{a^2 + (n\pi)^2}\right] + \frac{\pi a\, e^{-2a}}{[a^2 + (n\pi)^2]^2}$$

which is the result quoted in Appendix A.

2. Truncation Error

This appendix will calculate the error made in approximating

$$I(n,1) = \int_{-\infty}^{\infty} \left(\frac{\sin(x-n\pi)}{(x-n\pi)}\right)^2 \frac{dx}{|x|}$$

by the finite integral

$$XINT(N,1) = \int_{-A}^{B} \left(\frac{\sin(x-n\pi)}{(x-n\pi)}\right)^2 \frac{dx}{|x|}$$

We begin by writing

$$I(n,1) = I_L + XINT(N,1) + I_R$$

where

$$I_L = \int_{-\infty}^{-A} \left(\frac{\sin(x-n\pi)}{(x-n\pi)}\right)^2 \frac{dx}{|x|}$$

$$I_R = \int_{B}^{\infty} \left(\frac{\sin(x-n\pi)}{(x-n\pi)}\right)^2 \frac{dx}{|x|}$$

Since B is positive we have on writing the sinc squared as half of one minus the cosine of the double angle that

$$I_R = \tfrac{1}{2}\int_B^\infty \frac{dx}{x(n\pi-x)^2} - \tfrac{1}{2}\int_B^\infty \frac{\cos 2(n\pi-x)}{x(n\pi-x)^2}\,dx$$

The first integral can be integrated by DW 101.2 to give

$$-\frac{1}{2(n\pi)^2}\left[\frac{n\pi}{n\pi-B} - \ln\left[1-\frac{n\pi}{B}\right]\right]$$

Since we expect to take $B \gg n\pi$ it is convenient to write this as

$$+\frac{1}{2(n\pi)^2}\left[\frac{n\pi}{B}\,\frac{1}{(-\frac{n\pi}{B}+1)} + \ln\left(1-\frac{n\pi}{B}\right)\right]$$

and expand in powers of $(n\pi/B)$ obtaining

$$\frac{1}{2(n\pi)^2}\left[\left(\frac{n\pi}{B}\right) - \left(\frac{n\pi}{B}\right)^2 + \left(\frac{n\pi}{B}\right)^3 - \left(\frac{n\pi}{B}\right)^4 + \cdots - \left(\frac{n\pi}{B}\right) - \tfrac{1}{2}\left(\frac{n\pi}{B}\right)^2 - \tfrac{1}{3}\left(\frac{n\pi}{B}\right)^3 - \tfrac{1}{4}\left(\frac{n\pi}{B}\right)^4 - \cdots\right]$$

from which we obtain finally

$$-\frac{1}{2(n\pi)^2}\left[\frac{3}{2}\left(\frac{n\pi}{B}\right)^2-\frac{2}{3}\left(\frac{n\pi}{B}\right)^3+\frac{5}{4}\left(\frac{n\pi}{B}\right)^4\ \ldots+(-1)^r\left(\frac{r+(-1)^r}{r}\right)\left(\frac{n\pi}{B}\right)^r+\ldots\right]$$

for the contribution to I_R from the first integral in Equation (B4). The contribution from the second term in that equation becomes on integrating by parts once

$$\frac{\sin 2(n\pi-x)}{4\,x(n\pi-x)^2}\Bigg|_B^\infty+\int_B^\infty\frac{\sin 2(n\pi-x)}{4\,x(x-n\pi)^3}\left(3-\frac{n\pi}{x}\right)dx$$

which is approximately

$$+\frac{\sin 2B}{4B^3(1-\frac{n\pi}{B})^2}-\int_B^\infty\frac{\sin 2x}{4x^4}\left[3+8\left(\frac{n\pi}{x}\right)+15\left(\frac{n\pi}{x}\right)^2+24\left(\frac{n\pi}{x}\right)^3+\ldots\right]dx$$

Integrating by parts again we have

$$\frac{\sin 2B}{4B^3}\left\{1+2\left(\frac{n\pi}{B}\right)+3\left(\frac{n\pi}{B}\right)^2+\ldots\right\}-\frac{\cos 2B}{8B^4}\left[3+8\left(\frac{n\pi}{B}\right)+15\left(\frac{n\pi}{B}\right)^2+24\left(\frac{n\pi}{B}\right)^3+\ldots\right]$$

$$+\int_B^\infty\frac{\cos 2x}{8}\left(\frac{12}{x^5}+40\,\frac{n\pi}{x^6}+90\left(\frac{n\pi}{x^7}\right)^2+148\left(\frac{n\pi}{x^8}\right)^3+\ldots\right)dx$$

so that we have finally that the contribution from this term is

$$\frac{\sin 2B}{4B^3}+\left[\frac{n\pi}{2}\sin 2B-\frac{3}{8}\cos 2B\right]\frac{1}{B^4}+\mathcal{O}\left(\frac{1}{B^4}\right)$$

where the order notation indicates that the latter term goes to zero faster than $\frac{1}{B^4}$. Combining the two contributions now yields

$$I_R = -\frac{3}{4B^2} + \frac{1}{B^3}\left(\frac{n\pi}{3} + \frac{\sin 2B}{4}\right) + \frac{1}{B^4}\left(\frac{n\pi}{2}\sin 2B - \frac{3}{8}\cos 2B - \frac{5}{8}(n\pi)^2\right) + \mathcal{O}\left(\frac{1}{B^4}\right) \tag{D5}$$

Proceeding in a similar manner for I_L we have first

$$I_L = -\int_{-\infty}^{-A}\left[\frac{\sin(x-n\pi)}{(x-n\pi)}\right]^2 \frac{dx}{x}$$

which becomes on changing variables

$$I_L = \frac{1}{2}\int_A^\infty \frac{du}{u(u+n\pi)^2} - \frac{1}{2}\int_A^\infty \frac{\cos 2(n\pi+u)}{u(n\pi+u)}\,du \tag{D6}$$

As can be seen by comparing Equation (D4) and (D6) the contribution for both terms in latter equation can be obtained by substituting A for B and changing the sign on the $n\pi$ terms. We have then

$$I_L = \frac{-3}{4A^2} + \frac{1}{A^3}\left(\frac{-n\pi}{3} + \frac{\sin 2A}{4}\right) - \frac{1}{A^4}\left(\frac{n\pi}{2}\sin 2A + \frac{3}{8}\cos 2A + \frac{5}{8}(n\pi)^2\right) + \mathcal{O}\left(\frac{1}{B^4}\right) \tag{D7}$$

Substituting Equations (D5) and (D7) into (D1) now yields

$$I(n,1) = XINT(N,1) - \frac{3}{4}\left(\frac{1}{A^2} + \frac{1}{B^2}\right) + \frac{n\pi}{3}\left(\frac{1}{B^3} - \frac{1}{A^3}\right) + \frac{1}{4}\left(\frac{\sin 2A}{A^3} + \frac{\sin 2B}{B^3}\right)$$

$$+ \left(\frac{n\pi}{2}\right)\left(\frac{\sin 2B}{B^4} - \frac{\sin 2A}{A^4}\right) - \frac{3}{8}\left(\frac{\cos 2A}{A^4} + \frac{\cos 2B}{B^4}\right)$$

$$- \frac{5}{8}(n\pi)^2\left(\frac{1}{A^4} + \frac{1}{B^4}\right) + \mathcal{O}\left(\frac{1}{B^4}\right)$$

if we now make the assumption that for calculational convenience we take A = B this becomes

$$I(n,1) = XINT(N,1) - \frac{3}{2A^2} + \frac{\sin 2A}{2A^3} - \frac{1}{4A^4}\left[3\cos 2A + 5(n\pi)^2\right] + \mathcal{O}\left(\frac{1}{A^4}\right)$$

which is the result used in Appendix A.

REFERENCES

1. Bell, D. A., "Semiconductor Noise as a Queuing Phenomenon," Proceedings of the Physcial Society of London, July 1963, V 82 n 525 part 1, pg. 117-120.

2. Rollin, B. V., and Templeton, I. M., "Noise in Semiconductors at Very Low Frequencies," Proceedings of the Physical Society of London, 1953, Vol. 66B, pg. 259.

3. Rollin, B. V., and Templeton, I. M., "Noise in Germanium Filaments at Very Low Frequencies," Proceedings of the Physical Society of London, 1954, Vol. 67B, pg. 271.

4. Winston, H., and Firle, T. E., "Noise Measurements in Semiconductors at Very Low Frequencies," Journal of Applied Physics, Vol. 26, No. 6, 1955.

5. Blackman, R. B., and Tukey, J. W., "The Measuremement of Power Spectra from the Point of View of Communications Engineering," Bell System Technical Journal, Vol. XXXVII, January and March 1958.

6. Parzen, E., "On Consistent Estimates of the Spectrum of a Stationary Time Series," Annuals of Mathematical Statistics," Vol. 28, 1957.

7. Parzen, E., "On Choosing an Estimate of the Spectral Density Function of A Stationary Time Series," Annuals of Mathematical Statistics, Vol. 28, 1957.

8. Priestley, M. B., "Basic Considerations in the Estimation of Spectra," Technometrics, Vol. 4, No. 4, pgs. 551-564, November 62.

9. Watts, P. G., "Optimal Windows for Power Spectrum Estimates," Wisconsin University, A65802.

10. Davenport and Root, "Random Signals and Noise," McGraw Hill, 1958.

11. Mood, Alexander M., and Graybill, Franklin A., "Introduction to the Theory of Statistics," Second Edition, McGraw Hill, 1963.

12. Dwight, "Tables of Integrals," Fourth Edition, MacMillian Co., New York, 1961.

13. Wideow, B., "A Study of Rough Amplitude Quantization by Means of Nyquist Sampling Theory," IRE Transactions on Circuit Theory, December 1956, pg. 266.

14. Franklin, Philip, "Functions of Complex Variables," Prentice-Hall, Inglewood Cliffs, New Jersey, 1958.

15. Jolley, L. B. W., "Summation of Series," Second Revised Edition, Dover, New York, 1961.

16. Hoffait, A. H., and Throton, R. D., "Limitations of Transistor DC Amplifiers," Proceedings of the IEEE, February 1964.

17. Middlebrook, R. D., "Differential Amplifiers," Wiley, New York, 1963.